Development and application of *in vitro* and *in vivo* microdialysis methods contributing to biomarker profiling and characterisation of drug distribution processes

Inaugural-Dissertation
to obtain the academic degree
Doctor rerum naturalium (Dr. rer. nat.)

submitted to the Department of Biology, Chemistry and Pharmacy
of Freie Universität Berlin

by

Claudia Kirbs

from Magdeburg

2015

Diese Dissertation wurde unter der Leitung von Frau Professorin Charlotte Kloft von 2009 bis 2013 an den Instituten für Pharmazie der Martin-Luther-Universität Halle-Wittenberg und der Freien Universität Berlin angefertigt.

1. Gutachter: Prof. Dr. rer. nat. habil. Charlotte Kloft

2. Gutachter: Prof. Dr. med. Christoph Stein

Disputation am 09. November 2015

TABLE OF CONTENTS

LIST OF ABBREVIATIONS AND SYMBOLS

AD	Assay Diluent
AE	Adverse event
ASCII	American Standard Code for Information Interchange
AFST	Subcommittee on Antifungal Susceptibility Testing of the ESCMID European Committee for Antimicrobial Susceptibility Testing (EUCAST)
AUC	Area under the curve
BASG	Austrian Federal Office for Safety in Health Care ("Bundesamt für Sicherheit im Gesundheitswesen")
BCVA	Best-corrected visual acuity
BD	Becton Dickinson
BLQ	Below lower limit of quantification
BMV	Bioanalytical method validation
BP	Blood pressure [mmHg]
BSA	Bovine serum albumin
Cal	Calibration solution, - sample
CBA	Cytometric Bead Array
C	Concentration(s)
C_{calc}	Calculated concentration
C_{max}	Maximum concentration
C_{nom}	Nominal concentration
C_{RP}	Concentration of retroperfusate
G-CSF	Granulocyte colony-stimulating factor
CDER	Center for Drug Evaluation and Research
CI	Confidence interval
CSF	Cerebrospinal fluid
GM-CSF	Granulocyte-macrophage colony-stimulating factor
CV	Coefficient of variation (imprecision)
D	Dose
Dev	Deviation
EC_{50}/EC_{80}	Half maximal effective concentration/effective concentration on 80% of microbes
ECG	Electrocardiogram
ELISA	Enzyme-linked immunosorbent assay
EMA	European Medicines Agency
ESCMID	European Society of Clinical Microbiology and Infectious Diseases

EUCAST	European Committee for Antimicrobial Susceptibility Testing (ESCMID)
FACS	Fluorescence activated cell sorting/sorter
FDA	Food and Drug Administration
FR	Flow rate
HA	Human albumin (5% solution)
HR	Heart rate [1/min]
ICH	International Conference on Harmonisation (of Technical Requirements for Registration of Pharmaceuticals for Human Use)
ICU	Intensive care unit
ID	Individual subject record
IFI	Invasive fungal infections
IL	Interleukin
IL-6	Interleukin-6
IL-8	Interleukin-8
IL-10	Interleukin-10
IFN (-α, -γ)	Interferon (-alpha, -gamma)
ISF	Interstitial fluid
IV	Intravenous
IVMS	*In vitro* microdialysis system
LBA	Ligand Binding Assay
LLOQ	Lower limit of quantification
LOD	Limit of detection
LOQ	Limit(s) of quantification
µD	Microdialysis
µDialysate	Microdialysate
µPerfusate	Microperfusate
M-CSF	Macrophage colony-stimulating factor
Mean	Arithmetic mean
MFI	Median fluorescence intensity
MFI_{obs}	Observed median fluorescence intensity
MFI_{pred}	Predicted median fluorescence intensity
MIC	Minimal inhibitory concentration
M_r	Relative molar mass
MWCO	Molecular weight cut off (molecular mass cut off)
NCA	Noncompartmental analysis
NIBSC	National Institute for Biological Standards and Control
NIR	Near infrared light detector → identification signal (+red light detector (Red))
PAES	Polyarylethersulphone
PBS	Phosphate buffered saline

PD	Pharmacodynamic(s)
PK	Pharmacokinetic(s)
PO	Per os (drug administration route)
PP	Polypropylene
QC	Quality control sample
QC_{lin}	Dilutional linearity quality control sample
QC_{stab}	Quality control sample for stability testing
R/R^2	Correlation coefficient/coefficent of determination
rD	Relative delivery
RD	Retrodialysis
RE	Relative Error (inaccuracy)
Rec	Recovery (accuracy)
Red	Red light detector → identification signal (+near infrared light detector (NIR))
RP	Retroperfusate
RR	Relative recovery
RS	Ringer's solution
rSEM	Standard error of the mean divided by the arithmetic mean
RS/HA	Proxy matrix consisting of Ringer's solution and human albumin solution 5 % (ratio 10:1 V/V)
RT	Room temperature
RT-PCR	Real-time polymerase chain reaction
SD	Standard deviation
SEM	Standard error of the mean
SL	Stock solution
SOP	Standard operating procedure
SPC	Summary of product characteristics
$T_H0/1/2/17$	T-helper cell, type 0/1/2/17
TNF-α (/TNF)	Tumour necrosis factor alpha
UF	Ultrafiltration, i.e. fluid loss along microdialysis membrane (projects II+III)
	Ultrafiltrate, i.e. ultrafiltered plasma (project IV)
ULOQ	Upper limit of quantification
VRC	Voriconazole
WT	Body weight
Yellow	Yellow light detector → quantification signal
1-/2-CMT	One-/Two-compartment pharmacokinetic model
4-PL	4-parameter-logistic

LIST OF TABLES

LIST OF FIGURES

1 INTRODUCTION

1.1 Drug monitoring and biomarker profiling at the target site

The optimisation of extisting drug therapies is one pillar of pharmaceutical research and of patient care. Commonly, therapeutic drug monitoring (TDM) is one method to individualise patient therapy with a highly variable drug by analysing blood samples and adapting the dose regimen [1; 2]. However, basic data for this approach, e.g. the pharmacokinetic/pharmacodynamic (PK/PD) relationship or the therapeutic range of the drug of interest, are often missing. Prior to a monitoring in the clinical routine, data concerning the drug exposure and the affected compartment, i.e. the target site, has to be obtained in addition to phase I to phase III studies to optimise drug therapy.

This thesis focuses on drug therapy for diseases caused by infections and regularly associated with inflammation. Inflammation is a host defensive reaction to tissue injuries initiated by various conditions such as trauma, infections, invasion of foreign particles, ischemia-reperfusion syndrome, malignant tumors, and autoimmune diseases [3]. Besides sepsis and other systemic diseases, inflammation takes commonly place in specific tissue environments. Therefore, it is beneficial to investigate the target site [4] instead of monitoring unspecific biomarkers (e.g. C-reactive protein [5; 6]) in the circulation. For the investigation of tissue concentrations of endogenous and exogenous analytes there are a handful of techniques only [7], and these are linked to a number of advantages and disadvantages [8]. A promising tool for the investigation of unbound analytes in the interstitial space at the target site over time is provided by microdialysis (µD) [9]. For example, drug monitoring in the tissue can be realised by this technique [10], if the analyte is determinable by µD.

Furthermore, the determination of pharmacodynamic (PD) parameters from the investigated tissue would be favourable. Commonly, surrogate parameters are used to substitute the measurement of the PD at the target (e.g. at a receptor) due to not realisable or extremely complex analyses of these effects. Biomarker monitoring is a common tool employed as a surrogate for diagnosis, prognosis and clinical outcome of drug therapies [11; 12]. Biomarker profiling consists of the assessment of the time course of (different) biomarkers and of the relations between them (‘patterns’) as a prerequisite for biomarker monitoring in patient care settings [13].

The most representative instrument for pharmacological research in humans, especially at a late developing phase or in routine-use status, consists of well-planned clinical studies of high quality [14; 15]. So called ‘pilot studies’ represent means to obtain first indications or to preliminary evaluate hypotheses on aspects that have not been investigated *in vivo* before

[16]. Prerequisites for an appropriate data analysis from the results of these studies are valid and reliable bioanalytical methods [17]. To obtain further knowledge from the results, pharmacokinetic (PK) analysis in addition to explorative and descriptive analysis of data can be performed.

1.2 Microdialysis

Recently, determination of tissue concentrations of antiinfective drugs was primarily based on one of the following methods: 1) intraoperative tissue sampling and determination of the concentration in the homogenised matrix, 2) skin blister fluid sampling technique (collection of the drug-containing exudate from small skin vesicles caused by e.g. cantharidine plasters), 3) imaging methods (e.g. magnetic resonance tomography) as well as 4) evaluation of tissue drug concentrations in 'surrogate compartments' [7; 18]. The most obvious disadvantages of these methods are that in homogenised tissue it is not possible to differentiate between plasma, intra- and extracellular concentrations. In addition, due to the limited number of samples no assessment of the entire concentration-time course can be made without a-priori information. Finally, imaging methods require considerable instrumental equipment.

In contrast to these methods, µD is an approach for determination of drug concentrations in virtually all tissues and has been widely used *in vivo* in animal experiments since 1980s and in human studies for more than two decades [9; 19; 20]. µD as a minimally invasive technique enables the sampling of analytes in the interstitial fluid (ISF) of tissues. Essentially, µD was designed to collect small endogenous analytes such as glucose or neurotransmitters from the extracellular fluid [19; 21; 22]. µD may be used for *in vitro* experiments as well as *in vivo* investigations of (body) fluids or of the ISF of selected tissues [23]. µD enables the sampling of drugs and their metabolites on the one hand and of endogenous analytes on the other hand [24].The most important fields in which µD technique has been applied are the following: (i) the determination of neurotransmitter concentrations in brain, (ii) the monitoring of endogenous metabolism in several tissues (e.g. posttraumatic reactions) and (iii) the measurement of antiinfective drug concentrations in target tissues, respectively [10; 23; 24]. The advantages of this technique are its easy handling and reduction of the patient's burden to a minimum since tissue extraction is not required. µD allows a continuous determination of tissue drug concentrations over a defined time interval. In addition, this technique enables to determine specifically the unbound, i.e. pharmacodynamically active, fraction of the extracellular drug concentration at the site of action due to its 'filtering' effect. This effect is caused by the semipermeable µD membrane which only allows the diffusion of selected analytes limited by the molecule volume (and associated mass).

The relevance of the measurement of unbound drug concentrations at the site of action and infection has been recognised by regulatory authorities in the US and Europe. The European Agency for the Evaluation of Medicinal Products (EMA) has focused on unbound tissue concentrations of antiinfective angents rather than plasma concentrations to predict the outcome of antimicrobial therapy [25–27]. The US ”Food and Drug Administration” (FDA) released a draft guideline recommending that concentrations of antiinfectives should be determined at the site of action [28]. In addition, the establishment of the relationship of the unbound drug concentration and the *in vitro* susceptibility of the infecting organism is required if the dossier of a new antiinfective is submitted to regulatory authorities in the US. Finally, FDA acknowledged µD as an attractive approach for the determination of the distribution of antiinfectives to the tissue [28; 29].

Nonetheless, the most recent development of large-pore membranes (cut-off ≥100 kDa) of µD catheters has enabled to sample molecules with higher molecular mass directly at the site of *in vivo* synthesis [30]. Hence, it is appealing to apply µD as a technique to sample macromolecules (e.g. proteins) in ISF, i.e., at the site of inflammation.

1.2.1 System and principle of microdialysis

A µD system consists of the µD pump, the µD catheter (for clinical purposes), also called ‘µD probe’ (*in vitro* or in preclinical use), and a microvial for sample collection [19; 23]. The core of the µD catheter is represented by a semi-permeable membrane. Diffusion of solute analyte molecules takes place across this membrane in both directions driven by the concentration gradient. This semi-permeable membrane is characterised by a molecular mass cut-off value (commonly called ‘molecular weight cut-off’ (MWCO)), which is determined by the pore size of the membrane and reduces the range and the quantity of analytes passing the membrane. MWCO usually is 6 kDa, 20 kDa or 100 kDa for commercially available µD catheters; only analytes with a molecular mass lower than the MWCO are capable of passing the membrane. However, even if the molecular mass falls below the MWCO an acceptable amount of passing molecules will only be attained with analytes having a mass lower than approximately one-fourth of the MWCO [23].

The functional µD principle is as follows: a microperfusate (µPerfusate) is pumped into the inlet tubing at a flow rate (FR) in the range of 0.3-10 µL/min and enters the µD membrane. In general the perfusate is an aqueous solution that mimics the composition of the surrounding medium around the µD catheter [18; 23]. The fluid, called ‘microdialysate’ (µDialysate) after passing the membrane, flows through the outlet tubing and is sampled at the end of it into a microvial. In Fig. 1-1, µPerfusate (blue arrows) enters the membrane part of a concentric catheter via in inner tube and changes the flow direction at the end of the cylinder. Solutes of the µPerfusate (green) can pass through the membrane while solutes of the surrounding

medium (red), e.g. of ISF, can diffuse into the tube and are transported by the flowing µDialysate.

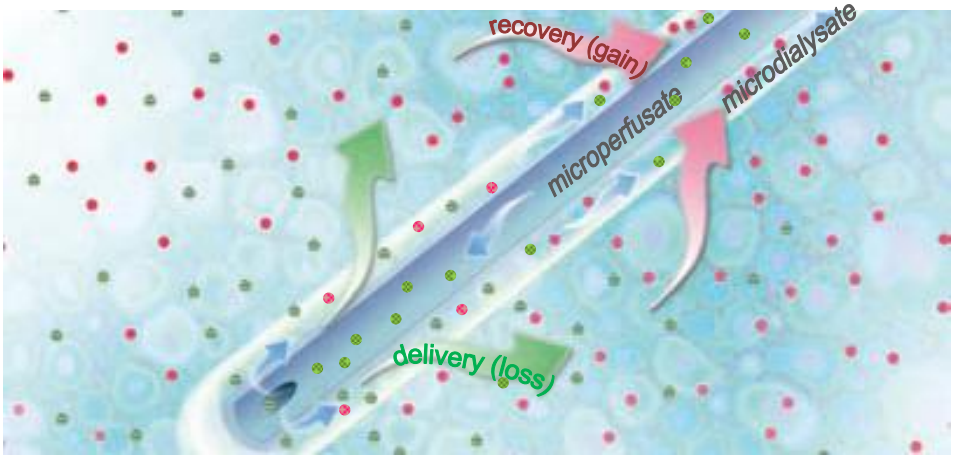

Fig. 1-1: Principle of microdialysis (modified from [31])

Besides the concentric catheters (shown in Fig. 1-1), linear ones are in (clinical) use as well. Inlet and outlet tubing are connected to the membrane tube on opposite sites, resulting in a continuously monodirectional flow of the µPerfusate.

Due to the continuous flow of the µPerfusate and to the diffusion velocity across the membrane, which both hinder an equilibrium of solute concentrations between ISF and µDialysate, concentrations quantified in µDialysate will only represent a fraction of the actual concentration in the surrounding medium or in ISF.

1.2.2 Relative recovery and relative delivery

The fraction of analyte gain or loss in µDialysate through the µD membrane is called ‘relative recovery’ (RR) or ‘relative delivery’ (rD) [23; 29], respectively. This fraction has to be determined to calculate actual concentrations in the investigated matrix by means of the analysed µDialysate. Determination is performed *in vitro* and/or *in vivo* by calibration techniques. Usually, µD is applied for the purpose of obtaining analytes from the catheter-surrounding tissue fluid. However, the equality of analyte permeation between recovery (gain, i.e., during the collection of µD samples in an investigation) and delivery (loss, i.e., during the calibration procedure) provides the theoretical concept for most of the calibration techniques [29].

Generally, RR and rD are calculated using the following equation:

$$RR, \% \; or \; rD, \% = \frac{C_{\mu Dialysate} - C_{\mu Perfusate}}{C_{ISF} - C_{\mu Perfusate}} \cdot 100 \qquad (1)$$

$C_{\mu Dialysate}$, $C_{\mu Perfusate}$ and C_{ISF} represent the concentration of the analyte in µDialysate, µPerfusate or catheter-surrounding medium/ISF, respectively.

The quantity of the gained or lost fraction depends on several factors, i.e. FR, MWCO, membrane area, temperature, pH of ISF, tortuosity and hydrophilicity of the membrane material, tortuosity of the catheter-surrounding matrix etc. [19; 23], and is, thus, in general not equal between *in vitro* and *in vivo* settings.

1.2.3 Calibration of microdialysis catheters

A catheter calibration has to be performed in order to determine the ratio which relates the measured concentration in µDialysate to the catheter-surrounding concentration in *in vitro* as well as *in vivo* settings [23; 29].

To obtain interstitial fluid concentrations of exogeneous analytes (e.g. drugs) from measured concentrations in µDialysate, µD catheter calibration can be assessed according to the retrodialysis (RD) method [32; 33]. Applying the common method of RD, the analyte is spiked to the µPerfusate and the lost fraction of the 'delivered' analyte is determined by measuring the residual concentration in µDialysate. The *in vivo* rD will thus be calculated according to Eq. (1) with C_{ISF}=0 as follows:

$$rD_{RD}, \% = 100 - \left(\frac{C_{\mu Dialysate}}{C_{\mu Perfusate}} \cdot 100\right) \qquad (2)$$

The assumption of equal rD (determined by RD) and RR (during the µD sampling of the analyte) presents the basic principle of RD. Therefore, rD_{RD} is equated with RR_{RD} (i.e. RR indirectly determined by RD) and ISF concentrations (C_{ISF}) of the analyte will be calculated with the following equation:

$$C_{ISF} = 100 \cdot \left(\frac{C_{\mu Dialysate}}{RR_{RD}}\right) \qquad (3)$$

In some cases an *in vivo* calibration procedure by analyte delivery is not appropriate for the investigated analyte or tissue, for example, if it is an endogenous analyte with pathophysilogical effects or if C_{ISF} cannot be assumed to be zero. In such cases, techniques applying analyte gain instead of loss are required. The flow-rate-variation method provides such a procedure [34]. Applying this method, µDialysate is sampled over a wide range of different FR. A constant concentration of the analyte in ISF presents the basic condition for the success of this calibration procedure. The determined concentrations in µDialysate are then plotted versus FR. Assuming equilibrium of concentrations at both sides of the membrane at a FR of 0.0 µL/min, i.e. under static conditions without a flow of µPerfusate/µDialysate, the concentration in ISF can be extrapolated from a mathematical function, which describes the plotted relation. Typically, an exponential function is applied.

Several further calibration methods, gain as well as loss procedures, were published [19; 23], which are only mentioned for the sake of completeness, but have not been employed in this

thesis: (i) the method of no-net-flux (also zero-net-flux) [35; 36], adding the analyte, which is also present in ISF, to µPerfusate in different concentrations and interpolating the surrounding concentration by plotting $C_{\mu Dialysate}$-$C_{\mu Perfusate}$ versus $C_{\mu Perfusate}$; (ii) the dynamic no-net-flux method applys the same principle but with different individuals, a single concentration is spiked in µPerfusate of every individual and data are pooled [9]; (iii) an endogenous reference analyte [37] can be used for calibration purposes as well if a correlation between its µDialysate concentration and RR of the analyte of interest was confirmed.

1.2.4 Considerations and challenges in microdialysis sampling

An important objective of the application of µD for the determination of analytes in the tissue is the observation of concentrations over time. Consequently, a good temporal resolution of such concentration determinations is intended, i.e., the sampling schedule has to consist of time intervals as small as possible. In addition, low FR are usually applied to provide an adequate gain of analyte molecules and, hence, result in reproducible, reliable high RR for the calculation of analyte concentrations in ISF. The low FR and the high temporal resolution cause small sample volumes, which lead to analytical challenges. Therefore, appropriate bioanalytical methods have to be developed for or adapted to the analyte quantification from µDialysate, considering the special (simple) composition of this matrix as well.
Furthermore, there is a potential volume loss during µD sampling, defined as ‘ultrafiltration’ (UF), which in particular occurs with the application of a membrane with a high MWCO. Ultrafiltration describes the process of increased water transport across the membrane caused by osmotic, hydrostatic and hydrodynamic, and further undefined forces [38–41].
The small sample volume and the occurrence of UF present the major drawbacks, which have to be solved via the development of adequate bioanalytical and µD methods for the determination of analytes, especially of those with a high molecular mass.

µD technique was originally in the 1970s/80s established for small endogenous analytes [22; 24] and since the 1990s later on used for drug molecules [10] and their PK analysis or PK/PD investigations [9] as well. In the last years an increasing number of the application of this technique for endogenous molecules of high molecular mass has been observed [30; 42–44]. One important consideration during determination of endogenous analytes, e.g. cytokines, is the effect of the applied technique on the tissue and, hence, on the analyte of interest itself. In the case of µD, which in general represents a minimally invasive method, the insertion of the µD catheter via a common cannula predominantly influences the peri-catheter environment. Consequently, the response of the tissue to the trauma of this catheter

insertion [45–48] and its impact on the analyte determination has to be considered for the application of μD for endogenous analytes.

1.3 Cytokines as a biomarker model for microdialysis

Cytokines (M_r 8-80 kDa) as immunomodulatory proteins are secreted by innate and adaptive immune cells, e.g. macrophages, neutrophils, B- and T-cells, as well as by tissue cells (e.g. fibroblasts) mediating all types of immune responses such as inflammation, infection and allergic or autoimmune reactions.

“Individually, cytokines are potent molecules which, *in vitro*, can cause changes in cell proliferation, differentiation and movement at nanomolar to picomolar concentrations” [49]. Cytokines influence the transcription of cellular genes and the production of other cytokines in networks and cascades [50]. Therefore, cytokines are not secreted *in vivo* individually rather than with other cytokines in patterns specific for the particular stimulus or inflammation. The cytokine network can be either protective or damaging by counteracting or supporting pathophysiologically important functions [51]. Either systemically or locally injected cytokines can also have tremendous effects on leukocyte migration and function, acute phase responses, temperature regulation, tissue structure (e.g. wound healing), cell survival, and haematopoietic cell numbers [49].

For the investigations in this thesis four model cytokines were selected on the basis of their multiple biological activities and wide-spread physicochemical properties. The physicochemical properties of the four model cytokines, i.e. Interleukin-6 (IL-6), Interleukin-8 (IL-8), Interleukin-10 (IL-10) as well as the Tumour Necrosis Factor-alpha (TNF-α), are listed in Tab. 1-1.

Tab. 1-1: Physicochemical properties of the four model cytokines [38; 49; 52]

Cytokine	Molar mass [kDa]	Isoelectric point (pI)
Interleukin-6	26.0 (21.5-28.0)	6.5
Interleukin-8	8.0	8.6
Interleukin-10	18.6 (homodimer 37.6)	8.0
Tumour Necrosis Factor-alpha	17.3 (homotrimer 53.9)	5.6

The four cytokines cover a wide range of molar mass (8.0-54 kDa), which is not only dependent on the number and kinds of amino acids but also on the glycosylation and quarternary structure (which might change during transport or functional processes). Furthermore, different isoelectric points were observed for these cytokines, which influence

the molecule charge in polar media and, consequently, contribute to hydrophilic/lipophilic properties.

Three of the four cytokines belong to the class of interleukins. Interleukins were originally defined as mediators between different populations of leukocytes and have a broad spectrum of effects concerning immune cells [50]. Nonetheless, they are involved in signalling pathways of other human cells as well.

1.3.1 Interleukin-6

IL-6 is a glycoprotein with a biological half-life of 3 min [50]. Therefore, systemic concentration measurements as well as determinations at one time point only can hardly describe the status of IL-6 secretion at the site of inflammation. It is a terminal factor of differentiation for antibody-stimulated B-cells, enhances Ig secretion by plasma cells and is involved in the activation and proliferation of thymocytes and T-cells. Indeed, IL-6 together with IL-1 appears to be one of the most important macrophage-derived mediators of T-cell activation [53]. This multifunctional cytokine is secreted by both lymphoid and non-lymphoid cells and regulates B- and T-cell function, haematopoiesis and acute-phase reactions [49; 53; 54]. IL-6 is also produced by macrophages, bone marrow stromal cells, fibroblasts, keratinocytes, mesangium cells, astrocytes and endothelial cells [49].

In humans, titers higher than 1000 U/mL have been measured in the cerebrospinal fluid (CSF) of patients with acute viral or bacterial infection of the central nervous system [55; 56]. Elevated IL-6 concentrations were also found in the serum of patients with severe burns, and a significant correlation was observed between IL-6 titers, fever and acute-phase proteins [57]. Similar correlations were observed in rheumatoid arthritis patients [58]. With regards to invasive fungal infections (IFI), IL-6 was produced rapidly after intranasal infection with the mould species *Aspergillus fumigatus*, and appeared to have a protective pro-inflammatory and immunomodulatory role in pulmonary host defence in response to organism-mediated pulmonary injury [59; 60].

1.3.2 Interleukin-8

IL-8 is a pro-inflammatory, non-glycosylated chemokine produced by many cell types, which mainly functions as a neutrophil chemoattractant and activating factor [61]. As a chemokine, IL-8 presents a secondary mediator that is induced by a primary pro-inflammatory mediator such as Interleukin-1 (IL-1) or TNF-α [62]. IL-8 mediates the local inflammation by inducing neutrophils to migrate from circulation into the tissue [50]. Unlike the classic leukocyte chemoattractants, which have little specificity, members of the chemokine family induce recruitment of well-defined leukocyte subsets [51; 62]. Like other pro-inflammatory cytokines, IL-8 is pleiotropic and acts on multiple cell types in addition to neutrophils, such as basophils

and subpopulation of lymphocytes (T-lymphocytes), keratinocytes, monocytes, and melanoma cells [49; 63]. However, the predominant function remains the recruitment and stimulation of neutrophils [62]. IL-8 is secreted by multiple cell types, including monocytes, lymphocytes, granulocytes, fibroblasts, endothelial cells, bronchial epithelial cells, keratinocytes, hepatocytes, mesangial cells and chondrocytes [49]. Its production is induced by pro-inflammatory agents [62], such as lipopolysaccharides, bacteria [64; 65], viruses [66], immune complexes [67], and integrin activation [68].

Elevated concentrations of IL-8 were recovered from inflammatory sites [62; 63] such as psoriatic scales [69], synovial fluid from rheumatoid joints [70] and bronchial lavage fluids from patients with respiratory distress syndrome [71; 72]. By recruitment of leukocytes, chemokine activity led to activation of host defence mechanisms and stimulated the early events of wound healing [62]. Increases in circulating IL-8 were part of the acute inflammatory response of humans to endotoxin as investigated by intravenous (IV) administration of endotoxins to 25 healthy volunteers [73]. IL-8 resulted in enhanced cytostatic effects of neutrophils on the yeast species *Candida albicans* [63; 74].

1.3.3 Interleukin-10

IL-10 is an acid-labile cytokine secreted by T_H0 and T_H2 subsets of $CD4^+$ T-lymphocytes and activated $CD8^+$ human T-cells [49] that blocks activation of cytokine synthesis by T_H1 T-cells [50], activated monocytes and NK-cells [75]. Conversely, it also stimulates and/or enhances proliferation of B-cells, thymocytes and mast cells. It reduces antigen presentation and inhibits T-cell activation [76]. Therefore, it is called an ‘anti-inflammatory’ cytokine. Thus, most cytokines are inhibited by IL-10, including crucial first-line defence cytokines, e.g. TNF-α, IL-1, and IL-6 [64; 77] and T_H1-inducing cytokines like IL-12 and IL-18 [76]. Furthermore, phagocytosis is increased by IL-10 in monocytes [78], a function that is rather associated with inflammation [76]. Additionally, the production of chemokines (e.g. IL-8), which recruit immune cells to the inflammatory site and activate them, is inhibited by IL-10 [76; 77].

The anti-inflammatory potential of IL-10 has encouraged clinical trials with IL-10 to treat chronic inflammatory diseases including inflammatory bowel disease, rheumatoid arthritis, and psoriasis [79]. Unfortunately, so far, these efforts have achieved only limited success. *C. albicans* induces immunosuppression through TLR_2-mediated IL-10 release [59; 80]. IL-10 suppresses the antifungal activity of mononuclear cells against *Aspergillus* hyphae, while increasing their phagocytic activity [59; 81].

1.3.4 Tumour Necrosis Factor-alpha

TNF-α is a potent paracrine and endocrine mediator of inflammatory and immune functions [82]. It does physiologically form homodimers or –trimers [50]. It is also known to regulate

growth and differentiation of a wide variety of cell types and is primarily produced by macrophages, T-cells and NK-cells [50; 83]. It is selectively cytotoxic for many transformed cells [51], especially in combination with IFN-α [49]. The TNF-α gene is silenced under normal circumstances and TNF-α concentrations in tissues are barely detectable [84]. TNF-α takes part in defence against infections, in amplification of inflammatory reactions as well as in stimulation of wound healing [50; 85]. Many of the actions of TNF-α occur in combination with other cytokines as part of the cytokine network. TNF-α appears to have a significant role in coordinating the inflammatory response and activating the cytokine cascade [64]. TNF-α is rapidly degraded in the circulation and has a short plasma half-life (15 to 30 min) when administered IV [86]. High-affinity membrane receptors for TNF-α exist on many tissues, including adipose tissue, liver, muscle, gut, and kidney [83]. The skin and lung may have extremely large numbers of TNF-receptors. The overall effect of TNF-α on various tissues appears to be regulated by the concentration of the mediator [49; 83]. I.e. the effect on a particular tissue could eventually depend on a specific threshold which has to be evaluated for each state of immune response or tissue composition, respectively. Furthermore, the trend of increasing or decreasing concentrations could be of predictive value for the grade of inflammation. TNF-α is stimulated by fungal, parasitic, viral, and bacterial agents [83].
TNF-α specifically activates neutrophils to phagocytise and inhibits the growth of *Candida* [87]. TNF-α stimulates neutrophils to damage *Aspergillus* hyphae, enhances phagocytosis of conidia, and augmentes neutrophil oxidative respiratory burst and degranulation induced by opsonised fungi [88; 89]. An overexpression of this mediator results in pathological effects, e.g septic shock [64; 82] or cachexia in tumor patients [50; 85].

1.3.5 Cytokines as diagnostic and prognostic biomarkers

The *in vivo* effect of a cytokine depends on the surrounding cytokine environment [49]. This is best illustrated in the context of inflammation [90]; at an inflamed site, many different cytokines and their inhibitors can be detected. It is the balance of activating and inhibitory cytokines that will determine the outcome in the inflamed tissue.
Altered cytokine responses caused by anti-inflammatory therapy may have important implications for both host defense and injury during septicaemia [73]. However, mediators of the inflammatory diseases itself do not always represent optimal biomarkers. For example, the leading role of C-reactive protein (CRP) as an inflammatory biomarker in cardiovascular disease is not primarily based on its pathogenic role in these disorders, but rather on its ability to reflect upstream inflammatory activity [91].

Surgical investigators used IL-6 as an index of the magnitude of systemic inflammation [84]. Profound morning elevations of plasma IL-6 and a reversal of its circadian rhythm were

reported in nine patients with major depressive disorder, in the absence of hypercortisolism. These observations may contribute to the increased risk for coronary heart disease and bone loss in this disease population [92].

Several studies have shown elevated concentrations of inflammatory cytokines such as TNF-α, IL-1β and IL-6 in heart failure patients in plasma and circulating leukocytes, as well as in the affected myocardium itself [91]. Some of these cytokines were also able to give useful prognostic information as reliable biomarkers in this disorder. A variety of inflammatory cytokines were upregulated in chronic heart failure, and several studies suggested that TNF-α, IL-6 or IL-1β could predict adverse outcome in these patients, although these studies were often limited in sample size and lack full standardisation [93; 94].

A huge part of life-threatening diseases are caused by the different kinds of pathogens such as viral, bacterial or fungal infections. The plasma samples from 56 HIV-seropositive and 15 HIV-seronegative individuals from the Multicenter AIDS Cohort Study population were measured for concentrations of cytokines and soluble markers [95]. When the HIV-positive individuals were stratified by $CD4^+$ levels, progressive increases in the concentrations of IFN-γ, TNF-α, and IL-6 were generally seen.

Although a large variety of mediators have been implicated in the development of sepsis syndrome, a rapidly growing body of experimental evidence suggests that cytokines are decisive factors in determining the pathobiology of sepsis syndrome [64; 96]. TNF-α and IL-1β have been most strongly associated with sepsis syndrome as early or ‘proximal’ cytokines, whereas IL-6- and IL-8 production is stimulated by these as well as by endotoxins resulting in a function as ‘distal’ cytokines intensifying the inflammatory response. Based on the available information on IL-6 in human disease, plasma IL-6 concentration in sepsis appears to be a good indicator of activation of the cytokine cascade and predicts subsequent organ system dysfunction and death. TNF-α serum concentrations were significantly raised in culture-positive pediatric patients in general and in gram-negative infections in particular [97]. They can be used as a surrogate marker of sepsis and aggressive treatment initiated in patients with elevated concentrations of TNF-α. In human sepsis, Hack et al. [98] and Marty et al. [99] have reported that plasma IL-8 concentrations are elevated in patients with sepsis and that higher concentrations correlate with mortality [64]. Van Deuren et al. [100] and Marchant et al. [101] reported higher plasma IL-10 concentrations in meningococcal infected patients with septic shock compared with patients without shock. In adult emergency department patients with suspected sepsis, IL-6 and CRP highly correlate with several infection parameters, but are inadequately discriminating to be used independently as diagnostic tools [102]. In contrast, results of 31 patients with febrile neutropenia indicate that procalcitonin and IL-6 were more reliable markers than C-reactive protein for predicting bacteraemia [103].

Aside from sepsis or other systemic immune responses, cytokines circulate at low concentrations, thus increasing analytical variability, and therefore require expensive high-sensitivity assays that need a large sample volume [91]. Alternatively, cytokines are to be determined at the target site, which reveal high pathophysiological concentrations of the mediators.

The μD technique provides a promising tool for target-site investigations, as reported Andersen et al.: IL-6 was markedly increased in the peritendinous tissue around the human Achilles tendon following exercise, suggesting that it may be involved in transforming mechanical loading into collagen synthesis in human tendon tissue [104]. Cameron et al. [105] hypothesised patients with high synovial fluid concentrations of IL-1β and TNF-α after acute knee injury to post-operatively develop osteoarthritis. IL-6 activity was significantly elevated in synovial fluid from patients with rheumatoid arthritis or other inflammatory arthritides, as compared with that in a group of patients with osteoarthritis [58]. From 125 arthritis patients and 20 healthy volunteers, patients with seropositive rheumatoid arthritis had the highest concentrations of IL-8 in the synovial fluids [67]. Rheumatoid arthritis, in which TNF-α had been strongly implicated as a mediator of the disease, was the first disease to be targeted by anti-TNF-α antibodies [106].

An increased IL-6 production was detected in lesional skin of psoriasis patients [107], therefore, IL-6 may be of major importance as a mediator of local and systemic inflammation, but also relevant for the epidermal hyperplasia observed in psoriasis [108]. The skin of psoriasis patients contained elevated concentrations of IL-8 as well [69; 108; 109]. Significant amounts of TNF-α could be detected in psoriatic skin lesions using immunohistochemical techniques [110]. TNF-α could not be determined in psoriatic scales or in suction blister fluid of lesional skin by Takematsu et al. [111]. It is likely that these results do not exclude a potential role of TNF-α in the initial step of the psoriatic inflammation [108], as also confirmed by the efficacy of psoriasis therapy with anti-TNF-α agents [109].

Bronchoalveolar lavage fluid IL-8 concentrations correlated with neutrophil counts and increased mortality in patients with adult respiratory distress syndrome [71; 72]. IL-8 concentrations in bronchoalveolar lavage fluid above a cut-off value of 2000 pg/mL showed high diagnostic specificity (83%) and sensitivity (81%) for patients with ventilator-associated pneumonia (VAP) [112]. A pilot study by Swanson et al. [113] indicated pulmonary concentrations of IL-8 and TNF-α to decrease in microbiologic responders with VAP. Conversely, clinical response parameters were discordant with the microbiologic response.

Compared with systemic cytokines, peritoneal cytokines (TNF-α, IL-6 and IL-10) responded extensively after major surgery, indicating that measurement of peritoneal cytokines was a more sensitive method to determine postoperative inflammatory reaction [114]. An

uncomplicated postoperative course was characterised by decreasing concentrations of peritoneal cytokines. Van Deuren et al. [100] found elevated TNF-α concentrations in the CSF of patients suffering from meningitis without septic shock, reflecting an intrathecal compartmentalised cytokine production.

A proper balance between pro- and anti-inflammatory mediators is necessary for regulating an adequate immune response toward a pathogen [64; 76], e.g. bacteria, vira or fungi. The pro-inflammatory response is essential for fighting the pathogen. Conversely, it is absolutely necessary to limit and resolve the inflammatory process to avoid damaging the host itself.

1.4 Voriconazole as a model antiinfective drug

Voriconazole (VRC) represents a second-generation triazole antifungal agent, which is indicated for IFI and was launched in 2002. Incidences of severe invasive fungal infectious diseases have increased at intensive care units (ICU) worldwide since the 1980s. Patients in critical care settings generally have a higher incidence of fungal infection [115].The increase of the prevalence was caused amongst others by the medical progress [116]: today a larger number of patients is immunosuppressed (e.g. HIV, transplantation patients, chemotherapy patients), being highly susceptible to invasive fungal infections [117]. As an example, approximately 25% of lung transplanted patients will develop an aspergillosis [118]. Another risk factor for the development of an invasive mycosis is a pharmacotherapy with antibiotics or/and corticoids [117].

Most of these opportunistic fungal infections are candidiasis and aspergillosis. In 2007 the results of EPIC II study including 1,265 ICU in 75 countries revealed that 19% of pathogens isolated in ICU patients were fungi [119; 120]. *Candida* species (spp) were predominantly isolated (17% of pathogens) followed by *Aspergillus* species (1.4%). Overall, Candida continues to be the predominant fungal pathogen [117; 121]. The yearly invasive candidiasis incidence reported on the USA National Center for Health Statistics is 8 to 10 cases per 100,000 people of general population [122]. Except for Denmark (8.6-9.4/100,000), incidence of invasive candidiasis in Europe (1.9-4.3/100,000) is lower than in the USA [117]. *Candida albicans* is the most common causative species, being responsible for 44.0% to 65.3% of *Candida* infections [117]. High mortality associated with candidaemia can be reduced by prompt, appropriate antifungal therapy [123]. Although *Aspergillus* species are a less common cause of infection, accounting for approximately 4% to 5% of all nosocomial fungal infections, they have emerged as an important cause of life-threatening invasive mycosis in immunocompromised patients [115; 124]. The epidemiology of aspergillosis in the ICU is difficult to establish due to the inhomogeneity of hospitalised patients, the diagnostic

difficulties necessitating a biopsy and the difficulty in discriminating between colonisation and disease [120]. However, incidence of invasive aspergillosis was published to range from 5 percent to more than 20 percent in high-risk groups [118; 125]. Both, *Candida* bloodstream infections and invasive aspergillosis, are associated with a high mortality rate in general [117; 118; 126] and with significant morbidity and mortality in immunocompromised patients, they can lead to extended stays on the ICU as well [116; 127]. In the US, candidaemia has a crude case fatality rate of 40%, whereas the corresponding rate with regards to invasive aspergillosis approaches 85%, even under aggressive antifungal therapy [115; 128; 129].

In the last 20 years amphotericin B has been the most important antifungal drug to treat severe IFI, but its implementation is linked with serious side effects. Antifungal agents which possess less side effects and thus better risk/benefit ratios are the triazoles. Particularly, the newer azole derivative, VRC, represents a progress in the treatment of IFI. VRC, a broad-spectrum triazole antifungal agent, was approved by the US Food and Drug Administration (FDA) in May 2002. It is structurally derived from fluconazole, with 1 triazole moiety replaced by a fluoropyrimidine group and a methyl group added to the propanol backbone, which provided VRC with fungicidal activity against *Aspergillus* spp. and other moulds [115; 130]. Therefore, VRC displays a higher efficacy against aspergillosis and other rare fungal pathogens. Therefore, it can be considered as a true broad-spectrum antifungal agent. In the last years, VRC replaced amphotericin B as the first-line treatment of invasive aspergillosis. VRC has been successfully used in other IFI as well, such as candidiasis, fusariosis or scedosporidiosis [130].

In clinical trials of aspergillosis in which patients were usually infected with wild-type isolates and treated with standard dose of VRC, the 6 week survival rate was approximately 80% [125; 131]. VRC has been assessed for the treatment of invasive aspergillosis in two clinical trials. During an open, non-comparative clinical trial on VRC treatment (primary or salvage therapy) of histopathologically or microbiologically proven or probable invasive aspergillosis, in a total of 116 eligible patients with various underlying conditions, the proportion of patients with complete or partial response at their respective end of VRC therapy was 48% and a stable response was seen in 21% [129]. A randomised prospective clinical trial compared VRC with amphotericin B deoxycholate. 381 patients were enrolled in this study, which demonstrated that VRC was significantly more effective than amphotericin B deoxycholate and was associated with a survival advantage. The rates of complete or partial response in acute invasive aspergillosis ranged from 41% to 53% after approximately 80-100 days of therapy [132].

1.4.1 Pharmacodynamic properties, indication and dosage regimen

VRC exerts its effect primarily through inhibition of cytochrome P450 (CYP)-dependent 14α-sterol demethylase, an enzyme responsible for the synthesis of 14α-demethyl lanosterol in the ergosterol biosynthetic pathway [133]. Ergosterol is an essential component of the fungal cell membrane, which regulates membrane fluidity and permeability as well as the activity of membrane-embedded enzymes. Furthermore, ergosterol is a major component of secretory vesicles in yeasts and plays an important role in oxidative phosphorylation reactions [115].

As mentioned in the previous section, VRC is an antifungal agent active against primary opportunistic fungal pathogens, e.g. *Candida* species, *Cryptococcus* species, *Aspergillus* species, *Scedosporium apiospermum*, common dermatophytes, fungi which cause endemic mycoses and other less common pathogens. The approved indications in Europe are the treatment of (i) invasive aspergillosis; (ii) candidaemia in non-neutropenic patients; (iii) serious invasive candidosis due to fluconazole-resistant *Candida* species (including *Candida krusei*); and (iv) serious invasive fungal disease caused by *Scedosporium* spp. and *Fusarium* spp. [134].

For yeasts, VRC appears to be fungistatic, as are other azoles [130]. However, for some filamentous organisms, VRC and other second-generation azoles are fungicidal [133]. VRC appears to be broadly active against many species of *Aspergillus*, including *Aspergillus terreus*, which is often resistant to amphotericin B [133; 135]. Consequently, therapy with VRC is the treatment of choice in patients with documented invasive aspergillosis [136] and invasive candidiasis (targeted therapy), even in the case of deep-sited infections such as osteomyelitis, meningitis, endophtalmitis etc. [130].

With regards to the dosage regimen, sequence therapy has been introduced apart from only multiple IV administration of VRC, i.e. a switch from direct administration into the systemic circulation to an absorption-based administration process, introducing further variability on the PK. In the currently approved dosing regimens, the IV dose is normalised to body weight (WT) but the oral dose is given independently of this demographic dimension [137]. VRC therapy can be initiated with a loading dose of 6 mg/kg IV every 12 h for two doses, followed by a maintenance dose of 4 mg/kg IV in the same interval. When patients are able to tolerate oral medications, oral therapy for patients weighing ≥40 kg can be initiated at 200 mg PO twice daily and increased to 300 mg PO twice daily if the response is inadequate [115].

1.4.2 Pharmacokinetic properties

The pharmacokinetics (PK) of VRC (VFEND®) have been studied in mouse, rat, rabbit, dog, guinea pig, and humans after single and multiple administration by both oral and IV routes. In brief, VRC was rapidly absorbed (t_{max} 1-2 hours) and displayed a high oral bioavailability (96%) which was reduced by fat food [115; 130]. Absorption of VRC was complete in all

species. VRC demonstrated 58% plasma protein binding and a volume of distribution of 4.6 L/kg [138]. VRC was predominantly cleared by hepatic metabolism, with 2% excretion unchanged in urine or faeces [115]. VRC was extensively metabolised in all species by cytochrome P 450 isoenzymes. The major pathways in humans involved fluoropyrimidine N-oxidation, fluoropyrimidine hydroxylation, and methyl hydroxylation. The major circulating metabolite in rat, dog, and human was the N-oxide of VRC. It has not been considered to contribute to efficacy since it was at least 100-fold less potent than VRC against fungal pathogens *in vitro* [115; 137].

Furthermore, VRC was characterised by non-linear, dose-dependent PK in all species. Consequently, PK parameters changed in dependence upon dose, and a superproportional increase in area under the curve (*AUC*) was observed with increasing dose. Significant accumulation on multiple dosing due to saturation of first-pass metabolism and systemic clearance led to this increase in systemic exposure. This was most pronounced in mouse and rat, less so in dog, and not observed in guinea pig or rabbit [137–139]. VRC appears to exhibit non-linear pharmacokinetics over the tested dose-range of 100-400 mg or at 4 mg/kg WT [134; 138] in humans as well [140; 141], possibly due to saturation of metabolism, with a 2-compartment model of disposition and widespread tissue penetration [115].

VRC demonstrates good tissue penetration, e.g. in CNS [115]. Antifungals such as VRC should display their pharmacodynamic activity in tissue, more precisely in ISF of tissue, because this is the site where most of the fungal pathogens are considered to reside. However, currently available PK data on VRC are almost exclusively based on the measurement of VRC plasma concentrations [141]. Additionally, total drug concentrations in plasma were evaluated without distinguishing between the protein-bound and unbound drug fraction. But only the unbound fraction of a drug is responsible for antifungal activity [142; 143], due to its ability to penetrate into tissues and reach the site of infection. Therefore, for the assessment whether effective drug concentrations at the site of action will be reached, it is highly important to know the distribution behaviour of the antifungal agent into the ISF of the infected tissue. Diffusion barriers and various transport processes may lead to a decreased or delayed drug penetration into the ISF. Thus, total plasma concentration-time profiles do not allow drawing the same conclusion about the unbound tissue-concentration time course [10; 24; 144].

Coming back to the systemic PK of VRC, additional factors that have been shown to impact PK parameters of VRC include liver disease, age, CYP2C19- and CYP3A-interacting comedications, and changes from IV to PO therapy [145]. The variable and hitherto unpredictable metabolism related to genetic factors, age, compliance, gastrointestinal

absorption during oral treatment or drug interactions may result in an insufficient exposure of the fungal pathogen to VRC or excess drug concentrations with potential toxicity.

1.4.3 Drug safety and interactions

VRC is generally well tolerated. Adverse effects of VRC are usually mild and transient [132]. The most common adverse effect - one not previously noted with other azoles - is a reversible disturbance of vision (photopsia). This occurs in approximately 30% of patients but rarely leads to discontinuation of the drug. Visual disturbances include altered colour discrimination, blurred vision, the appearance of bright spots and wavy lines, and photophobia [135; 140; 146]. In clinical studies, these undesirable effects occurred during the first week of therapy, yet rarely led to withdrawal of VRC treatment [132]. Skin rashes are the second most common adverse effect noted with VRC therapy. Most of these are mild and constitute no major problem. However, severe reactions, including Stevens-Johnson syndrome and toxic epidermal necrolysis, have been reported in a very small number of patients. Patients should be warned to avoid direct sunlight, because photosensitivity reactions can occur [135].

Elevations in hepatic enzyme concentrations occur with VRC therapy as well, as they do with other azole therapy [132]. The usual reversible pattern described consisted of elevations in the serum concentrations of alanine aminotransferase and aspartate aminotransferase, but elevations in alkaline phosphatase concentrations have also been noted [135].

Other less commonly noted adverse events include headache, nausea and vomiting, diarrhoea, abdominal pain [135], neurological side effects such as hallucinations, abnormal dreams, confusion, hypoesthesia, neuropathy, and paraesthesia; hepatic toxicity, QT interval prolongation [130], and increased photosensitivity [128; 147] were further reported. The latter was made responsible for cutaneous squamous cell carcinomas and melanomas emerging in patients after ultra-long-term VRC ingestion (>12 months) [132; 148; 149]. Visual hallucinations occurred at a rate of 5% in one clinical trial and clearly differed from photopsia [135].

VRC is not only a substrate but also a potent, competitive inhibitor of the cytochrome P450 isozymes CYP2C19, CYP2C9 and CYP3A4. Thus, co-administration of VRC is contraindicated with drugs that are highly dependent on these isoenzymes for clearance and for which elevated plasma concentrations are associated with serious and/or life-threatening events. In addition, coadministration of VRC is contraindicated with drugs that significantly decrease VRC plasma concentrations due to induction of these isozymes [115].

In plasma, inter-individual variability of VRC concentrations was observed that might be attributable to e.g. the genotype of the two known metabolising enzymes that show polymorphism: the isoenzymes CYP2C9 and CYP2C19 [115] or other influencing factors.

The polymorphism of the main metabolising enzyme CYP2C19 [150; 151] was shown to contribute to inter-individual variability of VRC [152]. For example, poor metabolisers (PM) showed 4-fold increased concentrations of VRC than extensive metabolisers (EM) in clinical studies [115; 135].

1.5 Objectives

In order to optimise an antiinfective therapy, different complementary approaches have to be evaluated and preferably combined. With regards to the applied drug therapy, for example, these different methodologies can consist of the observation of drug concentrations itself and of markers for the drug effects.

Monitoring of immunomodulatory mediator concentrations such as cytokines could provide important information about the state and progression of disease and the effect of drug therapy. However, in most cases cytokine concentrations in plasma do not represent concentrations in the inflamed tissues. The use of µD catheters might provide the basis for the development of a cytokine analysis procedure at the irritated tissue and, thus, for a biomarker profiling of various diseases and monitoring of therapy effects. As a first prerequisite for a possible use in clinical studies, the applicability and feasibility of µD of cytokines as well as the dependence of the analyte recovery on conditions of the µD system has to be explored *in vitro*. So far, results of published *in vitro* and *in vivo* µD investigations regarding RR and measured concentrations of determined cytokines revealed large variability. This finding probably rose from the large heterogeneity of catheter material and µPerfusate as well as the different FR used and from other experimental conditions, which all influence the extraction efficiency, i.e. RR or rD. Thus, the objectives of this thesis were to develop reproducible *in vitro* settings of the µD system to sample cytokines and quantify them. As model cytokines for these µD investigations, the pro-inflammatory modulators IL-6, IL-8, and TNF-α as well as the anti-inflammatory cytokine IL-10 were selected. The developed bioanalytical and µD methods were applied to define the potential and the limits of the applicability and feasibility of µD of cytokines. This would contribute to accurately implement the sampling of cytokines in future *in vivo* µD studies and assure the opportunity of prospective data comparison.

As a next step, monitoring of antiinfective agents in the tissue presents a mean for the verification of probably effective concentrations, i.e. known from *in vitro* investigations, at the target site. Moreover, PK parameters can be evaluated in comparison to parameters generated from plasma data. Thus, µD could be a tool for drug monitoring and potentially for the development of suggestions for an optimisation of drug therapy. Determination of an antiinfective agent at the target site was to be demonstrated using the antifungal substance

VRC. To compensate the lack of currently available information on the target-site distribution of VRC, the unbound, i.e. microbiologically active, concentrations of VRC in ISF of subcutaneous adipose tissue were to be measured and compared to unbound plasma concentrations after single and multiple dosing during sequence therapy.
The combination of both approaches could lead to the development of minimally invasive methods to rapidly monitor drug concentrations of antiinfective drugs at the target site simultaneously to the biomarker profiling for diagnosis and prognosis of the underlying disease. Consequently, after the assessment of therapeutic concentration ranges of the antiinfective drug as well as of diagnostic and prognostic concentration profiles of the biomarkers, this would result in the ability of monitoring such surrogates for therapy effects as a tool of therapy evaluation and optimisation.

The work of this thesis consisted of four projects, stepwise realising the development of the tools for the aforementioned approaches:

Project I: Validation of an adaption of a commercially available bioanalytical method, i.e. a ligand-binding assay, to the matrix of interest, as a prerequisite for the reliable quantification of cytokines from µDialysate. (The modification of the original method had previously been developed in the diploma thesis.)

Project II: *In vitro* characterisation of µD of cytokines to assess the performance (i.e. applicability) of µD for these analytes as a proof of principle and to determine the set-up conditions for the following *in vivo* µD investigations.

Project III: *In vivo* pilot study to investigate the feasibility (practical aspects) and applicability (possibility of determination of cytokines from *in vivo* µDialysate) of the developed µD system for clinical studies.
Evaluation of the application of flow-rate-variation method within this study as a mean for *in vivo* catheter calibration.

Project IV: A clinical long-term µD study with multiple doses of VRC as a clinically relevant model substance for a lipophilic antiinfective drug in healthy volunteers. Monitoring of the pharmacodynamically active fraction of the extracellular concentrations of this antifungal drug in ISF of the tissue commonly affected by IFI and comparison to systemic concentrations. Reflections of the dosage regimen employed in therapeutic use with particular focus on sequence therapy, single dose, and steady-state concentrations at the site of action. PK analysis of the observed concentrations over time by means of the non-compartmental approach and genotype influence on the PK parameters.

2 MATERIALS AND METHODS

2.1 Chemicals, drugs and pharmaceutical products

2.1.1 Projects I-III: Bioanalysis and microdialysis of IL-6, IL-8, IL-10 and TNF-α

Albiomin® 5% (50 human albumin g/L), solution for infusion	Biotest Pharma, Dreieich, Germany
BD™ CBA Human Soluble Protein Flex Sets IL-6, IL-8, IL-10, TNF-α: BD™ CBA Capture Beads BD™ CBA Detection Reagent BD™ CBA Standards	BD Biosciences, San Diego, USA
BD™ CBA Human Soluble Protein Master Buffer Kit: BD™ CBA Assay Diluent BD™ CBA Capture Bead Diluent BD™ CBA Detection Reagent Diluent BD™ CBA Instrument Setup Bead A1 BD™ CBA Instrument Setup Bead A9 BD™ CBA Instrument Setup Bead F1 BD™ CBA Instrument Setup Bead F9 BD™ CBA PE Instrument Setup Bead F1 BD™ CBA Wash Buffer	BD Biosciences, San Diego, USA
BD™ CBA lyophilised recombinant standards IL-6, IL-8, IL-10, TNF-α	BD Biosciences, San Diego, USA
BD™ FACSClean	BD Biosciences, San Diego, USA
BD™ FACSFlow	BD Biosciences, San Diego, USA
BD™ FACSRinse	BD Biosciences, San Diego, USA
Ringer's solution B.Braun 147 mM Na^+, 4 mM K^+, 2.2 mM Ca^{2+}, ~156 mM Cl^- in 1 L water for infusion	B. Braun, Melsungen, Germany
WHO International Standards IL-6, human rDNA derived, NIBSC code: 89/548 IL-8, human, rDNA derived NIBSC code: 89/520 IL-10, human, rDNA derived, NIBSC code: 93/722 TNF-α, human, rDNA derived NIBSC code: 88/786	National Institute for Biological Standards and Control, Potters Bar, UK

2.1.2 Project IV: Clinical long-term microdialysis study with voriconazole in healthy volunteers

2.1.2.1 Clinical study

Aqua ad iniectabilia	Mayrhofer Pharmazeutika, Leonding, Austria
Isotonic physiological NaCl solution 154 mM Na^+, Cl^- in 1 L WFI	Mayrhofer Pharmazeutika, Leonding, Austria
Isozid®-H colourless/coloured	Gebro Pharma, Fieberbrunn, Austria
Ringer's solution ÖAB (Austrian pharmacopoeia) 154 mM Na^+, 4 mM K^+, 2.7 mM Ca^{2+}, ~163.4 mM Cl^- in 1 L aqua ad iniectabilia	Mayrhofer Pharmazeutika, Linz, Austria

Study drugs:

Vfend® (VRC) 200 mg powder for solution for infusion	Pfizer, Vienna, Austria
Vfend® (VRC) 200 mg tablet	Pfizer, Vienna, Austria

Preparation of the IV infusion solution: Prior to the administration, one powder-containing vial was resuspended with 19 mL aqua ad iniectabilia resulting in a clear solution of 10 mg VRC/mL. The solution was further diluted with isotonic physiological NaCl solution to an IV infusion solution with a maximum concentration of 5 mg/mL.

Preparation of the retroperfusate (RP) (see section 1.2.3): VRC (Vfend®) was added to the perfusion medium resulting in a concentration (C_{RP}) of 200 µg/mL. All study preparations used during the trial were stored at the study site at room temperature (RT) and protected from light.

2.1.2.2 Bioanalysis

Acetonitrile (ACN) (HPLC grade)	Roth, Karlsruhe, Germany; VWR, Fontenay-sous-Bois, France
Ammonium dihydrogen phosphate	Merck, Darmstadt, Germany
Ammonia (30%)	Merck, Darmstadt, Germany
Isopropanol (HPLC grade)	Roth, Karlsruhe, Germany
Methanol (HPLC grade)	Roth, Karlsruhe, Germany
Ringer's solution	See section 2.1.1
Voriconazole LOT No. 052301-008-09 purity ≥98% [153]	Pfizer Global Research and Development, Sandwich, United Kingdom
Water, purified Milli-Q® plus purified-water system	Millipore, Molsheim, France

2.2 Laboratory and study equipment

2.2.1 Project I: Bioanalytical method for quantification of IL-6, IL-8, IL-10 and TNF-α from microdialysate

BD FACSArray™	BD Biosciences, San Diego, California, USA
Falcon™ conical tubes (15 mL)	BD, Franklin Lakes, NJ, USA
Falcon™ 96-well microtitre plates, U-bottom	BD, Franklin Lakes, NJ, USA
LaminAir® HB 2448	Heraeus Instruments, since 2005: Thermo Fisher Scientific, Langenselbold, Germany
MultiScreen®$_{HTS}$-BV Plate, 1.2 µm, nonsterile	Millipore, Schwalbach, Germany
MultiScreen®$_{HTS}$ Vacuum Manifold	Millipore, Schwalbach, Germany
Safe lock tubes (0.5 – 1.5 mL)	Eppendorf, Hamburg, Germany
Microtitre plate shaker	Grant, Shepreth, United Kingdom
Vacuum pump	Millipore GmbH, Schwalbach, Germany
Vortex mixer	IKA, Staufen, Germany

2.2.1.1 BD™ Cytometric Bead Array for cell-culture supernatant samples

The BD™ Cytometric Bead Array (CBA) is an immunological sandwich technique similar to common ligand-binding assays (e.g. ELISA) [154]. Instead of a solid immobile phase, the CBA consists of multiple sets of small microspheres with a uniform diameter together denoted the ‘bead population’ (see Fig. 2-1, left, A-F) [155]. One individual bead set comprises microspheres (‘beads’) conjugated with a cytokine-specific monoclonal antibody (i.e. the capture antibody). A distinct concentration of a fluorescent dye is incorporated into the bead material of each set, enabling detection of individual median fluorescence intensities (MFI). Consequently, the set and (thus) the bound cytokine can be identified. The selected fluorophore emits fluorescence detectable by near infrared (NIR) and red light detectors (“Red”; see next subsection) at wavelengths of ca. 660 nm to 680 nm.

Detection antibodies, linked to another dye, bind the complexes of antibody-conjugated-bead and captured cytokine (see middle part of Fig. 2-1). The dye of the detection antibody emits fluorescence at a different wavelength (approximately 576 nm), and is, therefore, detected by a yellow light detector (“Yellow”). The more cytokine molecules came in contact with one bead and bound to it, the more detection antibodies bind to the complexes on the bead. Hence, the amount of detection-antibody-conjugated fluorophores increases, resulting in an amplified MFI of that particular bead. Thus, the quantification MFI provides a measure for the specific cytokine concentration in the surrounding solution.

Summarised, *identification* of the targeted cytokine was attained by the fluororescent dye incorporated into the bead material, and *quantification* of this cytokine was enabled by the amount of dye-conjugated detection antibodies bound to the formed complexes on the bead.

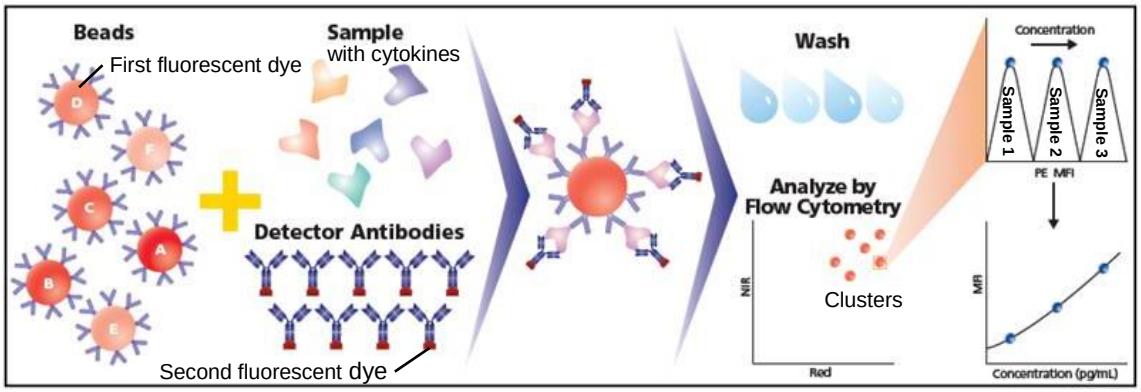

Fig. 2-1: Functional scheme of BD™ Cytometric Bead Array (modified from [156])

As a result of the principle, the BD™CBA represents a multiplex-assay with the option to determine up to 30 bead sets and, therefore, up to 30 individual cytokines simultaneously in a single sample of 50 µL [157]. Throughout the investigations of this thesis, the four cytokines IL-6, IL-8, IL-10 and TNF-α were analysed applying the BD™CBA. Cytokine containing samples, which were incubated with the reagents provided by the CBA, were subsequently analysed with the BD FACSArray™ device.

2.2.1.2 BD FACSArray™ - Data acquisition and analysis

Data acquisition and first data analysis were performed on the BD FACSArray™ bioanalyzer [158]. One sample, mixed with a high amount (>>50) of beads from each individual bead set, was processed in a cavity of a microtitre plate (see previous section and section 8.1). The number of bead sets in this sample was determined by the number of cytokines to quantify.
A defined fluid volume of the sample, containing the suspended microspheres, was then injected to the fluidics system of the device (see Fig. 2-2, left panel). The injected sample was coated by a sheath fluid resulting in hydrodynamic focusing, i.e., the sample was configured to a fluid stream with a diameter allowing only a single bead to pass the laser beam at a particular time point.

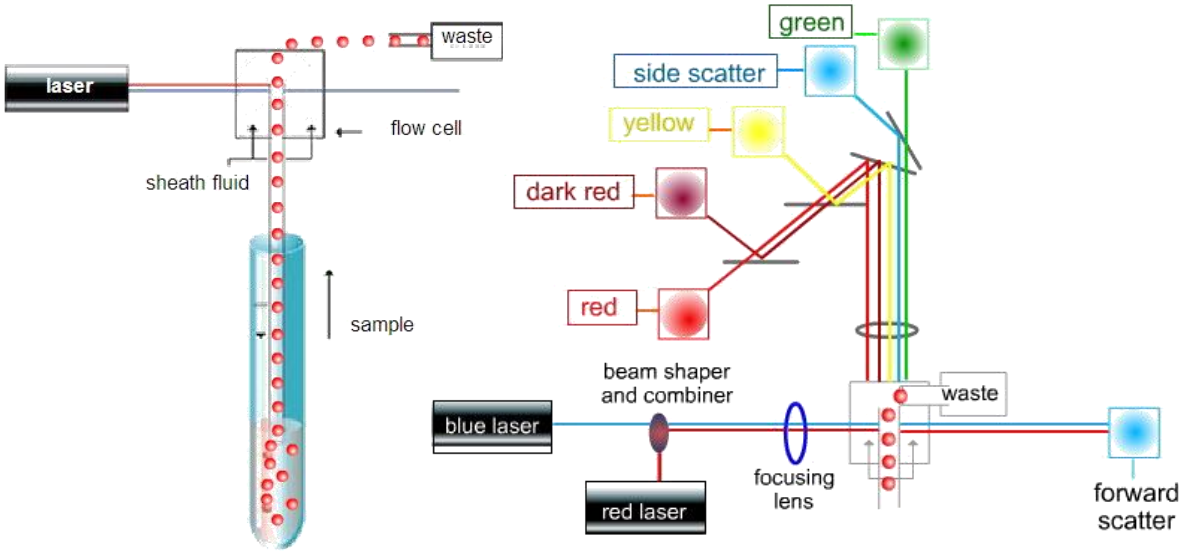

Fig. 2-2: Fluidics and optics system of a flow common cytometer [159]

One bead at the time, hence, streamed through the beam of two light lasers, one green (λ= 532 nm) and one red (λ= 635 nm) laser. The red laser radiation excites the fluorophore incorporated into the bead material, whereas the green beam initiates fluorescence from the dye bound to the detection antibody.

The optical system of the BD FACSArray™ bioanalyzer (Fig. 2-2, right panel) furthermore consists of a variety of detectors for forward scatter, side scatter and light emission of different wavelengths [158]. The individual identification fluorescence intensities of the different bead sets were distinguished by NIR (dark red) and Red detectors (see also previous subsection).

The detection of one bead is described as an ‘event’. Subsequent to the sample analysis, all events of one sample injection were presented in a plot displaying the MFI detected by NIR versus the one detected by Red (Fig. 2-1, left plot on the right side). Due to the specific concentrations of incorporated dye, the bead sets are arranged in clusters. One cluster represents one cytokine. For reasons of statistical significance, exclusively bead clusters with a minimum of 50 beads are analysable for MFI. This limitation has to be considered throughout sample processing and analysis.

The signal of the quantification fluorescence detector (Yellow, ‘PE MFI’ in Fig. 2-1) is subsequently assigned to the particular bead cluster, i.e. a bead set for one individual cytokine. Due to the high number of beads per set in a sample, signals are presented as MFI of the microspheres of the individual set. MFI of every cytokine were determined and obtained as raw data output [160].

2.2.2 *In vitro* (Project II) and *in vivo* (Project III) microdialysis of cytokines

This section outlines the µD equipment for the determination of cytokines used throughout the *in vitro* µD investigations (see section 2.5) or in the clinical study (see section 2.7).

2.2.2.1 Microdialysis pumps and syringes

106® Pump Syringe (*in vivo*)	M Dialysis, Stockholm, Sweden
BD Luer-Lok™ 1 mL Syringe (*in vitro*) polycarbonate	BD, Singapore, Singapore
CMA102® Pump (*in vitro*)	CMA Microdialysis, Solna, Sweden
CMA107® Pump (*in vivo*)	CMA Microdialysis, Solna, Sweden

All µD pumps used during the experiments and studies were checked for accuracy and precision of the FR: microtubes were weighed before and after µD applying different FR of 0.3, 0.5, 1.0, 2.0, 3.0, 5.0 and of 10 µl/min (n=5). The precision and accuracy of the obtained volume were calculated (accounting for density of water).

2.2.2.2 Microdialysis catheters and accessories

Linear and concentric (see section 2.2.4.1) µD catheters are illustrated in the description of the *in vitro* µD system (IVMS, see section 2.6.1 and Fig. 2-4).
All catheters used were CE marked according to the Medical Device Directive, 93/42/EEC, sterilised by β-radiation, stored according to the requirements in the product sheet (4 °C – 25 °C), were used once only except during *in vitro* studies and were purchased from CMA Microdialysis/M Dialysis, Solna, Sweden.

66® linear microdialysis catheter membrane: length 30 mm, MWCO 100 kDa, polyarylethersulphone (PAES)	M Dialysis, Solna, Schweden
CMA66® microdialysis catheter (see above)	CMA Microdialysis, Solna, Sweden
Safe lock tubes (0.5 mL)	See section 2.2.1
Culture Tube, 12 mL, Ø 17 x 77 mm round (U) bottom, polypropylene, sterile	Greiner Bio-One, Monroe, USA

2.2.3 Project III: Long-term pilot study on microdialysis of cytokines in healthy volunteers

2.2.3.1 Clinical study

The following equipment was employed for the *in vivo* µD setting throughout the clinical study at or outside of the study location enabling the participants to move unrestrictedly.

Alcohol Pads	B. Braun, Melsungen, Germany
Askina Derm sterile 10 x 12 cm	B. Braun Hospicare, Collooney, Ireland
Askina Elast fine 4 m x 10 cm	B. Braun, Melsungen, Germany

Hansaplast sensitive 5 m x 2.5 cm	Beiersdorf, Hamburg, Germany
Leukosilk 5 m x 2.5 cm	BSN medical, Hamburg, Germany
Octenisept disinfection spray	Schülke & Mayr, Norderstedt, Germany
Outlet tubing guide channels with connection for microvials	Technical laboratory at the Institute of Pharmacy, Martin-Luther-Universitaet, Germany
Safe lock tubes (0.5 mL)	See section 2.2.1

2.2.3.2 Bioanalysis

Bioanalysis of the study samples was conducted with the adapted and validated bioanalytical method for quantification of cytokines from µDialysate (see section 2.2.1).

2.2.4 Project IV: Clinical long-term microdialysis study with voriconazole in healthy volunteers

2.2.4.1 Clinical study

CMA60® microdialysis catheter membrane: length 30 mm, MWCO 20 kDa, polyarylethersulphone (PAES)	CMA Microdialysis, Solna, Sweden
106® Pump Syringe	M Dialysis, Solna, Schweden
CMA102® Pump	CMA Microdialysis, Solna, Sweden
Butterfly sets and luer adapter	Greiner Bio-one, Kremsmünster, Austria
Combi-stopper	Braun, Melsungen, Germany
Infusomat IP 85-2	Döring, Munich, Germany
Injekt Luer Solo 2 mL, 5 mL	Braun, Melsungen, Germany
Mini-Spike Plus®	Braun, Melsungen, Germany
Outlet tubing guide channels with connection for microvials	Technical laboratory at the Institute of Pharmacy, Martin-Luther-Universitaet, Germany
Perifix® Catheter Connector	Braun, Melsungen, Germany
Safe lock tubes (0.5 mL)	See section 2.2.1
Steristrip® 3M	Health Care, Neuss, Germany
Tegaderm® 3M	Health Care, Neuss, Germany
TriCath In®	Codan Medizinische Geräte, Lensahn, Germany
Venflon® IV cannula	BD, Heidelberg, Germany
Vacuette®/Vacuette® Premium blood collection tubes	Greiner Bio-one, Kremsmünster, Austria

2.2.4.2 Bioanalysis

Centrifree® Ultrafiltration devices	Millipore, Eschborn, Germany
Centrifuge 5417 R	Eppendorf, Hamburg, Germany
HPLC column (sorbent, pore size [Å], type, modification e (endcapped), particle size [µm], internal diameter × length [mm], precolumn)	
LiChrospher®-100 RP-18	Merck, Darmstadt, Germany

e, 5, 4.0 × 125	
LiChroCART® 4-4 guard column	
HPLC systems (modular)	
1 Controller LC-Net II/ ADC	JASCO, Gross-Umstadt, Germany
Pump (PU-2080 Plus)	
Peltier cooling and heating autosampler (AS-2051)	
Degasser module (DG-2080-53)	
Air-cooled Peltier element column thermostat Jetstream Plus	
Ultraviolet (UV)/Visible (VIS) detector (UV-2075) using deuterium lamps	
ChromPass Chromatography Data System (Version 1.8.6.1)	
2 UltiMate 3000	Thermo Scientific Dionex, Germering, Germany
Degasser/Solvent Rack (SRD-3200 2-channel)	
Pump (HPG-3200SD)	
Peltier cooling and heating autosampler (WPS-3000TSL analytical)	
Air-cooled Peltier element column thermostat (TCC-3000SD)	
DAD-Detektor (DAD-3000SD analytical, 13 µL, SST)	
Chromeleon Datasystem (7.1 Build 1541)	
Micro scales:	
Mettler AT 250	Mettler Instruments, Greifensee, Switzerland
Sartorius analytic A200S	Sartorius, Göttingen, Germany
pH meter pH315i (electrode SenTix®41)	WTW, Weilheim, Germany
Safe lock tubes (0.5 mL)	See section 2.2.1
Ultrasonic bath Sonorex RK 100	Bandelin electronic, Berlin, Germany
Vortex mixer	IKA, Staufen, Germany
96 well microtitre plate conical PP RNAse/DNAse-free	Thermo Fisher Scientific, Rochester, USA

2.3 Software

FCAP Array™ v1.0.1	Soft Flow, Burnsville, Minnesota, USA
Microsoft® Office Excel 2010	Microsoft Corporation, Bellevue, Washington, USA
Phoenix™ WinNonlin® 6.1-6.3	Pharsight/Certara, Mountain View, California, USA
R, version 2.15.1	R Development Core Team, 2012

Phoenix™ WinNonlin® Software was used to generate 4-parameter-logistic calibration functions [161] by non-linear regression based on the measurements of the calibration samples of the bioanalytical method (see section 2.4.1.1). This software was also used to: (i)

determine the mass transfer coefficient *r* [23] from recovery and delivery µD investigations and from the clinical study by non-linear regression (see sections 2.6.5, 2.6.6 and 2.7.3.3); and (ii) to perform non-compartmental (see section 2.8.3.3) and compartmental (see section 2.7.3.3) PK analysis [2]. Cytokine and VRC concentrations of analysed µD and UF samples were calculated in Microsoft® Office Excel 2010. Descriptive statistics were performed with Phoenix® WinNonlin® and Microsoft® Office Excel 2010. Statistical tests [162] were carried out in 'R' [163].

2.4 Project I: Bioanalytical method for quantification of IL-6, IL-8, IL-10 and TNF-α from microdialysate

2.4.1 Method development

In view of the recommendation in the European Medicines Agency (EMA) Guideline on Bioanalytical Method Validation (BMV) [17], the commercially available BD™ CBA assay for cytokines from cell-culture supernatant samples was adapted and validated for the quantification of cytokines from the considered matrix, i.e. µDialysate obtained from 100-kDa-cut-off membranes.

The adaption of the method to µDialysate was attained in the diploma thesis prior to the pre-study validation described herein. In brief, for quantification of cytokines in small sample volumes a mixture of Ringer's solution (RS) and human albumin solution (HA) (RS/HA, 10/1 v/v, HA concentration 0.5% m/v) was established as an alternative matrix for µDialysate due to the very limited availability. Since samples obtained via µD are diminutive in volume, the following reduction of required sample volume was achieved: from 50 µL, according to manufacturer's instructions, to 25 µL. The upper limit of quantification was increased and the background signal reduced compared to the settings of the original assay via an additional dilution step during sample processing.

Finaly, all investigated samples were processed according to the adapted method (see 8.1) and measured with the BD FACSArray™ Bioanalyzer (see section 2.2.1 and 8.1.3).

2.4.1.1 Non-linear regression of the calibration function

To achieve a (software) independent and reproducible generation of the calibration function, non-linear regression of calibration solution (Cal 1-12, see 2.4.2.1) concentrations was performed in Phoenix™ WinNonlin® using a 4-parameter-logistic (4-PL) equation in the format of the American Standard Code for Information Interchange (ASCII).

$$Log(MFI) = D + \frac{(A-D)}{1+(Log(concentration)/C)^B} \qquad (4)$$

In Eq. (4) *Log(concentration)* is the independent (x) and *Log(MFI)* the dependent variable (y). The parameters *A* and *D* represent upper and lower limit values of y, whereas *B* corresponds to the slope and *C* characterises the inflection point of the sigmoidal curve (see Fig. 2-3).

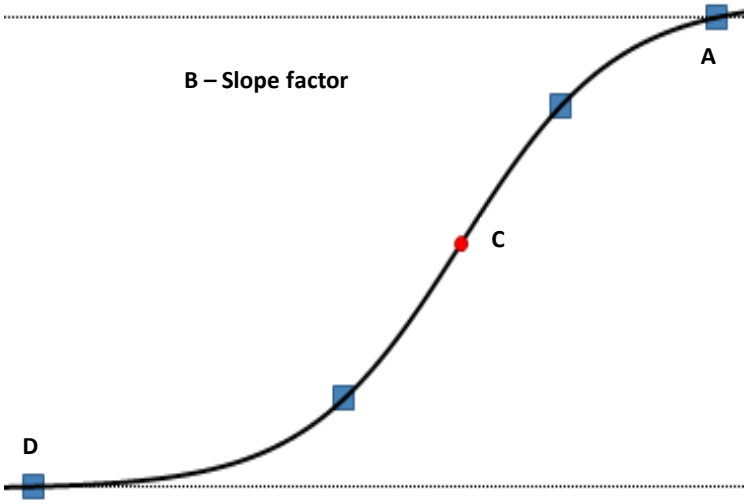

Fig. 2-3: 4-parameter-logistic function with parameters A (Max), B (slope), C (inflection point), and D (Min) (modified from [164])

Since the concentration scale and the signal (MFI) scale are converted logarithmically, the 4-PL incorporates the transforming-both-sides methodology [165], which is a mode of weighting. Due to the computing capacity of the software, the simultaneous logarithmic transformation of MFI and concentration values during the algorithmic iterations was not applicable and data had to be transformed into logarithms before conducting the non-linear regression.

Therefore, the equation was modified:

$$F = D + \frac{(A-D)}{1+(X/C)^B} \qquad F = Lg(MFI) \qquad (5)$$

$$X = Lg(concentration)$$

The following settings were applied for non-linear regression:

- Boundaries of initial parameters: 0.1 (lower) and 15 (upper)
- Algorithm: Gauss-Newton (Levenberg and Hartley)
- Convergence criteria: 0.0001 difference between objective function values of subsequent iterations
- 50 iterations as the maximum
- As heteroscedasticity was accounted for by the transforming-both-sides methodology [165] via logarithmic function of both scales, no further weighting was applied

2.4.2 Method validation

2.4.2.1 Preparation of stock solutions, calibration samples and quality control samples

Validation was performed to comply with the EMA Guideline on BMV [17] while applying twelve Cal solutions and six QC solutions. Stock solutions for Cal and QC used in the course of pre-study validation were prepared by solubilising lyophilised cytokine standards (CBA standards, see section 2.1.1) into assay diluent (AD) resulting in 150,000 pg/mL for each cytokine solution. Appropriate volumes (30-114 µL) of the corresponding stock solution were diluted with HA (6-74970 µL) to generate twelve Cal and six QC working solutions, respectively. The individual working solutions were finally diluted with RS/HA in the ratio of 1:15 to obtain the Cal and QC solutions, which were subsequently aliquoted. Concentrations of Cal and QC solutions were 4, 6, 10, 20, 50, 100, 500, 1000, 4000, 6000, 9000, 10000 pg/mL and 5, 15, 200, 1000, 7000, 9500 pg/mL, respectively.

Preparation of in-study Cal and QC

Cal and QC had to be produced to assure the quality of analysed study samples for the in-study validation. Stock solutions for Cal and QC were prepared by solubilising lyophilised CBA cytokine standard into RS/HA (SL-Cal: 10000 pg/mL) and AD (SL-QC: 150,000 pg/mL), respectively. Cal 1-12 were directly generated from SL-Cal and aliquoted. For QC, SL-QC was diluted with HA to working solutions according to the previous subsection. QC were prepared by diluting working solution with RS/HA at the ratio of 1:15.

2.4.2.2 Cytokine stability in microdialysate

Stability QC solution (QC_{Stab}) sets underwent stability testing to ensure stability of the analytes during sampling, sample processing, analysis, and under storage conditions. For this purpose QC_{Stab} sets were investigated for freeze-and-thaw cycles as well as applying further conditions similar to the actual study sample handling. One set consisted of three individual aliquots (n=3) per three different concentrations of the four model cytokines resulting in QC_{stab} 1, QC_{stab} 2 and QC_{stab} 3 for low (10^1-10^2 pg/mL), middle (10^2-10^3 pg/mL) and high concentrations (10^3-10^4 pg/mL), respectively. Additionally the stability of the QC stock solution was evaluated.

In order to generate QC_{stab} 1, QC_{stab} 2 and QC_{stab} 3, the stock solution (see section 2.4.2.1) was diluted 1:33$\overline{3}$, 1:20 and 1:2 with AD to obtain QC working solution 1, 2, and 3. QC_{stab} were freshly prepared from working solutions at the beginning of the individual stability test by mixing the aliquots with RS/HA in a ratio of 1:15. All frozen QC_{stab} were thawed directly before processing for sample analysis. One set of QC_{stab} was freshly prepared (set as 100%

stability) at the beginning of sample processing for analysis of QC_{stab} of an individual stability test and served as a reference. Stability was calculated using Eq. (6).

$$\text{Stability,\%} = \frac{C_{QC_{stab\,(stored)}}}{C_{QC_{stab\,(freshly\,prepared)}}} \cdot 100 \qquad (6)$$

1. For SL-QC stability, aliquots of the stock solution were stored for 6 h at RT (22 °C) and at 5 °C, respectively, and immediately frozen at -80 °C afterwards. One set of SL-QC aliquots was deposited at -80 °C directly after preparation and remained in the ultra-freezer until analysis.
2. Freeze-and-thaw stability was examined utilising six sets of QC_{stab} frozen at -80 °C. Following a storage period of 24 h, one set was unassistedly thawed at RT for 2 h representing one freeze-thaw cycle. Subsequently the set was refrozen for 24 h. The procedure was repeated five times with the same QC_{stab} set. The five remaining sets were treated in the same manner for 5, 4, 3, 2, and 1 cycles, respectively.
3. For short-term stability assessment, eight individual sets of QC_{stab} were stored at RT subsequent to preparation for 1, 2, 4, 6, 9, 12, 15, and 24 h, respectively, and frozen afterwards. The samples could not be analysed immediately for logistic reasons and for the reason that samples from several stability investigations were analysed together for a reduction of analytical time and costs. The validated method was, therefore, only applied to frozen samples.
4. For long-term stability, two sets of QC_{stab} were frozen at -80 °C and analysed after a time period of 2 as well as 8 months, respectively.
5. To determine stability of processed samples (post-preparative stability), QC_{stab} 1, QC_{stab} 2, and QC_{stab} 3 were processed for bioanalysis on a microtitre plate (see 8.1.2). A second QC_{stab} set was processed 1 h later than the first set on a second plate. Both sets were measured directly after the end of the sample processing, i.e. separated by 1 h.

2.4.2.3 Specificity and selectivity of the analytical method

Results of cross-reactivity investigations of the capture and detection antibodies belonging to the commercial kits were provided by the manufacturer [166] and did not reveal any interactions between the individual investigated cytokines and the antibodies.

Since no related or unrelated compounds were expected to occur during the long-term µD study with healthy volunteers, no further specificity and selectivity testing according to the EMA Guideline on BMV [17] was performed.

2.4.2.4 Limit of detection and carry-over effect

The limit of detection (LOD) was calculated from the MFI of six blank samples, i.e. pure sample matrix, via the test method developed by Rodbard et al. [167]. This method constitutes a t-test, in which the corresponding equation is converted to calculate LOD as the sample signal that is significantly different from the blank signal.
A carry-over effect was considered by placing six blank samples subsequent to five replicates of the highest concentrated QC sample.

2.4.2.5 Precision, accuracy, and lower limit of quantification

Six independent analysis runs implementing Cal 1-12 and QC 1-6 (see section 2.4.2.1) were evaluated for validation purposes.
Twelve Cal, covering the anticipated concentration range, were run at least in duplicate (i.e. using two wells per Cal sample) at the six individual validation days. At two of these analysis days Cal were analysed in triplicate and in five replicates, respectively. The lowest concentrated Cal solution (4 pg/mL) served as an anchor point beyond the quantifiable range to improve, stabilise, and optimise fitting of the calibration function [17; 161].
Six QC samples (anticipated LLOQ (i.e. 5 pg/mL), three times LLOQ, lower mid, higher mid, high and anticipated upper limit of quantification (ULOQ)) were used to access accuracy and precision of the method at six independent runs over several days. QC were analysed in triplicate at five analysis runs and once employing five replicates.

2.4.2.6 Dilutional linearity

Dilutional linearity was investigated to assure the appropriate quantification of samples with a concentration above ULOQ. An ultra-high concentrated solution (142,500 pg/mL cytokines, i.e. 14.25-fold ULOQ) was diluted 1:15 ($QC_{lin}1$). Additionally a dilution series was produced: non-serially diluted samples were prepared from a high concentrated solution (15000 pg/mL) applying ratios of 1:1 (QC_{lin} 2), 1:3 (QC_{lin} 3) and 1:6 (QC_{lin} 4). Subsequent samples were serially diluted from the next higher concentrated dilution in ratios of 1:10 (QC_{lin} 5, 6) and 1:5 (QC_{lin} 7). All samples were prepared using RS/HA as the blank matrix and resulting in nominal concentrations of 9500, 7500, 5000, 2500, 250, 25 and 5 pg/mL.

2.4.2.7 Parallelism of dilution series from a study sample and spiked in-study validation samples

In order to investigate whether the dilution behaviour of study samples (i.e. the matrix of interest) is equal to that of the in-study validation samples (i.e. spiked artificial matrix), the parallelism of a dilution series, produced from a study sample, to the Cal and QC curves has to be confirmed. A high concentrated study sample (see section 2.7) was diluted with RS/HA

in the ratios of 1:2, 1:5 and 1:10. The three diluted aliquots and the original study sample were analysed in duplicate. Cal and QC samples served as the reference.

2.4.2.8 Intermediate precision

The robustness of an analytical method is defined as a measure of its capacity to obtain constant results when perturbed by small variations in processing parameters [168]. Varied method parameters include e.g. pH values of buffers or incubation times and are supplemented with established 'system suitability parameters' (e.g. wavelength, flow rate) as well [169; 170]. Ruggedness is defined as the degree of reproducibility of QC results under a variety of external conditions, for example different laboratories, analysts, and reagent lots [168; 169]. The entire range of variations is currently considered by the term 'intermediate precision' [171], which is categorised by the additional term 'internal' or 'external'. Adjustments of the detector voltages, which are conducted in general during the monthly instrument setup (see 8.1.3), represented internal variations of method or instrument parameters, whereas several external variations were conducted:

Placement of QC samples in microtitre plate

One QC set was pipetted into wells in an ascending concentration sequence subsequent to cavities filled with Cal solutions. Aliquots of the second QC set were randomly placed across the wells of the entire microplate. The solutions were processed and analysed.

Analyst replacement (inter-analyst reprocibility)

A second analyst processed Cal 1-12 (n=2) and QC 1-6 (n=3) applying the adapted bioanalytical BD™CBA method and analysed the samples using the BD FACSArray™ Bioanalyzer.

Reinjection reproducibility of processed samples

After the first analysis of all samples (Cal and QC) of a microtitre plate, an assortment of samples was analysed again (ca. 2 h after beginning of first injection). The plate was located on the plate-loader of the BD FACSArray™ Bioanalyzer at RT for the whole time of injection and reinjection. One replicate of Cal 1-12 as well as one individual replicate of QC 2, QC 3, and QC 5 were reinjected in order to evaluate accuracy and deviation from results of the first injection. Four replicates of Cal 7 (500 pg/mL) were analysed to calculate precision.

pH value of sample matrix

Three aliquots of blank matrix solution were spiked with different amounts of the four model cytokines to obtain a final concentration of $\leq 10^1$, $<10^2$, and $\leq 10^4$ pg/mL of each cytokine,

respectively. Each individually concentrated solution was split into three aliquots. The first and the third aliquot were adjusted with HCl or NaOH solution to pH 5 and pH 8, respectively, whereas the second aliquot remained untreated with a pH value of 7 (i.e. pH value of RS/HA solution). Subsequently, three replicates of each of the nine solutions were analysed and the relative deviation of the concentration of the acidic or basic pH-adjusted samples from the concentration of the sample at pH 7 was calculated (concentration recovery (Rec), see Eq. (7)):

$$\mathrm{Rec,\%} = \frac{C_{calc}}{C_{nom}} \cdot 100 \qquad (7)$$

In Eq. (7) C_{calc} represents the observed concentration, whereas C_{nom} corresponds to the nominal concentration, i.e. mean concentration at pH value of 7.

2.4.2.9 Inter-laboratory comparability: Comparison of the in-house Cal with the NIBSC/WHO standards

To compare in-house Cal with international standards, reference Cal solutions were prepared resuspending lyophilised NIBSC/WHO standards for IL-6, IL-8, IL-10, and TNF-α. The lyophilisates with a cytokine mass of 1 µg (denoted as ‘approximated’ mass) were separately dissolved in 1 mL AD and aliquoted (preliminary stock solutions of IL-6, IL-8, IL-10 and TNF-α, 1 µg/mL). 500 µL of the individual preliminary stock solutions were pooled resulting in a final stock solution of 250,000 pg/mL per cytokine. Cal 12 (10,000 pg/mL) was prepared from the stock solution, and Cal 6 (100 pg/mL) was diluted serially from Cal 12 solution. Cal 7-11 were non-serially generated from Cal 12, Cal 1-5 were diluted from Cal 6 non-serially as well and solutions were subsequently aliquoted. Accordingly, Cal 1-12 had the same nominal concentrations as in-house Cal 1-12 (see section 2.4.2.1), which were 4, 6, 10, 20, 50, 100, 500, 1000, 4000, 6000, 9000, and 10000 pg/mL. In-house and NIBSC Cal were processed and analysed (n=2) applying the validated bioanalytical method.

2.6 Project II: *In vitro* microdialysis of cytokines

2.6.1 *In vitro* microdialysis system (IVMS)

All µD experiments were performed with an *in vitro* microdialysis system (IVMS) shown in Fig. 2-4 and previously developed to standardise conditions (e.g. heights, distances, lengths, temperature etc.) for *in vitro* µD investigations [172; 173]. Glass tubes, containing the catheter-surrounding medium throughout µD investigations of hydrophilic drugs, were replaced by polypropylene tubes for cytokine investigations with the intention to reduce adsorption effects.

Three linear µD catheters (CMA66® / 66® linear µD catheters, see section 2.2.2.2) were fixed in a tube containing the catheter-surrounding medium. This medium container was tempered at the intended temperature and medium was stirred at 600-700 rpm. The inlet tubings of the linear µD catheters were connected to syringes placed in the *in vitro* µD pump (see section 2.2.2.1). µPerfusate and catheter-surrounding medium consisted of the physiologically related matrix RS/HA (see section 2.4.1). Before each experiment, catheters were rinsed with µPerfusate and equilibrated in tempered surrounding medium for at least 60 min. Time point “0 min” was the start of the first µD sampling interval at the particular FR and the beginning of the first µD sampling interval of the entire µD experiment for stability testing at 37 °C (see section 2.6.3), respectively.

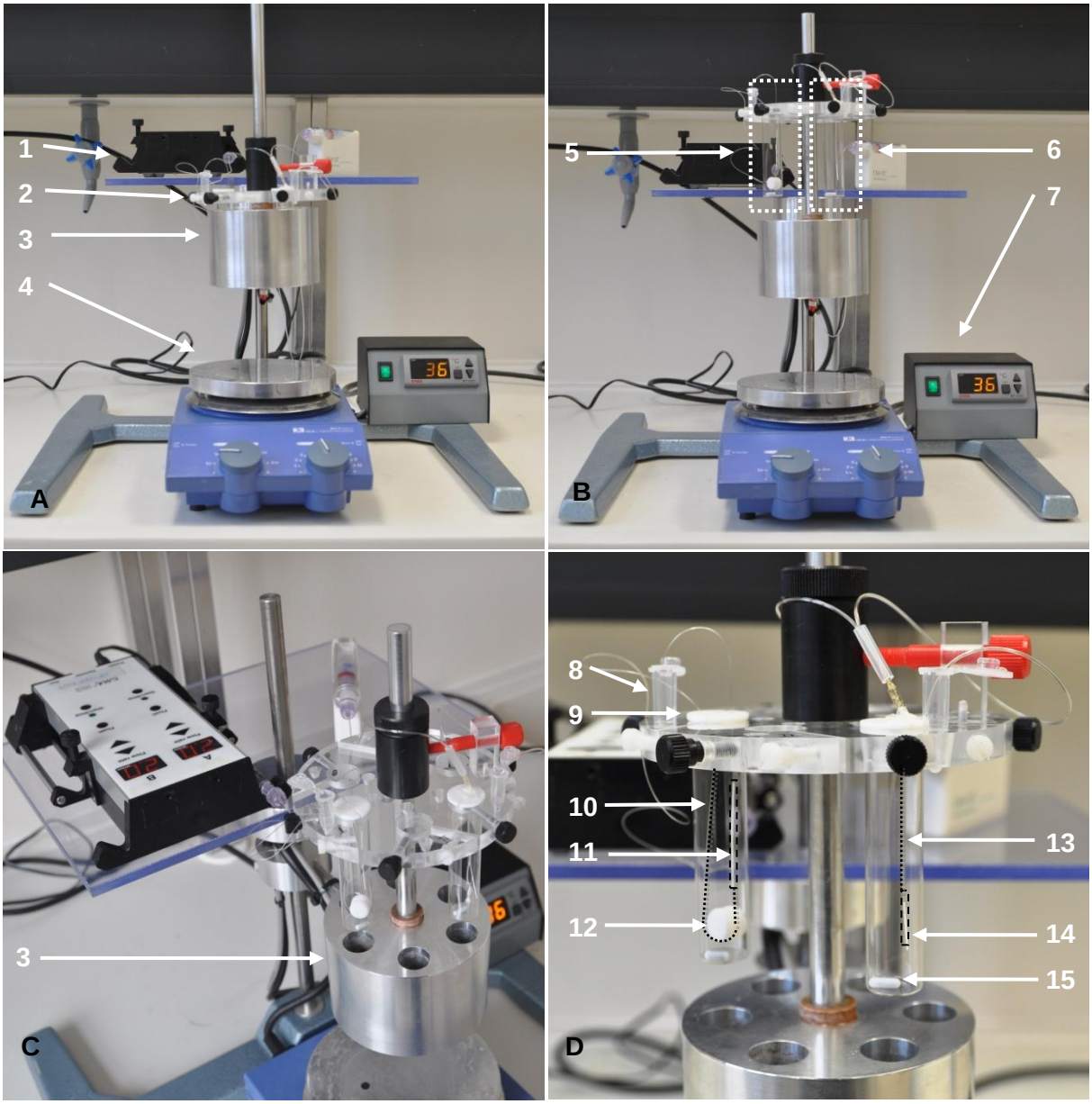

Fig. 2-4: *In vitro* microdialysis system without cover lid

Legend for Fig. 2-4

A	System in working position without cover lid	6	Unit ‘concentric catheter‘
B	System in preparation position	7	Thermoblock temperature control module
C	Pumps, platform and thermoblock	8	Dialysate collection vial
D	Platform with vials in preparation position	9	Guide cap for linear catheter
1	Platform with stationary and portable microdialysis pumps	10	Linear catheter, e.g. CMA66® / 66® MD Catheter
2	Multifunctional hardware adapter platform	11	Semi-permeable membrane of linear catheter
3	Thermoblock with wells for medium container	12	Guide lug for linear catheter
4	Magnetic stirrer	13	Concentric catheter, e.g. CMA60® / 63® MD Catheter
5	Unit ‘linear catheter‘	14	Semi-permeable membrane of concentric catheter
		15	Magnetic stir bar

2.6.2 Preparation of solutions used as perfusate or medium

Solutions serving as µPerfusate or catheter-surrounding medium were spiked by adding negligible volumes of high-concentrated cytokine solutions (matrix composed of AD or HA) to large volumes of analyte-free RS/HA. High-concentrated solutions were suspensions/lyophilisates remaining from method development (see section 2.4.1), and therefore, were of heterogenous character and consequently varied in concentrations of the individual cytokines as well as in concentrations ranges of the applied solutions. Uniformity of spiked concentrations of the solutions was not required for recovery/delivery investigations since calculations were related to the determined concentrations. However, equally concentrated solutions would have been beneficial for non-linear regression in section 2.6.6 (Eq. (14) and Eq. (15)) and estimation of catheter-surrounding medium- and µPerfusate concentrations.

2.6.3 Investigation of influence of microdialysis system settings

Stability of cytokines in catheter-surrounding medium over up to 6 h at 37 °C

Throughout recovery investigations (see section 2.6.5) samples of the cytokine containing catheter-surrounding medium were collected consecutively in intervals of 2 h over a period of 6 h. Collected samples were immediately frozen at -80 °C to explore stability of the model cytokines at 37 °C over a time period exceeding the longest µD intervals. Concentrations at different points in time were compared to concentrations at the starting time (0 min) and stability was calculated according to Eq. (6) (see section 2.4.2.2).

Assessment of sample volume loss by ultrafiltration or evaporation

For determination of the dimension of fluid loss and dependence of observed UF or evaporation on FR (and temperature), the volume of every individual sample of investigations concerning recovery and delivery at 25 °C and 37 °C (see section 2.6.5) was determined. For this purpose microtubes were weighed prior and subsequent to µDialysate sampling and the resulting mass difference was converted into volume (density was assumed to be equal to that of water and temperature as well as atmospheric pressure considered for calculation). Calculated volumes were compared to nominal volumes, i.e. the product of the interval/collection period (min) and FR (µL/min). Lost as well as recovered fluid were determined using the relative error (RE, see section 2.9) or volume recovery (i.e. $(100 + RE)$). Additionally, open microvials with 30 µL of blank matrix solution were placed on the multifunctional hardware adapter platform of the IVMS (see Fig. 2-4 in section 2.6.1) and

potential evaporation determined gravimetrically for the time intervals equivalent to the µD intervals.

2.6.4 Adsorption of cytokines to the catheter components

Polyurethane tubings, 0.38 mm in diameter and 400 mm in length, were perfused with µPerfusate containing intermediate (C_{IL-6}= 600 pg/mL, C_{IL-8}= 500 pg/mL, C_{IL-10}= 300 pg/mL, $C_{TNF-\alpha}$= 800 pg/mL) and low (C_{IL-6}= 100 pg/mL, C_{IL-8}= 90 pg/mL, C_{IL-10}= 40 pg/mL, $C_{TNF-\alpha}$= 80 pg/mL) concentrations of the model cytokines. Following an initial perfusion at FR of 2.0 µL/min for four intervals of 15 min (30 µL per sample), FR was switched to 0.5 µL/min and three aliquots were sampled in 60 min intervals (30 µL per sample).

In the second part of adsorption testing, three catheter-surrounding medium containers were filled with 12 mL of medium containing 1000-4000 pg/mL of cytokines. Three linear catheter membranes including 100 mm tubing were placed in the solutions and equilibrated for 10 min at 37 °C. Afterwards, aliquots of 30 µL of the surrounding solutions were sampled.

For the determination of the adsorption of cytokines to the tubings and to the outer µD membrane surface, the different adsorption samples were analysed and signals were compared with those of the initial µPerfusate or the initial medium samples, respectively.

2.6.5 Dependence of relative recovery and relative delivery on variations of flow rate, temperature, catheter-surrounding medium concentration and pH value

Tab. 2-1 gives an overview of the *in vitro* recovery and delivery investigations performed with the IVMS to evaluate relative fractions of cytokine concentration gain and loss via the µD catheter membrane, i.e. RR and rD. µD sampling intervals ranged between 7 min and 200 min and were set according to the applied FR to obtain a nominal volume of approximately 35-60 µL.

Tab. 2-1: Experimental settings to investigate the dependency of relative recovery (RR) and relative delivery (rD) on flow rate (0.3, 0.5, 1.0, 2.0, 5.0 µl/min) and on cytokine concentration. Stirring velocity: moderate (600-700 1/min). w/o: without.

Experimental arrangement	Temperature [°C]	Flow rate [µL/min]	Cytokine concentration [pg/mL]		
			Medium	Perfusate	Dialysate
Recovery investigations					
Dependence on flow rate	25/37	0.3-5.0	10^3-10^4	RS/HA w/o cytokines	To be measured
Dependence on concentration	37	0.5	10^2-10^4	RS/HA w/o cytokines	To be measured
Dependence on pH value	37	0.5	10^3-10^4 (pH 5, 7 and 8)	RS/HA w/o cytokines	To be measured
Delivery investigations					
Dependence on flow rate	25/37	0.3-5.0	RS/HA w/o cytokines	10^3-10^4	To be measured

Relationship between relative recovery of cytokines and flow rate at 25 °C and 37 °C

In vitro µD RR was determined employing FR of 0.3, 0.5, 1.0, 2.0 and 5.0 µL/min and sampled for 7-200 min leading to nominal µDialysate volumes of 35-60 µL. Catheter-surrounding medium was spiked with 10^3-10^4 pg/mL for each cytokine. Recovery investigations were performed over three subsequent sampling intervals per FR at surrounding medium temperatures of 25 °C and 37 °C, respectively. Medium was sampled simultaneously to the µDialysate with an additional sample at the beginning of the experiment (0 min). *In vitro* RR at a particular FR was calculated in accordance with Eq. (1) from medium (i.e. representing ISF *in vitro*) and µDialysate concentrations:

$$RR\ (in\ vitro), \% = \frac{C_{\mu Dialysate} - C_{\mu Perfusate}}{C_{medium} - C_{\mu Perfusate}} \cdot 100 \qquad (8)$$

$C_{\mu Dialysate}$, $C_{\mu Perfusate}$, and C_{medium} represented the µDialysate, µPerfusate, or catheter-surrounding medium concentration of the individual cytokine, respectively. As $C_{\mu Perfusate}$ was zero, calculation of RR was reduced to:

$$RR\ (in\ vitro), \% = \frac{C_{\mu Dialysate}}{C_{medium}} \cdot 100 \qquad (9)$$

To establish the relationship between RR and FR, non-linear regression with RR data was performed applying Eq. (10) [23].

$$RR = (1 - e^{-\frac{rA}{FR}}) \cdot 100 \qquad (10)$$

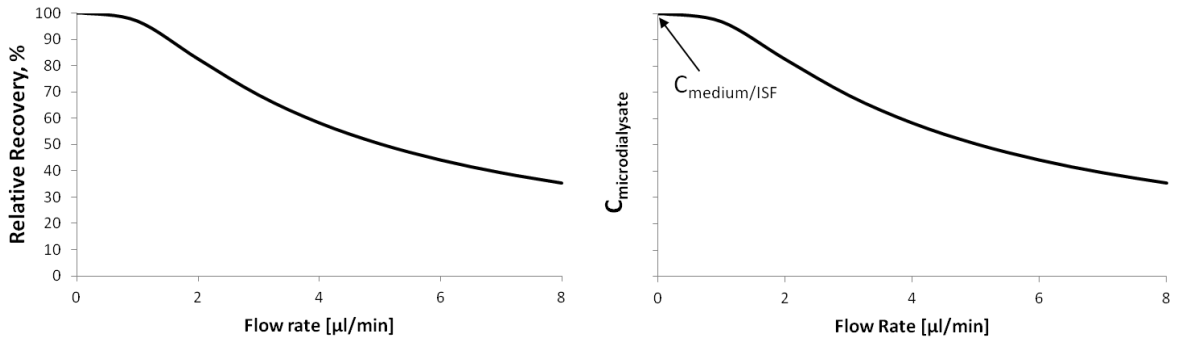

Fig. 2-5: Relationshipt between flow rate and relative recovery (left panel) and relationship between flow rate and microdialysate concentration (right panel)

In Eq. (10) *r* represents the mass transfer coefficient as the parameter to be estimated, *A* the catheter surface (47 mm^2), and *FR* the perfusion flow rate as the independent variable. A typical graph of the mathematical description is presented in Fig. 2-5 (left panel).

Relationship between relative delivery of cytokines and flow rate at 25 °C and 37 °C

For *in vitro* µD relative delivery (rD) experiments, µPerfusate was spiked with 10^3-10^4 pg/mL for each cytokine and sampling was accomplished over three equal, subsequent sampling intervals of 7-200 min for FR of 0.3, 0.5, 1.0, 2.0 and 5.0 µL/min. Delivery investigations were performed at 25 °C or 37 °C, respectively, with a µDialysate volume of 35-60 µL. µPerfusate was sampled directly from the µD syringe previous to and following the µDialysate sampling, i.e. samples were acquired prior to the start of the first of three µD sampling intervals for a particular FR and as soon as the third interval had been finished.
In vitro rD at a particular FR was calculated in accordance with Eq. (1) from µPerfusate and µDialysate concentrations:

$$rD\ (in\ vitro), \% = \frac{C_{\mu Dialysate} - C_{\mu Perfusate}}{C_{medium} - C_{\mu Perfusate}} \cdot 100 \qquad (11)$$

As C_{medium} was initially zero and only negligibly increased over time, calculation of rD was reduced to:

$$rD\ (in\ vitro), \% = (1 - \frac{C_{\mu Dialysate}}{C_{\mu Perfusate}}) \cdot 100) \qquad (12)$$

To establish the relationship between rD and FR, non-linear regression with rD data was performed analogous to Eq. (10) (see above).

$$rD = (1 - e^{-\frac{rA}{FR}}) \cdot 100 \quad (13)$$

Relative recovery of cytokines at varying surrounding medium concentrations

RR was investigated at 37 °C employing a FR of 0.5 µL/min over three subsequent sampling intervals of 70 min per concentration level of the catheter-surrounding medium. The three different medium solutions contained 80-170 pg/mL, 300-800 pg/mL and 1000-3000 pg/mL of cytokines, respectively.

Relative recovery of cytokines at different pH values

Cytokine-spiked surrounding medium ($C_{IL\text{-}6}$= 6500 pg/mL, $C_{IL\text{-}8}$= 5500 pg/mL, $C_{IL\text{-}10}$= 3500 pg/mL, C_{TNF}= 6500 pg/mL) was split into three aliquots. Solutions were adjusted to the same pH values as for the investigation of the effect of pH value on bioanalysis of cytokines (see section 2.4.2.8): The resulting aliquots had pH values of 5, 7 (pH of RS/HA solution) and 8, respectively. RR from each individual surrounding medium was investigated at 37 °C with FR of 0.5 µL/min over three sampling intervals of 70 min.

2.6.6 Prediction of catheter-surrounding medium concentrations by non-linear regression of microdialysate concentrations

In view of the subsequent *in vivo* µD applying the flow-rate-variation method (see section 1.2.32.7), equations (10) and (13) from subsection 2.6.5 were transformed to determine the catheter-surrounding medium concentration as an estimated parameter. Throughout *in vivo* investigations, catheter-surrounding fluid concentrations of cytokines will not be directly determinable and, therefore, indirect determination methods for RR had to be examined. To qualify the selected determination method (i.e. the flow-rate-variation method, see 2.7.1.3) *in vitro* as a prerequisite for the *in vivo* application (see Eq. (16) in section 2.7.3.3), Eq. (9) was plugged in Eq. (10) and rearranged for $C_{\mu Dialysate}$ (see Eq. (14)). Consequently, µDialysate concentrations instead of RR values were subjected to weighted non-linear regression (weight: $1/y_{predicted}$) and the intercept (which was 100% RR) was replaced by C_{medium} [23] (see also Fig. 2-5).

$$C_{\mu Dialysate} = (1 - e^{-\frac{rA}{FR}}) \cdot C_{medium} \quad (14)$$

For recovery experiments, $C_{\mu Dialysate}$ represents the directly determined µDialysate concentrations, whereas in delivery investigations, the term corresponds to the lost fraction, which is the result of the subtraction of µDialysate concentrations from µPerfusate concentrations.

$$C_{\mu perfusate} - C_{\mu Dialysate} = (1 - e^{-\frac{rA}{FR}}) \cdot C_{\mu Perfusate} \qquad (15)$$

In both equations (Eq. (14) and Eq. (15)), *r* represents the mass transfer coefficient with regard to absolute concentrations instead of relative recovery/delivery (see Eq. (10) and (13) in section 2.6.5).

2.7 Project III: Long-term pilot study on microdialysis of cytokines in healthy volunteers

The study "Microdialysis of Healthy Volunteers to Determine Cytokines" (official title "Mikrodialyse zur Gewinnung von Zytokinen am gesunden Probanden") was approved by the local ethics committee of the Charité Universitaetsmedizin Berlin and was conducted by the Department of Clinical Pharmacy and Biochemistry of the Freie Universitaet Berlin in cooperation with the Department of Anesthesiology and Operative Intensive Care Medicine of the Charité, in accordance with the Declaration of Helsinki, as amended in Fortaleza 2013 [174], and the ICH guideline for good clinical practice [14]. The study was registered at German Clinical Trials Register, which automatically included registry at the WHO International Clinical Trials Registry Platform (DRKS and ICTRP, identifier: DRKS00005420; www.germanctr.de, http://www.who.int/ictrp/en/). The study site was at the Department of Clinical Pharmacy and Biochemistry, Institute of Pharmacy of the Freie Universitaet Berlin, Germany.

2.7.1 Clinical study protocol

2.7.1.1 Study design

The investigation was designed as an exploratory, prospective, uncontrolled study without an investigational medicinal product. Four healthy volunteers were recruited for this explorative investigation, applying one µD catheter per individual for a study period of three days. Tab. 2-2 and Tab. 8-1 give an overview of procedures performed at the different study days.

Tab. 2-2: Study design of the long-term pilot study on microdialysis of cytokines in healthy volunteers

Study days		
----------1----------	----------2----------	----------3----------
Sampling schedule		
Insertion of microdialysis catheter (x) and microdialysate sampling intervals (⌐¬*)		
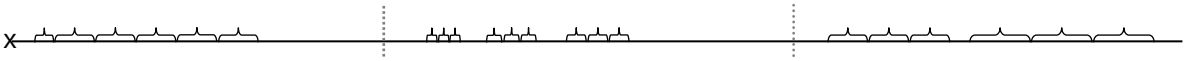		
Baseline and 5 samples	3 samples per FR	3 samples per FR
Flow rate (length of sampling interval)		
0.5 µL/min (70 min)	5.0 (7 min), 2.0 (18 min) and 1.0 µL/min (35 min)	0.5 (70 min) and 0.3 µL/min (120 min)

*length indicates duration of sampling interval

The different lengths of the µD sampling intervals (⌐¬) were selected considering the sample volume required for bioanalysis (i.e. 25 µL) and potential volume loss by UF (see sections 1.2.4 and 2.7.1.2). Consequently, the planned intervals were chosen to obtain a nominal sampling volume of 35-36 µL.

During the study procedures, the volunteers were allowed to move freely and to carry out their regular activities. They were, however, recommended to refrain from physical exercises, excessive alcohol consumption, and from having a sauna.

2.7.1.2 *In vivo* long-term microdialysis study setting

Following skin disinfection the linear catheter was inserted to ISF of the abdominal subcutaneous tissue. A guiding cannula (21 G, 50 mm) was introduced into the tissue with a puncture into and out of the skin in a distance of circa 37 mm. The µD syringe, filled with the perfusion fluid (RS/HA 0.5%), was connected to the inlet tubing and the syringe plunger cautiously pushed to wet the catheter membrane. Subsequently, the outlet tubing of the catheter was pulled through the cannula to place the membrane within the tube of the cannula. As the last insertion step, the inlet tubing was manually fixed on the skin and the cannula was removed while the membrane remained within the subcutaneous tissue.

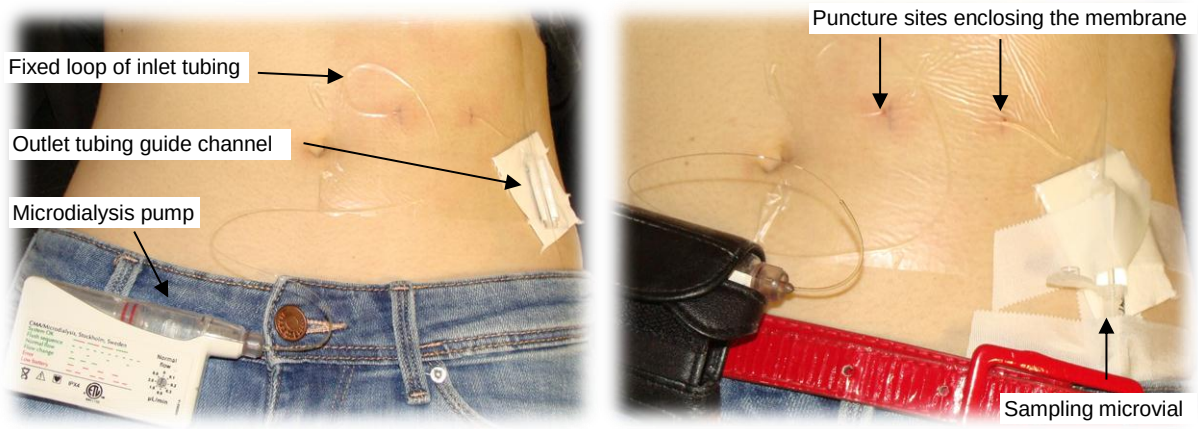

Fig. 2-6: *In vivo* microdialysis setting previous to final fixation (left) and with fixation of pump and microvial (right)

The syringe was placed in the portable µD pump and pumping started with a flush period of 5 min followed by an automatic decrease to the pre-set FR (i.e. 0.5 µL/min).

The skin area above the µD membrane including the two puncture sites was covered by a transparent adhesive tape enclosing a formed loop of the inlet tubing and a small part of the outlet tubing (see Fig. 2-6, left panel). An outlet tubing guide channel with connection for 500-µL-microtubes was fixed and a sampling vial connected, the pump was attached to a belt (see Fig. 2-6, right panel).

Assessment of sample volume loss by ultrafiltration or evaporation

In accordance with *in vitro* investigations (see section 2.6.3), phenomena related to UF or evaporation were examined, contributing to the exploration of the *in vivo* feasibility of the developed µD setting for determination of cytokines from subcutaneous tissue. Actual volumes of µDialysate were determined gravimetrically and volume loss and recovery calculated using RE (see section 2.9) and volume recovery (i.e. $(100 + RE)$), respectively.

2.7.1.3 Study procedure applying the flow-rate-variation method

Prior to inclusion, the healthy volunteers were informed about the background, the nature and the objectives, procedures, and risks of the study. Upon signature of the informed consent form (at the earliest 24 h after receiving the study information) and considering inclusion and exclusion criteria (Tab. 2-3), individuals were enrolled into the study.

Tab. 2-3: Inclusion and exclusion criteria

Inclusion criteria	Exclusion criteria
Healthy volunteers between 25 and 40 years Body mass index between 18.5 and 30.0 kg/m^2 Anamnesis and screening without pathological findings	Long-term (drug) therapy (except hormonal contraception) Pregnancy or lactation period Irritations of abdominal skin area Contemporary participation in other clinical studies

Screening visit

Body weight (WT) and height as well as age and sex were documented at the screening visit, which was accomplished between seven to one days before study day 1. Each enrolled healthy volunteer was subjected to undergo an anamnesis, a physical examination, and a visual inspection of the abdominal skin for potential irritations.

Study day 1

On study day 1 the µD catheter was inserted (see section 2.7.1.2) and perfused with FR of 0.5 µL/min. Following an equilibration period of at least 20 min (including the flush of the µD system), one baseline sample and five samples of an interval duration of 70 min each were subsequently collected (see Tab. 2-2). Afterwards, the µD setting was checked and fixed in a comfortable position remaining overnight and individuals were able to leave the department. Visual inspection of the puncture sites and the affected skin area were performed frequently throughout the study course by the investigator.

Study day 2

At the beginning of study day 2, FR was increased to 5.0 µL/min followed by an equilibration period of 30 min. Subsequently, three consecutive samples were taken every 7 min and, afterwards, FR reduced to 2.0 min (followed by an equilibration period of 30 min). The sampling time was extended to three intervals of 18 min. Prior to the last equilibration period of study day 2, FR was decreased to 1.0 µL/min and sampling interval prolonged to 35 min. Following the last three samples, FR was reduced to 0.5 µL/min again and study day 2 ended with checking and overnight fixation of the µD system.

Study day 3

As the first examined FR (0.5 µL/min) was already set beforehand, three sampling intervals with a length of 70 min started directly at the beginning of the last study day without a preceding equilibration period. Afterwards, the pump was set to the final investigated FR of 0.3 µL/min and sampling continued every 120 min following an equilibration period of 30 min.

Once sampling had been completed, the µD pump was stopped and the catheter removed from the subcutaneous tissue. Hence, the outlet tubing was cut as close to the puncture site as feasible and the remaining part and surrounding skin area were disinfected. Subsequently, the membrane was carefully pulled out through the inlet puncture site. The puncture sites were covered by a plaster if required. The µD catheter was then checked for leakage and integrity.

Final examination

The final examination was performed up to seven days after study day 3. The occurrence of potential adverse events (AE) and the healing process of the puncture sites were checked once again.

2.7.1.4 Documentation

Case report forms (CRF) were generated for the volunteers, recording all monitored observations during the entire study duration. CRF contained: the name of the study; initials and number of the participant; the written informed consent; dates of the study days for the individual volunteer; parameters recorded at the screening visit and at the final examination; sample collection times; any AE (with regards to the µD procedure) encountered; and other notes as required. Technical µD problems, e.g. functioning errors of the µD pump, were documented as well.

2.7.2 Bioanalysis of the microdialysis samples

Microtubes were weighed prior to connection to the µD system as well as after the sampling interval. Vials were stored at -80 °C within a time limit of 60 min after disconnection from the µD system and remained ultra-deep-frozen until bioanalysis.
Quantification of IL-6, IL-8, IL-10, and TNF-α from the µDialysate samples was realised applying the adapted, validated assay (see sections 2.4 and 8.1) incorporating Cal and QC samples.

2.7.3 Data analysis of the microdialysis data

Non-linear regression of the 4-PL was performed from the raw data of Cal plugging in logarithms of the nominal concentrations as the independent variable and Log(MFI) as the dependent one (see 2.4.1.1), and concentrations of QC and study samples were calculated via the calibration function obtained (see section 2.3 for the applied software). In-study validation was performed by determination of inaccuracy (expressed as RE, %) and imprecision (expressed as CV, %) of calculated concentrations of µDialysate Cal and QC samples.

2.7.3.1 Building the data set

Excel data files, compatible with Phoenix™ WinNonlin®, included: sampling time points; dependent variable (i.e. IL-6, IL-8, IL-10 and TNF-α concentrations); independent variables, such as basic or time-related items, e.g., the individual subject record (ID); covariates, i.e. demographic factors; and data considering µD procedures and UF (see Tab. 8-2). The different item labels were placed in different columns and the individual events of these items, e.g., dosing events and µDialysate concentrations, were sorted in rows by ID and time points in ascending order. Values below the LLOQ were included in data analysis (and particularly denoted by 'flag dependent variable (FLDV)'). Demographic data and other issues listed in CRF were manually transferred into electronical format and were combined with concentration data to a complete data set. The obtained data set was subject to intensive data checkout analysis.

2.7.3.2 Data set checkout

Before data analyses the data set was systematically checked in terms of completeness, correctness and plausibility. In a first exploration, the data set was subjected to a column check in Excel (see section 2.3). Single columns were examined for their minimum and maximum values to check overall plausibility of the values. In addition, a cross-column check was performed, identifying logical combinations within one row. The plausibility check was assisted by creation of so called "index plots" in 'R' (see section 2.3): in these plots each item in the data set was plotted versus ID.

2.7.3.3 Explorative data analysis, non-linear regression and compartmental pharmacokinetic analysis

Calculated concentrations of study samples were subjected to descriptive and explorative analysis. Furthermore, in accordance with the *in vitro* approach (refer to section 2.6.6), µD concentrations obtained during the performance of the flow-rate-variation method were used to estimate the cytokine concentration of the catheter-surrounding ISF and, consequently, to calculate the *in vivo* RR. The mass transfer coefficient *r* and the ISF concentration (C_{ISF}) were estimated (see Eq. (16)), if data was adequate for weighted non-linear regression (weight: $1/y_{predicted}$) of sample concentrations in dependence of FR. The equation for this relation was similar to that applied for *in vitro* RR data (see section 2.6.6, Eq. (10)). It was used to derive *in vivo* cytokine concentrations of ISF (comparable to the *in vitro* cytokine concentrations of the catheter-surrounding medium) from µDialysate concentrations, since measured µD sample concentrations were the exclusive information resulting from *in vivo* µD.

$$C_{\mu Dialysate} = \left(1 - e^{-\frac{rA}{FR}}\right) \cdot C_{ISF} \qquad (16)$$

In Eq. (10) *A* represents the catheter surface (47 mm^2) and *FR* the perfusion flow rate. A typical graph of the mathematical description is presented in Fig. 2-5 (right panel).

A PK model, commonly applied for modelling of drug concentrations in a body compartment, was used to describe the pathophysiological process of endogeneous cytokine secretion into ISF of the abdominal subcutaneous adipose tissue activated by the insertion of the µD catheter. I.e., the compartmental PK approach was employed to describe the concentration-time profiles of each of the cytokines based on the explorative graphical analysis. For that reason, the one-compartment (1-CMT) model including first-order absorption, i.e. the Bateman function (Eq. (17) [2] and Fig. 2-7), was chosen. The following PK parameters were estimated via individual non-linear curve fitting:

$$C(t) = \frac{k_a \cdot F \cdot D}{V \cdot (k_a - \lambda_z)} \cdot \left(e^{-\lambda_z t} - e^{-k_a t}\right) \qquad (17)$$

C(t) represents the concentration at the time *t*, k_a and λ_z are the first-order absorption and elimination constants, respectively, *V* is the apparent volume of distribution, *F* denotes the bioavailability and *D* represents the dose. Since cytokines are endogenous substances and were not administered to the healthy volunteers, the dose (*D*) was a fictional parameter set to 100 µg and bioavailability (*F*) fixed to the value '1'. The implementation of a lag-time (t_{lag}) was investigated for the improvement of the model to describe the concentration-time profile.

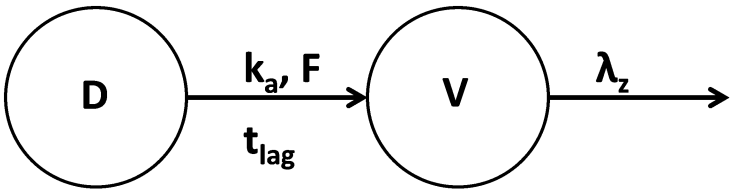

Fig. 2-7: One-compartment model with first-order absorption, delayed input and first-order elimination

2.8 Project IV: Clinical long-term microdialysis study with voriconazole in healthy volunteers

The clinical study "Assessment of target site pharmacokinetics of voriconazole in healthy volunteers during sequence therapy" was conducted by the Department of Clinical Pharmacy, Martin-Luther-Universitaet Halle, Germany, in cooperation with the Department of Clinical Pharmacology, Medical University Vienna, Austria, which provided the study location as well. The study was approved by the ethics committee of the Medical University Vienna, Austria, and the responsible competent federal authority (BASG). The clinical trial was

registered at ClinicalTrials.gov (identifier: NCT01539330) and the European Clinical Trials Database EudraCT (No. 2008-008524-32). The study was conducted in accordance with the Declaration of Helsinki as amended in Seoul 2008 [174], the ICH guideline for good clinical practice [14], and local regulatory requirements. Written informed consent was obtained from each volunteer prior to study enrolment.

2.8.1 Clinical study design

The investigation was designed as a prospective, open-labelled and uncontrolled clinical study in healthy volunteers and consisted of two parts:

A pilot study investigated for the first time the feasibility of long-term insertion and sampling from the µD catheter for single- and multiple-dose investigations of VRC. This part had been performed in three healthy volunteers and was published previously to the current investigation [173; 175]. Maintenance of functionality and sufficient drug diffusion across the µD membrane over the four-day insertion period was demonstrated, as was the tolerability of the procedure over the whole study duration. Consequently, the feasibility of the used µD catheters for accurate sampling over the entire period was confirmed for continuation of the second and main part of the study.

This thesis deals with the conduction of the main study with the best feasible µD catheter insertion duration and sampling schedule from the pilot part in an additional cohort of six healthy volunteers. For evaluation, catheter calibration and PK data were pooled from both parts of the study for data analysis.

Due to the exploratory nature of the study, no formal sample size calculation had to be performed. Additionally, as a prerequisite for sample size calculations the intra- as well as inter-individual variability of the primary outcome, i.e. the determination of PK of VRC in plasma and ISF during sequence therapy, was determined for the first time and was, thus, unknown a priori.

The approved VRC sequence dosing regimen (see section 1.4.1), consisting of initial IV and subsequent oral dose formulations, was applied in the study: VRC was administered twice a day (dosing interval, τ=12 h) on day 1 as an IV dose of 6 mg per kilogram WT over 2 h (initial two loading doses), followed by IV doses of 4 mg per kilogram WT (following two maintenance doses) over 1.3 h on day 2 (according to VFEND® SPC [138]). Three subsequent oral doses of 200 mg were administered in the form of tablets continuing the dosing interval of 12 h. Starting with the calibration procedure prior to drug administration (pilot part) or beginning simultaneously to the first drug administration (main part), respectively, sampling of µDialysate was initiated. Sampling of venous blood was started prior to the application of the first dose and continued according to the sampling schedule.

The schematic dosing and sampling schedule for the four study days is summarised in Tab. 2-4.

Tab. 2-4: Schematic dosing schedule, sampling time points and time intervals for single and multiple dose investigations

Study days						
----------1----------		----------2----------		----------3----------		-----4-----
Study visits						
1	2	3	4	5	6	7
Time [h]						
0-12	12-24	24-36	36-48	48-60	60-72	72-84
Sequence dosing schedule						
IV (6 mg/kg WT)	IV (6 mg/kg WT)	IV (4 mg/kg WT)	IV (4 mg/kg WT)	PO (200 mg)	PO (200 mg)	PO (200 mg)
Extensive sampling schedule						
Insertion (x) and retention time (--) of microdialysis catheter, retrodialysis in the pilot (..+_) and main (_) study						
x-..----------_			----------..			----------_
Microdialysate sampling (intervals)						
0-0.5, 0.5-1, 1-1.5, 1.5-2, 2-2.5, 2.5-3, 3-3.5, 3.5-4, 4-5, 5-6, 6-7, 7-8, 8-9, 9-10, 10-11, 11-12 h	0-20,20-40, 40-60, 60-80, 80-100, 100-120 min	0-20,20-40, 40-60, 60-80 min	0-20,20-40, 40-60, 60-80 min	0-0.5, 0.5-1, 1-1.5, 1.5-2, 2-2.5, 2.5-3, 3-3.5, 3.5-4, 4-5, 5-6, 6-7, 7-8, 8-9, 9-10, 10-11, 11-12 h	-	0-0.5, 0.5-1, 1-1.5, 1.5-2, 2-2.5, 2.5-3, 3-3.5, 3.5-4, 4-5, 5-6, 6-7, 7-8, 8-9, 9-10, 10-11, 11-12 h
Plasma sampling						
0, 0.5, 1, 1.5, 1.75, 2, 2.25, 2.5, 3.25, 4.5, 6, 8, 9, 10, 11, 12 h	2, 12 h	1.3, 12 h	1.3, 12 h	0.5, 1, 1.5, 1.75, 2, 2.25, 2.5, 3.25, 4.5, 6, 8, 9, 10, 11, 12 h	12 h	0.5, 1, 1.5, 1.75, 2, 2.25, 2.5, 3.25, 4.5, 6, 8, 9, 10, 11, 12 h

An extensive sampling scheme was applied to result in a rich data situation covering single and multiple dosing of VRC. Supplementary details of the study procedure are also listed in the study schedule (see Tab. 8-3). Recruited healthy volunteers were examined for inclusion and exclusion criteria (see Tab. 8-4) before enrolment into the study. Participants were instructed to adhere to lifestyle restrictions and to recommendations for appropriate handling of µD setting as stated in Tab. 8-5.

2.8.1.1 *In vivo* long-term microdialysis study setting

The µD setting for the long-term investigation illustrated in Fig. 2-8, which was confirmed to be feasible in functionality and in practical aspects during the pilot phase, was arranged at the abdomen of the individuals:

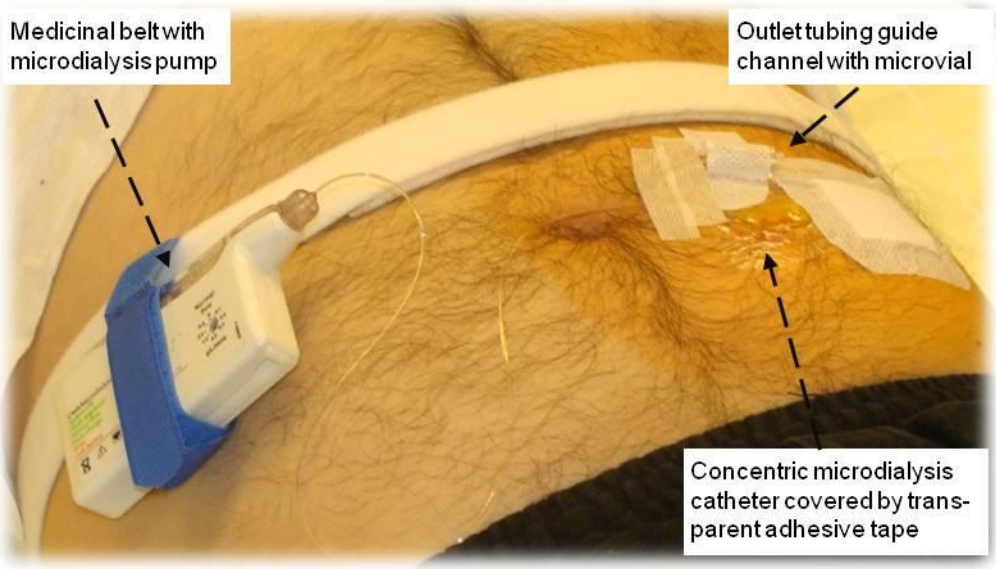

Fig. 2-8: *In-vivo* microdialysis setting for long-term investigation

The mobile µD pump was fixed on a modified medicinal belt directly at the human body. The inlet tubing led to the catheter membrane subcutaneously located in ISF of the abdomen and was partly covered by a transparent adhesive tape, which enclosed the affected area of the skin and a part of the outlet tubing as well. The outlet tubing was drawn through the tube of a guide channel connected to a microvial for µDialysate sampling.

2.8.1.2 Study procedure according to the clinical study protocol

The healthy volunteers had to take part in a screening visit prior to participation in the clinical trial. A study visit was defined as the time span between the start of a drug administration and the start of the next administration, i.e. 12 h in total. At all respective study visits vital signs were determined, AE, food intake within 2 hours prior to PO administration and concomitant drugs recorded, and, at study visit 1, the drug history of the previous 14 days was documented. During the study visits the volunteers were required to remain in a resting position for the majority of time.

Screening visit

Each recruited healthy volunteer was scheduled to undergo a general physical examination, including e.g. an anamnesis, determination of BMI, drawing of blood for laboratory screening tests and virology (see section 8.2), vital signs recording (BP and HR measured after 5 min rest in supine position) according to the study schedule (Tab. 8-3). In addition, ECG was performed and an ophthalmological examination had to take place to ensure the absence of abnormalities. For genotyping, one whole blood sample (~4 ml) was drawn. Moreover, drug screening in urine and urinanalysis was performed. The screening visit had to take place within 3 weeks before study day 1.

Prior to inclusion, the healthy volunteers were informed about the nature, scope and the procedures of the study and about the risks involved. Upon signature of the informed consent form and provided that volunteers fulfil all inclusion/exclusion criteria, the individuals were enrolled into the study and identified by a given consecutive individual number and initials (the first letter of the first name and the first letter of the surname).

Study day 1, visit 1

In the morning of the study day 1, the volunteers entered the clinical research ward. Heart rate, blood pressure and WT were obtained. A plastic cannula (Venflon®) was inserted into an arm vein, preferentially into the antecubital vein for the administration of VRC. A second plastic cannula with a switch-valve (TriCath In®) was inserted into the contralateral arm vein, preferentially into the antecubital vein, to monitor plasma concentrations of VRC. A µD catheter (CMA60®) was used to monitor ISF concentrations of VRC: The skin of the periumbilical abdomen was cleaned and disinfected at the site of the µD-catheter insertion and then punctured by a steel guidance cannula without anaesthesia. Using this guidance cannula, the µD catheter was inserted into the subcutaneous tissue. The µD system (see section 2.8.1.1) was connected and perfused with Ringer's solution at FR of 2.0 µL/min achieved by a microinfusion pump (CMA107®). After insertion of the catheter, an equilibration period of a minimum of 30 min and baseline sampling (15 min) was performed. Subsequently, 6 mg VRC per kg WT were administered IV over a period of 120 min. On completion of infusion, about 50 mL isotonic physiological NaCl solution were infused via the infusion tubing to rinse and to guarantee the complete administration of the dosage (infusion rate: same as for VRC infusion). At pre-defined time intervals, according to the sampling schedule (see Tab. 2-4), blood (~4 mL each) and µD (~60 to ~120 µL each, depending on the interval) samples were taken. The venous catheter was manually rinsed after each sampling with isotonic physiological NaCl solution.

Study day 1, visit 2

Study visit 2 started with the second IV administration of 6 mg VRC per kilogram WT over 120 minutes. During the administration blood (~4 mL each) and µD (~40 µL each) samples were taken according to the sampling schedule (see Tab. 2-4). The volunteers stayed at the research ward for the night.

Study day 2, visit 3

Study visit 3 started with the first IV administration of the maintenance dose of 4 mg VRC per kilogram WT. During administration, blood (~4 mL each) and µD (~40 µL each) samples were taken according to the sampling schedule (see Tab. 2-4). After the last sampling,

retrodialysis was performed as described in section 2.8.1.3. Following a short time under supervision (up to 30 min), the volunteers were permitted to leave the clinical research ward.

Study day 2, visit 4

Study visit 4 started with the second IV administration of the maintenance dose of 4 mg VRC per kilogram WT. During administration, blood (~4 mL each) and µD (~40 µL each) samples were taken according to the sampling schedule (see Tab. 2-4). Following a short time under supervision (up to 30 min), the volunteers were able to leave the clinical research ward for the night (until the next administration).

Study day 3, visit 5

Study visit 5 started with the first PO administration of 200 mg VRC tablets swallowed with circa 200 µL water. Before and after administration, blood (~4 mL each) and µD (~60 to ~120 µL each) samples were taken according to the sampling schedule (see Tab. 2-4).

Study day 3, visit 6

Study visit 6 started with the second PO administration of 200 mg VRC. Before administration, blood (~4 mL each) samples were taken according to the sampling schedule (see Tab. 2-4). Following a short time under supervision (up to 30 min), the volunteers were able to leave the clinical research ward for the night (until the next administration).

Study day 4, visit 7

Study visit 7 started with the third PO administration of 200 mg VRC. After administration, blood (~4 mL each) and µD (~60 to ~120 µL each) samples were taken according to the sampling schedule (see Tab. 2-4). Afterwards a retrodialysis was performed as described in section 2.8.1.3. Following a short time under supervision (up to 30 min), the volunteers left the clinical research ward.

The total blood loss of approximately 250 mL over the four day study period and the additional screening visit, final examination and genotype sample had been shown to be well tolerated by healthy volunteers in the pilot part of the study.

Final examination

Between 1 and 7 days after last drug administration, a final examination for safety was performed. The evaluation included vital signs, a physical examination (consisting of clinical chemistry, haematology, urinanalysis, WT, ECG and ophthalmological examination as at screening visit except from drug screening and virology) and AE monitoring (see Tab. 8-3).

2.8.1.3 Calibration procedure of microdialysis catheters

Calibration procedure was performed at four different visits throughout the pilot study (prior to drug administration at visit 1 and at the end of visits 3, 5 and 7). Since RR demonstrated excellent reproducibility [175], repetition of catheter calibration was reduced to two times for the main study. In view of the fact that small amounts of drug have to be administered to the tissue for RD, a washout phase has to follow after the calibration procedure. However, during the pilot study first µD samples (obtained before drug administration) contained VRC concentrations remaining from RD. Consequently, the washout phase of 30 min after retrodialysis prior to the start of the first drug administration (visit 1) revealed to be insufficient for subsequent PK sampling. Therefore, calibration procedure at the beginning of visit 1 was removed from study schedule for the main part and was, by amendment to the clinical study protocol, performed merely at the study visits 3 and 7 (see Tab. 2-4 and Tab. 8-3): For µD catheter calibration VRC was added to the perfusion medium (retroperfusate, RP) in a concentration of 200 µg/mL (see section 2.1.2.1). The calibration procedure at visit 3 started at the end of the µD sampling period (0-80 min) with an equilibration period of 10 min with RP as the perfusate, followed by retrodialysate sampling over two intervals of 15 min. Subsequently, no sampling was performed over a minimum of 10 h (see section 2.8.1.2 and Tab. 2-4). At visit 7 the retrodialysis was performed subsequently to the rich µD sampling period of 12 h.

2.8.1.4 Documentation

The study participants were monitored throughout the course of the trial and all findings were recorded in the CRF, which were referred to the participants by their ID and initials. The records included the study number, the written informed consent, visit dates of the individual, records of vital signs, medical history or examinations administered, laboratory results, concomitant treatment and sample collection times for diagnostic as well as PK samples, any AE encountered, and other required notes. A physician assessed the severity according to the predefined (ICH) criteria on the AE page [176; 177]. Clinical laboratory and haematology parameters were provided as print-outs which were signed and dated by the investigator. Comments on all values which were clinically significantly out of reference ranges were given by the investigator.

2.8.2 Bioanalysis of plasma and microdialysis samples

2.8.2.1 Sample collection, plasma ultrafiltration and HPLC analysis of the samples

Approximately 4 mL venous blood were drawn and collected into citrate tubes (Vacuette®) for the measurement of VRC plasma concentrations. Blood samples were kept in an ice bath for

a maximum of 60 min and centrifuged at approximately 4° C and 3720 *g* for 5 min, plasma was obtained and cells were discharged. Thereafter, samples were frozen and stored at -80 °C until analysis. µDialysates were frozen subsequent to the sampling interval at -80 °C and stored until analysis as well.

VRC concentration was assayed by two different HPLC devices depending on the location (Martin-Luther-Universitaet, Halle, or Freie Universitaet Berlin, respectively), where bioanalysis was accomplished. For that reason, sample injection was performed from microvials or microtitre plates determined by the individual autosampler requirements. The following section exemplifies the method with sample processing in microtitre plates.

A previously described validated bioanalytical method for quantification of VRC from µDialysates and ultrafiltrates (UF) was applied [173; 178]: Plasma samples were processed by ultrafiltration (UF) prior to HPLC analysis. For this purpose, 1 mL of the individual plasma sample (thawed at RT) was pipetted into an UF device (Centrifree®) and centrifuged as recommended in the operating manual provided by the manufacturer (20 min, 2000 *g*, RT). For HPLC analysis UF were subsequently pipetted into a microtube filled with ACN (40/60 v/v) and centrifuged at 25 °C and 13500 *g* for 15 min. A volume of 40 µL of the supernatant was applied to the microtitre plate for sample analysis. µDialysates were processed by a similar method: The individual sample was mixed with ACN (40/60 v/v) directly in the well of the microplate.

The six Cal solutions ranged from 0.156 up to 10.4 µg/mL and QC samples showed concentrations of 1.56 µg/mL (QC 1), 4.16 µg/mL (QC 2) and 8.32 µg/mL (QC 3). Both types were prepared in RS, as this was the previously validated proxy matrix for µDialysate and UF [173; 178]. A volume of 16 µL of Cal, QC as well as µDialysate samples was pipetted to the wells of the microtitre plate and mixed with 24 µL ACN (40/60 v/v; see last paragraph).

All samples remained at 10 °C in the autosampler prior to injection. A volume of 20 µl from each sample was directly injected into the HPLC system. The mobile phase, consisting of an ammonium phosphate buffer ($(NH_4)H_2PO_4$ + NH_3 + H_3PO_4; 40 mM; pH 6.0) and ACN (65/35 v/v) was used under isocratic conditions at a flow rate of 1 ml/min. All samples were separated by a LiChrospher®-100 RP-18 column with an integrated precolumn as the stationary phase. The column temperature was maintained at 25 °C. Quantification of VRC was realised with UV detection at a wavelength of 254 nm. Peak areas of unknown concentrations were calculated by use of the calibration function obtained from Cal determinations and weighted linear regression (weight: 1/concentration^2).

2.8.2.2 Analysis of genotype of Cytochrome P450 isoenzymes 2C9 and 2C19

Genotype analysis of the first five individuals

CYP2C9 and CYP2C19 genotyping of the first five study individuals was carried out at the Institute of Pharmacology, Medical Faculty, Ernst Moritz Arndt Universitaet, Greifswald, Germany, by means of DNA preparation and purification, amplification of the purified DNA and pyrosequencing (see section 8.3) [173; 179; 180]. The CYP2C9 alleles -*2 and -*3 and CYP2C19*2 were determined and if not confirmed positively, the gene was assumed to be composed of the wild type (CYP2C9*1/CYP2C19*1) sequence.

Genotype analysis of the subsequent four individuals

Genotype analysis of blood samples of the following four healthy volunteers was accomplished by the Department of Clinical Pharmacology and Pharmacoepidemiology at the University of Heidelberg, Germany, with additional determination of CYP2C19*3/-*4/-*17 alleles (see section 8.3). If the presence of CYP2C9*2 or -*3 and CYP2C19*2, -*3, -*4 or -*17 was not verified, the wild type genotype was postulated.

2.8.3 Data analysis of study samples

2.8.3.1 Building the data set and handling of missing values

PK data of the main part of the study was merged with equally structured data from the pilot phase. Excel data files, compatible with most common and also more specialised PK software (e.g., Phoenix™ WinNonlin®, NONMEM™), included sampling time points, dependent variables (e.g. VRC concentrations in UF and ISF), independent variables such as basic or time-related items, for example ID, and covariates (e.g. demographic factors) (see Tab. 8-6). The different item labels were placed in the headers of columns and the individual events of these items, e.g. dosing events and UF/ISF concentrations, were sorted in rows by ID and time points in ascending order. Values below the LLOQ were included in data analysis (and particularly denoted as ‘below limit of quantification’ data). Covariates missing within an individual were replaced by the measured value closest to that certain time point (last observation carried forward or next observation carried forward method, whichever was closer in time). There were no covariates that were missing completely within any individual. Data were combined manually to a complete data set.

2.8.3.2 Data set checkout

Before analyses, data sets were systematically checked in terms of completeness, correctness and plausibility. In a first exploration the data set was subjected to a column check in Excel (see section 2.3). Single columns were examined for their minimum and

maximum values to check overall plausibility of the values. In addition, the data set was subject to a cross-column check, identifying logical or potentially erroneous combinations within one row. The plausibility check was assisted by the creation of “index plots” in ‘R’ (see section 2.3). In these plots every item in the data set was plotted against the ID data item. The appendix contains an example of such an index plot (see Fig. 8-1).

2.8.3.3 Explorative and pharmacokinetic data analysis

The unbound VRC concentrations in UF (ultrafiltered plasma) and ISF of subcutaneous adipose tissue were determined. For characterisation of the unbound concentration-time profiles in both matrices, the following PK parameters of VRC after single (visit 1) and multiple dosing (visit 5 and 7) were estimated by non-compartmental analysis (NCA) [181; 182]:

The area under the curve (*AUC*) from start of last drug administration until the last measurable concentration was calculated applying the linear-up/log-down method, which operates with linear interpolation for the ascending and logarithmic interpolation for the descending part of the profiles. The linear method calculates the sum of trapezia between two successive measurement time points (see Eq. (18)) [2]:

$$AUC_{t_i - t_{i+1}} = \sum_{i=1}^{n} \frac{C_i + C_{i+1}}{2} \cdot (t_{i+1} - t_i) \qquad (18)$$

The area under the descending part of the curve was calculated with the log-linear trapezoidal rule (Eq. (19)) [2]:

$$AUC_{t_i - t_{i+1}} = \sum_{i=1}^{n} \frac{C_i - C_{i+1}}{\ln(\frac{C_i}{C_{i+1}})} \cdot (t_{i+1} - t_i) \qquad (19)$$

(C_i or $C_{i+1} \neq 0$)

In Eq. (18) and Eq. (19) t_i and $t+1_i$ correspond to two successive measurement time points with the concentrations C_i and C_{i+1}. The timepoints t_i, $t_{i+1, \ldots} t_n$ amount to the dosing interval τ if a concentration is measurable at t_n.

The terminal slopes (λ_z) were graphically estimated using a semi-logarithmic presentation of measured drug concentrations versus time. For this purpose and if feasible, the same number of concentration-time points (n) of the terminal phase of the curve was applied in order to describe the decline as a mono-exponential terminal phase. In order to reliably identify the mono-exponential terminal phase independently of point-of-view visual impressions, the same number of concentrations was chosen for the estimation of the terminal slope. Of course, it was visually checked, that these time points belonged to the phase of the profile already describing the drug elimination. Ten time points were selected for

ISF data. An exception of this number was visit 5 in the pilot study, in which the last µD sampling interval was replaced by the retrodialysis procedure, and hence, nine ISF concentration-time points were utilised. For UF, eight time points were selected for visits 1 and 7 along with nine data points for visit 5, if the planned number of samples was completely obtained throughout the visits. Once the time points for regression had been determined, λ_z was estimated by performing a linear regression of the natural logarithm of the related concentration values. λ_z is defined as:

λ_z = *-1 m* (estimated slope)

Next, λ_z was used for calculating the terminal half-life according to Eq. (20).

$$t_{1/2} = \frac{ln2}{\lambda_z} \quad (20)$$

Clearance (CL) was determined from dose (*D*) and AUC_τ.

$$CL = \frac{D}{AUC_\tau} \quad (21)$$

For oral administration, the administered amount $(D \cdot F)$ has to include bioavailability (96% for VRC [183]), which was set to '*F=1*' for PK analysis.
Volume of distribution (V) was obtained:

$$V = \frac{CL}{\lambda_z} \quad (22)$$

C_{max} and t_{max} were directly determined from the concentration-time profiles.

In addition, in order to illustrate tissue fluid (i.e. ISF) penetration *AUC* ratios were calculated by dividing the *AUC* in ISF by the *AUC* in plasma. Comparison was drawn between the individuals, the matrices, the dosing and the administration routes. Drug accumulation was calculated via the accumulation factor using the following equation (Eq. (23)):

$$Accumulation\ factor = \frac{AUC_{\tau\ (multiple\ doses)}}{AUC_{\tau\ (single\ dose)}} \quad (23)$$

To compare concentration-time profiles and PK parameter between single and multiple dosing as well as IV and PO doses, dose-normalised concentrations were determined using Eq. (24) with the individual dose administered in the current study visit and NCA as well as accumulation factors calculated for a second time.

$$C_{dose-normalised} = C \cdot 1000/D \quad (24)$$

Due to the nature of the study, all PK parameters were compared in an explorative approach between single and multiple dosing and between both sampling fluids. For comparison, appropriate statistical tests were performed if possible (see section 2.9).

2.9 Descriptive and explorative statistics

Common standard localisation and dispersion parameters (see Tab. 2-5) were calculated to describe and characterise data obtained in projects I to IV, according to the attributes of the respective data variable [162]. While localisation parameters illustrate the central tendency, dispersion parameters describe the variability of a distribution.
The confidence interval (CI) was utilised to provide a measure of parameter uncertainty. The calculation of the standard error (SE) was applied to estimate the standard deviation (SD) of a series of measurements over all possible samples.

Tab. 2-5: Localisation and dispersion parameters

Parameters	
Localisation parameters (continuous data)	
Arithmetic mean($\bar{x}$)	$\bar{x}=\frac{\sum_{i=1}^{n} x_i}{n}$
Geometric mean ($\bar{x}_{geom}$)	n^{th} root of the product of the n observations
Median ($\tilde{x}$)	Value which divides the data ranked in order in half; a half being smaller and a half being larger than the median; 50^{th} percentile
Relative error (RE)	$RE,\%=\frac{C_{calc}-C_{nom}}{C_{nom}}\cdot 100$
Dispersion parameters (continuous data)	
Range (R)	Minimum (Min) – Maximum (Max)
Standard deviation (SD)	$SD=\sqrt{\frac{\sum_{i=1}^{n}(x_i-\bar{x})^2}{n\text{-}1}}$
Coefficient of variation (CV)	$CV,\%=\frac{SD}{\bar{x}}\cdot 100$
Standard error or the mean (SEM)	$SEM=\frac{SD}{\sqrt{n}}$ $\quad rSEM,\%=\frac{SD}{\sqrt{n}}\cdot\bar{x}^{-1}\cdot 100$
Geometric standard deviation (SD_{log})	$SD_{log}=e^{\sqrt{\frac{\sum_{i=1}^{n}(\ln x_i-\ln\bar{x}_{geom})^2}{n}}}$
Geometric coefficient of variance (CV_{geom})	$CV_{geom},\%=100\cdot\sqrt{e^{(SD_{log})^2}-1}$

Apart from t_{max} and $t_{1/2}$, which were given as median and range, geometric localisation and dispersion parameters were applied to most of the PK parameters (C_{max}, λ_z, AUC).

Explorative statistical analysis was carried out applying appropriate statistical tests (see Tab. 2-6) [162]. Selection of a test was dependent on the problem, the distribution of the data, the homogeneity of variance of the parameter and the sample size (n). The significance level α was set to 0.05, i.e., probability values (p) less than 5% ($p<0.05$) were considered to indicate statistically significant differences (rejection of null hypothesis). The Shapiro-Wilk normality test was selected since the test reveals high power particularly for small sample sizes ($n<50$). Tested groups consisted either of at least six replicates each or of one group with three replicates and another group with a minimum number of nine replicates.

Tab. 2-6: Statistical hypothesis tests

Statistical test	**Description**
Test on normal distribution	
Shapiro-Wilk normality test	Test of normality of the data ($n<50$)
Kolmogorov-Smirnov test (K-S test)	Test of normality of the data ($n\geq50$)
Test on homogeneity of variance	
F-test	Test of homogeneity of two variances
Parametric test (applied for normally distributed data and homogeneous variances)	
Student's t-test	Test of the significance of the difference between two sample means (two unpaired samples)
Student's paired t-test	Test of the significance of the difference between two sample means (two dependent samples)
Parametric test (applied for normally distributed data and heterogeneous variances)	
Welch test	Test of the significance of the difference between two sample means (two independent samples)
Non-parametric test (applied for not normally distributed data)	
Wilcoxon signed-rank test	Rank test to compare two paired samples
Friedman test	Rank test to compare multiple paired samples
Wilcoxon-Mann-Whitney test (rank-sum test)	Rank test to compare two unpaired samples
Kruskal-Wallis test	One-way analysis of variance by ranks to compare multiple unpaired samples

Regression analysis described the functional relationship between values of a dependent variable (response variable, y) and one or more independent variables (explanatory variables, x_i). A regression equation $y=f(x, \beta)$ modelled the dependent variable (outcome of a measurement, y) as a function of the independent variables x, the unknown model

parameters β, and corresponding constants. Model parameters were estimated to result in the optimal fit of the data, which was evaluated by using the least squares method, i.e., minimising the distance between the measured and predicted values of the dependent variable y.

To characterise and confirm the goodness of fit, the correlation coefficient r ($-1 \leq r \leq 1$) or the coefficient of determination r^2 ($0 \leq r^2 \leq 1$) were calculated using the observed as well as the predicted y-values. Goodness-of-fit plots (observed versus predicted values) were generated to graphically demonstrate appropriateness of estimated parameters. Generally, two types of regression analysis exist, these are linear (see section 2.8.3.3) and non-linear regression (see sections 2.4.1.1, 2.6.5 and 2.7.3.3), which were both applied in the present work.

3 RESULTS

3.1 Project I: Bioanalytical method for quantification of IL-6, IL-8, IL-10 and TNF-α from microdialysate

A robust and rapid flow cytometry-based multiplex assay enabled the simultaneous determination of IL-6, IL-8, IL-10, and TNF-α. In the preceding diploma thesis the assay was successfully adapted to the investigated matrix, i.e. 100-kDa-µDialysate, with a sample and reagent volume reduction from 50 µL to 25 µL per test and an increase of ULOQ from 5000 pg/mL to 10000 pg/mL (see also 2.4.1). The target matrix was substituted by the appropriate proxy matrix RS/HA due to comparable properties to µDialysate and an essentially similar assay performance applying this matrix. The developed method was documented in the SOP "Quantification method of the cytokines IL-6, IL-8, IL-10 and TNF-α from µDialysate by BD™CBA/BD FACSArray™" (see Appendix 8.1).

3.1.1 Non-linear regression of the calibration function

In order to calculate sample concentrations, non-linear regression was performed utilising the 4-PL equation (see 2.4.1.1) to generate calibration functions for each cytokine in the range of 6-10,000 pg/mL with an additional 'anchoring' point of 4 pg/mL for improving the goodness of fit [161; 184]; the correlation coefficient between observed and predicted Log(MFI) was at least 0.999. The ranges of the parameters of the 4-PL functions for the different cytokines are summarised in Tab. 3-1, furthermore, Tab. 8-16 lists the individual parameters of all six validation days.

Tab. 3-1: Ranges of parameters of non-linear regression (4-parameter logistic) over the six validation days

Parameter	Range of parameter value			
	IL-6	**IL-8**	**IL-10**	**TNF-α**
A	1.05 - 1.10	1.03 – 1.25	0.71 – 1.15	0.41 – 0.61
B	1.97 – 2.36	1.80 – 2.68	1.74 – 2.61	1.61 – 2.04
C	3.88 – 5.16	3.74 – 5.61	3.90 – 6.36	4.24 – 8.02
D	6.30 – 8.36	5.85 – 9.19	6.26 – 10.6	7.23 – 13.6

3.1.2 Method validation

3.1.2.1 Cytokine stability in microdialysate

Different storage conditions, to which cytokines were exposed throughout routine bioanalysis or in the course of prospective *in vitro* and *in vivo* µD studies, revealed no degradation tendency of cytokines in spiked µDialysates over the time periods relevant to sample handling. Stability results are summarised in Tab. 8-7.

Stability of stock solution aliquots stored in the ultrafreezer (-80 °C), refrigerator (ca. 5 °C) or at the bench top (RT, ca. 22 °C) for 6 h was comparable between different storage conditions and did not deviate from freshly prepared QC_{stab} ($p \geq 0.118$, t-test): mean cytokine concentrations of diluted, measured stock solution were between 102% and 112% (CV: 1.92%-7.27%) at -80 °C, 92.2% and 102% (CV: 6.95%-10.7%) at 5 °C and between 98.4% and 101% (CV: 0.00%-7.17%) at RT for the individual cytokines.

Following freeze-and-thaw cycles, mean stability was demonstrated to exceed 80% for two cycles at the minimum (see Fig. 8-2). IL-6 and IL-10 were stable at the three investigated concentrations throughout all of the six conducted freeze-and-thaw cycles: stability ranged between 87.3% and 112% (CV: 4.00%-11.3%) for IL-6 and 82.7% and 109% (CV: 1.96%-15%) for IL-10, respectively. IL-8 was stable over all six cycles at the intermediate and the high concentration (≥81.2% (CV≤15.0%)), however, stability of the lowest concentration was only acceptable for the first four cycles (≥81.2% (CV≤11.9%)) and decreased to 79.9% (CV: 6.00%) and 68.8% (CV: 4.96%) at the last two cycles, respectively. QC_{Stab} 1 (low concentration) revealed stability for TNF-α until the last two freeze-thaw cycles: recovery was ≥82.8% (CV≤9.70%) for cycle 1 to 4; for cycle 5 and 6 stability showed 77.5% (CV: 2.72%) and 69.7% (CV: 3.07%). Following constant stability over two cycles (≥92.0% (CV≤10.0%), $p \geq 0.15$), TNF-α concentration of QC_{Stab} 2 was reduced to 77.6%, 73.8%, 78.2% and 74.6% (CV≤10.5%, $p \leq 0.01$) at the last four freeze-and-thaw cycles, respectively. The solution containing high concentrations of TNF-α revealed scattering stability results over the six freeze-thaw cycles: consecutive recoveries of 104%, 83.5%, 97.4%, 80.6%, 78.5% and 85.8% (CV: 1.67%-16.5%) were observed. Consequently, the cytokine containing matrix should not be thawed more than twice before sample analysis.

Overall stability of the four cytokines at RT (see Fig. 8-3) was demonstrated up to 4 h. The aliquots of QC_{Stab} 3 obtained after 2 h revealed increased variability (CV: 23.8%-29.7%) and were, thus, considered to be an (bioanalytical) outlier. IL-6 and IL-10 remained stable over the complete time period of 24 h with results from 80.7% to 127% (CV: 0.77%-16.9%) for IL-6 and 80.6% to 117% (CV: 0.00%-13.7%) for IL-10. The storage of IL-8 at RT yielded in mean recoveries between 83.1% and 98.8% for low and intermediate concentrations. In the aliquots of the high concentrations IL-8 average stability varied from 80.1% to 106% and

77.6% at one occasion (9 h). A tendency towards degradation was detected for TNF-α in QC_{Stab} 1 and QC_{Stab} 2: In QC_{Stab} 1, mean TNF-α concentrations exceeding a time period of 6 h fell below 80% resulting in 78.2% at 9 h and 12 h (CV: 0.61% and 7.65%), 72.6% (CV: 0.88%) at 15 h and 59.1% (CV: 6.46%) at 24 h. Recovery of the intermediate concentrations was 78.2% (CV: 4.60%) at 1 h, however, the following time points (2 h and 4 h) revealed higher results of 98.2% (CV: 14.1%) and 83.0% (CV: 10.9%), respectively. From 6 h to 24 h mean concentrations of QC_{Stab} 2 varied between 64.6% and 79.0% (CV≤10.1%) and, therefore, TNF-α was not considered to be stable for more than 4 h in solutions of intermediate concentrations. High concentrated solutions showed inconsistent average TNF-α concentrations with results of 78.6% (CV: 7.33%), 74.6% (CV: 3.85%) and 77.1% (CV: 7.07%) at 4 h, 9 h and 12 h, respectively, and recoveries ranging between 86.1% and 117% (CV: 1.47%-8.55%) for 1 h, 2 h, 6 h, 15 h and 24 h. Since concentrations of all individual cytokines were reduced in QC_{Stab} 3 at 4 h, 9 h and 12 h, followed by higher concentrations at the subsequent time points, the reductions were regarded as random errors and not as observations of cytokine degradation. The cytokine solutions should, therefore, not be stored on the benchtop at RT for more than 4 h.

For results of short-term stability at 37 °C as part of the *in vitro* microdialysis investigations see section 3.2.1.

Long-term storage of cytokine samples at -80 °C was observed not to have an influence on stability. Average recoveries ranged between 85.0% and 116% (CV: 3.18%-17.8%) after storage for a period of 2 months, except for the lowest concentration (QC_{Stab} 1) of IL-8: the three aliquots showed recoveries of 59.0%, 71.3% and 84.6%; since the concentrations of the entire aliquots of the other solutions (after 2 and 8 months) were consistently above 80%, the two of the three aliquots of QC_{Stab} 1, whose stability was not given for IL-8, were considered to be (analytical) outliers. Subsequent to a period of 8 months mean cytokine concentrations varied from 83.7% to 90.7% (CV: 3.27%-9.48%). Cytokine containing µDialysate samples can be stored in the ultrafreezer for a minimum of 8 months, e.g., on behalf of clinical study purposes.

Different processing time points revealed an influence on processed sample stability (i.e. post-preparative stability) and on concentration variability of the cytokines. Mean IL-6 and TNF-α concentrations exceeded 80% (82.3% to 93.0%, CV: 7.52%-17.0%). However, one aliquot of QC_{Stab} 1, QC_{Stab} 2 and QC_{Stab} 3 solutions, respectively, resulted in IL-6 concentrations below 80% (76.2%, 74.6% and 68.0%), and one aliquot of QC_{Stab} 3 showed insufficient TNF-α recovery of 70.9%. QC_{Stab} 1 to QC_{Stab} 3 also exposed at least one aliquot with decreased concentrations for IL-8 and IL-10. Average recoveries from the low, intermediate and high concentrated solutions were 79.2% (CV: 15.5%), 83.9% (CV: 10.6%), 73.9% (CV: 15.6%) for IL-8 and 77.8% (CV: 20.7%), 81.9% (CV: 13.3%), 82.6% (CV: 14.3%)

for IL-10, respectively. Stability cannot be assured if samples are processed with a time delay to the processing of the Cal and QC samples. Consequently, Cal samples will have to be added for samples which are processed with a time delay (e.g. on a second microtitre plate) to guarantee accurate concentration measurement. Alternatively, QC samples can be placed on the last cavities of a run with more than one microtitre plate to check the post-preparative stability over the entire set of samples of the analytical run.

3.1.2.2 Limit of detection and carry-over effect

The calculated MFI results at LOD were 11.2, 15.8, 12.5 and 2.53 for IL-6, IL-8, IL-10, and TNF-α, respectively, and therefore, were significantly ($p<0.005$, t-test) lower than mean MFI results for QC LLOQ, which amounted to 16.5 (CV: 2.39%), 18.0 (CV: 2.51%), 16.5 (CV: 3.85%) and 5.89 (CV: 4.26%) on this validation day.
Six aliquots of blank samples placed subsequent to five samples of the highest QC sample did not reveal any calculated concentration above 0 pg/mL for the individual cytokines and showed mean MFI of 10.5 (CV: 3.98%), 15.1 (CV: 2.96%), 11.9 (CV: 3.12%) and 2.17 (CV: 11.2%).

3.1.2.3 Precision, accuracy and lower limit of quantification

The bioanalytical method was validated by QC samples over a quantification range of 5 pg/mL to 10000 pg/mL. Results of the validation parameters, i.e. intra- and inter-assay accuracy and precision, met requirements of the EMA Guideline on BMV [17] for ligand binding assays over a concentration range of 10-10,000 pg/mL, except for mean intra-assay inaccuracy of TNF-α (≤23.7% RE, 93% of mean RE <20%). For concentrations between LLOQ (5 pg/mL) and 10 pg/mL intra-assay imprecision and inaccuracy of the QC replicates were less or equal 16.8%/±14.9% (IL-6), 30.4%/±36.5% (IL-8), 26.9%/±29.5% (IL-10) and 27.8%/±10.1% (TNF-α), while inter-assay precision and accuracy were within the international acceptance criteria. Considering Cal solutions, 99% of mean intra- and inter-assay imprecision and inaccuracy results met guideline recommendations. Individual validation results for Cal and QC are listed in Tab. 8-8 to Tab. 8-15 in the appendix and summarised in Tab. 3-2.

Tab. 3-2: Validated concentration range with intra-assay imprecision (expressed as coefficient of variation, CV, %) and inaccuracy (as mean percentage deviation, RE, %) of determined cytokine concentrations in microdialysate quality control samples

Cytokine	Range of concentration (pg/mL)	Maximal Imprecision CV, %	Maximal Inaccuracy RE, %
Intra-assay variability (n=3 or 5)			
IL-6	≥5 - ≤10	16.8	+14.9
	>10 - ≤10000	12.0	-15.0
IL-8	≥5 - ≤10	30.4	-36.5
	>10 - ≤10000	12.3	-17.0
IL-10	≥5 - ≤10	26.9	+29.5
	>10 - ≤10000	11.6	-10.7
TNF-α	≥5 - ≤10	27.8	+10.1
	>10 - ≤10000	16.5	+23.7
Inter-assay variability (n=20)			
IL-6	≥5 - ≤10	11.6	+2.30
	>10 - ≤10000	7.89	-4.49
IL-8	≥5 - ≤10	19.2	-22.6
	>10 - ≤10000	9.81	-8.95
IL-10	≥5 - ≤10	17.8	+4.52
	>10 - ≤10000	7.20	+4.47
TNF-α	≥5 - ≤10	17.0	+2.65
	>10 - ≤10000	10.1	+16.5

3.1.2.4 Dilutional linearity

Results of investigation of dilutional linearity are displayed in Tab. 3-3 and Fig. 8-4. Imprecision and inaccuracy of the QC_{lin} samples were acceptable (overall CV and RE for concentrations higher than 10 pg/mL: ≤7.30% and ≤±15.5%; for 5 pg/mL (QC_{lin} 7): ≤19.4% and ≤±18.4%) and dilutional linearity was established. Thus, samples assumed to be concentrated higher than ULOQ can be processed and analysed applying this quantification method as well.

Tab. 3-3: Linearity (Mean of calculated concentrations; CV, %; RE, %) of diluted solutions from high-concentrated samples

Linearity sample	$Conc_{pred}$ (pg/mL)	$Conc_{calc}$ (pg/mL)				CV, %				RE, %			
		IL-6	IL-8	IL-10	TNF-α	IL-6	IL-8	IL-10	TNF-α	IL-6	IL-8	IL-10	TNF-α
QC_{lin} 1 non-serial	**9500**	8839	9104	9333	9863	2.90	3.62	1.85	2.91	-6.96	-4.17	-1.76	+3.83
QC_{lin} 2 non-serial	**7500**	7329	6923	7578	7659	1.43	2.43	3.37	4.67	-2.27	-7.69	+1.04	+2.12
QC_{lin} 3 non-serial	**5000**	5132	4832	5129	5208	2.99	1.95	2.00	2.66	+2.64	-3.36	+2.58	+4.16
QC_{lin} 4 non-serial	**2500**	2358	2270	2440	2704	3.15	1.57	3.14	3.49	-5.67	-9.21	-2.39	+8.15
QC_{lin} 5 serial	**250**	219	211	233	250	7.12	6.38	6.42	7.30	-12.6	-15.5	-6.63	+0.01
QC_{lin} 6 serial	**25**	22.0	22.4	24.3	27.2	5.17	1.03	0.44	4.88	-12.2	-10.3	-2.71	+8.78
QC_{lin} 7 serial	**5**	4.24	4.08	5.09	5.38	10.4	19.4	16.5	15.6	-15.2	-18.4	+1.76	+7.53

3.1.2.5 Parallelism of dilution series from a study sample and spiked in-study validation samples

Parallelism of the MFI-concentration curves of Cal and a dilution series of one incurred study sample from the long-term µD study (section 2.7) was demonstrated (see Tab. 3-4 and Fig. 8-5). Since the study sample did not contain IL-10 and TNF-α, parallelism was demonstrated for IL-6 and IL-8 by this *in vivo* solution. Imprecision and inaccuracy of diluted parallelism samples did not exceed 6.54% CV and ±7.59% RE, respectively. Compared to first analysis of the incurred study sample (MFI: 1076 pg/mL for IL-6 and 974 pg/mL for IL-8), reanalysis via parallelism investigation resulted in congruent concentration results (RE: -2.80% (IL-6) and -2.07% (IL-8)).

Tab. 3-4: Mean concentrations, imprecision (CV, %) and inaccuracy (RE, %) of parallelism samples

Parallelism sample	Mean $Conc_{calc}$ (pg/mL)		CV, %		RE, %	
	IL-6	IL-8	IL-6	IL-8	IL-6	IL-8
Study sample	1046	954	3.66	6.54	-	-
1:2	549	474	2.72	0.00	+5.04	-0.56
1:5	218	188	0.00	2.34	+4.10	-1.41
1:10	112	96.9	2.08	7.02	+7.59	+1.53

3.1.2.6 Intermediate precision

The MFI-concentration relationships of the validation sets from all six analysis runs are presented in Fig. 3-1; the correlation coefficient *r* consistently achieved values ≥0.9995. Goodness-of-fit plots revealed essential similarity of observed and predicted signals (see Fig. 8-6).

On validation days 2, 4 and 5 the voltage of the NIR and Red detectors, which detected the signal for the identification and differentiation of the analytes, were changed to separate the cytokine cluster from one another in an optimal mode. The adjusted settings were retained for the subsequent validation days. Therefore, quantification MFI results of the Yellow detector could have shifted due to a slightly modified selected cluster of detected beads for one individual cytokine. Additionally, the voltage of the Yellow detector was adjusted at day 5 and maintained for the last validation day. Goodness of non-linear regression results and of calculated concentrations were not influenced by these marginal detector voltages adjustments (see Fig. 8-6 and Tab. 8-16). QC and Cal did not show modified concentration results for the validation days with adjusted voltages.

Reproducibility of non-linear regression parameters (see Tab. 8-16) over the six validation runs was shown since variability amounted to ≤23.5% CV only, notwithstanding the changes of the detector voltages of the device on three of the six days, which resulted in divergent MFI values for the individual calibration curves.

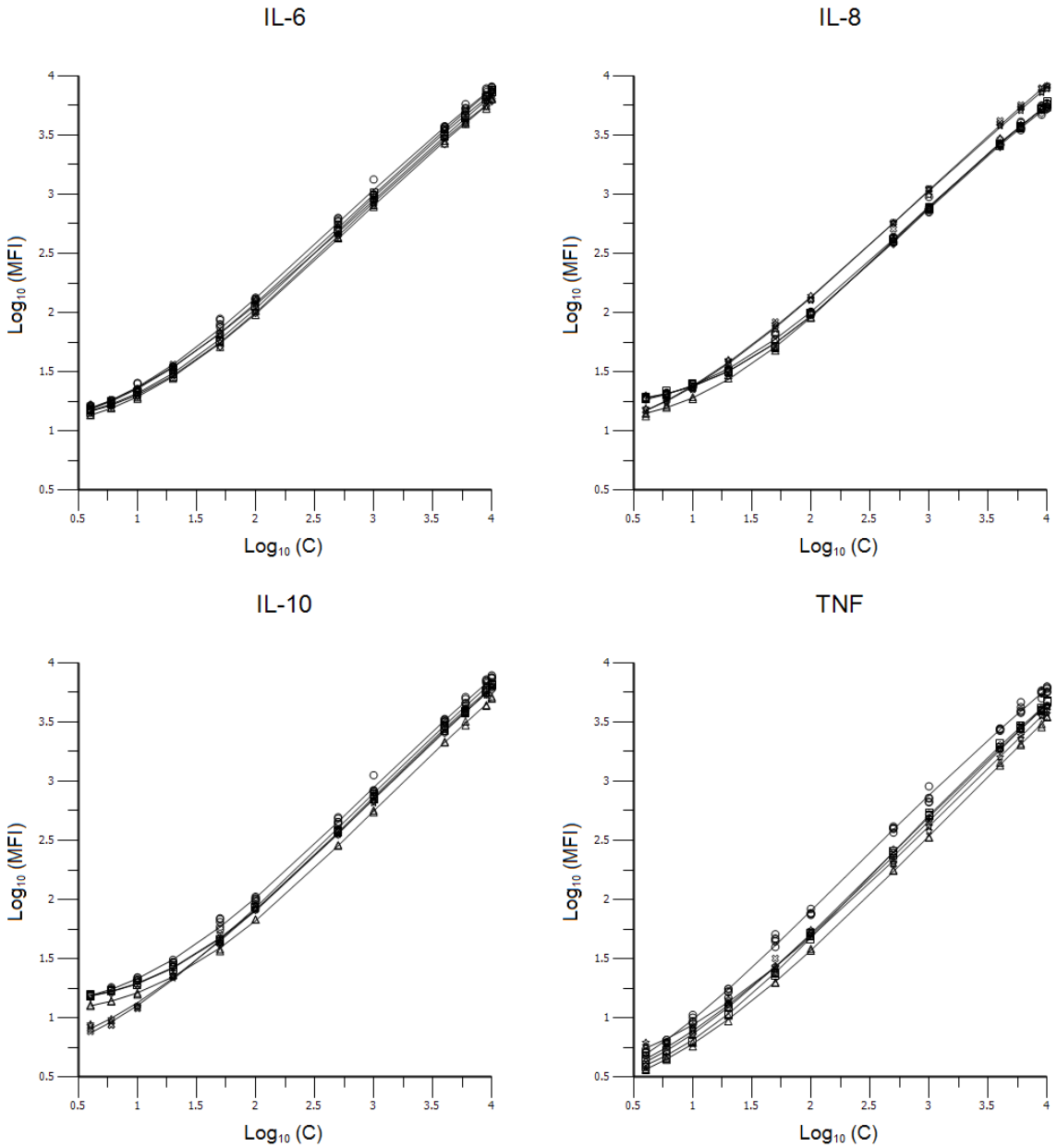

Fig. 3-1: MFI of calibration solutions in dependency of nominal concentration at six validation days. Symbols: Validation day 1 (□), 2 (○), 3 (◊), 4 (Δ), 5 (※), 6 (*)

Placement of QC samples on microtitre plate

Imprecision and inaccuracy of randomly placed QC replicates were not increased regarding QC replicates located next to Cal samples (see Tab. 3-5). CV and RE of sequentially placed QC replicates were ≤11.4% and ≤±15.7%, respectively, whereas these quality criteria of randomly placed QC remained within 13.6% and ±13.0%.

Tab. 3-5: Imprecision (CV, %) and inaccuracy (RE, %) of sequential and randomly placed quality control samples

$Conc_{pred}$ (pg/mL)	CV, %				RE, %			
	IL-6	**IL-8**	**IL-10**	**TNF-α**	**IL-6**	**IL-8**	**IL-10**	**TNF-α**
				Sequentially placed QC				
5	4.40	4.98	4.33	2.60	+0.01	+0.54	-10.9	-13.1
15	4.41	1.22	3.83	3.42	-12.0	-6.85	-13.4	-15.7
200	2.82	4.00	6.66	5.13	-11.2	-6.63	-9.52	-7.55
1000	10.6	2.85	3.33	4.85	+2.70	-2.67	-2.12	+1.43
7000	11.4	4.93	3.57	3.84	-10.1	-0.51	-7.32	-12.6
9500	6.28	5.64	3.11	6.18	-7.09	-1.20	-10.5	-12.5
				Randomly placed QC				
5	7.30	6.41	9.69	13.6	-0.56	-1.64	-8.01	-0.77
15	1.12	8.42	9.94	13.3	-9.34	-2.05	-13.0	-8.85
200	9.00	2.38	10.8	11.6	-8.42	-12.8	-10.2	-6.33
1000	5.02	2.08	7.45	7.97	-5.77	-2.36	-5.76	-1.96
7000	12.8	4.17	5.77	10.0	+1.60	-2.80	-7.73	-7.08
9500	7.28	3.59	5.85	7.10	-5.59	+2.94	-0.59	-10.5

Analyst replacement (inter-analyst reproducibility)

QC samples, analysed by a second, ‘untrained’ analyst, were within validation acceptance limits for ligand binding assays of the EMA Guideline on BMV [17] (see Tab. 3-6). Inaccuracy of 96% of QC replicates were ≤±18.4% RE, whereas imprecision of the complete QC set ranged between 0.90% and 16.1% CV.

Tab. 3-6: Imprecision (CV, %) and inaccuracy (RE of the means, %) of quality control samples analysed by a second analyst

$Conc_{pred}$ (pg/mL)	CV, %				RE, %			
	IL-6	**IL-8**	**IL-10**	**TNF-α**	**IL-6**	**IL-8**	**IL-10**	**TNF-α**
5	7.94	5.32	16.1	15.0	+7.66	-7.81	+9.58	-1.40
15	3.91	0.90	6.00	3.83	-4.00	-1.10	+2.53	+2.08
200	11.7	3.84	7.37	7.13	-9.34	-10.2	-3.86	-8.36
1000	10.7	7.20	7.15	11.1	-6.99	-13.7	-1.67	-4.36
7000	2.77	3.72	1.44	4.88	+8.04	+4.09	-8.81	-2.12
9500	6.33	1.82	4.82	3.86	-4.90	-2.04	-20.8	-16.4

Reinjection reproducibility of processed samples

Reinjected QC generated lower fluorescence signals than samples injected beforehand as exposed by the absolute calculated concentrations and deviations between concentrations of QC samples injected first and reinjected (see Tab. 3-7). These concentrations were calculated from the calibration curve of the first injection.

Tab. 3-7: Concentration and deviation (with respect to the first injection) of injected and reinjected QC (calculated by non-linear regression of Cal of the first injection)

$Conc_{nom}$ [pg/mL]	**$Conc_{calc}$ [pg/mL] first injection**				**$Conc_{calc}$ [pg/mL] reinjection**				**Deviation, %**			
	IL-6	**IL-8**	**IL-10**	**TNF-α**	**IL-6**	**IL-8**	**IL-10**	**TNF-α**	**IL-6**	**IL-8**	**IL-10**	**TNF-α**
15	12.4	13.3	13.5	14.6	9.58	11.1	13.0	14.0	-23.0	-16.6	-3.65	-3.79
200	169	176	183	168	139	136	151	140	-17.8	-23.0	-17.4	-16.6
7000	6794	7052	7055	7233	6478	6277	5986	6629	-4.66	-11.0	-15.2	-8.35

Cytokine concentrations of all three reinjected QC were below the concentrations of the first injection with predominantly high inter-injection differences (58% of deviations higher than 15%). These differences fluctuated between the cytokines at the three concentrations, a general trend in the cytokine concentration changes was thus not observed.
Since the mentioned processes were not limited to QC samples, reinjected Cal solutions had to reveal lower signals as well. Therefore, RE of the observed QC concentrations of reinjection decreased when calculated via reinjected Cal compared to the RE of reinjected QC concentrations calculated via Cals of the first injection (Tab. 3-8 and Tab. 3-9).

Tab. 3-8: Concentrations and relative error (RE,%) of reinjected QC (calculated by non-linear regression of Cal of the first injection)

$Conc_{pred}$ [pg/mL]	**$Conc_{obs}$ [pg/mL]**				**RE, %**			
	IL-6	**IL-8**	**IL-10**	**TNF-α**	**IL-6**	**IL-8**	**IL-10**	**TNF-α**
15	9.58	11.1	13.0	14.0	-36.1	-26.1	-13.4	-6.64
200	139	136	151	140	-30.4	-32.2	-24.6	-30.0
7000	6478	6277	5986	6629	-7.46	-10.3	-14.5	-5.30

In Tab. 3-9 the prerequisite of the reinjection of Cal additionally to samples, which have to be reanalysed, was demonstrated (RE decreased regarding Tab. 3-8). RE were occasionally outside the limit of 20%.

Tab. 3-9: Concentrations and relative error (RE,%) of reinjected QC (calculated by non-linear regression of reinjected Cal)

$Conc_{pred}$ [pg/mL]	$Conc_{obs}$ [pg/mL]				RE, %			
	IL-6	IL-8	IL-10	TNF-α	IL-6	IL-8	IL-10	TNF-α
15	11.6	15.9	15.6	15.1	-23.0	+6.23	+4.32	+0.52
200	150	174	170	147	-25.2	-12.8	-15.0	-26.7
7000	6936	7223	6626	7014	-0.92	+3.18	-5.35	+0.20

Imprecision was calculated from four replicates of Cal 500 pg/mL from injection and reinjection (see Tab. 3-10). CV were slightly increased for the reinjected Cal solution, however, all CV were more than 10% lower than the acceptance limit of 20%.

Tab. 3-10: Mean concentrations and imprecision (CV, %) of injected and reinjected Cal 500 pg/mL (n=4, calculated by non-linear regression of $Cal_{injected}$ and $Cal_{reinjected}$, respectively)

$Conc_{obs}$ [pg/mL]				CV, %			
IL-6	IL-8	IL-10	TNF-α	IL-6	IL-8	IL-10	TNF-α
Cal							
528	534	550	533	4.96	2.88	4.73	8.67
Cal reinjected							
520	522	530	515	9.38	5.30	6.46	8.89

pH value of sample matrix

Concentration measurements of IL-6 and IL-8 were not influenced by the pH value of the matrix solution as deviation in the mean concentration of the replicates was within intra-assay inaccuracy of ±20% (±25% at the lower limit of quantification). One aliquot of the low concentration of IL-8 showed only 74.8% concentration recovery at pH 8. However, concentration recovery of IL-10 and TNF-α remarkably decreased when de- or increasing pH from 7 (see Fig. 3-2). At pH 5 and pH 8, IL-10 concentration recovery of differently spiked solutions exceeded the intra-assay inaccuracy limits by 7.97% to 59.6%, except for the high concentration at pH 8. TNF-α concentration recoveries of the low and intermediate concentrations were reduced at pH 5 and pH 8 down to 3.72% and 69.3%, respectively, while deviation of the high-concentrated solution did not exceed intra-assay inaccuracy of ±20% at pH 5 and pH 8.

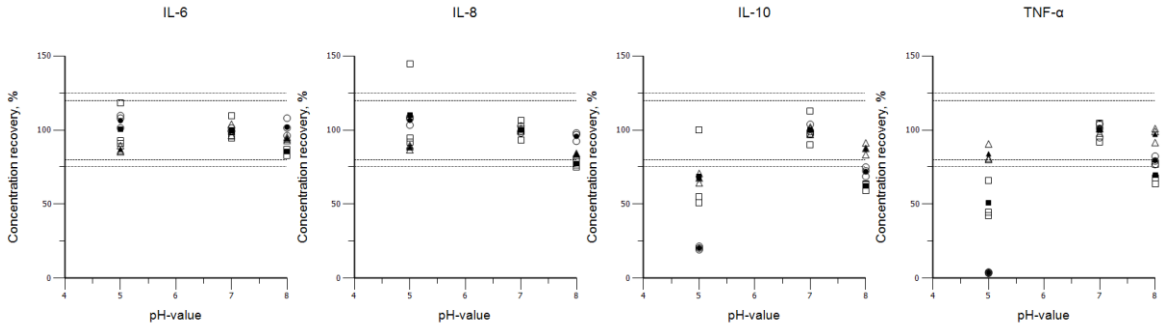

Fig. 3-2: Influence of pH value on concentration recovery (n=3) for the four cytokines. Symbols: spiked concentrations of 10^1 pg/mL (□), 10^2 pg/mL (○) and 10^4 pg/mL (Δ); means of concentration recovery (filled symbols), ±20% (---), ±25% (···) intra-asssay inaccuracy limits.

3.1.2.7 Inter-laboratory comparability: Comparison of in-house Cal with NIBSC/WHO standards

Tab. 3-11: Calculated ratios of the mean logarithmic MFI of in-house and NIBSC Cal

C_{nom} [pg/mL]	Ratio of mean $log(MFI_{In\text{-}house})/log(MFI_{NIBSC})$			
	IL-6	**IL-8**	**IL-10**	**TNF-α**
4.00	0.99	0.98	1.06	1.02
6.00	1.00	0.98	1.13	1.06
10.0	1.00	0.99	1.16	1.13
20.0	0.98	0.96	1.12	1.05
50.0	0.97	0.94	1.07	1.05
100	1.00	0.97	1.12	1.08
500	1.00	0.98	1.09	1.06
1000	0.99	0.97	1.07	1.05
4000	0.99	0.97	1.03	1.02
6000	0.98	0.97	1.03	1.03
9000	0.99	0.98	1.04	1.04
10000	1.00	0.98	1.03	1.03
Mean	**0.99**	**0.97**	**1.08**	**1.05**
CV, %	***0.96***	***1.25***	***4.12***	***3.06***
Min	0.97	0.94	1.03	1.02
Max	1.00	0.99	1.16	1.13

Calculated concentration results of in-house and NIBSC Cal are listed in Tab. 8-17. Inter-replicate variability of NIBSC Cal was similar to in-house Cal (NIBSC: CV ≤20.9%, 41 of 48 samples <10%; in-house: CV ≤15.3%, 46 of 48 samples <10%). Accuracy (related to non-linear regression of in-house Cal) differed substantially between the two sets of Cal (NIBSC: RE ≤±50.7%, 10 of 48 samples <±10%; in-house: RE ≤±14.3%, 46 of 48 samples <±10%). Systematic deviations of the signals were observed for IL-8, IL-10 and TNF-α shown by Tab. 8-17 and Fig. 8-7.The signal-concentration relations of IL-6 were approximately congruent. The other cytokines showed approximately parallel curve shapes when visually inspected. For IL-8, the NIBSC Cal distinctly exceeded the in-house Cal, while for IL-10 and TNF-α, the NIBSC Cal considerably deceeded the in-house Cal solutions. Since the curve shapes were approximately parallel, ratios between logarithms of the MFI for the twelve Cal

concentrations of the two sets should amount to similar values across the different concentrations. Consequently, calculation of the ratios would provide a potential tool for comparison of study samples between different laboratories. Ratio results are presented in Tab. 3-11. For IL-6 from Cal 20.0, 50.0 and 6000 pg/mL, the ratio deviated the most from '1' as also observed in Fig. 8-7 resulting from Cal signals deviating from the typical MFI-concentration relation.

For IL-8, Cal 50.0 pg/mL and for IL-10 as well as TNF-α, Cal 10.0 pg/mL showed ratios the most deviating from '1'. Variability of the ratios over the concentration range increased for IL-10 and TNF-α compared to the other cytokines.

For comparison of the analysis results with BD stated conversion factors, the ratio of the nominal and the calculated concentrations of the NIBSC Cal was determined over the concentration range.

Tab. 3-12: Calculated ratios of nominal and mean observed concentrations of NIBSC Cal

C_{nom} [pg/mL]	Ratio of NIBSC C_{nom}/C_{calc}			
	IL-6	**IL-8**	**IL-10**	**TNF-α**
4.00	0.86	0.68	1.56	1.02
6.00	1.03	0.75	2.03	1.37
10.0	0.96	0.75	1.83	1.64
20.0	0.98	0.75	1.66	1.33
50.0	0.89	0.72	1.47	1.30
100	0.96	0.83	1.64	1.34
500	0.93	0.82	1.58	1.38
1000	0.94	0.82	1.56	1.34
4000	0.98	0.78	1.42	1.31
6000	0.92	0.73	1.40	1.35
9000	0.93	0.73	1.43	1.36
10000	0.86	0.69	1.27	1.24
Mean	**0.94**	**0.75**	**1.57**	**1.33**
CV, %	***5.41***	***6.64***	***13.0***	***10.2***
Min	0.86	0.68	1.27	1.02
Max	1.03	0.83	2.03	1.64

Ratios provided by BD were as follows: Concerning BD CBA Flex Set Standards (at 2500 pg/mL, 1 CBA standard batch), ratios of 1.25 (IL-6), 1.04 (IL-8), 1.01 (IL-10) and 1.54 (TNF-α) were published; for BD CBA Kit Standards (at 2500/5000 pg/mL, 1 CBA standard batch), calculations of 1.01 (IL-6), 0.74 (IL-8), 1.14 (IL-10) and 1.38 (TNF-α) were indicated [185].

Stated ratios of NIBSC and BD CBA Flex Set Standards should at least approximately be consistent with calculated ratios of Tab. 3-12. However, in-house ratios did not simply diverge from BD ratios, the trends of the ratios for the four cytokines compared to one another tremendously varied as well. Consequently, ratios published by BD cannot be used to compare concentration measurements from other laboratories to measurements with the here-presented method.

3.1.3 Recommendations for in-study validation acceptance limits

Based on the results of the bioanalytical method validation and on experiences obtained throughout the process of method development and validation, the following recommendations for in-study validation performance and their acceptance criteria were generated: QC samples replicated (at least measured in duplicate) at a minimum of four concentrations, one LLOQ (5 pg/mL), one within three times of the LLOQ (low QC, 15 pg/mL), one in the midrange (middle QC, 200 pg/mL), and one approaching the high end of the range (high QC, 9500 pg/mL), have to be incorporated into the individual runs. Additionally, the other validated QC solutions (1000 pg/mL and 7000 pg/mL) can be included in an optional manner. The results of the QC samples provide the basis of accepting or rejecting the run.

At least 67% of QC samples should be within the acceptance criteria (Tab. 3-13); a maximum of 33% of QC samples (not all replicates at the same concentration) is permitted to be outside the presented inaccuracy range from the nominal value.

Tab. 3-13: In-study-acceptance criteria of RE and CV (intraassay, interassay) over the validated concentration range

Cytokine	**Range of concentration**	**Intraassay**		**Interassay**	
		Maximal Imprecision	**Maximal Inaccuracy**	**Maximal Imprecision**	**Maximal Inaccuracy**
	(pg/mL)	**CV, %**	**RE, %**	**CV, %**	**RE, %**
IL-6	≥5 - ≤10	25	±25	25	±25
	> 10 - ≤10000	20	±20	20	±20
IL-8	≥5 - ≤10	40	±40	25	±25
	> 10 - ≤10000	20	±20	20	±20
IL-10	≥5 - ≤10	30	±30	25	±25
	> 10 - ≤10000	20	±20	20	±20
TNF-α	≥5 - ≤10	30	±30	25	±25
	> 10 - ≤10000	20	±20	20	±20

3.2 Project II: *In vitro* microdialysis of cytokines

3.2.1 Influence of microdialysis-system settings

Stability of cytokines over up to 6 h at 37 °C

Measurements of cytokine concentrations of the catheter-surrounding medium, which was sampled at 37 °C in intervals of 2 h over a period of 6 h, did not reveal IL-6 and IL-8 degradation over the investigated time. Stability ranged from 101% to 110% (CV: 1.53%-5.86%) for IL-6 and from 97.1% to 97.5% (CV: 2.76%-6.99%) for IL-8, respectively. IL-10 concentrations were within limits of postulated stability over that period of time as well, though a trend of decreasing concentrations was observed: mean recoveries at 2 h, 4 h and 6 h were found to be 90.3% (CV: 10.8%), 85.8% (CV: 2.06%) and 84.5% (CV: 4.30%). For TNF-α, degradation was observed with stability below 80% for the last occasion: concentrations were 88.5% at 2 h, 83.9% at 4 h and 75.7% at 6 h (CV ≤4.21%). Therefore, TNF-α containing solutions cannot be stored at 37 °C for more than 2 h. However, if the initial concentration gradient between the catheter-surrounding medium and the µPerfusate is sufficiently high and concentrations are determined frequently for RR and rD calculations, slow degradation of TNF-α does not limit *in vitro* µD investigations.

Loss of sample volume by ultrafiltration or evaporation

Fig. 3-3 shows the medians of µDialysate volume recovery values determined at the different FR, complemented by the observed minima and maxima (left panel) of 36 measurements each. The dispersion of the determined volumes was widened by individual outliers as demonstrated by the interval between the 10^{th} and 90^{th} percentiles (right panel), which was distinctly decreased compared to minimal and maximal data.

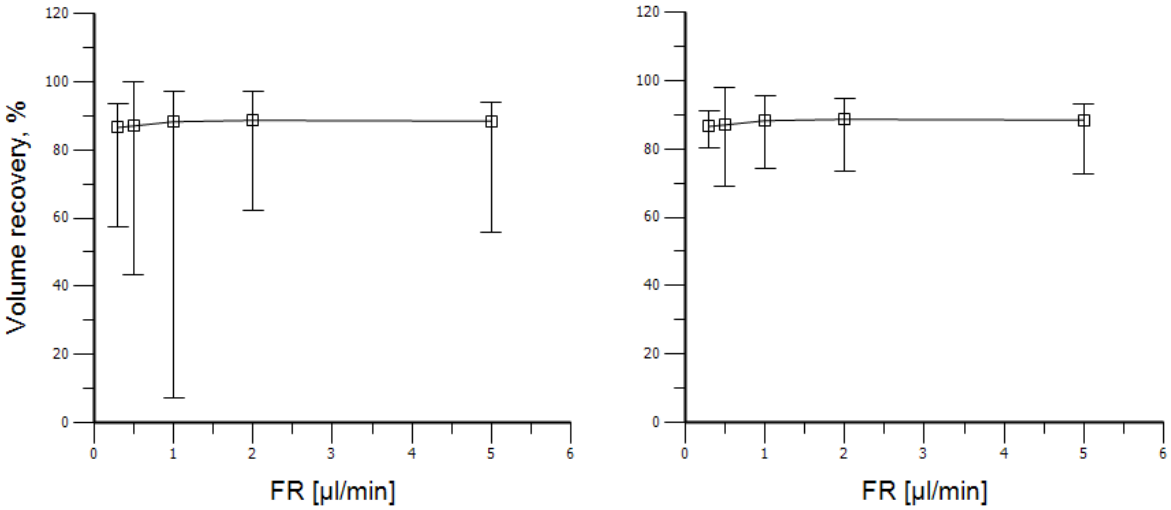

Fig. 3-3: Volume recovery of *in vitro* microdialysate samples vs. flow rate (FR). Symbols: Median (squares), Min-Max (error bars, left panel), 10th-90th percentiles of measured volumes (error bars, right panel)

The median volumes negligibly increased from the lowest FR (0.3 µL/min) to 1.0 µL/min (86.5% to 88.2%) and remained virtually constant at the higher FR (88.6% at 2.0 µL/min and 88.4% at 5.0 µL/min). In order to investigate potential differences caused by the temperature of the catheter-surrounding medium, the volume recoveries were stratified by temperature (ca. 25 °C and 37 °C) and compared (see Fig. 3-4).

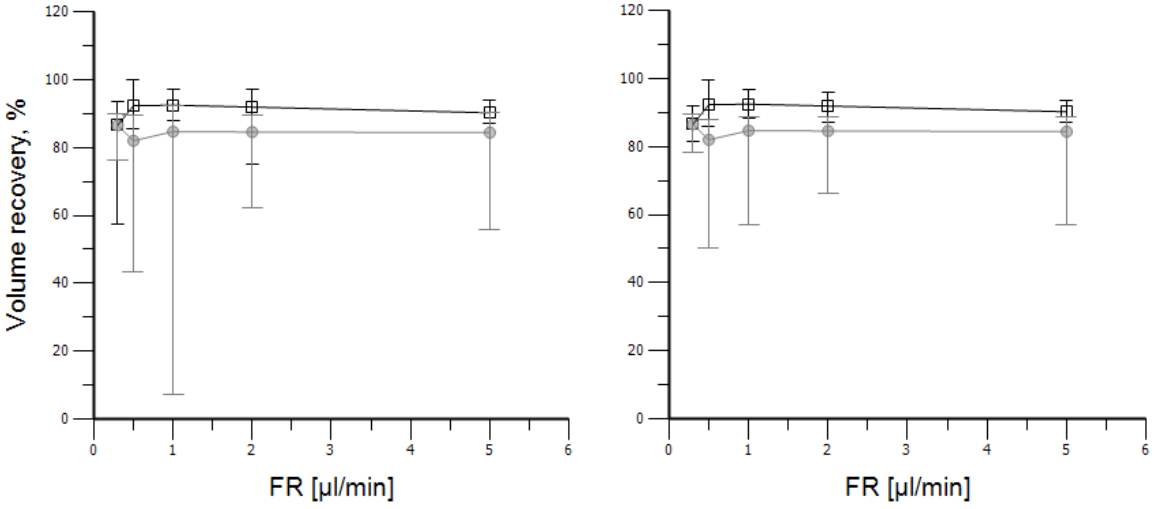

Fig. 3-4: Volume recovery of *in vitro* microdialysate samples vs. flow rate (FR) stratified by temperature: 25 °C (black) and 37 °C (grey). Symbols: Median (squares, circles), Min-Max (error bars, left panel), 10th-90th percentiles of measured values (error bars, right panel)

Loss of volume was found to be increased at 37 °C (13.8% median loss over all FR) compared to the lower temperature (25 °C, 11.3%) of the catheter-surrounding medium. However, the differences in volume recovery between 25° C and 37 °C were not statistically significant for individual FR ($p>0.2$, Kruskal-Wallis test). This fact was similarly observable by

the overlapping of the 10th percentile of 25 °C and the 90th percentile of 37 °C in Fig. 3-4 (right panel).

To assess whether the volume loss was due to UF or evaporation processes, fluid evaporation was preliminary examined individually and independently from µD-membrane-mediated fluid loss. For a fluid temperature of 25 °C and RT of approximately 22 °C, pure evaporation throughout the longest µD intervals of approximately 200 min (i.e. at 0.3 µL/min) was 11.2% compared to 13.1% for a fluid temperature of 37 °C and approximately 24 °C RT. For short µD intervals (e.g. at 2.0 µL/min), evaporation was reduced to 0.93% (in 30 min) for the low temperature and 3.23% (in 18 min) for the high temperature, respectively. Consequently, loss of fluid volume was not fully accounted for by pure evaporation and UF partially had to cause volume loss as well. The extent of the UF effect was not quantifiable by the data of these preliminary investigations. Consequently, the influence of evaporation and UF on the RR and rD data is currently not determinable as well.

3.2.2 Adsorption of cytokines to the catheter components

Assay signals of IL-6, IL-8, IL-10 and TNF-α caused by solutions with high cytokine concentrations having passed through µD tubing did not change over the investigated time period of 4 h (Fig. 3-5, left panel); signals (i.e. MFI) did not exceed deviations of ±15% and were not significantly different from signals of the perfused solution before entering the µD catheter (mean (CV) of pure solution (n=3) vs. mean (CV) of adsorption samples (n=21): 793 (1.04%) vs. 834 (4.90%) for IL-6, 582 (3.09%) vs. 624 (3.70%) for IL-8, 379 (3.13%) vs. 378 (4.52%) for IL-10 and 209 (5.97%) vs. 216 (5.47%) for TNF-α; $p>0.05$ (t-test) except for IL-8). Although for IL-8 non-difference of the means was not shown ($p<0.01$, t-test), the mean of solutions passing the tubings was not lower, as expected, but higher than the mean of the µPerfusate samples. Consequently, it was concluded that IL-8 signal deviation was caused by analytical inaccuracy of up to ±17% (see 3.1.2.3, Tab. 3-2), other unknown factors or by pure chance and that IL-8 as well as the other three cytokine molecules did not adhere to the inner tubing surface.

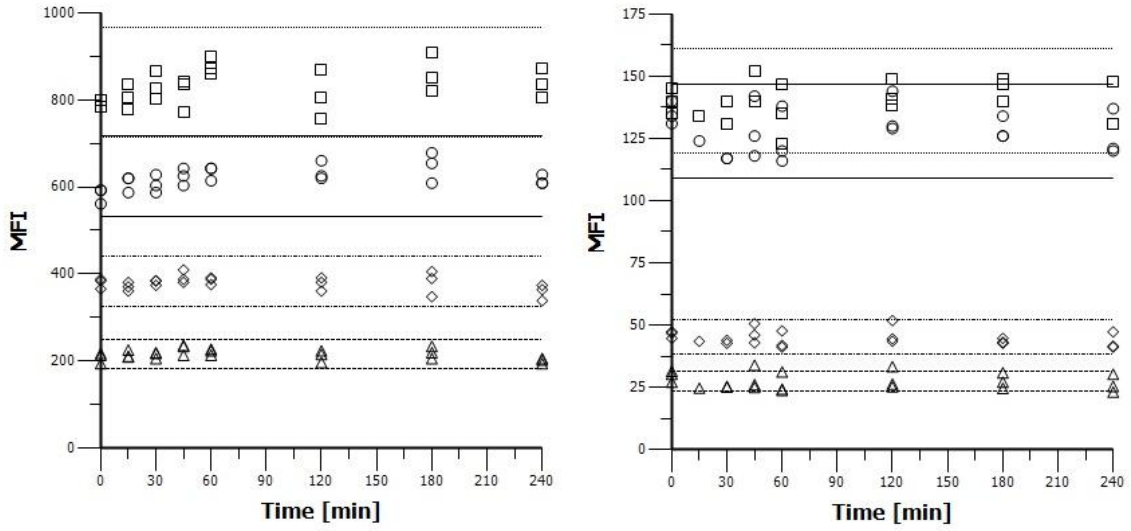

Fig. 3-5: Assay signals (median fluorescence intensities, MFI) of high (left panel) and low concentrated (right panel) cytokine solutions before (time=0 min) and after inlet tubing passage (n= 3 experiments each). Symbols: MFI of IL-6 (□), IL-8 (○), IL-10 (◊) and TNF-α (Δ), Lines: ±15% of overall means for (IL-6 (···), IL-8(—), IL-10 (-·-·-) and TNF-α (---)

The same non-adsorptive behaviour over 4 h was observed for low cytokine concentrations of solutions passing a 0.38 mm-diameter tubing (Fig. 3-5, right panel). Signals were not significantly different from signals of the perfusate (mean (CV) of pure solution (n=3) vs. mean (CV) of adsorption samples (n=18): 140 (3.6%) vs. 140 (5.6%) for IL-6, 135 (3.3%) vs. 127 (7.1%) for IL-8, 46.3 (2.9%) vs. 44.5 (6.9%) for IL-10 and 29.7 (7.6%) vs. 27.0 (12.5%) for TNF-α; $p>0.05$, t-test)).

Assay signals of the solutions of the medium with and without µD membrane and 100 mm tubing did not considerably vary either (MFI of pure solution (n=3) vs. solution containing µD membrane and tubing (n=3): 1793-1936 vs. 1730-1962 for IL-6, 1714-1777 vs. 1639-1859 for IL-8, 1133-1207 vs. 1008-1240 for IL-10 and 2547-2889 vs. 2266-3050 for TNF-α).

Consequently, adsorption of cytokines to the µD catheter components was not observed. This fact simplified the performance of the following *in vitro* and *in vivo* µD investigations, since precautionary measures accounting for adsorption were not required.

3.2.3 Dependence of relative recovery and relative delivery on flow rate

Recovery and delivery data were not normally distributed and homogeneity of µD results from the three individual catheters in the experiments could not be verified. Therefore, RR and rD data were tested non-parametrically and as paired (Wilcoxon signed-rank and Friedman test) within experiments and are presented showing the entire range of replicates.

Dependence of relative recovery on flow rate at 25 °C and 37 °C

RR versus FR at two different temperatures (see also Tab. 8-18) and non-linear regression of these relations are presented in Fig. 3-6.

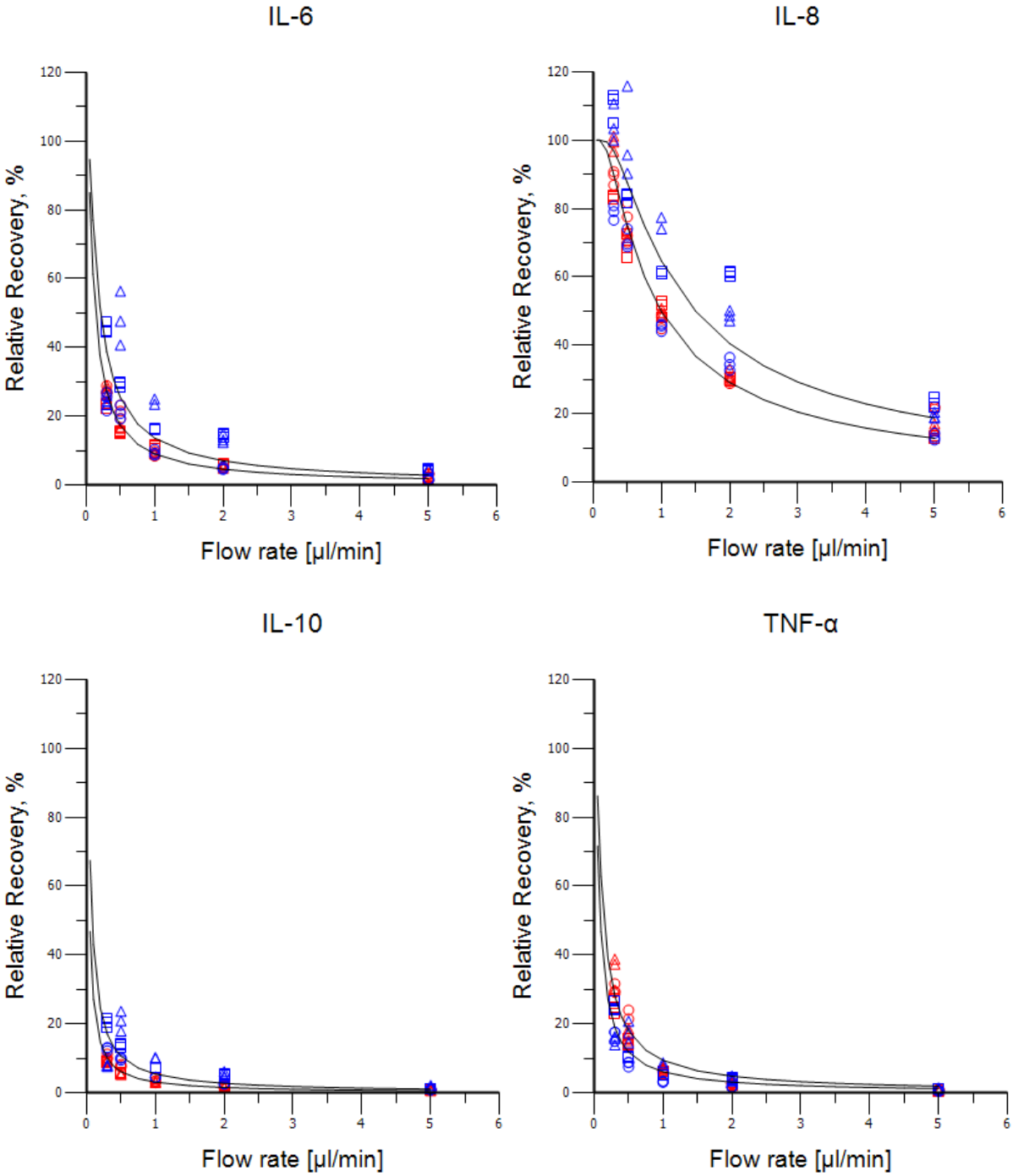

Fig. 3-6: Flow rate dependence of relative recovery (n=3) for IL-6, IL-8, IL-10, and TNF-α. Symbols: Three catheters (□, ○ and Δ), at a temperature of catheter-surrounding medium of 25 °C (red) and 37 °C (blue); non-linear regression lines (—)

RR of the individual cytokines decreased with increasing FR as expected. The range of RR over FR extensively differed for the four cytokines: IL-8 showed the highest values (12.4%-116%) followed by IL-6 (1.46%-56.4%), TNF-α (0.50%-38.8%) and IL-10 (0.62-23.7%). Thus,

the mass transfer coefficients *r* of the non-linear regression (see section 2.6.5) varied as well: IL-8 displayed the highest *r* values (0.0146 mm/min and 0.0221 mm/min), followed by IL-6 (0.0020 mm/min and 0.0031 mm/min), TNF-α (0.0021 mm/min and 0.0013 mm/min), and IL-10 (0.0007 mm/min and 0.0012 mm/min) at the temperatures of 25 °C and 37 °C, respectively, with correlation coefficients of the non-linear regression curves of ≥0.7629.

Intra-catheter imprecision of RR (n=3) revealed acceptable values at 25 °C. I.e., for each catheter at an individual FR, the range of RR (Min-Max) related to the median RR at this specific FR was ≤37.7% (62% of the median-related ranges ≤9.94%). At 37 °C the ranges were ≤37.3% (53.3% of the median-related ranges ≤9.88%). However, inter-catheter imprecision of RR (n=9) was ≤82.5% (70% of the ranges related to the median RR of all catheters ≤49.1%) and ≤129% (5% of the median-related ranges ≤35.2%) for the two temperature settings, respectively. Accordingly, RR showed increased variability between the catheters at 37 °C compared to 25 °C.

For IL-6, IL-8 and IL-10, RR values at 37 °C were mainly higher than at 25 °C. For TNF-α opposite results were obtained. Mass transfer coefficients were significantly different between the two temperature settings for the four cytokines (Fig. 3-7, left panel).

Dependence of relative delivery on flow rate at 25 °C and 37 °C

Fig. 3-8 depicts rD over FR at two different temperatures and the results from non-linear regression of these relations. rD of the individual cytokines decreased with increasing FR except for IL-10 at 37 °C. The range of rD over FR extensively differed between the four cytokines and even negative rD values occurred: IL-8 showed the highest rD (2.69%-92.0%), followed by IL-6 (-47.9%-48.4%), TNF-α (-36.7%-38.6%) and IL-10 (-39.3%-23.5%). Since negative values were considered not to be plausible and rational rD data, non-linear regression of rD over FR was confounded for IL-6, IL-10, and for TNF-α. IL-10 in particular showed a large number of negative rD values due to its extremely low membrane passing characteristics (see also RR results above). Therefore, values of the mass transfer coefficients *r* for IL-6, IL-10, and TNF-α should not be calculated and compared. The mass transfer coefficients *r* of the non-linear regression (see section 2.6.5) of rD for IL-8 was found to be 0.0159 mm/min and 0.0231 mm/min (correlation coefficients ≥0.9756) for 25 °C and 37 °C, respectively (see Fig. 3-7, right panel).

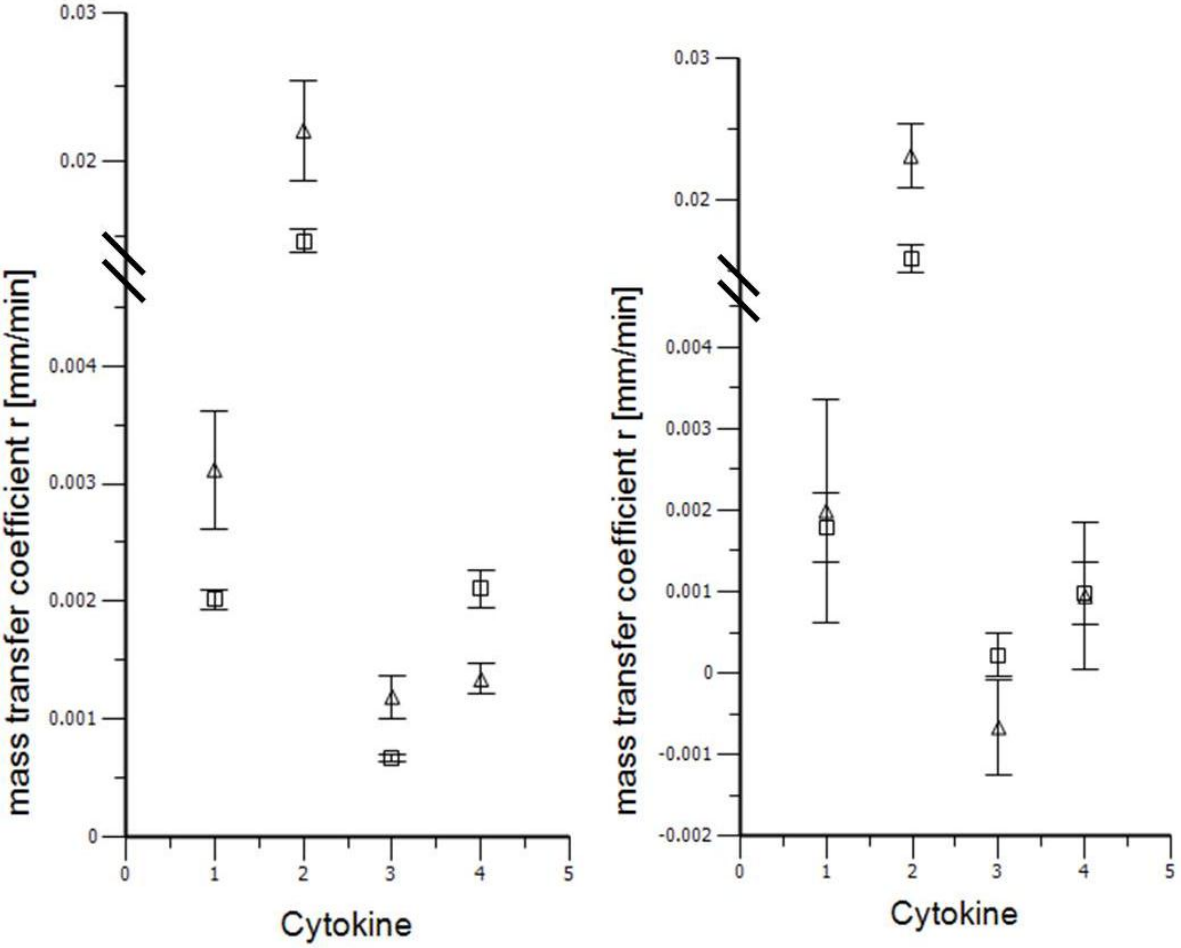

Fig. 3-7: Mass transfer coefficients *r* (error bars: 95% confidence interval) of the individual cytokines (1=IL-6, 2=IL-8, 3=IL 10, 4=TNF-α). Coefficients were estimated by non-linear regression from the relative recoveries (left panel) and the relative deliveries (right panel) at 25 °C (□) and 37 °C (Δ)

Intra-catheter imprecision of rD (n=3) for IL-8, calculated as range (Min-Max) at an individual FR related to the median value at this specific FR, was less or equal 74.4% (73% of ranges ≤8.05%) and 89.8% (79% of ranges ≤7.91%) at the two temperature settings, respectively. Inter-catheter imprecision of rD (n=9) of IL-8 was 10.4%, 11.1%, 35.7%, 43.8% and 110% at 25 °C and was 2.24%, 6.75%, 15.5%, 42.3% and 99.9% at 37 °C for individual FR of 0.3, 0.5, 1.0, 2.0 and 5.0 µL/min, respectively. Consequently, rD showed comparable variability between the individual samples and the catheters at the two different temperatures. rD values itself at 37 °C were predominantly higher than at 25 °C (Fig. 3-8). Accordingly, mass transfer coefficients were significantly different between the two temperature settings for IL-8 (see Fig. 3-7, right panel).

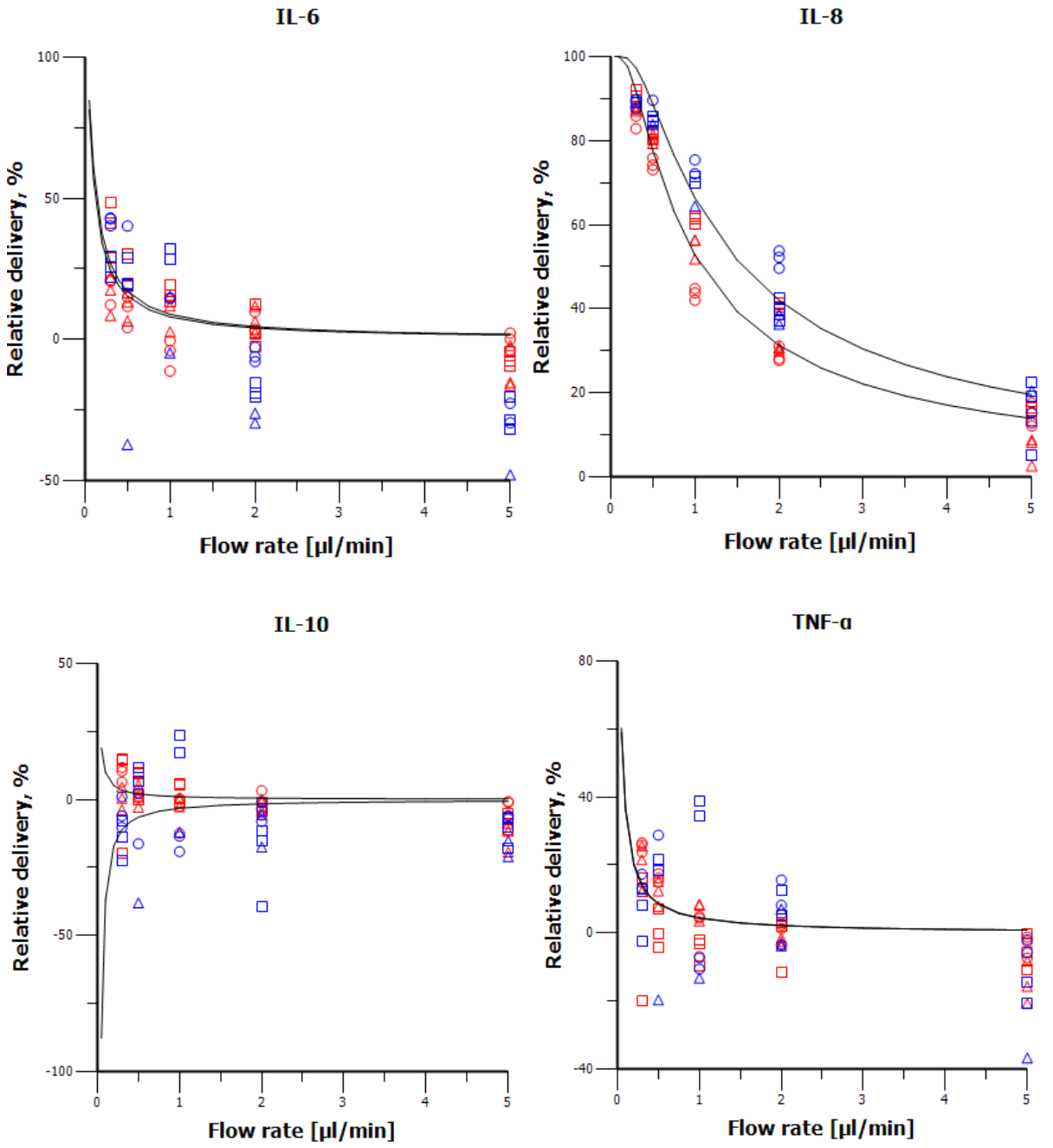

Fig. 3-8: Flow rate dependence of relative delivery (n=3) for the four cytokines. Symbols: Three catheters (□, ○ and Δ), at 25 °C (red) and 37 °C (blue) catheter-surrounding medium temperature, non-linear regression lines (—)

A systematic distribution of the negative values could not be confirmed, but a tendency for negative rD with higher FR and at the increased temperature was observed: The percentage of negative rD (all cytokines, all catheters) added up to 8.4% for FR of 0.3 µL/min as well as 0.5 µL/min, 31% for 1.0 µL/min, 25% for 2.0 µL/min and 69% for 5.0 µL/min at 25 °C and 26% for 0.3 µL/min, 19% for 0.5 µL/min, 35% for 1.0 µL/min, 58% for 2.0 µL/min and 76% for 5.0 µL/min at 37 °C .

Comparison of relative recovery and relative delivery

Measurements of µPerfusate revealed slightly higher variability than analysis of concentrations of the catheter-surrounding medium at 37 °C: the relative standard error of the mean (rSEM, see section 2.9) for all µPerfusate samples of one experiment was 3.98%-6.63%, whereas rSEM for all catheter-surrounding medium samples of one experiment was 1.94%-2.86%. Changes of concentrations between two subsequent time points did not follow any trend, and was thus considered to result from bioanalytical imprecision or to be of random error nature and not due to e.g. stability problems. Random errors could, for example, have been caused by phenomena of inhomogeneity.

Due to the negative rD values found for IL-6, IL-10 and TNF-α, rD and RR were solely comparable for IL-8 (see Fig. 3-9): rD and RR values equally decreased with increasing FR both at 37 °C and 25 °C. The mass transfer coefficients *r* of the non-linear regression for IL-8 were 0.0159 mm/min and 0.0146 mm/min for rD and RR at 25 °C and 0.0231 mm/min and 0.0221 mm/min at 37 °C, respectively. Comparison of mass transfer coefficients between rD and RR settings did not reveal any significant differences for IL-8 at 25 °C or 37 °C (see Fig. 3-10).

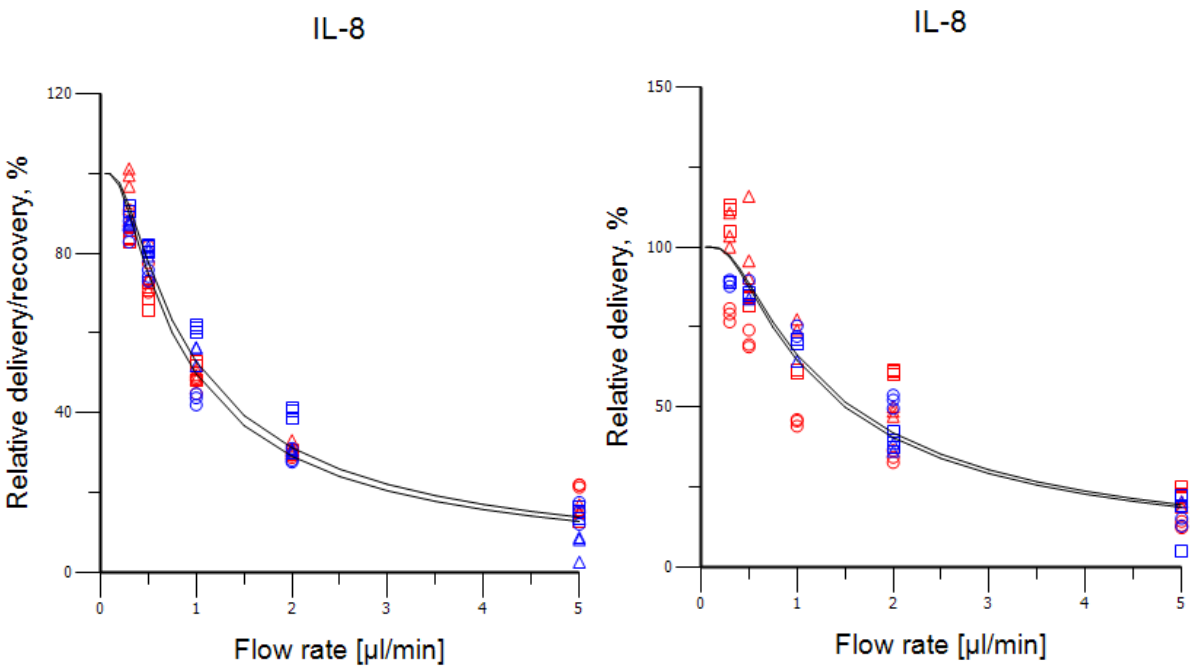

Fig. 3-9: Flow rate dependence of relative delivery (blue) and recovery (red) (n=3) for IL-8 at 25 °C (left panel) and 37 °C (right panel). Symbols: 3 catheters (□, ○ and Δ), non-linear regression lines (—)

Intra-catheter imprecision was considerably increased for rD at 25 °C and 37 °C (ranges related to the median: ≤74.4% and ≤89.8%, see previous subsection) compared to RR (ranges related to the median: ≤37.7% and ≤37.3%, see above). Inter-catheter imprecision of

rD was equal or less 110% at 25 °C and 99.9% at 37 °C, and thus, in the same magnitude as ranges of RR (≤82.5% and ≤129%).

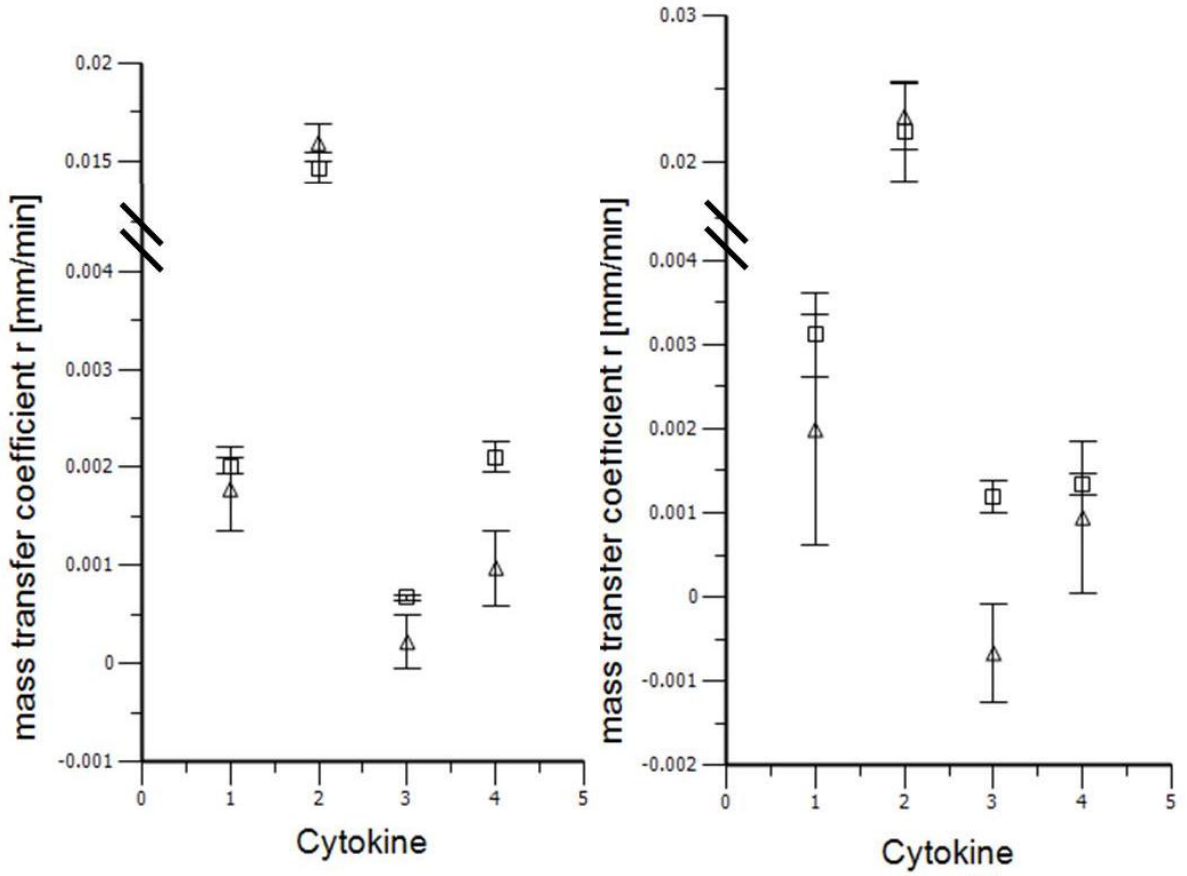

Fig. 3-10: Mass transfer coefficients r (error bars: 95% confidence interval) of the individual cytokines (1=IL-6, 2=IL-8, 3=IL 10, 4=TNF-α). r values were estimated by non-linear regression from the relative recoveries (□) and deliveries (∆) at 25 °C (left panel) and 37 °C (right panel)

3.2.4 Prediction of concentrations of the catheter-surrounding medium by non-linear regression of microdialysate concentrations

Comparison of observed and predicted cytokine µDialysate concentrations for recovery investigation at 37 °C are illustrated in Fig. 3-11. The cytokine concentrations of the medium (for recovery experiments) and the µPerfusate (for delivery experiments) were estimated by application of Eq. (14) and Eq. (15) (see section 2.6.6), respectively, as one parameter of the non-linear regression function, i.e. cytokine concentrations at a FR of 0 µL/min (C_{medium} or $C_{\mu Perfusate}$).

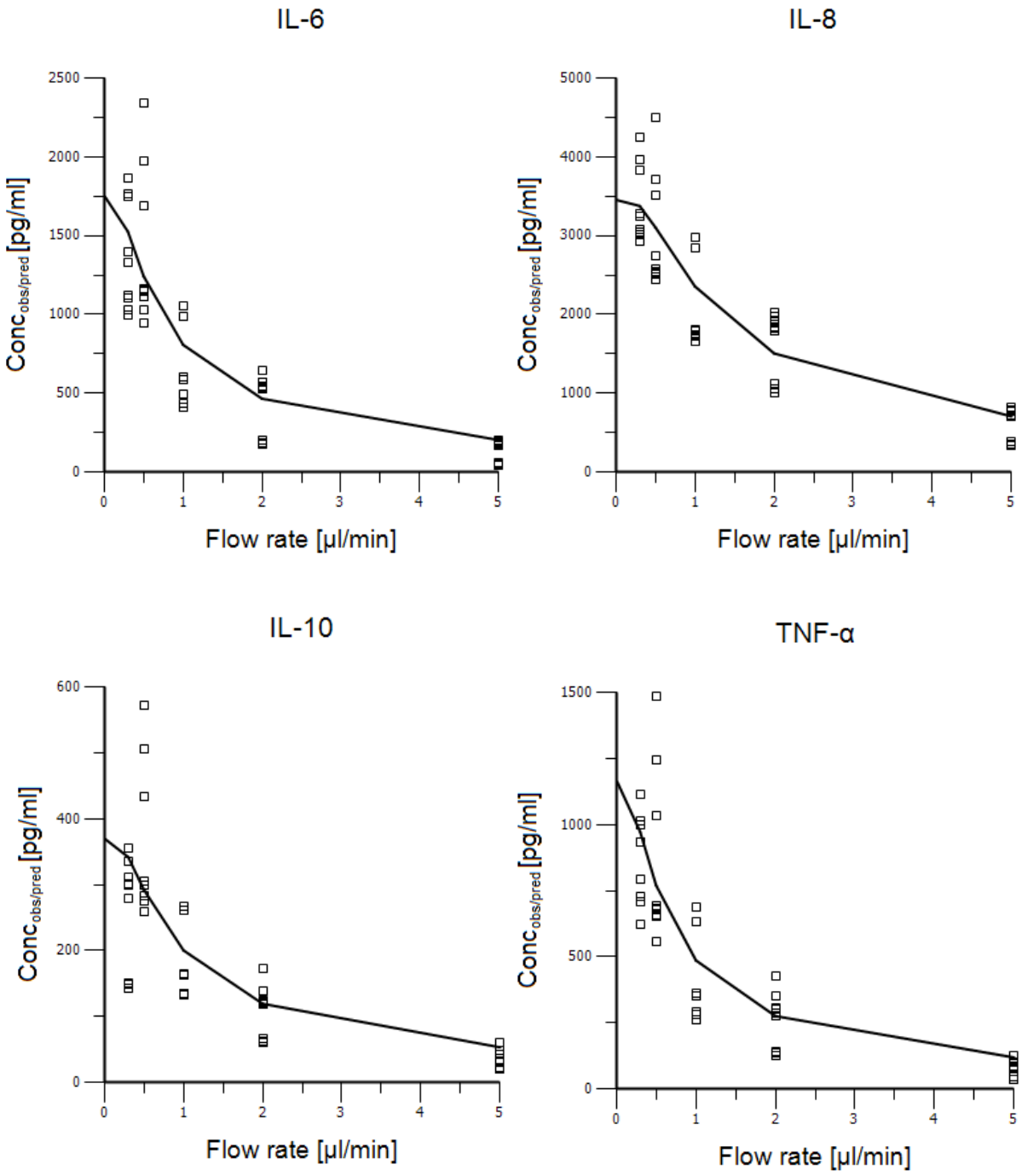

Fig. 3-11: Observed (□) and predicted (line) microdialysate concentrations of *in vitro* recovery investigation vs. flow rate at 37 °C

Columns three to five of Tab. 3-14 show the results of the non-linear regression in comparison to the observed mean medium or µPerfusate concentration over all investigated FR of the individual experiments. In this way, the predictions basing on µDialysate data of the *in vitro* experiments, which will be the only available type of data in the following *in vivo* µD investigation (see section 3.3), were compared to the measured concentrations to assess the accuracy of this approach.

Tab. 3-14: Observed mean concentrations [pg/mL] (± standard deviations) of medium (recovery experiments) and microperfusate (delivery experiments), corresponding concentrations estimated by non-linear regression and relative deviations. Non-linear regression of data over all flow rates (FR) and selected FR of 1, 2 and 5 µL/min.

Cyto-kine	Investigation	All FR			FR:1-5 µL/min		
		Observed $C_{medium/\mu Perfusate}$	Estimated $C_{medium/\mu Perfusate}$	Dev, %	Observed $C_{medium/\mu Perfusate}$	Estimated $C_{medium/\mu Perfusate}$	Dev, %
IL-6	Recovery, 25 °C	6914 (±374)	3037	-56.1	6934 (±434)	1467	-78.8
	Recovery, 37 °C	4172 (±564)	1746	-58.1	4048 (±448)	2472	-38.9
IL-8	Recovery, 25 °C	5941(±313)	5389	-9.29	6000 (±356)	3744	-37.6
	Recovery, 37 °C	3468 (±470)	3451	-0.49	3445 (±314)	3980	+15.5
	Delivery, 25 °C	6793 (±248)	6611	-2.68	6740 (±198)	7713	+14.4
	Delivery, 37 °C	4338 (±713)	4132	-4.75	4761 (±340)	8007	+68.2
IL-10	Recovery, 25 °C	4908 (±252)	894	-81.8	4956 (±275)	981	-80.2
	Recovery, 37 °C	2361 (±415)	369	-84.4	2560 (±302)	1190	-53.5
TNF-α	Recovery, 25 °C	7889 (±706)	10353	+31.2	8242 (±626)	4110	-50.1
	Recovery, 37 °C	6970 (±1500)	1160	-83.4	7889 (±707)	2170	-72.5

Non-linear regression of the lost fractions of the concentrations of IL-6, IL-10 and TNF-α from delivery experiments was not realisable due to high variability and occurrence of negative values. For recovery experiments, medium concentrations of these three cytokines were not appropriately estimated (RE between observed and estimated concentrations: -84.4% up to +31.2%). However, catheter-surrounding medium as well as µPerfusate concentrations of IL-8 were adequately calculable for recovery and delivery investigations (RE: -9.29% up to -0.49%).

Constant concentrations of the catheter-surrounding fluid are not likely to occur in *in vivo* investigations, in particular over a long period of time. To result in conditions comparable to *in vivo* calculations, the calculation was repeated for a reduced sample set, i.e. for FR investigated in a shorter period of time (see Tab. 3-14, three columns on the right). Concentration data were selected for FR of 1.0 µL/min, 2.0 µL/min and 5 µL/min due to short µD intervals for sample collection. The assumption of moderately constant ISF concentrations is rather suitable for the short time period of 21 to 108 min than for a prolonged period of three and a half to six hours at FR of 0.5 µL/min and 0.3 µL/min (refer to

section 2.7.1.1). Predicted concentrations showed increased inaccuracy for IL-8 up to ±68.2%; however, estimations were appropriate for recovery measurements at 37 °C (RE: +15.5%), most likely representing *in vivo* conditions. Parameter estimations for the other cytokines revealed considerable underestimations of the concentrations of the surrounding fluid to an extent comparable to a regression utilising the entire range of FR. Consequently, predictions of the ISF concentrations from *in vivo* µDialysate data applying the flow-rate-variation method (see section 3.3.6) can only be accurately performed for IL-8.

3.2.5 Dependence of relative recovery on concentration

Since previous investigations revealed differences in adjustments of the catheter-surrounding medium temperature, settings for the following examinations were selected such as applying optimal µD adjustments (see section 4.2.3) and representing *in vivo* conditions. For this purpose, to reduce the number of influencing factors and for the reason that delivery experiments yielded implausible, irreproducible results for IL-6, IL-10 and TNF-α, exploration of the dependence of the extraction fraction on varying concentrations was performed at a temperature of 37 °C and at a FR of 0.5 µL/min only in recovery experiments (i.e., utilising a catheter-surrounding medium spiked with cytokines).

Fig. 3-12 shows RR values in relation to concentrations of the catheter-surrounding medium. The different ranges of RR values of the four individual cytokines are underlined by this diagram as well: the median RR of this individual experiment at 37 °C and FR of 0.5 µL/min were 21.4%, 94.0%, 7.00% and 5.72% for IL-6, IL-8, IL-10 and TNF-α, respectively. RR did not vary over the concentration range for all cytokines. The linear regression slopes of RR values vs. concentrations of the medium were -0.0009 (95% CI: -0.0053 - +0.0035), -0.0005 (-0.0053 - +0.0044), 0.0005 (-0.0023 - +0.0034) and -0.00008 (-0.0010 - +0.0008) for IL-6, IL-8, IL-10 and TNF-α, respectively, and thus, approximately equal to zero as zero was within the CI.

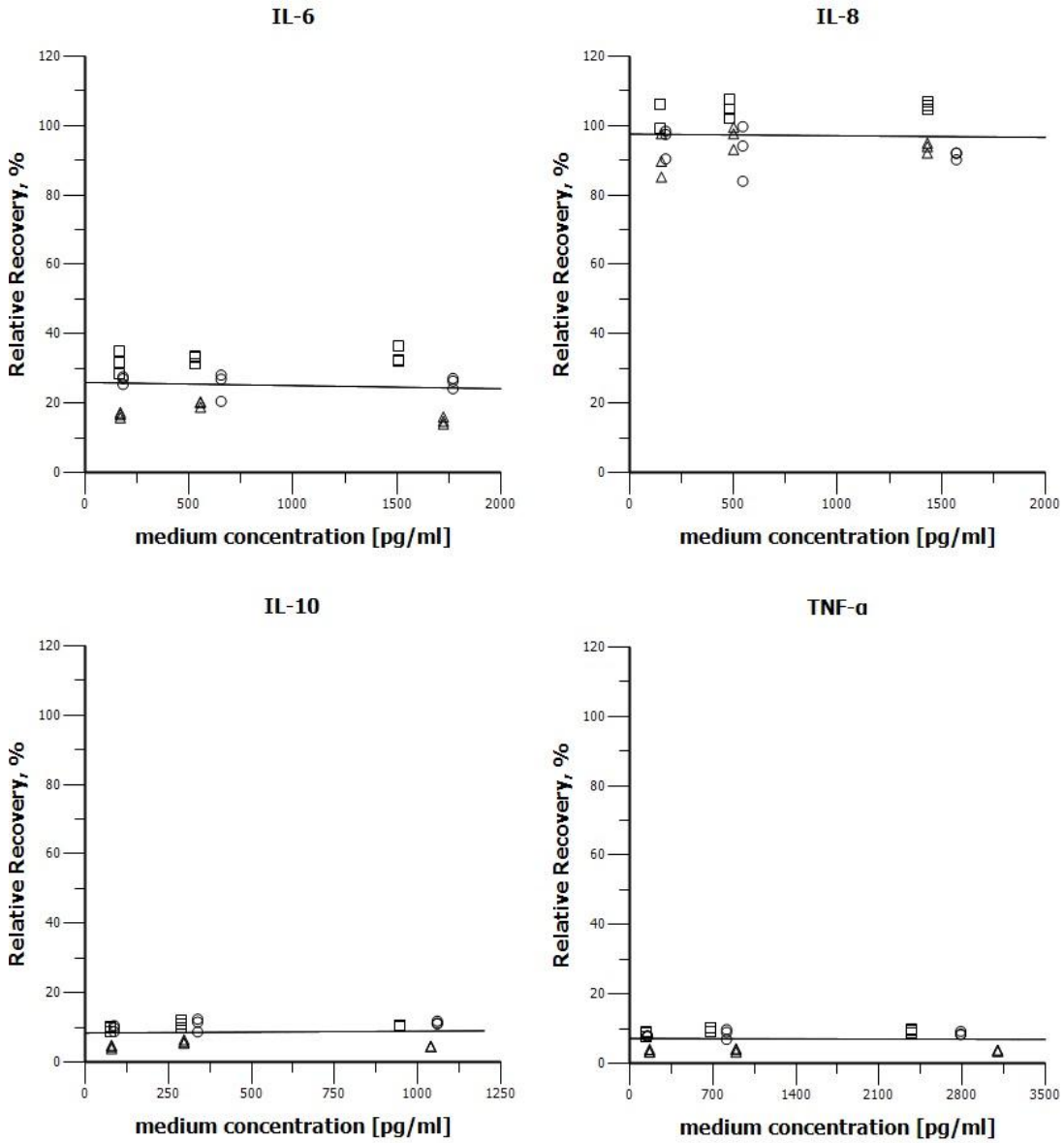

Fig. 3-12: Relative recovery of the four cytokines vs. concentrations of the catheter-surrounding medium. Experiment was performed three times. Symbols: Three catheters (□, ○ and ∆), linear regression lines (—)

3.2.6 Effect of pH value on relative recovery

RR of IL-8 at different pH values of catheter-surrounding medium did not indicate any dependence on the pH value (see Fig. 3-13). RR of IL-6 remained constant at pH 5 (28.4%-44.1%) and pH 7 (26.4%-42.2%), but decreased at pH 8 (14.1%-21.3%). For IL-10 and TNF-α, RR increased with increasing pH values (pH 5, 7 and 8, respectively: 0.91%-5.62%, 10.9%-19.0% and 13.4%-34.6% for IL-10 and 0.95%-14.2%, 11.9%-18.1% and 13.0%-57.3% for TNF-α). Values for these two cytokines revealed higher intra- and inter-catheter variability than those for IL-6 and IL-8: the inter-catheter ranges related to the median RR at

the specific pH value were between 58.0% and 112% for IL-10 and between 43.6% and 316% for TNF-α, respectively, whereas for IL-6 and IL-8 these ranges were between 9.65% and 44.8%. The intra-catheter ranges related to the median RR at the specific pH value ranged from 8.78% to 33.8% for IL-10 and from 15.3% to 288% for TNF-α, respectively, whereas for IL-6 and IL-8 these ranges were between 2.64% and 26.8%.

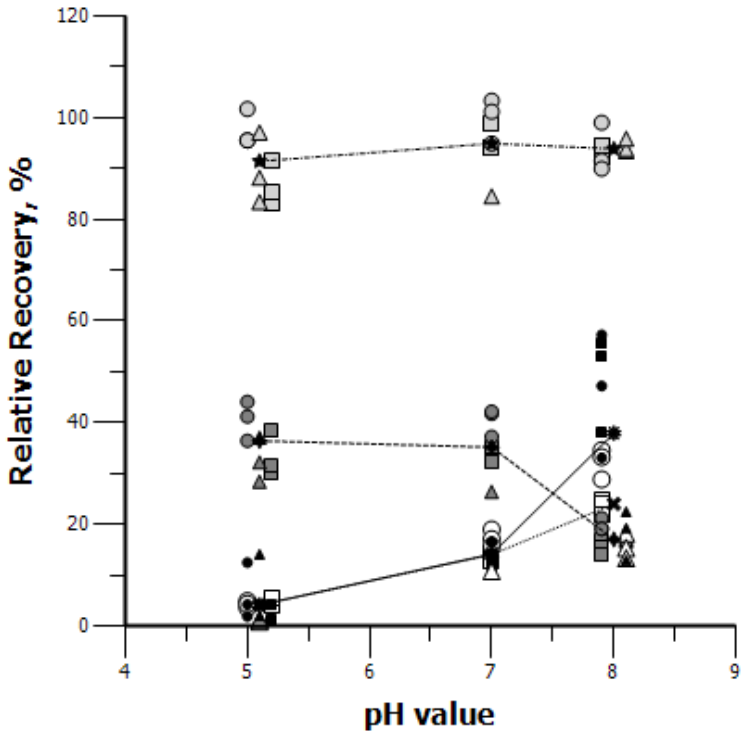

Fig. 3-13: Influence of pH value on relative recovery (n=3) for the four cytokines. Symbols: Three catheters (□, ○ and Δ), colours: IL-6 (grey), IL-8 (light grey), IL-10 (white), TNF-α (black); Median values for IL-6 (four-point star), IL-8 (five-point star), IL-10 (cross), TNF-α (ten-point star) connected by lines. Isoelectric points: 6.5 (IL-6), 8.6 (IL-8), 8.0 (IL-10), 5.6 (TNF-α)

No statistically significant difference was shown between different pH values ($p=0.87$, Friedman test) for RR of IL-8. Comparing RR at the individual pH values by Wilcoxon signed-rank test, IL-6 RR were not significantly different for pH 5 and 7 ($p=0.81$). However, RR at pH 7 and 8 revealed a significant difference ($p<0.001$). RR of IL-10 and TNF-α significantly varied for pH 5 and 8, respectively, compared to pH 7 ($p<0.05$).

3.3 Project III: Long-term pilot study on microdialysis of cytokines in healthy volunteers

3.3.1 Demographic data

Four healthy volunteers (all caucasian) were enrolled in the study. Their demographic data are listed in Tab. 3-15.

Tab. 3-15: Demographics of the individuals 01-04

ID	Sex	Age [Years]	Weight [kg]	Height [cm]	BMI[a] [kg/m^2]
01	female	28	72	167	25.8
02	female	28	69	170	23.9
03	male	36	70	178	22.1
04	female	25	50	165	18.5
Median		28	69.5	168.5	23.0

[a] Body mass index

Three female and one male individual, aged 25 up to 36 years, were enrolled in the study. ID 04 nearly showed underweight and ID 01 was slightly overweighted within the pre-obese range. The remaining two study participants were within the moderate range.

3.3.2 Safety assessment during the clinical study

AE appearing throughout the study period are listed in Tab. 3-16. No serious adverse events appeared and events, occurring during study performance, were predominantly caused by skin punctuation or covering with the transparent adhesive tape. Problems concerning µDialysis sampling were resolved within appropriate time to continue with the study without failing. Severity of the AE did not exceed an intensity of ‘mild’.

Tab. 3-16: Adverse events (AE) occurring in the pilot study. (The entire range of AE was assigned certainly related to the performance of microdialysis or to the *in vivo* microdialysis setting.)

ID	AE	AE onset/end	Severity	Action taken	Outcome
01	Blood drop within microdialysate	First interval of 70 min at study day 1	-	No	Data included in data set
02	Slightly haemolytic microdialysate	First interval of 70 min at study day 1	-	No	Data included in data set
02	Bloody oozing at insertion site	After catheter insertion until ca. 15 min later	Mild	Exchange of transparent adhesive tape	Recovered/ Resolved; data included in data set
02	Skin irritation under transparent adhesive tape	After displacement of adhesive tape for catheter removal	Mild	No	Recovered/ Resolved within a few days
02	Slight haemorrhage from insertion sites	After catheter removal	Mild	No	Recovered/ Resolved within one minute
03	Minimal abrasion of skin covered by outlet tube guide channel	Visible after catheter removal	Mild	No	Recovered/ Resolved within a few days
04	Foreign body sensation at catheter site	Intermittent during all study days	Mild	No	Recovered/ Resolved after catheter removal
04	Pruritus under transparent adhesive tape	Starting from second interval of 4 h at study day 3	Mild	Cooling of skin area with thermal pack	Recovered/ Resolved after catheter removal

The study design (e.g. changing FR) and the preliminary character of this pilot study did not allow evaluating the impact of AE on the cytokine concentration-time course.

3.3.3 Feasibility of long-term application of clinical microdialysis

Long-term µD investigation was performed over ca. 56 h without any drop-outs or µDialysis performance failures. Individuals were able to leave the study site and to proceed with their daily routine throughout the course of the clinical study. Overall, the procedure was well-tolerated by the study participants as well as it was practically performable by the study personnel. µD catheters worked over the entire study duration and were not damaged; perfusion ran consistently, consequently, sampling of µDialysate was performed over time as planned. Some technical problems with regards to the µD system came up, were noted in the CRF, and are listed in Tab. 3-17.

Tab. 3-17: Technical microdialysis events/errors occurring in the pilot study

ID	Event	Onset/end	Action taken	Outcome
01	Microdialysate flow reduced	0 - ca. 1.5 h	Flush of microdialysis system	Resolved; equilibration time extended
01	“Low battery” pump failure	Last interval of 70 min at study day 1	Pump device exchanged	Resolved; data included in data set

The µDialysate flow could be stabilised at the beginning of study day 1 in ID 01 and the µD pump operated in an accurate manner after exchanging the device.The sampling volumes almost unexceptionally reached extents required for bioanalysis; only one out of the eighty study samples from all healthy volunteers had to be diluted with AD prior to sample processing. µDialysate did not run back into the tube of the outlet tubing guide channel during daily sampling, as it had been observed before during µD studies. However, µDialysate accumulating over-night spread to the guide channel and had to be removed before start of µD intervals.

Sample volume loss by ultrafiltration or evaporation

Data concerning acquired µD sampling volumes were separated according to the study days. The first subset described volume recoveries in the course of study day 1, when five subsequent samples were obtained at 0.5 µL/min. Baseline samples could not be used for volume determinations as FR had regularly been changed during baseline sampling due to the initital system flush or manual FR adjustments. The sample volume from the last µD interval at study day 1 in ID 01 was decreased by a pump failure, and thus, excluded from this analysis. The second subset included the volume loss throughout application of the flow-rate-variation method (on days 2 and 3) and thus, provided data directly comparable to volumes obtained from the *in vitro* relative recovery investigations at 37 °C (see section 3.2.1).

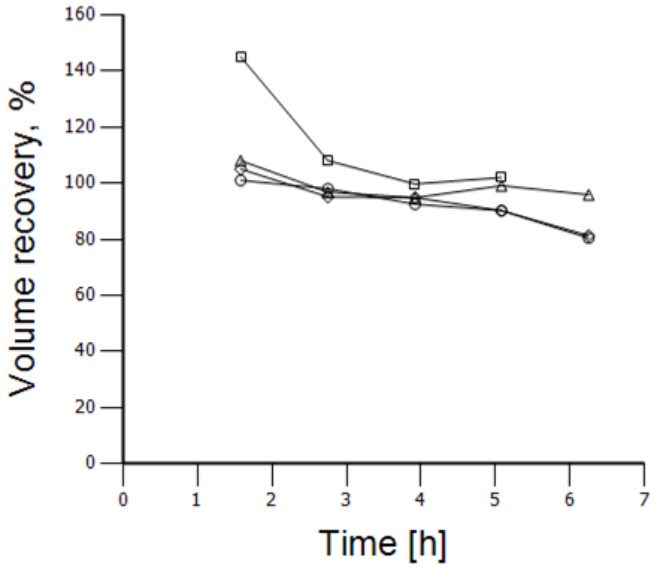

Fig. 3-14: Volume recovery of the individual microdialysate samples at a flow rate (FR) of 0.5 µL/min at the start of study day 1 (first five microdialyis intervals). The x-axis refers to the planned time (i.e. at the middle of the microdialysis interval) after insertion of the microdialysis catheter. Symbols: ID 01 (□), ID 02 (○), ID 03 (◊) and ID 04 (Δ)

Data from the first subset is presented in Fig. 3-14. Volume recovery predominantly showed 100% for the initial samples. A trend concerning decreasing volumes over time was observed for all the individuals with the steepest initial decline in ID 01. Volume recovery in ID 01 and ID 04 approached to 100% at the end of the first study day (102% and 95.9% for the last samples), whereas an approximate loss of 20% in sample volume was finally observed in ID 02 and ID 03 (80.4% and 81.3%). The volume recovery at the following study days did not show any trend (see Fig. 8-8).

Values of the obtained volumes of samples from the varying FR (study day 2 and 3) are illustrated in Fig. 3-15.

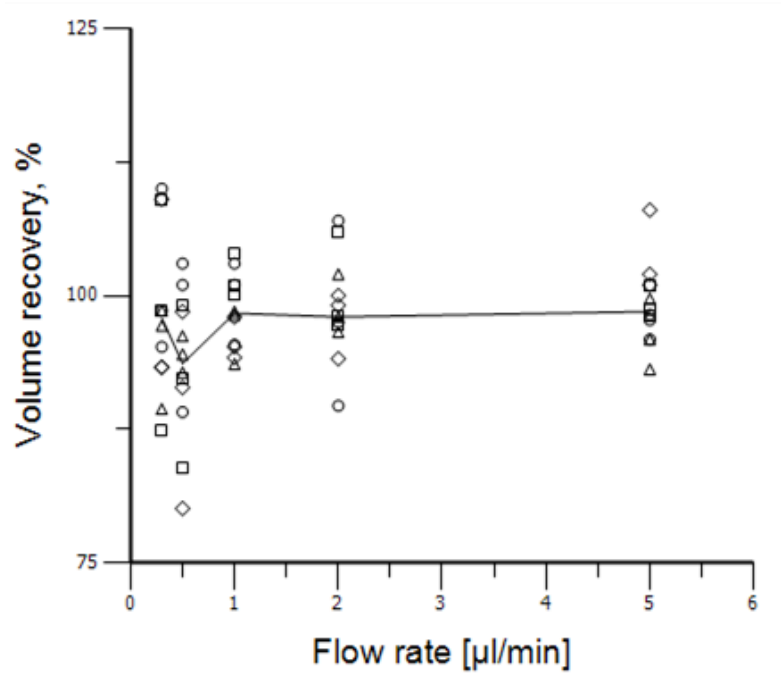

Fig. 3-15: Individual and median (line) volume recovery of the microdialysate samples in dependence on flow rate (FR). Symbols: ID 01 (□), ID 02 (○), ID 03 (◊) and ID 04 (Δ)

Similar to the *in vitro* results (see section 3.2.1), a decrease of fluid volume was demonstrated between 0.3 µL/min and 0.5 µL/min followed by an increase back to the starting value at 1.0 µL/min and a further slight increase of volume recovery at the subsequent FR.

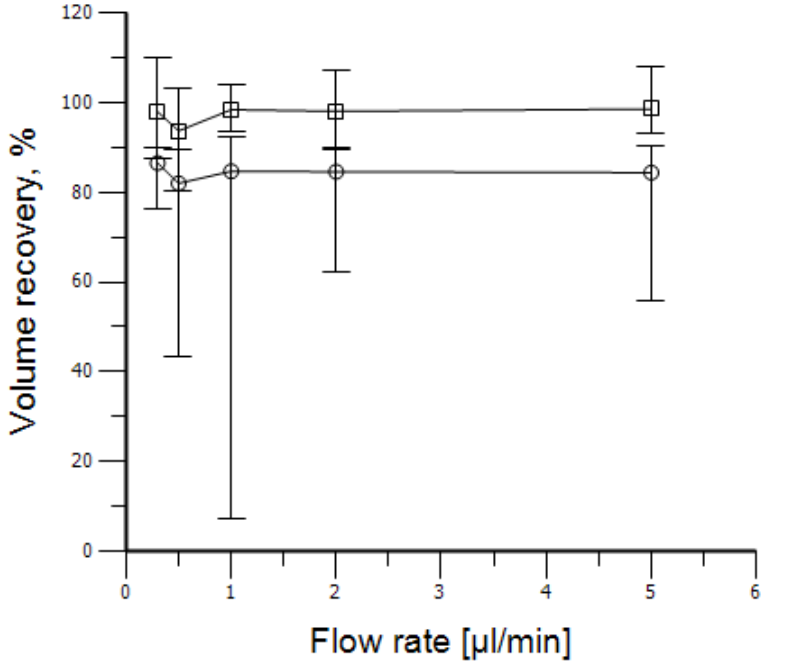

Fig. 3-16: Volume recovery of the microdialysate samples obtained in *in vitro* (recovery/delivery experiments at 37 °C (○)) and *in vivo* (study samples (□)) investigations. Symbols: median ± Min/Max (error bars)

To compare volume loss *in vitro* and *in vivo*, volume recovery data were simultaneously evaluated (Fig. 3-16). This result revealed an approximately parallel course with the lowest volume recovery for both settings at 0.5 µL/min. An almost constant volume loss during all laboratory investigations compared to the pilot study was observed. Deviations between volume recoveries varied between 11.4% at the lowest FR and 14.2% at 5.0 µL/min. Increased variability was observed for *in vitro*- compared to *in vivo* volumes. Differences between *in vitro* and *in vivo* fluid volume loss were statistically significant over the entire FR range ($p<0.001$, Wilcoxon rank-sum test).

3.3.4 Bioanalysis of the study samples

Application of the adapted and validated bioanalytical method (see section 3.1) to the study samples was successfully performed. Quality assessment during the study sample measurements was accomplished by QC samples. The high number of cavities on the used microtitre plate (n=96) enabled bioanalysis of all study samples in only two analytical runs. Both runs met the criteria for precision and accuracy described in the international EMA Guideline on BMV [17], as well as the in-house acceptance limits (see section 3.1.3) and were, therefore, considered as accepted/passing. The results for accuracy and precision supported the results regarding robustness and ruggedness of the method: intra-assay inaccuracy was lower than or equal to ±17.2% RE in the concentration range of 10-10000 pg/mL and ±27.0% RE from 5 pg/mL up to 10 pg/mL; and imprecision maximally reached 12.1% CV. Overall inter-assay RE and CV were within ±18.2% and 15.3%, respectively. Considering individual QC aliquots, one of 36 aliquots was lost due to a pippetting error and 6 out of 140 (4.29%) concentration results exceeded in-study validation acceptance limits (established in section 3.1.3).

3.3.5 Data set and data set checkout

The final data set contained IL-6, IL-8, IL-10, and TNF-α µD concentration data of four healthy individuals as well as their demographic data, and other study characteristics and documentation. 100% of the planned samples (n=20 per ID) were available from the observation period of 56 h. For the investigation of the flow-rate-variation method, fiveteen samples per individual (nine at day 2 and six at day 3) were included, since a period of at least 20 h after µD catheter insertion was considered for cytokine concentrations to attain constant baseline values in ISF again. ‘Kinetic’ analysis of the cytokine concentration-time profiles consisted of eight samples per individual as those were all sampled at the same FR of 0.5 µL/min (five samples at day 1 and three at day 3).

3.3.6 Flow-rate-variation method for calibration of relative recovery of cytokines

Concentrations of the four evaluated cytokines in µDialysate at different FR are presented in Fig. 3-17. IL-10 and TNF-α were excluded from further data analysis, since the two cytokines revealed concentrations below the lower limit of quantification. Further, for ID 01 Fig. 3-17 shows that concentrations of IL-6 and IL-8 did not follow the typical exponentially decreasing course (see section 2.6.6) with increasing FR. IL-6 concentrations from ID 02 slightly decreased from 0.3 µL/min to 0.5 µL/min and escalated at 1 µL/min. Subsequently, cytokine concentrations declined in an approximately exponential course. IL-8 concentrations showed a nearly exponential decrease over the entire FR range. In ID 03 concentration-FR profiles of both cytokines approached to the typical exponential reduction with increasing FR. The differences between courses of the profiles from the three FR investigated at study day 2 (1-5 µL/min) and those from low FR (0.3 µL/min and 0.5 µL/min, study day 3) were particularly obvious for ID 04: while concentrations were low and slightly decreasing at low FR, they tremendously increased at 1 µL/min and successively followed an exponentially decreasing course. The tremendous increase in IL-6 concentrations from 0.5 to 1.0 µL/min was more pronounced in ID 04 than in ID 02.

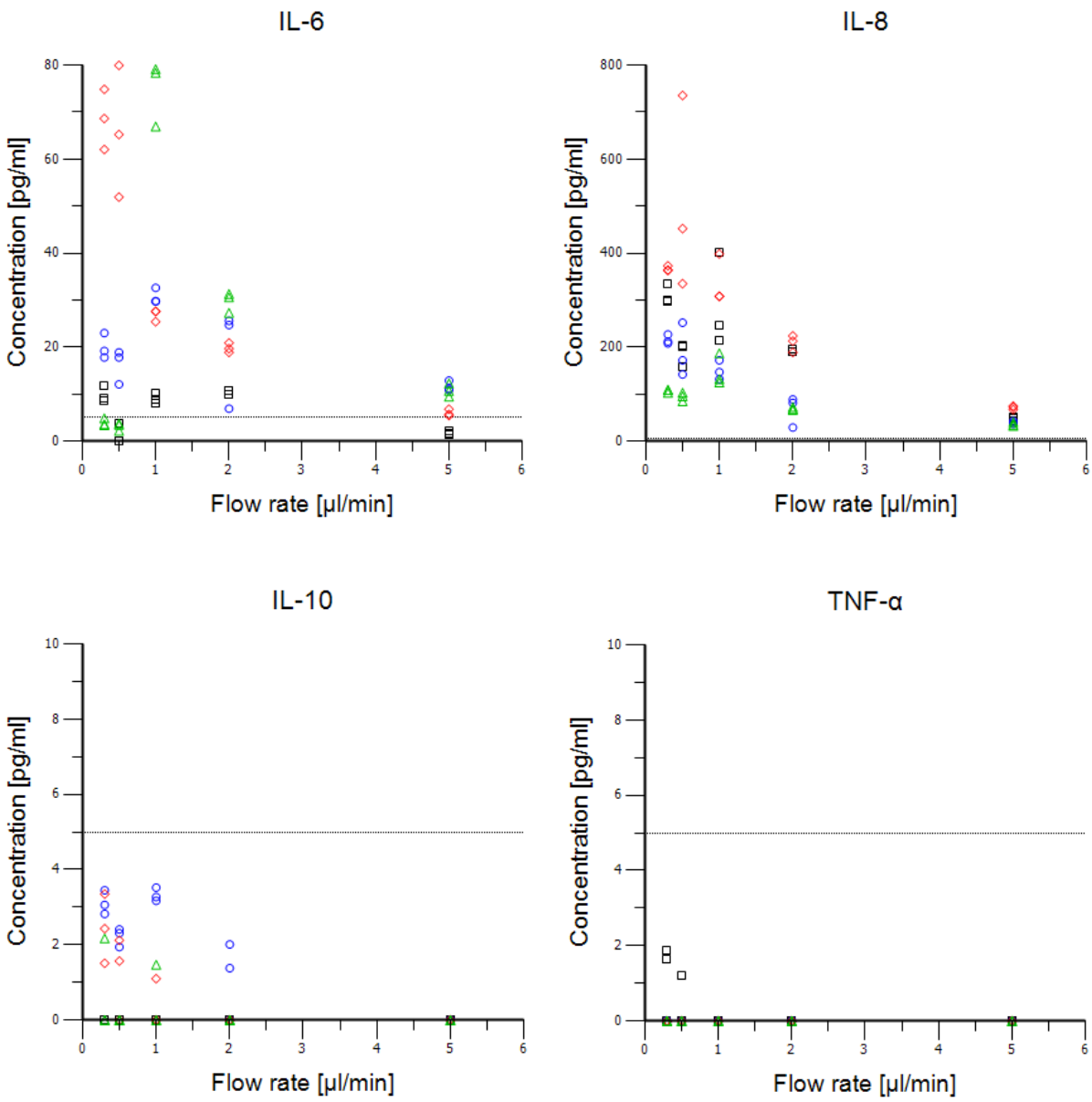

Fig. 3-17: Individual concentrations of IL-6, IL-8, IL-10 and TNF-α from *in vivo* microdialysate in dependence on flow rate (FR). Symbols: ID 01 (□), ID 02 (○), ID 03 (◊) and ID 04 (Δ); LLOQ (···)

In Fig. 3-18 the *in vivo* µDialysate concentrations in the logarithmic scale in relation to FR was compared to results of the *in vitro* recovery investigation at 37 °C (see section 3.2.3). The sample of the third µD interval at FR of 2.0 µL/min for ID 02 showed enormously deviating (low) concentrations of IL-6, IL-8 and IL-10 (TNF-α concentrations were not quantifiable in all samples at 2.0 µL/min). Hence, this sample was considered to be an outlier and was excluded from the non-linear regression.

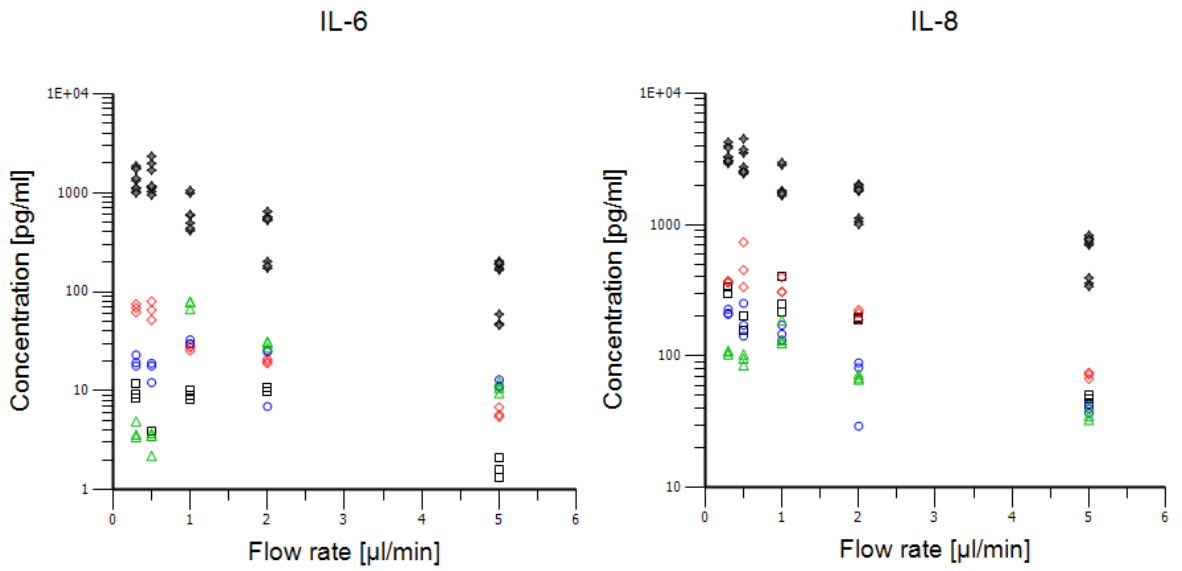

Fig. 3-18: Individual concentrations of IL-6 and IL-8 from *in vivo* and *in vitro* (✧) microdialysate in dependence on flow rate (FR). Symbols: ID 01 (□), ID 02 (○), ID 03 (◊) and ID 04 (Δ)

Profiles of IL-6 and IL-8 for ID 03 and ID 04 (1 µL/min to 5 µL/min) were comparable to *in vitro* profiles of these cytokines. Concerning IL-8, µDialysate concentrations in ID 02 visually followed an exponential couse as in the *in vitro* experiments.

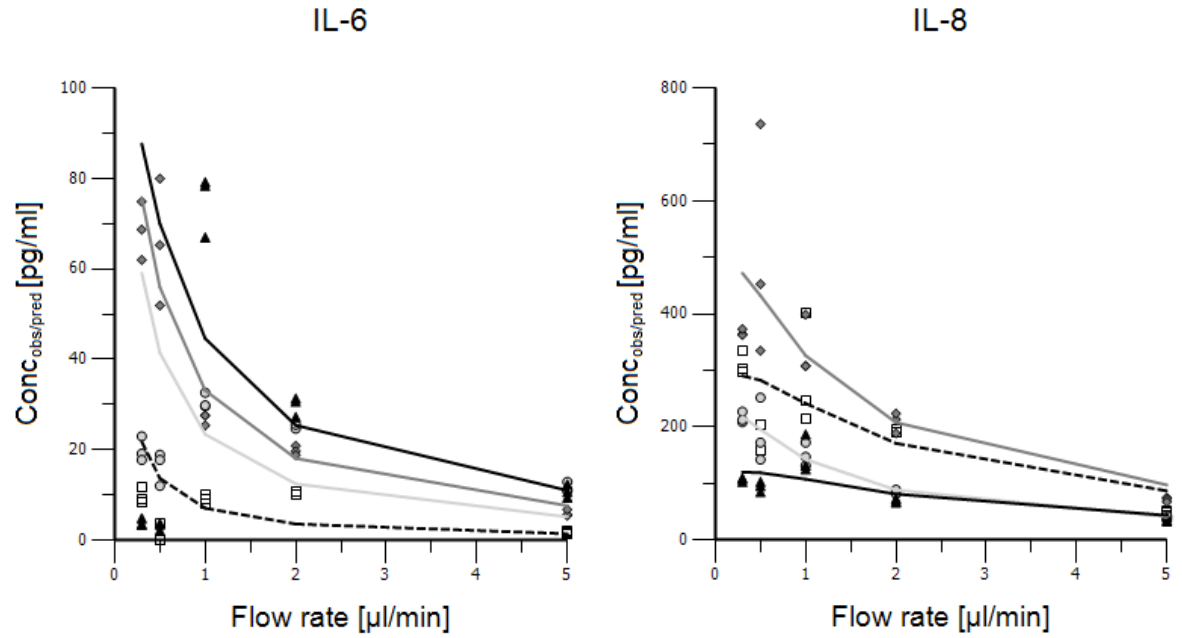

Fig. 3-19: Observed and predicted (lines) microdialysate concentrations of IL-6 and IL-8 from the four study individuals. Symbols: ID 01 (□), ID 02 (○), ID 03 (◊) and ID 04 (Δ), non-linear regression lines: ID 01 (dashed), ID 02 (light grey), ID 03 (grey) and ID 04 (black)

µD concentrations predicted by non-linear regression using the flow-rate-variation method (see 2.7.3.3, Eq. (15)) and individual µDialysate concentrations are jointly illustrated in Fig. 3-19. Parameter values and standard errors are presented in Tab. 8-20, the weighted

correlation coefficients between the observed and the predicted µD concentration values are summarised in Tab. 8-21. Measured concentrations of IL-6 could be adequately predicted for ID 03 (CV of predicted parameters ≤33.9%, R=0.9654), since concentrations were not remarkably decreased at the low FR in this individual. IL-8 concentrations were adequately described for all healthy volunteers (CV of predicted parameters ≤30.4%, R≥0.8363), they were also significantly higher than the set of IL-6 cocnentrations.

However, predicted values did not sufficiently describe the trend of the individual concentrations as a result of the decreased concentrations at the low FR of 0.3 µL/min and 0.5 µL/min (see weighted residuals in Fig. 8-9). These decreased concentrations at low FR (0.3 µL/min and 0.5 µL/min) had probably been the result of essentially decreased ISF concentrations at the last study day. Consequently, the assumption of constant catheter-surrounding cytokine concentrations was rejected for these data points. Therefore, non-linear regression was repeated for a reduced data set without the two lowest FR.

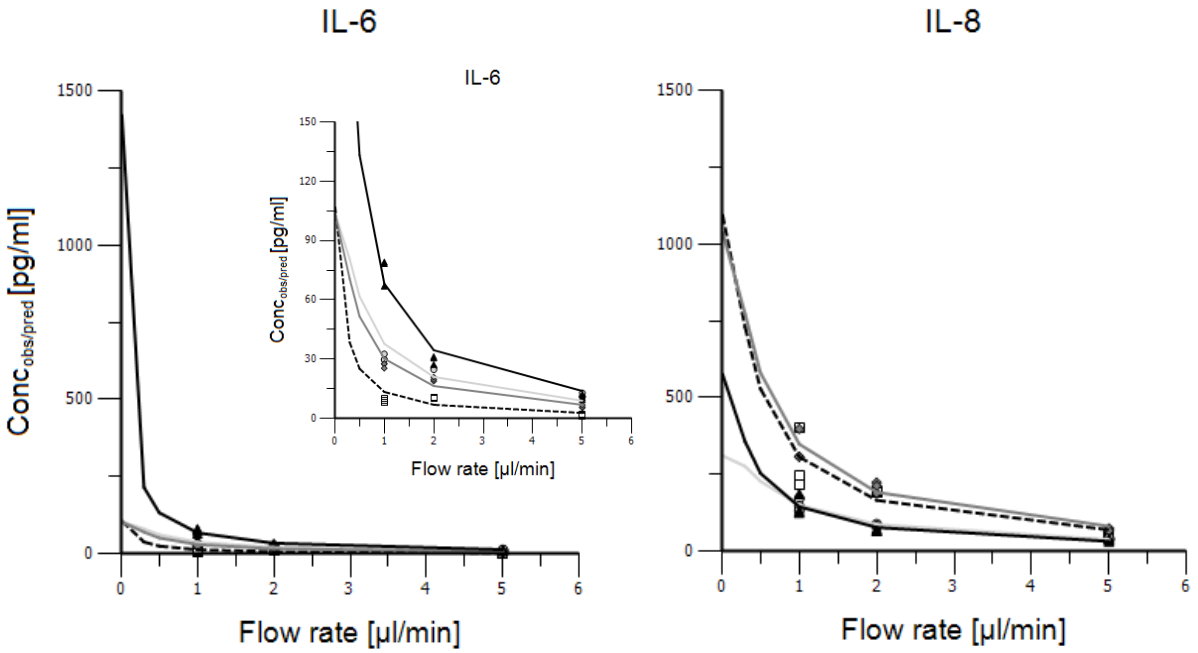

Fig. 3-20: Observed and predicted (lines) microdialysate concentrations of IL-6 and IL-8 at 1-5 µL/min from the four study individuals. Symbols: ID 01 (□), ID 02 (○), ID 03 (◊) and ID 04 (Δ), lines: ID 01 (dashed), ID 02 (light grey), ID 03 (grey) and ID 04 (black)

Predicted values estimated from reduced µDialysate concentration data sufficiently described the trend of the individual concentrations (see Fig. 3-20). Weighted resisuals were decreased after non-linear regression with the reduced data set and were randomly spread around zero (see Fig. 8-10).

The objective of the flow-rate-variation method was to enable the calculation of *in vivo* RR of the cytokines by the µDialysate concentrations. For this purpose, ISF concentrations, which were not measurable *in vivo*, had to be determined and µDialysate concentrations set in

relation to those. As previously introduced (see sections 2.6.6 and 2.7.3.3), ISF concentrations can be estimated from the µDialysate concentrations over a range of different FR by the flow-rate-variation method. This approach is based on the assumption that µDialysate concentrations equal the ISF concentration at a FR of 0 µL/min. Section 3.2.4 revealed sufficient predictability of concentrations of the catheter-surrounding medium (representing ISF *in vitro*) by non-linear regression only for IL-8. Consequently, the estimation of C_{ISF} from clinical data was performed individually for IL-8. The calculated C_{ISF} was then used to calculate RR of IL-8 *in vivo* (with Eq. (3)) at selected FR employed for parameter estimation (1 µL/min to 5 µL/min). In a subsequent step, calculated RR for the four individuals of the study were pooled due to the proof-of-principle concept of the study and the limited number of sample replicates at the individual FR. Non-linear regression of the determined RR was performed applying Eq. (10). To compare determined *in vitro* and estimated *in vivo* RR, individual results and predictions from non-linear regression are shown in Fig. 3-21.

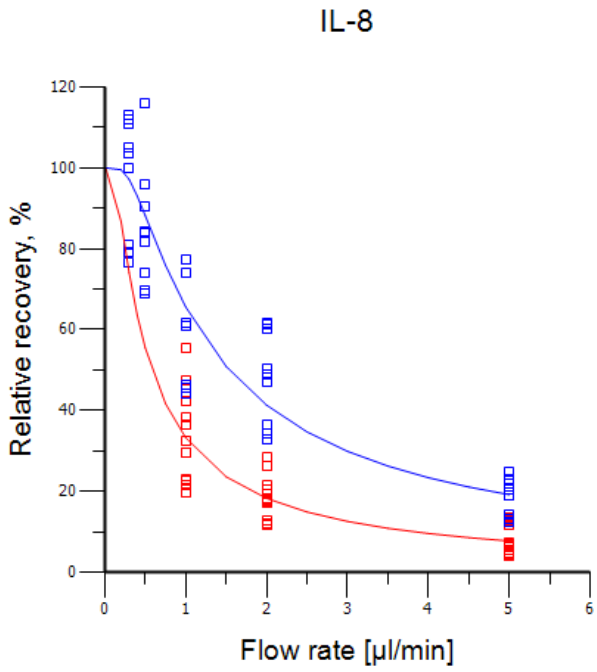

Fig. 3-21: Observed (squares) and predicted (lines) relative recoveries of IL-8 from *in vitro* recovery investigation at 37 °C (blue) and *in vivo* recovery estimations from the four study individuals (red).

Estimated *in vivo* RR were decreased with regard to RR determined *in vitro*. The course of the RR at the highest FR (1.0, 2.0 and 5.0 µL/min) was shifted vertically to lower RR and the distance between the RR values was maximal at 1.0 µL/min (difference of 32.3%) and decreased at 2.0 µL/min (23.0%) as well as at 5.0 µL/min (11.4%).

3.3.7 Individual concentration-time profiles of cytokines in microdialysates

Individual µDialysate concentration-time profiles of IL-6, IL-8, IL-10 and TNF-α from the four individuals sampled at FR of 0.5 µL/min are displayed in Fig. 8-11. The same data are presented in Fig. 3-22 utilising a logarithmic y-scale to improve the illustration of the kinetics and the decreased concentrations after ca. 48 h. Data points are connected by lines to outline the profiles of the individuals.

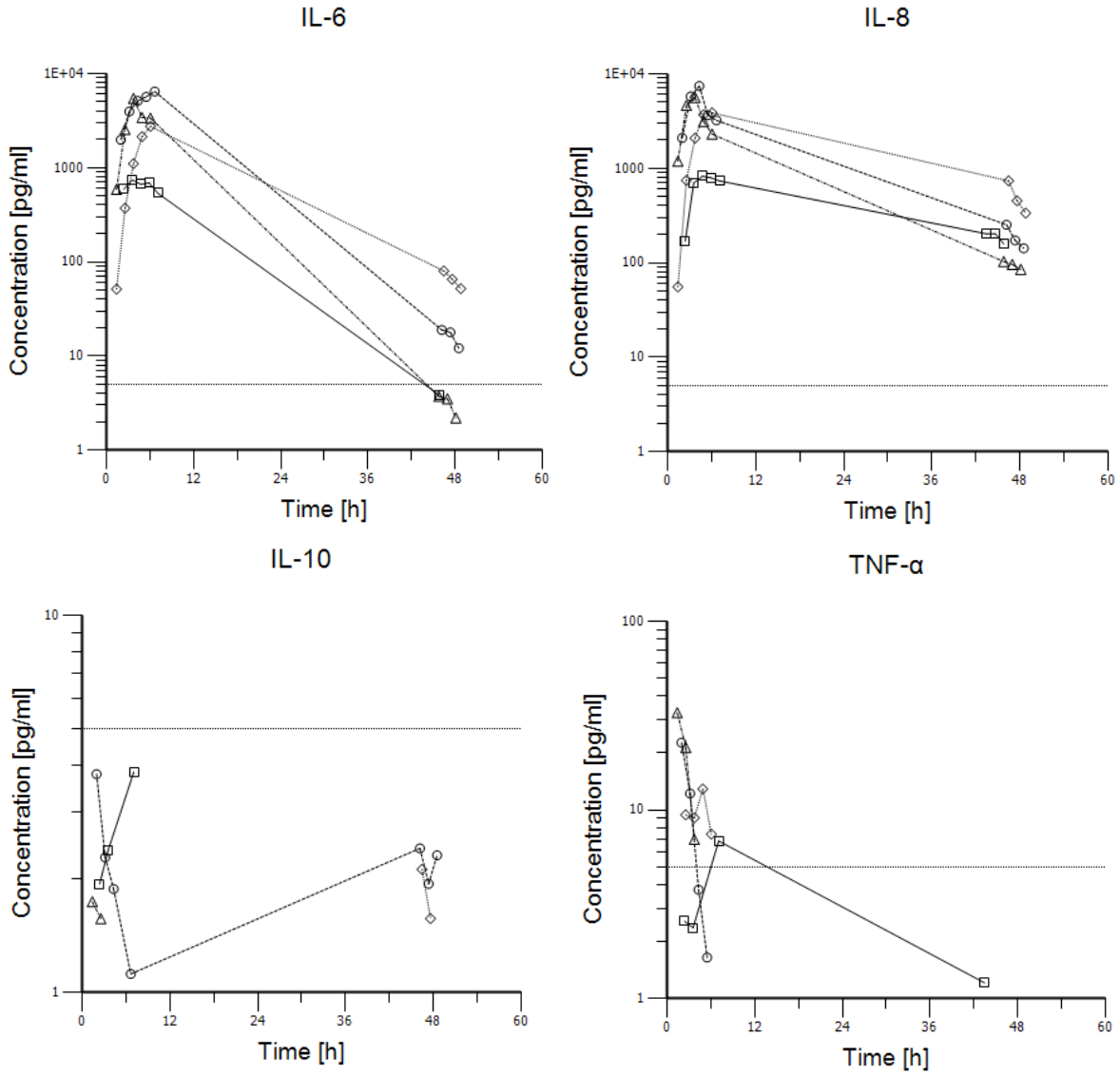

Fig. 3-22: Semi-logarithmic concentration-time plots of IL-6, IL-8, IL-10 and TNF-α in ID 01 (□), ID 02 (○), ID 03 (◊) and ID 04 (Δ); LLOQ (¨). The time after insertion of the µD catheter is shown on the x-axis.

IL-6 and IL-8 initially showed increasing concentrations in all individuals with C_{max} ranging from 740 pg/mL to 6423 pg/mL and 824 pg/mL to 7421 pg/mL, respectively. Concentrations in ID 01 exhibited a short plateau phase within the time period of the first four µD intervals (up to 390 min after insertion of the µD catheter) before starting to decrease. ID 04 already

revealed C_{max} in the third µD interval (190-260 min) and concentrations subsequently decreased rapidly to the fourth interval (260-330 min) followed by a subsequent slight decrease for IL-8 and a marginal decrease for IL-6.
ID 02 and ID 03 showed continuously ascending IL-6 concentrations during the first five µD intervals (up to 400 and 430 min, respectively). Overall, concentrations at approximately 48 h were remarkably decreased compared to the initial ones. For ID 02, ID 03, and ID 04, last measured concentrations were consecutively descending. Only one of the last concentration values of IL-6 was determinable (i.e. above LOD) in ID 01. Similar to IL-6, ID 03 revealed steeply ascending initial IL-8 concentrations at the first day as well as steeply declining last concentrations (day 3). For the other individuals, C_{max} values of the first five µD intervals were followed by slightly (ID 01) and steeply (ID 02 and ID 04) decreasing concentrations, respectively. The entire concentration data of IL-10 were BLQ or even below LOD and did, therefore, not present consistent concentration-time profiles. TNF-α demonstrated a decrease of the first concentrations from initial C_{max} of 22.7 pg/mL in ID 02 and 32.7 pg/mL in ID 04 falling below the LLOQ and subsequently below LOD at the third or fourth µD interval. For ID 01 and ID 04 a slight concentration decrease between the first and second µD interval was followed by an increase throughout the last µD intervals of study day 1 (C_{max}: 6.84 pg/mL and 12.9 pg/mL, respectively). At study day 3 TNF-α was detectable in one unique sample in ID 01, however, the sample concentration was BLQ as well.
Since IL-10 and TNF-α revealed low concentrations (partially BLQ) and no systematic increase followed by decreasing concentrations was observable for all individuals, mathematical description of the profiles was applied only for the other two cytokines.

Although endogenous compounds, based on explorative graphical analysis a 1-CMT PK model was implemented to describe the ascending and subsequently descending concentration-time profiles of the cytokines in response to tissue trauma due to the µD catheter insertion. Since cytokines are endogenous substances and were not administered to the healthy volunteers, the oral dose (D) was a fictional parameter set to 100 µg and bioavailability (F) fixed to the value ‘1’. To sufficiently describe the concentration-time profiles, a delayed absorption was implemented incorporating t_{lag}. This implementation was plausible with respect to the study procedure, i.e., the first concentration data point was placed to the middle of the first µD interval of 70 min subsequent to an equilibration phase of 50-110 min. Observed and predicted cytokine concentrations are presented in Fig. 3-23, parameter estimates are summarised in Tab. 8-22. CV of the parameters for IL-6 were overall high, whereas CV of parameters for describing IL-8 concentrations were low except for ID 03.

Concerning IL-6, early µDialysate concentrations (prior to 7 h) were accurately predicted in ID 01, ID 02 and ID 03 (see Fig. 3-23, upper left panel). In ID 04 observed C_{max} was not captured by the prediction. One explanation could be that the following two data points were immensely lower than C_{max} and deviated from one another to a minor extent. Therefore, a 2-CMT model was also tried to apply, but was not feasible due to an error in curve stripping.

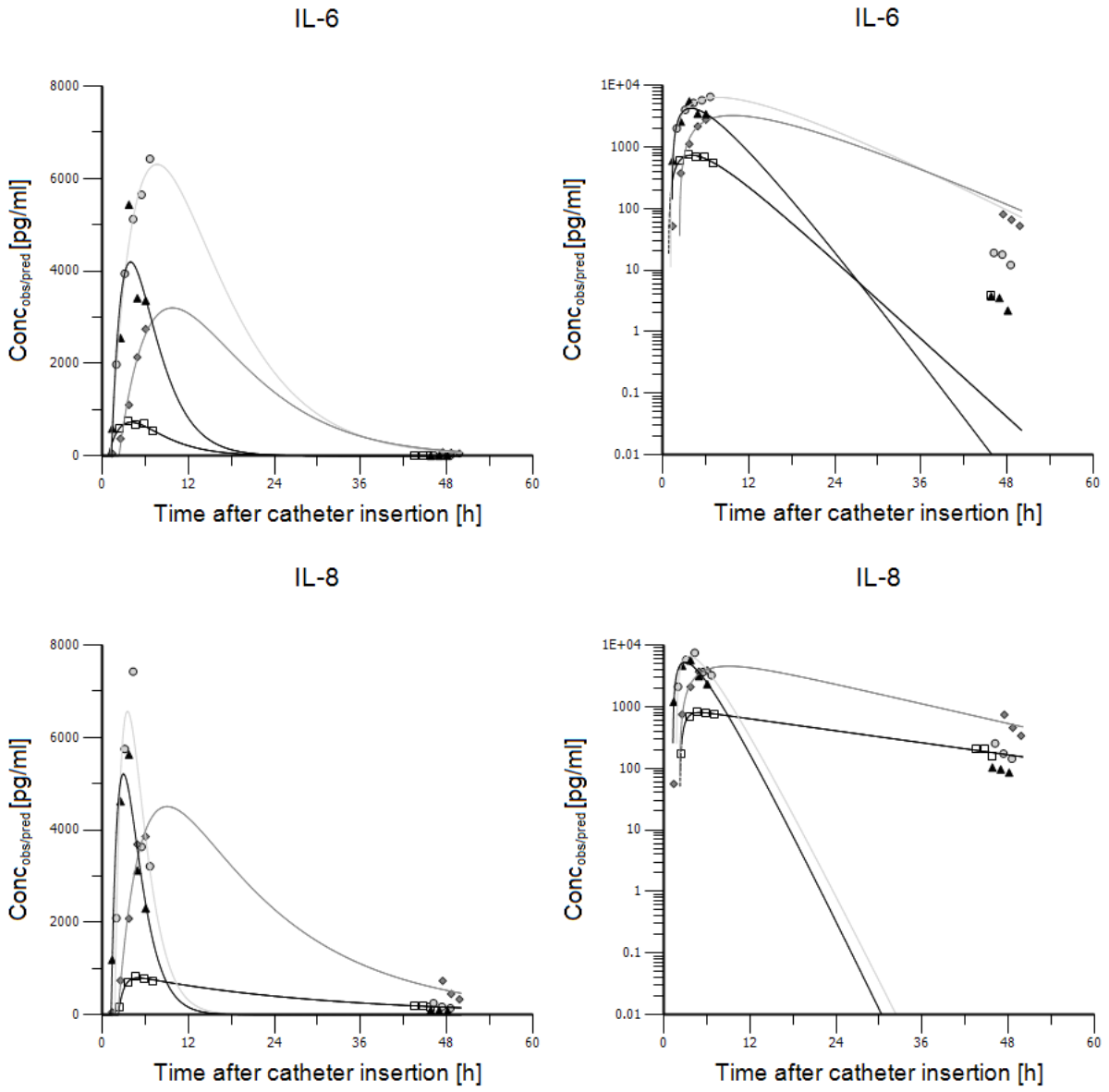

Fig. 3-23: Observed and predicted (lines) microdialysate concentrations of IL-6 and IL-8 over time from the four study individuals (linear scales: left panels; semi-logarithmic plots: right panels). Symbols: ID 01 (□), ID 02 (○), ID 03 (◊) and ID 04 (Δ), lines: ID 01 (dashed), ID 02 (light grey), ID 03 (grey) and ID 04 (black)

As visible in the upper right panel of Fig. 3-23 considering the semi-logarithmic plotting, late (around 48 h) IL-6 concentrations were sufficiently described by predictions, except for ID 02: the major deviations between observed and predicted concentrations were from 3.86 pg/mL to 0.07 pg/mL in ID 01, 18.9 pg/mL to 119 pg/mL in ID 02, 79.9 pg/mL to 122 pg/mL in ID 03

and 3.72 pg/mL to 0.01 pg/mL in ID 04 (Fig. 8-12). Depending on whether C_{max} was achieved within the µD intervals of study day 1 or C_{max} had to be estimated by the 1-CMT model, observed t_{max} of IL-6 concentrations were 3.6 h and 3.8 h in ID 01 and ID 04, whereas predicted t_{max} in ID 02 and ID 03 amounted to 7.7 h and 9.7 h, respectively.

Early and late IL-8 concentrations were appropriately predicted in ID 01 and ID 03 (Fig. 3-23, lower left and right panels, and Fig. 8-12). In ID 02 and ID 04 predictions did not capture C_{max} as well as late observed data (major deviations C_{obs}/C_{pred}: 252/0.00 pg/mL and 103/0.00 pg/mL, respectively). In ID 01, ID 02 and ID 04 observed t_{max} of IL-8 concentrations were 4.8 h, 4.3 h and 3.8 h, respectively, whereas predicted t_{max} in ID 03 accounted for 9.1 h.

The terminal slopes of the individual concentration-time profiles, represented by λ_z in the 1-CMT model, ranged between 0.1373 h^{-1} and 0.3715 h^{-1} (CV up to 11253%) for IL-6 as well as 0.0375 h^{-1} and 0.5861 h^{-1} (CV up to 87288%) for IL-8 and were, thus, highly variable. Due to the missing goodness of this parameter, $t_{1/2}$ was not calculated from λ_z.

In order to determine patterns of potential interactions of the cytokines among each other, the concentration-time profiles of IL-6, IL-8, IL-10 and TNF-α were grouped and plotted per ID (Fig. 3-24).

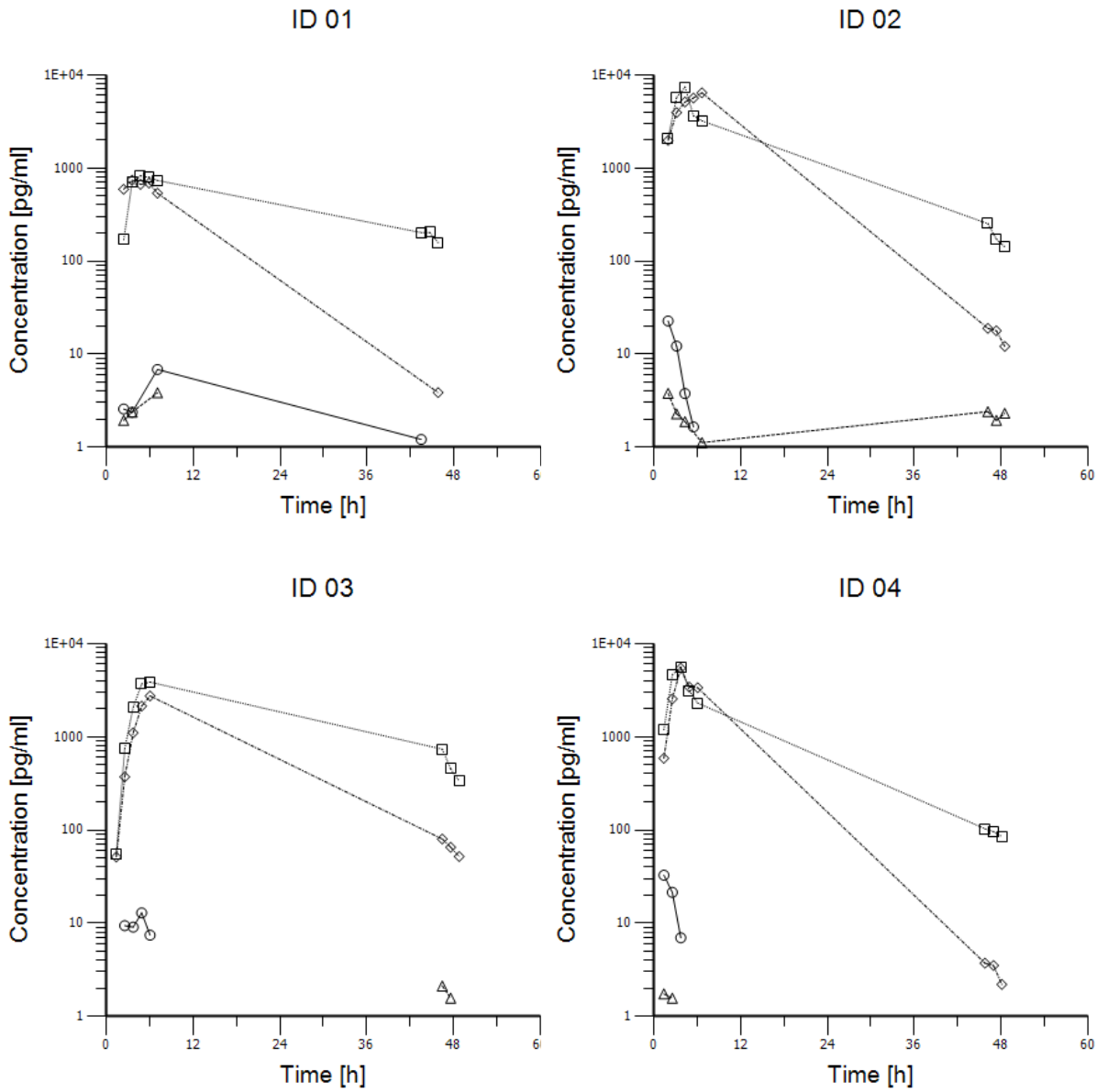

Fig. 3-24: Semi-logarithmic concentration-time plots of IL-6 (◊), IL-8 (□), IL-10 (Δ) and TNF-α (○) in ID 01, ID 02, ID 03 and ID 04. The time after insertion of the µD catheter is shown on the x-axis.

In Fig. 3-24, concentrations of IL-6 and IL-8 increased nearly simultaneously and showed almost equal t_{max}. However, C_{max} of IL-6 in ID 02 was shifted to µD intervals (i.e. 140 min) later than C_{max} of IL-8. IL-6 subsequently decreased to a higher extent than IL-8. No trends were evaluable for IL-10 and TNF-α since the concentrations were spread around LLOQ and frequently were BLQ. Nonetheless, in ID 02 and ID 04, concentrations of TNF-α apparently declined during the first µD intervals.

3.4 Project IV: Clinical long-term microdialysis study with voriconazole in healthy volunteers

Feasibility of long-term µD insertion and of sampling of VRC from ISF throughout the applied sequence dosing schedule was successfully confirmed in the main study, after being previously demonstrated during the pilot study [175].

The main study comprised the recruitment of additional six healthy volunteers. One participant was considered a drop-out after removal of a failing catheter at around 59 h (end of visit 5). The catheter was not replaced due to non-adherence of the study individual to behavioural requirements and therefore, less than 90% of planned data was sampled from this individual. This non-evaluable drop-out was replaced by an additional participant as pre-specified in the clinical study protocol. In the course of visit 5 the µD catheter of ID 09 had to be removed due to absent µDialysate in the sampling vial (sample "1 h 30 min-2 h"). A new CMA60® catheter was inserted immediately followed by an equilibration period of 10 min. Subsequently, µDialysate sampling was resumed with sample "3 h-3 h 30 min". Randomly, a few µD samples showed a lack or a shortage of sample volume, respectively, without any apparent reason. Apart from these incidents the study was conducted as planned.

3.4.1 Demographic data and genetic characteristics

Demographic information of the nine Caucasian, healthy male participants are listed in Tab. 3-18. Age ranged between 21 and 46 years, median BMI (24.0 kg/m^2) was within the normal range [186] with three individuals (ID 01, ID 02 and ID 03) laying in the lower segment of the pre-obese range (25.3, 25.3 and 25.4 kg/m^2). Tab. 3-18 gives genetic information about CYP 450 isoenzymes as well. Two individuals showed polymorphic genotypes of the isoenzyme CYP2C9, i.e. individual heterozygous mutants consisting of the alleles *2 and *3. The genotypes of CYP2C19 revealed a widespread spectrum of polymorphisms: ID 02 was a homozygous mutant for the allele *2, whereas this allele was incorporated in one homologous chromosome of ID 04, ID 08 and ID 09. There were two heterozygous mutants with the CYP2C19*17 allele as well (ID 06 and ID 09). Accordingly, ID 09 exhibited a heterozygous genotype of the loss-of-function allele CYP2C19*2 and the gain-of-function allele CYP2C19*17.

ID 01, 03, 04 and 05 were excluded from further consideration of the influence of the genotype state on PK parameters (see section 3.4.9) due to unknown genetic information about the presence of CYP2C19*4/*17 alleles.

Tab. 3-18: Individual characteristics: demographics and genetic variations of isoenzymes CYP2C9 and CYP2C19 within the individuals 01-09

ID	Age [years]	Height[a] [cm]	Weight[b] [kg] Median (range)	BMI[c] [kg/m^2] Median (range)	CYP2C9 genotype	CYP2C19[d] genotype
01	43	181	83.0 (82.2-83.7)	25.3 (25.1-25.5)	*1/*3	*1/*1 (unknown)
02	46	176	78.4 (77.0-80.2)	25.3 (24.9-25.9)	*1/*1	*2/*2
03	34	183	82.0 (82.0-82.2)	24.5 (24.5-24.5)	*1/*1	*1/*1 (unknown)
04	28	171	74.4 (73.1-75.2)	25.4 (25.0-25.7)	*1/*1	*1/*2 (unknown)
05	21	179	70.5 (69.5-71.0)	22.0 (21.7-22.2)	*1/*1	*1/*1 (unknown)
06	22	177	65.5 (65.1-65.9)	20.9 (20.8-21.0)	*1/*1	*1/*17
07	26	181	67.2 (67.1-67.7)	20.5 (20.5-20.7)	*1/*2	*1/*1
08	28	184	72.4 (72.2-73.0)	21.4 (21.3-21.6)	*1/*1	*1/*2
09	24	181	76.8 (76.7-77.3)	23.4 (23.4-23.6)	*1/*1	*2/*17
Median (range)	**28 (21-46)**	**181 (171-184)**	**76.0[e] (65.1-83.7)**	**24.0[e] (20.5-25.9)**	**-**	**-**

[a] Once determined at screening visit

[b] Four times determined for ID 01-03 (at screening visit, at visit 1 and 5, and at final examination), three times determined for ID 04-09 (at screening visit, at visit 1 and at final examination).

[c] Body mass index

[d] Genotype analysis in terms of CYP2C9*2, *3 and CYP2C19*2 performed for all IDs, CYP2C19*4 and *17 additionally determined for ID 06-09 (wild-type (*1) assumed if no mutant allele was detected (see section 2.8.2.2))

[e] Median of median values

3.4.2 Dose characteristics

The approved and recommended clinical routine dose regimen was applied in this study. This regimen consisted of four initial IV administrations, i.e. two loading doses of 6 mg/kg WT and two maintenance doses of 4 mg/kg WT, and three subsequent PO administrations. The dosing interval for this sequence therapy was 12 h. Tab. 3-19 summarises the administered individual doses, the total dose amounts for IV and PO administrations, respectively, and the total amounts of the entire doses administered throughout the course of the study. The second loading dose in ID 03 deviated from the first one as a result of air bubbles in the tubing at the beginning of the infusion, which led to a difference of the infused solution of about 40 mL accounting for approximately 79 mg VRC.

The individual administered doses clearly show the difference between IV and PO dose amounts. The loading IV doses ranged from 390 mg to 498 mg (24.3% difference related to the arithmetic mean), while maintenance IV doses varied between 260 mg and 332 mg

(difference of 24.3%), resulting from the differences in WT for which IV doses were individualised. Subsequently, equal PO doses of 200 mg were administered to all individuals.

Tab. 3-19: Dose characteristics

	Intravenous dosing				*Oral dosing*		
	6 mg/kg WT		4 mg/kg WT		Independent from WT – 200 mg		
ID	Visit 1	Visit 2	Visit 3	Visit 4	Visit 5	Visit 6	Visit 7
	Time since first dose [h]						
01-09	0.00	12.00	24.00	36.00	48.00	60.00	72.00
	Dose amount [mg]						
01	498	498	332	332	200	200	200
02	480	480	320	320	200	200	200
03	492	413	328	328	200	200	200
04	450	450	300	300	200	200	200
05	420	420	280	280	200	200	200
06	390	390	260	260	200	200	200
07	406	406	271	271	200	200	200
08	438	438	292	292	200	200	200
09	461	461	307	307	200	200	200
	Total dose IV [mg]				*Total dose PO [mg]*		
01	1660				600		
02	1600				600		
03	1561				600		
04	1500				600		
05	1400				600		
06	1300				600		
07	1354				600		
08	1460				600		
09	1536				600		
	Median (Min-Max): 1500 (1300-1660)						
	Total dose [mg]						
01	2260						
02	2200						
03	2161						
04	2100						
05	2000						
06	1900						
07	1954						
08	2060						
09	2136						
	Median (Min-Max): 2100 (1900-2260)						

3.4.3 Safety assessment during the clinical trial

AE were recorded as described in section 2.8.1.4 and are outlined in Tab. 3-20. AE were observed in every study participant except for ID 09.

Tab. 3-20: Adverse events in certain/probable/possible/unlikely relationship to treatment

ID	AE	AE frequency/onset	Relationship to treatment	Severity	Action taken
01	Impaired vision when eyes closed	Intermittent	Certain	Moderate	No
01	Burning sensation at infusion site	Intermittent	Certain	Mild	No
02	Headache	Once, ~10 h after last study drug administration	Possible	Mild	Pharmacological treatment with paracetamol
02	Impaired vision when eyes closed	Intermittent	Certain	Moderate	No
02	Nausea	Once, ~3 h after last study drug administration	Probable	Moderate	No
03	Impaired vision when eyes closed	Intermittent	Certain	Mild	No
03	Headache	Once, ~3 h after last study drug administration	Possible	Mild	No
03	Slight dizziness	Once, ~1 h after last study drug administration	Possible	Mild	No
03	Slight drowsiness (asthenia)	Once, ~1/2 h after last study drug administration	Possible	Mild	No
04	Skin rash of the face	Intermittent	Possible	Mild	No
04	Colour visions	Intermittent	Certain	Mild	No
04	Dizziness	Twice, each ~1 ½ h after last study drug administration	Probable	Mild	No
04	Headache	Once, ~2 h after last study drug administration	Probable	Mild	No
04	Back pain	~23 h after last study drug administration, persistent for 3 days	Unlikely	Mild	No
04	Pain at the neck	~23 h after last study drug administration, persistent for 3 days	Unlikely	Mild	No
05	Headache	Once, ~5 h after last study drug administration	Probable	Mild	Pharmacological treatment with paracetamol
05	Dizziness	Twice, ~5 h and 11 h after last study drug administration	Probable	Mild	No
05	Sensation of heat	Once, 11 h after last study drug administration	Probable	Mild	No
05	Colour visions	Intermittent	Certain	Mild	No
06	Optical hallucination	Intermittent	Probable	Mild	No
06	Dizziness	Once, ~2 h after last study drug	Possible	Mild	No

		administration			
06	Headache	Twice, ~5 h and 7 h after last study drug administration	Possible	Mild	Pharmacological treatment with paracetamol (once)
06	Increased light sensitivity	Intermittent	Certain	Mild	No
07	Increased light sensitivity	Intermittent	Certain	Mild	No
07	Nausea	Once, ~5 hours after last study drug administration	Possible	Mild	No
08	Headache	Once, ~4 hours after last study drug administration	Possible	Mild	Pharmacological treatment with paracetamol
08	Optical hallucination	Intermittent	Certain	Mild	No
08	Increased light sensitivity	Intermittent	Certain	Mild	No
08	Watery stool	Once, ~5 hours after last study drug administration	Unlikely	Mild	No

32 AE were listed, ten (31.3%) of those with a certain relationship to the administration of the study drug and three AE (9.38%) were assessed to be ‘unlikely’ related to VRC. All AE were of mild severity except for three (9.38%), which showed moderate severity (impaired vision twice, nausea once). AE regarding the eye/vision were noticed ten times (31.3%), headache occured six times (18.8%). Dizziness and nausea were less frequent (four times (12.5%) and twice (6.25%)) and other AE were observed once (3.13%).The individuals completely recovered from all AE within the particular study visit. AE considered not to be related to treatment were as follows: ID 01 showed a small hematoma (∅ 1 cm) at probe insertion site; ID 04 had hematoma at both forearms at the blood catheter insertion site after catheter removal; in ID 07 recurrent bloody oozing from probe insertion site occurred during visit 1; ID 08 revealed an aphtha at the left buccal mucosa persistent over three days; ID 09 developed a dry cough three days after the last study drug administration and recovered within the four subsequent days.

3.4.4 Bioanalysis of the study samples

The bioanalytical method was successfully transfered to a second laboratory equipped with a different HPLC device thoughout the course of the study. Validity and robustness was demonstrated over the entire range of eighteen runs for study sample analysis. QC and Cal of all analytical runs met pre-specified acceptance criteria: Accuracy of 98% of all QC samples was higher or equal to 85%. Not more than one out of nine QC replicates of an individual run failed acceptance criteria. Intra-run (n=3) imprecision ranged from 0.39% to 12.4% CV. Overall QC replicate analysis at the different concentrations (n=54) exposed RE

of -6.63%, +1.38% and +3.28% and CV of 6.55%, 5.23% and 5.68% for QC 1, QC 2 and QC 3, respectively.

3.4.5 *In vivo* relative recovery

Results of *in vivo* relative recovery of the pilot phase published by Simmel et al. [175] were confirmed in the main study (see Fig. 3-25). Overall mean RR (CV) of CMA60® catheters for all RR samples obtained during the study was 85.2% (6.49%).

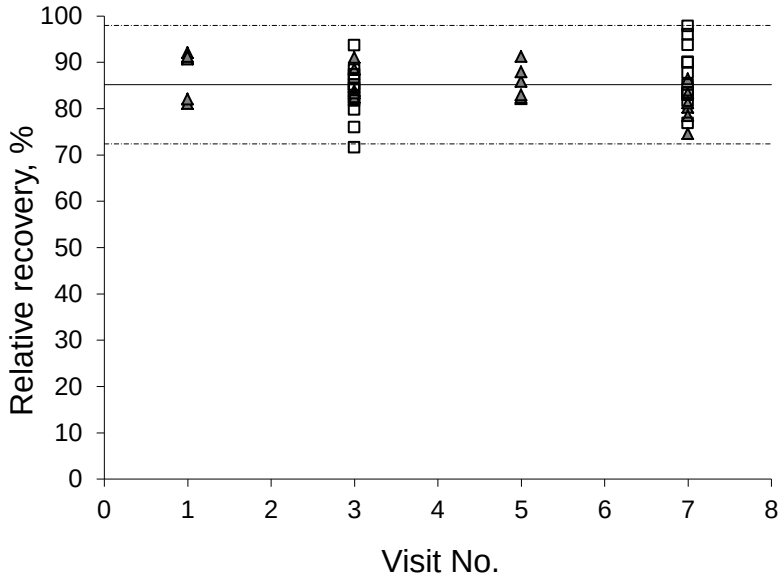

Fig. 3-25: Relative recoveries of microdialysis catheters. Triangles: pilot study, squares: main study; line: overall arithmetic mean, dotted line: ±15% of the mean

One single RD sample from ID 09 at visit 3 revealed RR outside the 15%-range around the overall mean, 98% of RR results were within this range. Mean RR for all study visits per individual during the whole study duration are presented in Tab. 3-21 and individual RR are listed in Tab. 8-23. The distribution of RR values was two- to three-fold higher in ID 09 (CV: 12.9%) than in the other study individuals (CV: 2.97%-7.89%). The related catheter was removed in visit 5 due to sampling volume loss or absence, respectively, and replaced by a new one. Corrections of µDialysate concentrations for ID 09 were calculated by RR of the first µD catheter (4.2% CV) for the related samples and by RR observed from the second µD catheter (2.8% CV) for samples obtained subsequent to the insertion of the new catheter. For the remaining study individuals, ISF concentrations were calculated incorporating arithmetic means of RR determinations from one individual (Tab. 3-21).

Tab. 3-21: Mean relative recovery (RR), standard deviation (SD) and coefficient of variation (CV) for all study visits per individual

Individual	Visit	$n_{RD\ samples}$	n_{total}	Mean RR, %	SD RR, %	CV, %
01	1, 3, 5, 7	2	8	85.7	4.75	5.55
02	1, 3, 5, 7	2 (1)	7	86.7	3.77	4.35
03	1, 3, 5, 7	2	8	82.6	5.16	6.25
04	3, 7	2	4	87.1	5.03	5.77
05	3, 7	2	4	85.1	2.53	2.97
06	3, 7	2	4	90.8	7.16	7.89
07	3, 7	2	4	86.1	3.32	3.85
08	3, 7	2	4	80.4	2.81	3.49
09[1]	3, 7	2	4	82.8	10.7	12.9

n=1 for visit 3 ID 02
[1] insertion of a new catheter during visit 5

Mean RR results for all study individuals and RD samples at the different study visits exposed comparable results (see Tab. 3-22): the highest average value (88.0%) was determined for visit 1, whereas the lowest one (79.4%) was calculated for the subsequent RD performance (visit 3).

Tab. 3-22: Mean relative recovery catheters for all study individuals at study visit 1, 3, 5 and 7

Study day	Visit	$n_{volunteers}$	$n_{RD\ samples}$	n_{total}	Mean RR, % (CV, %)
1	1	3	2	6	88.0 (5.7)[1]
2	3	9	2 (1)	17	79.4 (6.7)[2]
3	5	3	2	6	85.4 (4.3)[2]
4	7	9	2	18	85.1 (7.5)[2]

n=1 for visit 3 ID 02
[1]Concentration (µg/mL) of perfusate for retrodialysis within visit 1 (CV, %): 17.9 (4.2) (n=6).
[2]Concentration (µg/mL) of perfusate for retrodialysis within visit 3, 5 and 7 (CV, %): 172.3 (17.6) (n=41).

Calculations for the subsequent visits showed similar RR extents (85.4% vs. 85.1%); however, calibration procedures at visit 1 and 5 were solely performed during the pilot phase

of the study. There was no significant difference between the mean RR of the four visits (p=0.696).

3.4.6 Data set and data set checkout

All planned plasma samples were obtained, ultrafiltered and analysed, resulting in a total of 522 unbound plasma concentrations (i.e. UF). A number of 560 µDialysate samples were collected over the entire study period and VRC was quantified from 552 of these samples (see Tab. 3-23). Eight µD samples were lost due to the defect and exchange of the µD catheter of ID 09 and due to unsystematic lacks or shortages in the volume of individual samples. Corrections of µDialysate concentrations by means of calculated RR reflected unbound concentrations from ISF.

Tab. 3-23: Distribution of the observations for the matrices studied (available samples at the end of the study, taken from plasma or CMA60®; in percentage of number of planned samples)

Matrix	No. of samples planned	No. of samples obtained	No. of samples analysed	Samples obtained, %	Samples analysed, %
UF	522	522	522	100	100
ISF	564	560	552	99.3	98.6
Total	1086	1082	1074	99.6	98.9

The merged data set for the pilot and the main study individuals underwent a data set checkout. After it was judged to be plausible and constructed in a consequential manner, this final data set was applied for data analysis.

3.4.7 Unbound concentration-time profiles of voriconazole

Unbound VRC concentrations of a total of 1074 samples ranged between 0.08 µg/mL and 4.19 µg/mL (see Tab. 3-24).

Tab. 3-24: Concentration characteristics of voriconazole in ultrafiltrate and interstitial fluid during the entire study time

	C_{UF} [µg/mL]	C_{ISF} [µg/mL]
Min	0.08[1]	0.11[2]
Max	4.19	3.68
Median	1.09	0.87
Ratio of medians		0.8

[1] BLQ; seven samples: 0.08 to 0.14 µg/ml (considered for PK analysis); LLOQ: 0.16 µg/ml
[2] BLQ; six samples: 0.11 to 0.14 µg/ml (considered for PK analysis); LLOQ: 0.16 µg/ml

Individual concentration-time profiles of UF and ISF from the nine study individuals are illustrated in Fig. 3-26. The x-axis represents the time after first drug administration summarising the total study duration of approximately 84 h. Green squares show the (mean) amounts of the first four WT-individualised IV doses (two initial doses of 6 mg/kg, followed by two doses of 4 mg/kg) and the subsequent three PO doses of 200 mg. Consequently, the doses decreased over time from the initial two loading doses of 406-498 mg per individual to 260-332 mg of the following two maintance IV doses and, finally, to 200 mg of the last three PO doses (see also Tab. 3-19).

Rich sampling was performed throughout visit 1 (0-12 h), visit 5 (48-60 h) and visit 7 (72-84 h), whereas sampling was limited to the first 2 h/1.3 h of visit 2, visit 3, and visit 4 and no sampling was performed in visit 6 (see section 2.8.1, Tab. 2-4). The upper panel of Fig. 3-26 visualises the concentration range, covered by the individual profiles, from single dose observations (0-12 h) to multiple dose observations (48-60 h and 72-84 h). After multiple dosing ID 02 (circles) and ID 08 (six-point stars) revealed the highest UF and ISF concentrations, while UF and ISF exposure were around 4.5-fold and 3.2-fold smaller, respectively, in ID 01 (squares), ID 04 (triangles), and ID 06 (four-point stars). Overall C_{min}, i.e. the last concentration within the dosing interval of 12 h, varied between 0.08 µg/mL and 0.75 µg/mL after single dose, whereas after multiple doses it ranged from 0.35 µg/mL to 2.25 µg/mL (visit 5) and from 0.18 µg/mL to 2.49 µg/mL (visit 7) (see Tab. 8-29). C_{min} after single dose was significantly different from these after multiple doses ($p<0.001$, t-test of logarithmic values), whilst C_{min} were not different between visit 5 and visit 7 ($p=0.482$, t-test of logarithmic values).

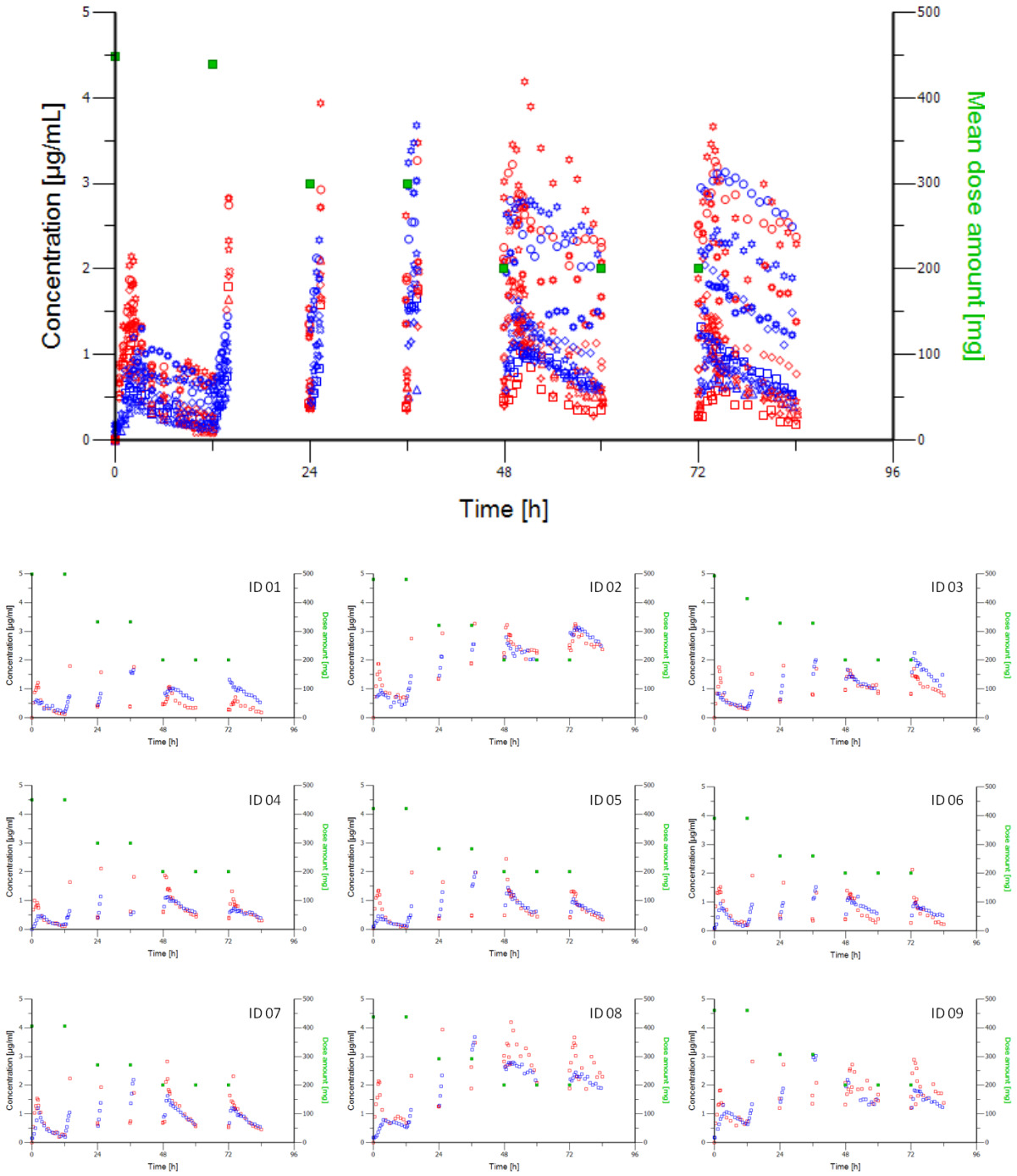

Fig. 3-26: Unbound plasma (UF (red)) and interstitial fluid (ISF (blue)) concentration-time profiles of voriconazole in ID 01 (squares), ID 02 (circles), ID 03 (diamonds), ID 04 (triangles), ID 05 (cross), ID 06 (four-point star), ID 07 (five-point star), ID 08 (six-point star) and ID 09 (ten-point star). Green squares: Mean dose amounts (upper panel) and individual doses (lower panel).

Individual profiles (Fig. 3-26, lower panel) displayed different VRC exposures in the study participants. The maximum drug accumulation after multiple dosing was observed in ID 02 and ID 08, and the lowest drug accumulation was shown by ID 01 and ID 06. The other concentration-time profiles were in-between with increased concentrations for ID 03 as well as for ID 09 and lower concentrations for ID 04, ID 05 and ID 07.

C_{max} of UF from ID 03 was decreased at visit 2 compared to C_{max} at visit 1, probably due to failures in the second dose administration to this participant (see section 3.4.2).
Comparing UF with ISF, UF revealed higher C_{max} compared to ISF after single and predominantly after multiple doses as well. Individual C_{max} showed different accumulations: C_{max} of UF generally increased from visit 1 to visit 2 except for ID 03; following values occasionally in- or decreased, but predominantly stayed within the same range. A considerable decrease was observed in ID 01 after the switch from IV to PO dosing, whereas most C_{max} showed a behaviour comparable to steady-state conditions, i.e., varied only within a small range. At the last visit the largest part of individual concentrations slightly decreased. C_{max} of ISF predominantly increased over the first four visits and subsequently decreased to a minor extent.
Whereas most individuals showed overlapping or contiguous ISF and UF profiles after multiple dosing, ISF concentrations were considerably higher than UF in ID 01 (visit 5 and visit 7) and ID 03 (visit 7). In contrast, in the last visits ID 08 and ID 09 showed principally higher UF concentrations related to ISF. The slopes of the ascending part of the profiles were generally steeper for UF data than for ISF data. For ID 08 and ID 09, concentration-time points of the descending parts of the profiles at visit 5 and visit 7 were highly scattered, resulting in increased residuals from the typical elimination behaviour for UF related to ISF data.
Each concentration-time profile was similar in concentration range and shape between visit 5 and visit 7, which led to the assumption of steady-state-like conditions starting at visit 5.

Fig. 3-27 considers UF data individually (left panel) and averaged by the geometric mean in the semi-logarithmical presentation (right panel). Descending parts of the individual profiles immensely varied in shape and steepness and progressively diverged after multiple dosing. Consequently, inter-individual variability increased with the number of administered doses. Variability of plasma concentrations already increased within the first 12 h as well (see Fig. 3-27, right panel), this fact resulted in a broad range of C_{min} ($CV_{geom.}$ of dose-normalised data: 99.7%), already reaching the extent of variability observed after multiple doses: $CV_{geom.}$ of dose-normalised data was 83.9% at visit 5 and 126% at visit 7. The slopes of the descending geometric mean profile parts were flatter after multiple dosing than after single dosing. Additionally, the illustration of the geometric mean underlines the assumption of having almost achieved steady-state concentrations at visit 5 and visit 7, respectively, since the fluctuation within one visit was smaller than after single dose and the concentration ranges were similar in visit 5 and visit 7. However, visit 7 showed marginally decreased concentrations compared to visit 5 resulting from the reduction in dose amounts.

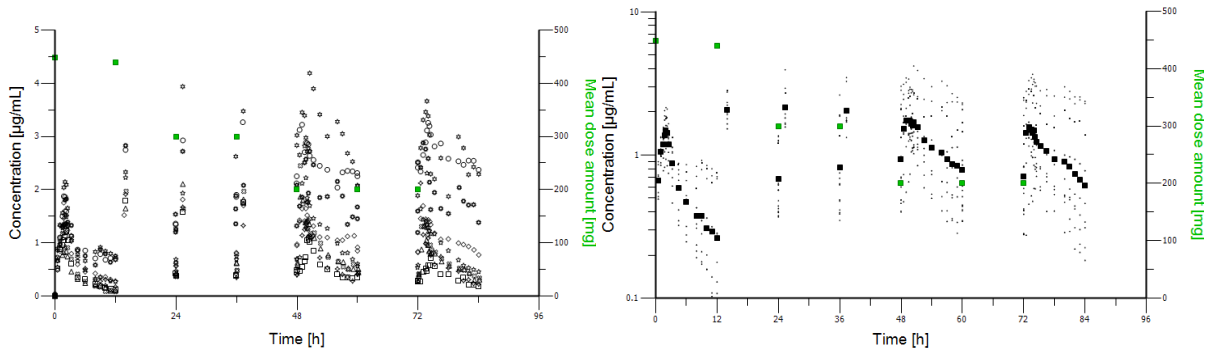

Fig. 3-27: UF concentration-time profiles of voriconazole in ID 01 (squares), ID 02 (circles), ID 03 (diamonds), ID 04 (triangles), ID 05 (cross), ID 06 (four-point star), ID 07 (five-point star), ID 08 (six-point star) and ID 09 (ten-point star) (left panel). Geometric mean (black filled squares) and individual (points) concentrations in semi-logarithmic plots (right panel). Mean dose amounts (green squares).

This observation was confirmed by minimum UF concentrations as well (Fig. 3-28): Following accumulation within the first four visits, geometric means of minimal concentrations slightly decreased subsequent to the switch from IV to PO dosing; Geometric means of unbound C_{min} in plasma started with 0.26 µg/mL at visit 1, increased to 0.65 µg/mL (visit 2), 0.79 µg/mL (visit 3), and 0.93 µg/mL (visit 4) and subsequently decreased to 0.61 µg/mL at visits 5 to 7. Geometric means of dose-normalised data more distinctly approached a plateau-like phase starting from 48 h after first dosing. Since there were no significant differences of dose- and WT-/dose-normalised concentrations, solely dose-normalised data will be presented in following sections of this thesis.

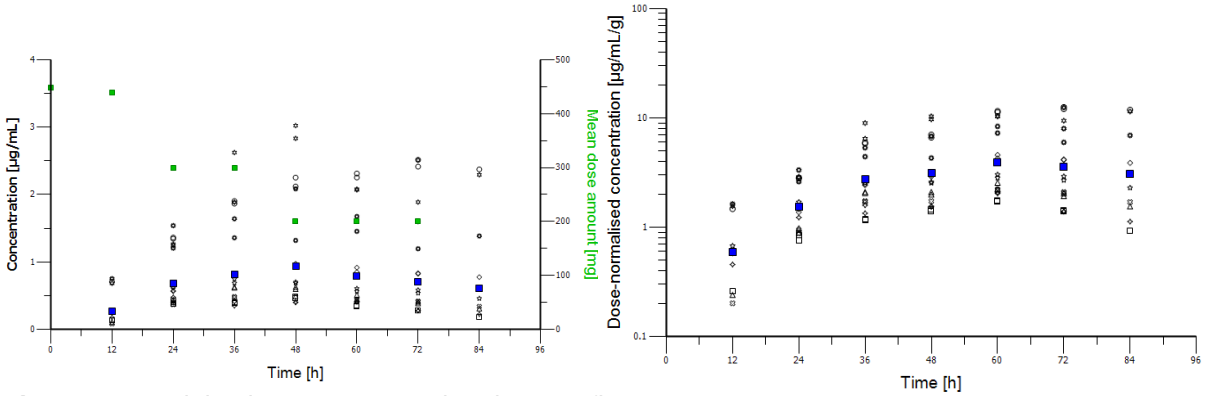

Fig. 3-28: Minimal UF concentration-time profile (left panel) and dose-normalised profile (right panel) in ID 01 (squares), ID 02 (circles), ID 03 (diamonds), ID 04 (triangles), ID 05 (cross), ID 06 (four-point star), ID 07 (five-point star), ID 08 (six-point star) and ID 09 (ten-point star) (left panel). Mean dose amounts (green squares).

ID 02, ID 08 and ID 09 showed enormously increased minimum concentrations compared to geometric means (approximately 2.6- to 3.9-fold), whereas values were intensely decreased in ID 01 (approximately 0.3-fold).

Individual (left panel) and geometric mean ISF concentrations in semi-logarithmic presentation (right panel) are displayed in Fig. 3-29. Descending parts of the individual profiles rather corresponded with one another in shape and steepness than UF data, but were still variable. While individual curves proceeded close to one another after single dosing, profiles of ID 02, ID 03, ID 08 and ID 09 intensely exceeded the other ones especially at visit 7.

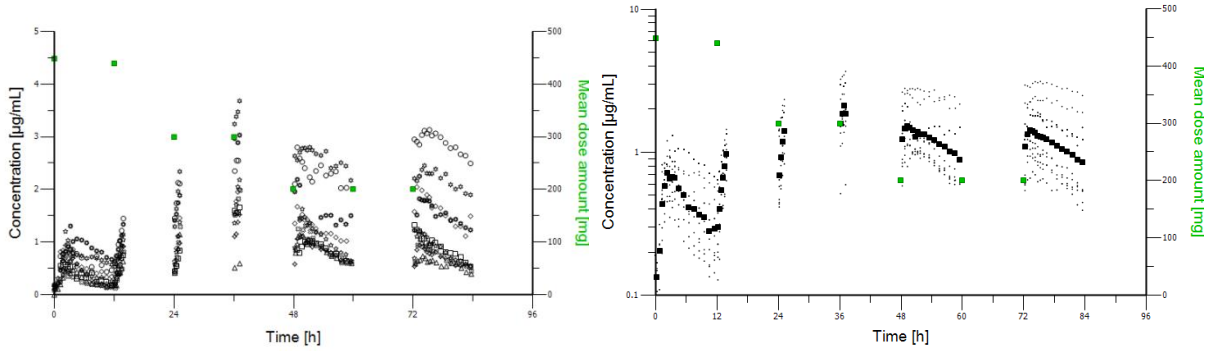

Fig. 3-29: ISF concentration-time profiles of voriconazole in ID 01 (squares), ID 02 (circles), ID 03 (diamonds), ID 04 (triangles), ID 05 (cross), ID 06 (four-point star), ID 07 (five-point star), ID 08 (six-point star) and ID 09 (ten-point star) (left panel). Geometric mean (black filled squares) and individual (points) concentrations in semi-logarithmic plots (right panel). Mean dose amounts (green squares).

ID 04 showed the lowest concentrations after multiple doses. The enlarged variability after multiple dosing is furthermore obvious in the right panel of Fig. 3-29, which, in addition, visualises the flatter slope of the geometric mean curve after multiple drug administration compared to visit 1. Analogously to UF data, concentrations in ISF accumulated and approached a phase of less fluctuation and similar concentration ranges from 48 h onwards (see also Fig. 3-31).

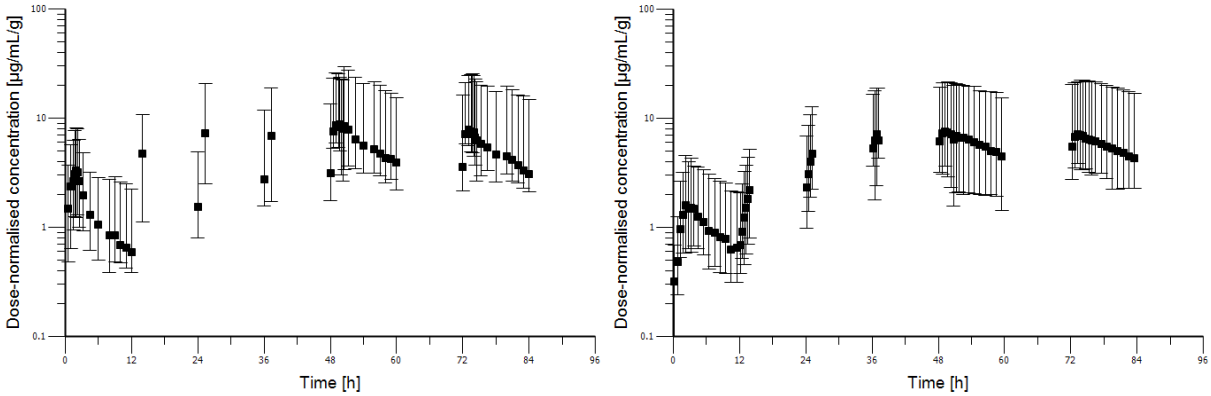

Fig. 3-30: Geometric mean (filled squares) and 5th/95th-percentiles (error bars) of dose-normalised UF (left panel) and ISF (right panel) concentrations

Dose-normalised data (Fig. 3-30, also Fig. 8-13 and Fig. 8-14) underlined this plateau-like phase, as confirmed by minimal ISF concentrations as well (see Fig. 3-31). Geometric means of minimum concentrations as well as of minimum dose-normalised concentrations considerably increased from visit 1 to visit 5 and decreased to a small extent until visit 7. At visit 5 two geometric means were determined, since the last µD sample was obtained at 10.5 h previous to RD throughout the pilot phase (ID 01-03), and at 11.5 h in the main study (ID 04-09) due to the aforementioned (section 2.8.1.3) abolishment of RD performance in this visit.

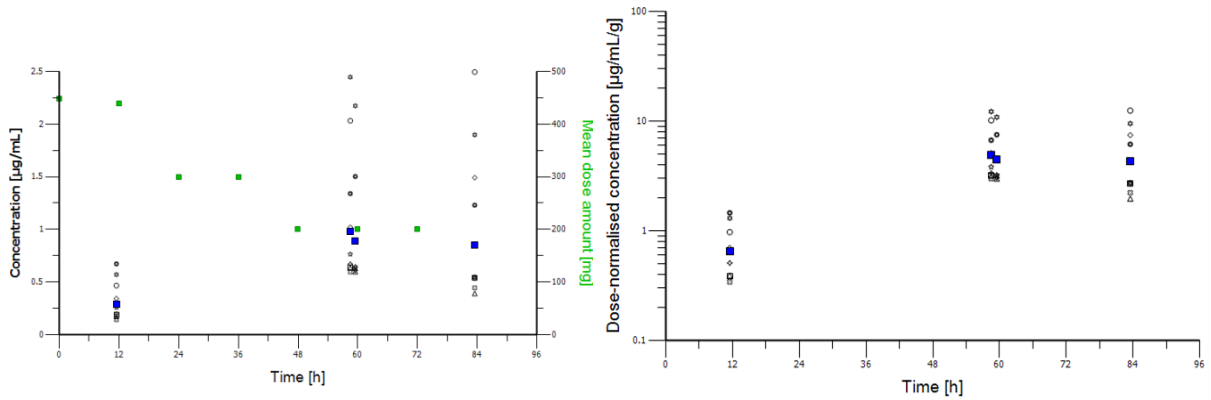

Fig. 3-31: Minimal ISF concentration-time profile (left panel) and dose-normalised profile (right panel) in ID 01 (squares), ID 02 (circles), ID 03 (diamonds), ID 04 (triangles), ID 05 (cross), ID 06 (four-point star), ID 07 (five-point star), ID 08 (six-point star) and ID 09 (ten-point star) (left panel). Mean dose amounts (green squares).

Inter-individual variability of geometric averaged C_{min} in ISF stayed constant from visit 1 to visit 5 (58.0% vs. 58.6%) and increased after multiple oral doses (79.0% at visit 7).

To directly compare UF and ISF data, individual (dots) and geometric mean (squares) concentration-time profiles are pooled in Fig. 3-32. The left panel shows the measured concentrations, whereas the right panel illustrates dose-normalised profiles, both in semi-logarithmic scales.

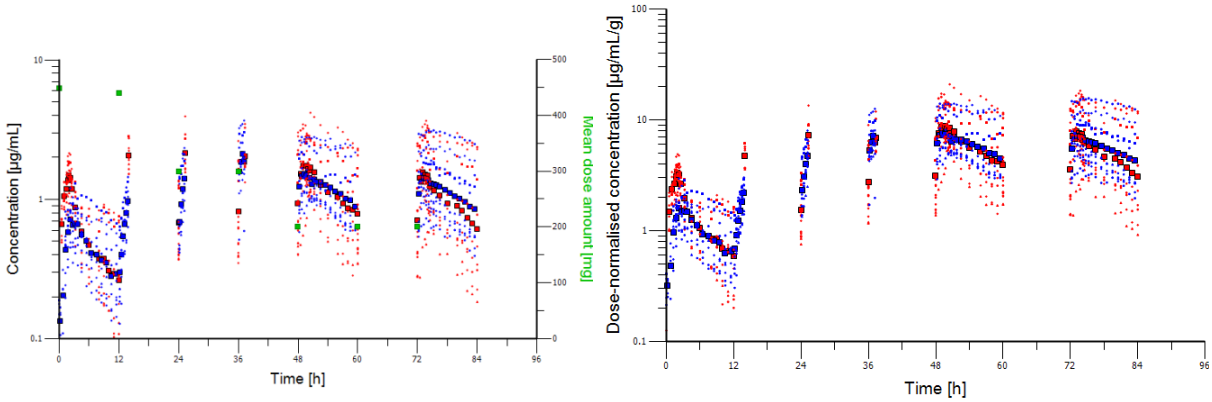

Fig. 3-32: Geometric mean (squares) and individual (points) concentration-time profiles in the two matrices (UF (red) and ISF (blue)) and in semi-logarithmic plots (left panel). Dose-normalised geometric mean and individual concentration-time profiles in the two matrices (right panel). Mean dose amounts (green squares).

Although higher early concentrations were observed in UF related to ISF, comparable late concentrations resulted after single dose. Early, increasing concentrations at visit 2 and visit 3 were higher for UF compared to ISF. This relation converged at visit 4, i.e., similar concentration ranges appeared at visit 4 and visit 5, progressing to higher late concentrations in ISF at the end of visit 7. The slopes of the terminal phases were congruent for both matrices at the start of the study (visit 1, see also Fig. 3-33). Nevertheless, the slope of the geometric mean UF profile was steeper than that of the ISF concentrations in visit 5 and visit 7. These observations are confirmed by the geometric mean values of λ_z shown in Tab. 8-25: terminal slopes in UF and ISF were 0.0999 and 0.0930 at visit 1, respectively, and decreased to 0.0585/0.0381 at visit 5 and 0.0616/0.0468 at visit 7. Inter-individual variability was slightly lower for UF than for ISF at the beginning of visit 1 (blue and red dots, also Fig. 3-30), changing to slightly increased variability of UF data at the end of the single dose interval. Whereas maximum concentrations were within the same range of variability after multiple doses, final UF concentrations of the dosing intervals varied more extensively than ISF concentrations (CV_{geom} of dose-normalised C_{min}: 83.9% (visit 5) and 126% (visit 7) for UF vs. 58.6% (visit 5) and 79.0% (visit 7) for ISF).

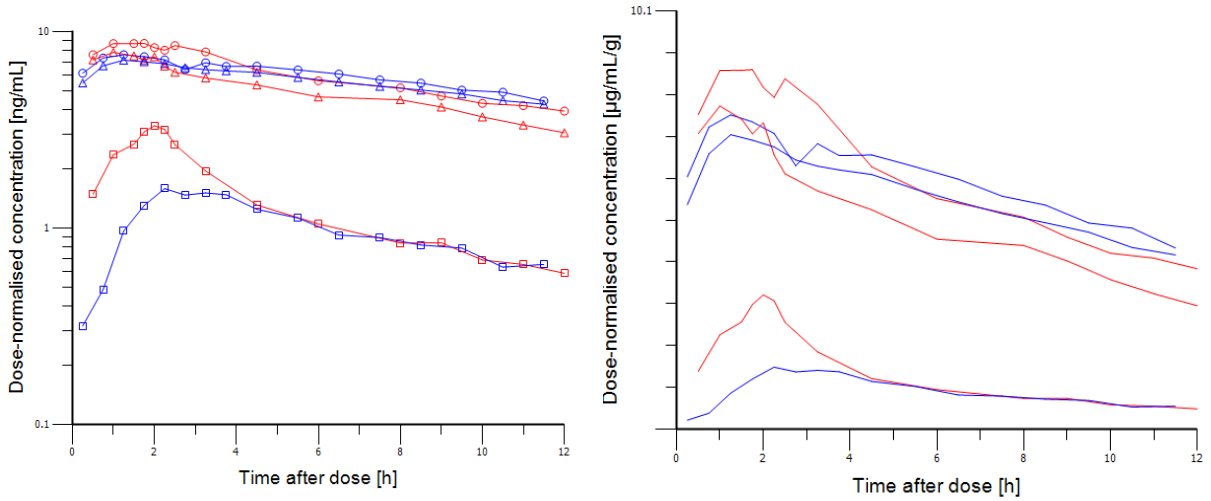

Fig. 3-33: Geometric mean dose-normalised concentration-time plots of voriconazole in UF (red colour) and ISF (blue colour). Visit 1 (squares), visit 5 (circles), visit 7 (triangles) (left panel). Right panel: spaghetti plot.

As prerequisite for elaboration of the number of PK disposition phases being contained in the descending part of the geometric mean profiles, dose-normalised concentration curves are presented in relation to time after the last administered dose applying semi-logarithmic scales (Fig. 3-33). Left and right panels differ in presentation of geometric mean data points additionally to lines. Following single dose administration, ISF and UF concentrations ascended in a parallel manner until C_{max}. Subsequent to t_{max}, UF concentrations initially descended more steeply than ISF data. Terminal slopes were congruent for both matrices at visit 1. ISF curve was shaped monophasically, whereas UF concentrations exhibited a biphasic shape. Following multiple doses, geometric mean profile of UF concentrations proceeded in a monophasic form with parallel slopes between visit 5 and visit 7. Dose-normalised concentrations in ISF showed corresponding profiles. However, declines of the monophasic ISF profiles after multiple dosing were slightly flatter in slope compared to UF profiles.

3.4.8 Pharmacokinetic parameters

Terminal slopes of the individual concentration-time profiles are listed in Tab. 8-24, amended by geometric means of the terminal slopes from all study individuals (Tab. 8-25). Values of r^2 from non-linear regression varied from 0.151 (ID 09, visit 7) to 0.993 (ID 05, visit 7) for UF and from 0.097 (ID 09, visit 5) to 0.988 (ID 07, visit 5) for ISF with median values of 0.923 (visit 1), 0.844 (visit 5) and 0.900 (visit 7) for UF and of 0.913 (visit 1), 0.932 (visit 5) and 0.895 (visit 7) for ISF, respectively. Terminal slopes were in the same range for UF and ISF after single dose and were predominantly higher for UF compared to ISF data after multiple dosing.

Tab. 3-25: Median and range of terminal half-life $t_{1/2}$ [h]

Matrix	Visit 1 x̃ (R)	Visit 5 x̃ (R)	Visit 7 x̃ (R)
UF	4.42 (2.96-29.7)	7.66 (6.18-73.3)	7.13 (5.11-45.6)
ISF	6.75 (3.67-27.8)	11.1 (8.24-85.9)	13.8 (9.38-27.6)

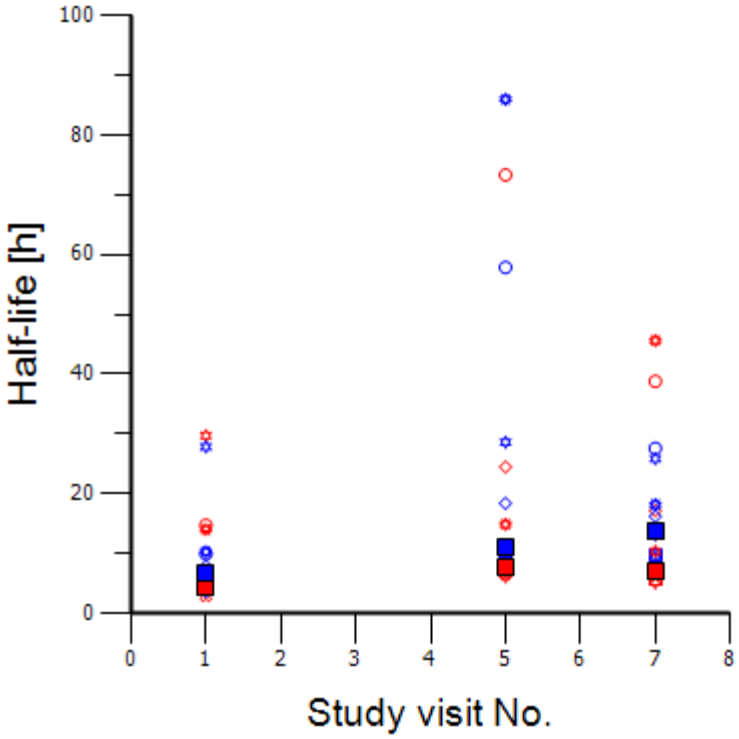

Fig. 3-34: Terminal half-life $t_{1/2}$ after single (visit 1) and multiple dosing (visits 5, 7) in ID 101 (squares), ID 02 (circles), ID 03 (diamonds), ID 04 (triangles), ID 05 (cross), ID 06 (four-point star), ID 07 (five-point star), ID 08 (six-point star) and ID 09 (ten-point star). UF (red colour) and ISF (blue colour). Median values (filled squares).

Calculated terminal half-lives are presented in Tab. 3-25 and Fig. 3-34. UF revealed shorter $t_{1/2}$ at visit 1 compared to visit 5 or visit 7 (approximately 60%), while values were similar between the last visits. Inter-individual variability was more than doubled from visit 1 to visit 5 and was subsequently reduced by 40% in visit 7. In accordance with UF data, ISF showed shorter $t_{1/2}$ after single dose related to multiple doses as well. The value extremely increased at visit 5 (to 164%) and further increased moderately at visit 7 (to 204%). Inter-individual variability of ISF $t_{1/2}$ at visit 1 and visit 7 was lower than UF data, however, the parameter dispersion was in a similar range for both matrices at visit 1 and visit 5. Comparing the median values in ISF and UF, higher $t_{1/2}$ were observed for ISF at all visits. UF and ISF $t_{1/2}$ values from ID 02, ID 08 and ID 09 were always above median values of the entire study population (145%-957% higher in UF and 148%-774% higher in ISF). However, the half-life

determined at visit 5 in ISF of ID 09 has probably to be considered as an outlier, since there was a gap of five µD intervals (three during the terminal phase) due to the catheter replacement and the slope could, therefore, be calculated with inadequate goodness (r^2 of 0.097) only.

With regards to $t_{1/2}$ over time, the individual values also predominantly increased from visit 1 to visit 5 and further to visit 7. These individual as well as the median $t_{1/2}$ indicated a time-dependent non-linear PK behaviour of VRC.

Individual C_{max} and t_{max} values are listed in Tab. 8-26. Additionally, Fig. 3-35 and Tab. 3-26 present individual as well as median values and ranges of t_{max}, respectively.

Tab. 3-26: Median and range of t_{max} [h]

Matrix	Visit 1 x̃ (R)	Visit 5 x̃ (R)	Visit 7 x̃ (R)
UF	2.00 (1.00-2.25)	1.50 (0.50-2.50)	1.00 (0.50-2.50)
ISF	2.75 (1.75-3.75)	1.75 (0.75-4.50)	1.25 (0.25-3.25)

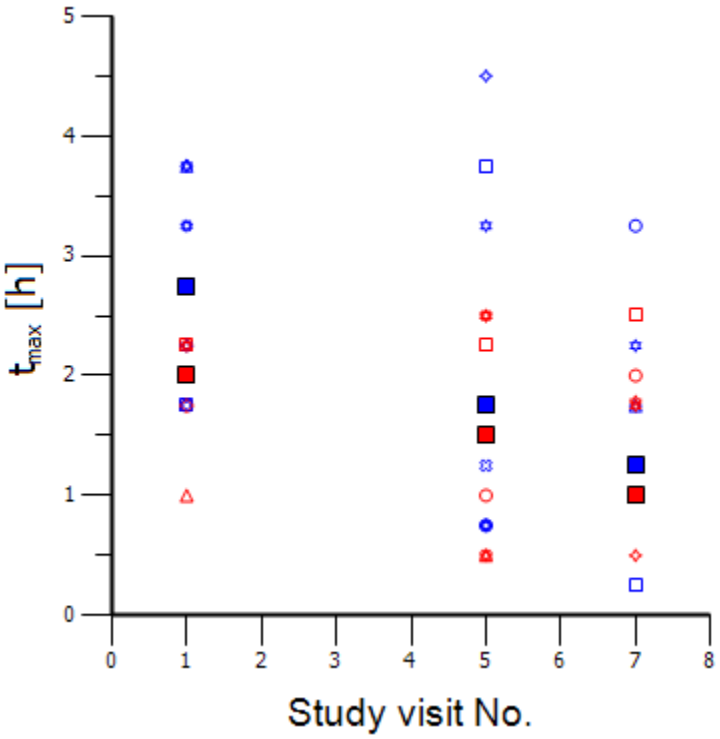

Fig. 3-35: t_{max} after single (visit 1) and multiple dosing (visits 5, 7) in ID 01 (squares), ID 02 (circles), ID 03 (diamonds), ID 04 (triangles), ID 05 (cross), ID 06 (four-point star), ID 07 (five-point star), ID 08 (six-point star) and ID 09 (ten-point star). UF (red colour) and ISF (blue colour). Median values (filled squares).

Median t_{max} in UF was equal to the infusion duration at visit 1 (2 h), whereas C_{max} occurred delayed for 45 min in ISF (at 2.75 h). t_{max} values decreased after PO dosing and were shortest at visit 7. The range of individual t_{max} was extended after PO doses. t_{max} in ISF were consistently increased compared to UF; however, the deviation was reduced to 0.25 h after multiple dosing. ISF t_{max} varied to a higher extent between the individuals compared to UF.
Individual dose-normalised values of C_{max} are presented in Tab. 8-27. Dose-normalised C_{max} of ID 02 as well as of ID 08 increased to the four-fold in UF and to the seven-fold in ISF after multiple dosing relative to single dose. In contrast, C_{max} was barely amplified to the two-fold in both investigated matrices from ID 06. Geometric means of C_{max} and dose-normalised C_{max} are shown in Tab. 3-27 and Fig. 3-36.

Tab. 3-27: Geometric mean, geometric SD, and geometric CV, % of observed C_{max} [µg/mL] and dose-normalised C_{max} [µg/mL/g].

	Single dose			*Multiple dose*					
	Visit 1			*Visit 5*			*Visit 7*		
Matrix	$\bar{X}_{geom}$	SD_{geom}	CV_{geom}	$\bar{X}_{geom}$	SD_{geom}	CV_{geom}	$\bar{X}_{geom}$	SD_{geom}	CV_{geom}
				Observed C_{max}					
UF	1.54	1.27	24.2	2.19	1.54	45.5	1.92	1.69	56.1
ISF	0.79	1.46	39.1	1.65	1.46	39.3	1.50	1.62	51.5
				Dose-normalised C_{max}					
UF	3.45	1.28	25.4	11.0	1.54	45.5	9.60	1.69	56.1
ISF	1.77	1.48	41.1	8.26	1.46	39.3	7.48	1.62	51.5

Geometric mean of C_{max} increased after multiple doses compared to single dose with a slight decrease from visit 5 to visit 7. It was consistently higher in UF than in ISF. The difference between both matrices decreased after multiple dosing. Inter-individual variability was lower for UF compared to ISF at visit 1, in contrast, UF variability slightly surpassed ISF at visit 5, whereas ISF variability stayed constant at visit 1 and visit 5 and only moderately expanded at visit 7. Variability of C_{max} exceeded 50% in both matrices at visit 7.

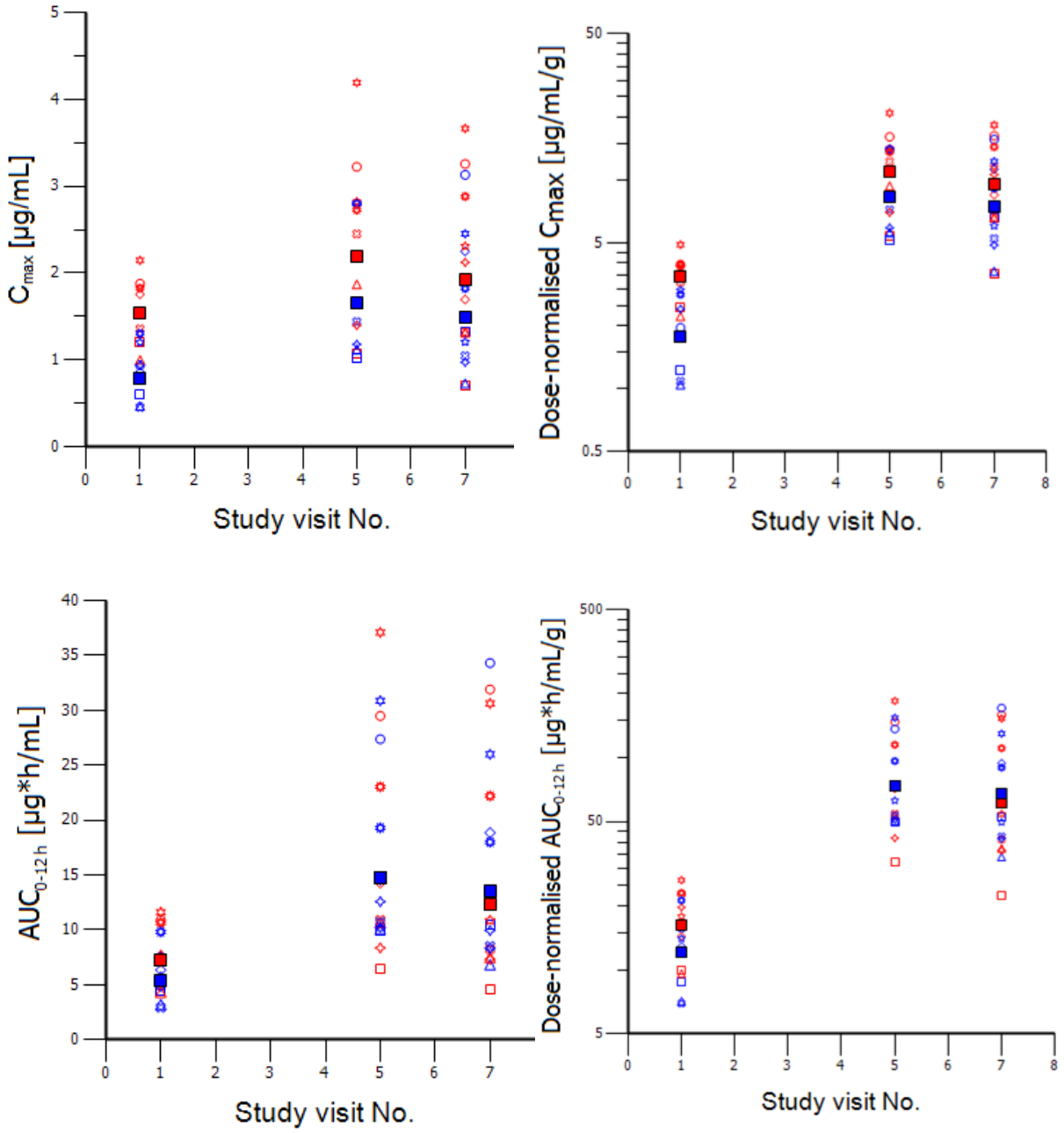

Fig. 3-36: C_{max} and AUC_{τ} after single (visit 1) and multiple dosing (visits 5, 7) in ID 01 (squares), ID 02 (circles), ID 03 (diamonds), ID 04 (triangles), ID 05 (cross), ID 06 (four-point star), ID 07 (five-point star), ID 08 (six-point star) and ID 09 (ten-point star). UF (red colour) and ISF (blue colour). Geometric means (filled squares).

AUC, as a further parameter of the extent of exposure, was tremendously increased after multiple doses compared to single dose administration and slightly decreased at visit 7 related to visit 5. Geometric mean of *AUC* derived from ISF data was overlaying *AUC* from UF at visit 5 illustrated in Fig. 3-36 and observable from data listed in Tab. 3-28. However, inter-individual variability of *AUC* from UF data corresponded to ISF at visit 1 and was higher

at visit 5. Both matrices revealed increased variability at visit 7 still showing higher values for UF than for ISF.

Tab. 3-28: Geometric mean, geometric SD, and geometric CV, % of determined partial *AUC* [µg·h/mL] and dose-normalised partial *AUC* [µg·h/mL/g]

	Single dose			*Multiple dose*					
	AUC0-12h			*AUC48-60h*			*AUC72-84h*		
Matrix	$\bar{X}_{geom}$	SD_{geom}	CV_{geom}	$\bar{X}_{geom}$	SD_{geom}	CV_{geom}	$\bar{X}_{geom}$	SD_{geom}	CV_{geom}
				Determined AUC					
UF	7.30	1.44	37.7	14.7	1.80	64.0	12.3	1.99	77.9
ISF	5.39	1.49	41.8	14.7	1.56	46.5	13.5	1.76	61.5
				Dose-normalised AUC					
UF	16.3	1.46	39.0	73.6	1.80	64.0	61.4	1.99	77.9
ISF	12.1	1.47	40.2	73.6	1.56	46.5	67.6	1.76	61.5

Tab. 3-29: *AUC* ratios (AUC_{ISF}/AUC_{UF})

ID	AUC_{ISF}/AUC_{UF}				
	Single dose	*Multiple dose*			
	Visit 1	Visit 5	Visit 7	*Δ, %*	
	AUC0-12h	*AUC48-60h*	*AUC72-84h*	Visit 1 → Visit 5	Visit 5 → Visit 7
01	0.89	1.55	2.33	+73.9	+50.4
02	0.69	0.93	1.08	+34.2	+15.9
03	0.90	1.02	1.42	+13.8	+39.2
04	0.74	0.94	0.91	+27.7	-3.51
05	0.56	0.98	1.03	+74.6	+5.30
06	0.63	1.22	1.13	+94.6	-7.39
07	0.79	0.87	0.91	+10.1	+5.65
08	0.62	0.83	0.85	+34.2	+1.98
09	0.92	0.84	0.81	-9.13	-3.26
Summary statistics					
$\bar{X}_{geom}$	0.74	1.00	1.10		
SD_{geom}	1.20	1.22	1.39		
CV_{geom} ,%	18.2	20.4	33.8		

To compare the extent of drug distribution in the subcutaneous tissue fluid to the drug exposure in plasma, ratios of AUC_τ between ISF and UF were calculated for the different visits. Results are displayed in Tab. 3-29. Individual ratios were lower than 1 at visit 1 (geometric mean: 0.74) and were spread around 1 at visit 5 (geometric mean: 1.00; 33.3% of individual ratios ≥1.00) as well as at visit 7 (geometric mean: 1.10; 55.6% ≥1.00). ID 01 showed remarkable high ratios at visit 5 and visit 7, tremendously exceeding ratios of the other individuals. The differences of the ratios at the individual visits considerably varied between the study participants (see right two columns of Tab. 3-29) and were predominantly of positive values due to ratios increasing with multiple dosing. ID 06 showed the highest relative increase from visit 1 to visit 5 followed by a slight decrease at the subsequent visit.

While AUC_{ISF} near steady state was occasionally (ten of 18 ratios) below AUC_{UF}, C_{min} in ISF consistently exceeded the one in plasma in the individuals except for ID 02, ID 08 and ID 09 (three of 18 C_{min} did not) (Tab. 8-29).

Tab. 3-30: Drug accumulation factors ($AUC_{\tau\,(multiple\ dose)}/AUC_{\tau\,(single\ dose)}$) ($AUC_{\tau\,(multiple\ dose)}$ of visit 5 and visit 7, $AUC_{\tau\,(single\ dose)}$ of visit 1)

Matrix	*Visit 5*			*Visit 7*		
	$\bar{X}_{geom}$	SD_{geom}	CV_{geom}	$\bar{X}_{geom}$	SD_{geom}	CV_{geom}
	Determined $AUC_{\tau\,(multiple\ dose)}/AUC_{\tau\,(single\ dose)}$					
UF	2.02	1.40	34.9	1.68	1.49	41.7
ISF	2.73	1.34	29.7	2.51	1.41	35.3
	Dose-normalised $AUC_{\tau\,(multiple\ dose)}/AUC_{\tau\,(single\ dose)}$					
UF	4.50	1.44	38.0	3.76	1.54	45.2
ISF	6.11	1.36	31.1	5.61	1.48	40.7

Drug accumulation factors were determined to quantify drug accumulation in plasma and subcutaneous tissue fluid after multiple doses (see Tab. 3-30). Considering dose-normalised data, AUC_τ increased to the four-fold value in plasma and six-fold value in ISF after multiple dosing. Factors were slightly higher at visit 5 compared to visit 7. Variability ranged from 31.1% to 45.2% and was marginally increased for UF related to ISF.

Assuming that steady-state conditions were almost reached and based on an oral bioavailability of 100%, comparison of dose-normalised AUC_τ at visit 7 with dose-normalised $AUC_{0-\infty}$ after single dose was performed. Since the common bioavailability/bioequivalence study criterion for the extrapolated part of $AUC_{0-\infty}$ to be ≤20% [181; 187] was only fulfilled for

UF data of ID 01, 04-07 and ISF data of ID 06, ratios were calculated exclusively for these *AUC* values. Dose-normalised AUC_{τ} at visit 7 were 22.5 µg·h/mL/g, 37.4 µg·h/mL/g, 41.2 µg·h/mL/g, 36.6 µg·h/mL/g, and 54.3 µg·h/mL/g for UF of ID 01, 04, 05, 06, and 07 and 41.5 µg·h/mL/g for ISF of ID 06 (see Tab. 8-28), respectively, and corresponding $AUC_{0-\infty}$ after single dose amounted to 9.91 µg·h/mL/g, 9.61 µg·h/mL/g, 12.4 µg·h/mL/g, 19.7 µg·h/mL/g, and 17.9 µg·h/mL/g for UF of ID 01, 04, 05, 06, and 07 and 12.4 µg·h/mL/g for ISF of ID 06. Ratios between AUC_{τ} and $AUC_{0-\infty}$ were 2.3, 3.9, 3.3, 1.9, and 3.0 for UF and 3.3 for ISF data.

Tab. 3-31: Voriconazole clearance (CL) [L/h/kg] and apparent volume of distribution (V) [L/kg] at visit 7

ID	Matrix	CL	V
01	UF	0.54	4.51
	ISF	0.23	3.27
02	UF	0.08	4.38
	ISF	0.07	2.90
03	UF	0.18	4.56
	ISF	0.13	3.03
04	UF	0.36	3.46
	ISF	0.39	7.74
05	UF	0.35	3.59
	ISF	0.34	4.72
06	UF	0.42	3.09
	ISF	0.37	7.01
07	UF	0.27	2.48
	ISF	0.30	4.02
08	UF	0.09	1.34
	ISF	0.11	3.94
09	UF	0.12	7.72
	ISF	0.14	3.80

CL and V were calculated from NCA at visit 7 and listed for the individuals in Tab. 3-31. In order to compare the individual values, CL and V were normalised to WT. CL ranged between 0.08 L/h/kg and 0.54 L/h/kg for UF as well as 0.07 L/h/kg and 0.39 L/h/kg for ISF. Arithmetic means and CV are presented in Tab. 3-32.

Tab. 3-32: Arithmetric mean of CL [L/h/kg] and V [L/kg] at visit 7

	CL		V	
Matrix	$\bar{x}$	CV	$\bar{x}$	CV
UF	0.27	60.2	3.90	45.4
ISF	0.23	52.9	4.49	38.7

Inter-individual variability high for both parameters and was approximately 15% higher for CL than for V. Whereas CL of UF exceeded the one calculated for ISF, V showed opposite results.

Non-normalised CL ranged from 6.27 L/h to 27.3 L/h for UF and from 5.83 L/h to 29.3 L/h in ISF. Arithmetic mean CL was 19.8 L/h and 16.8 L/h for UF and ISF, respectively.

3.4.9 Genotype effect on pharmacokinetic parameters

The potential influence of genotype of the metabolising enzymes cytochrome P450 (2C9, 2C19) on the PK of VRC was preliminary explored. Since genotypes of the study individuals

were analysed to a different extent of included alleles, less information was provided for the first five individuals (see Tab. 3-33).

Tab. 3-33: Detailed genetic variations for isoenzymes CYP2C9 and CYP2C19 within the individuals 01-09

ID	Isoenzymes						Pheno-type
	CYP2C9*2	CYP2C9*3	CYP2C19*2	CYP2C19*17	CYP2C19*3	CYP2C19*4	
01	0	1	0	3	3	3	
02	**0**	**0**	**2**	**0[a]**	**0[a]**	**0[a]**	**PM**
03	0	0	0	3	3	3	
04	0	0	1	3 (0/1)[a]	3 (0/1)[a]	3 (0/1)[a]	
05	0	0	0	3	3	3	
06	**0**	**0**	**0**	**1**	**0**	**0**	**UM**
07	**1**	**0**	**0**	**0**	**0**	**0**	**EM**
08	**0**	**0**	**1**	**0**	**0**	**0**	**IM**
09	**0**	**0**	**1**	**1**	**0**	**0**	**PM/UM**

0= wild type
1= heterozygous
2= homozygous
3= unknown
[a] conclusion from CYP2C19*2 homogenous/heterogenous status

CYP2C9 genotype analyses revealed only heterozygous mutations in two individuals. Due to the lack of homozygous CYP2C9 mutants and the occurence of only one of each mutant allele in the study population, data was considered not to be sufficient for an analysis of a potential influence of this genotype on PK parameters. Consequently, PK results were not presented in relation to CYP2C9 genotype.

The five individuals with known genotype alleles on both autosomal chromosomes (see Tab. 3-33, bold type), i.e. ID 02 as well as ID 06, 07, 08 and 09, were selected for the analysis of the potential influence of CYP2C19 on PK parameters. Each of the five individuals was a distinct genotype of the mentioned isoenzyme. While ID 02, who was a homozygous carrier of a mutation with reduced or absent enzyme activity, has the status of a PM [152; 188], ID 08 was an intermediate metaboliser (IM), i.e. a heterozygous mutant with reduced enzyme function [189]. The homozygous wild type (ID 07) was characterised as EM [151]. In view of the fact that CYP2C19*17 was associated with increased enzyme activity, ID 06 was referred to as an ultra-rapid metaboliser (UM) [190]. The status of ID 09 was assumed to be situated between PM and UM, considering that the individual carried one loss-of-function and a gain-of-function allele (PM/UM).

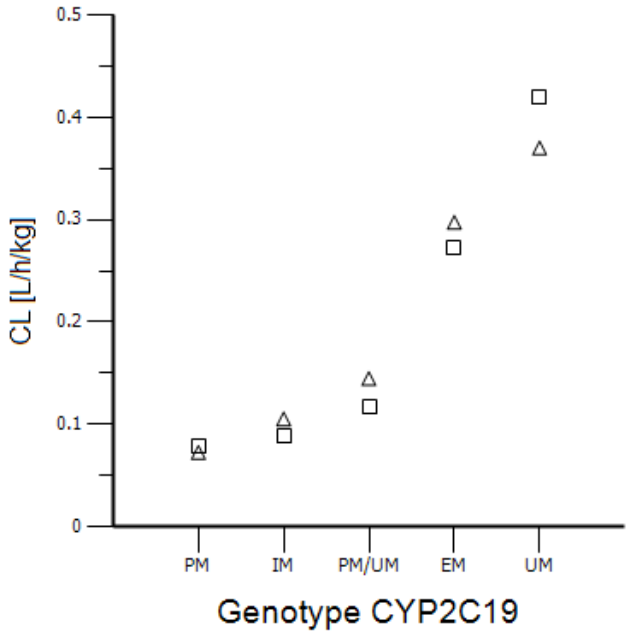

Fig. 3-37: Voriconazole clearance at visit 7 (CL [L/h/kg]) in dependence on CYP2C19 phenotype. UF (squares) and ISF (triangles).

CL of VRC increased with amplified enzyme activity hypothesised from CYP2C19 genotype, whereas CL of the individual with heterozygous *2/*17 alleles (PM/UM) lied between parameters of IM and EM. The relation between supposed phenotype and CL was similar for UF and ISF. Especially in UF the trend was shaped in an exponential manner. Since there were only five data points in each matrix (i.e. only one data point at each genotype), the data was considered not to be sufficient for a mathematical description of the supposed relation.

4 DISCUSSION

Cytokines represent a crucial component of various diseases; hence, reliable quantification at the site of inflammation would enable to monitor disease progression and therapeutic efficacy. The selection of the model cytokines IL-6, IL-8 and TNF-α as well as the anti-inflammatory cytokine IL-10 for the investigations of this thesis was based on clinical relevance [102; 114; 191; 192], on the wide range of physicochemical properties (e.g. molar mass, (see Tab. 1-1)) of these analytes and on the physiological release of the cytokines at subsequent time points during the process of appearing or disappearing inflammation.
µD of cytokines was investigated step by step, initially validating the adapted bioanalytical method (project I, section 4.1), subsequently evaluating feasibility and characteristics of µD of cytokines *in vitro* (project II, section 4.2), resulting in the optimal µD set up conditions for the pilot *in vivo* µD study (project III, section 4.3).
In order to complement the approach of optimisation of drug therapy, VRC quantification at the target-site was performed in a clinical long-term µD study (project IV, section 4.4) and compared to systemic VRC concentrations.

4.1 Project I: Bioanalytical method for quantification of IL-6, IL-8, IL-10 and TNF-α from microdialysate

Currently, a high proportion of research articles does not provide appropriate information about the validity of the applied assays for cytokine quantification. Additionally, no internationally approved standard for mass concentrations of cytokines is provided limiting the comparablility of results from bioanalyses from different laboratories. As a consequence of its composition, the BD™CBA represents a multiplex-assay with the option to determine up to 30 bead sets and therefore up to 30 individual analytes simultaneously in a single sample of 50 µL [193]. The here described bioanalytical method was adapted from the BD™CBA for cell-culture supernatant samples (see first paragraph of section 3.1). As one characteristic of this adaption, reagent consumption was reduced to 50%. HA was added to the matrix as a carrier protein to ensure protein stability and reduce unspecific adsorption of cytokines to vials, microtitre plates and µD component surfaces. Non-linear regression was arranged to be performed independently from the FACS software, resulting in a traceable and reproducible regression analysis process.
The validated assay was in accordance (see section 3.1.2) with requirements of the EMA Guideline on BMV [17] and forms the mandatory basis for *in vitro* and *in vivo* µD investigations of the four pro- and anti-inflammatory model cytokines.

4.1.1 Method validation

Since all (*in vitro* and *in vivo*) study samples were stored at -80 °C until analysis, all samples underwent at least one freeze-thaw cycle. Therefore, the evaluation of the stability (see section 3.1.2.1) after one freeze-thaw cycle was the basis for the reliable quantification of samples from *in vitro* and *in vivo* µD investigations of cytokines. Freeze-and-thaw investigations revealed stability for a minimum of two freezing cycles.

Furthermore, incorporation of Cal and QC samples in analytical runs are mandatory for in-study validation reasons. Therefore, the confirmed stability of stock solution provides the prerequisite for a reproducible Cal and QC preparation.

Study samples were exposed to temperatures between RT and ca. 34 °C at the abdominal body site of healthy volunteers, where they remained during the µD interval for up to 2 h (see section 2.7.1.1). µDialysate samples were subsequently stored at RT from the time of sample collection until freezing at -80 °C for a maximum of 60 min (see section 2.7.2). The four cytokines remained stable at 37 °C as well as at RT for at least 4 h as described in subsection 3.1.2.1 and section 3.2.1. Consequently, sampling and storing conditions throughout the *in vivo* study were appropriate to ensure stability of the investigated cytokines.

Bioanalysis of study samples should be performed within 2 months after freezing, since long-term storage investigation indicated a beginning degradation of cytokines between 2 and 8 months (section 3.1.2.1), i.e. stability recovery after 8 months of storage at -80 °C ranged between 83.7% and 90.7% (CV: 3.27%-9.48%), which was still within the acceptance criteria. In the study applying the validated method (see section 2.7), all study samples were analysed within 25 days after sampling.

The bioanalysis runs are supposed not to exceed a number of 96 tests including Cal and QC in view of post-preparative stability results: samples on a second microtitre plate, as processed 1 h subsequently to the first microplate, were reduced in cytokine concentration recovery for up to 26.1%.

Higher stability of IL-6 compared to TNF-α had been observed in EDTA treated plasma samples, which correlates to observations of this work in µDialysate [194]. IL-6 was stable over six freeze-thaw-cycles in EDTA plasma, whereas TNF-α consistently increased with each freezing step with statistical significance from the third cycle on [195]. Stability of IL-6, IL-8 and TNF-α was previously confirmed over 8 h at RT, over 24 h at 4 °C or deep-frozen in EDTA plasma [196]. Sample preparation and storage conditions were affecting cytokine stability and showed high variability of recovered concentrations in plasma samples [194–196].

Considering negative cross-reactivity investigations of capture and detection antibodies that had been conducted by the manufacturer [166] (see 2.4.2.3) and given the fact that no

related compounds were expected to occur during the µD study (2.7), no specificity testing according to the EMA Guideline on BMV [17] was performed throughout validation of the bioanalytical method.
For future studies, going beyond the objectives of an explorative pilot investigation, specificity tests by adding related exogenous or endogenous compounds to QC samples will need to be considered. For analyte-unrelated compounds, in particular study or concomitant drugs, selectivity tests with spiking at least 10 sources of samples matrix near or at LLOQ will have to be performed as well [17; 197].

LOD was calculated via a converted t-test as recommended by Rodbard et al. [167] for radioligand assays and was significantly lower than LLOQ. No carry-over effect was detected supporting independent (random) sample arrangement on the microtitre plate.
LLOQ was set to be 5 pg/mL and was validated with intra-assay imprecision (CV) and inaccuracy (RE) limits of 16.8%/±14.9% (IL-6), 30.4%/±36.5% (IL-8), 26.9%/±29.5% (IL-10) and 27.8%/±10.1% (TNF-α). Quantification within the concentration range of 10 to 10000 pg/mL was confirmed to fulfil requirements of the EMA Guideline on BMV [17] for ligand binding assays, except for mean intra-assay inaccuracy of TNF-α (≤±23.7% RE, 93% of mean RE <±20%). Consequently, the four model cytokines can be reliable determined by the validated method in a concentration range exceeding the one of e.g. the common ELISA technique (i.e. a range of about two decimal powers) [198–200]. Nonetheless, considering that lyophilisates for Cal and QC preparation are not available in a purified form fully characterised, or fully representative of an endogenous biomarker (since produced by non-human microorganisms), the method has to be defined as a ‘relative quantitative assay’ with ‘estimated’ accuracy [201; 202].
For concentrations exceeding the ULOQ, dilutional integrity was demonstrated up to ca. 150,000 pg/mL (see section 3.1.2.4). This finding enables the quantification of cytokines from µDialysate covering the reported physiological as well as the pathophysiological concentration range in tissues: Brennan et al. published IL-8 concentrations in a range of 830 pg/mL up to 8800 pg/mL in synovial fluid [70], whereas Cameron et al. found mean IL-6 and IL-8 concentrations of 51,302 pg/mL and 22,897 pg/mL, respectively, and low TNF-α concentrations in the double-digit pg/mL-range in synovial fluid of chronically inflamed knees [203]. Immense IL-6 concentrations higher than 100,000 pg/mL were measured from peritoneal fluid, whilst concentrations of IL-10 and TNF-α were predominantly lower than 1000 pg/mL [114]. The inter-quartile ranges of concentrations from bronchoalveolar lavage fluid sampled from seventeen patients suffering from ventilator-associated pneumonia were 105-503 pg/mL for IL-6, 2633-11762 pg/mL for IL-8, 0-9 pg/mL for IL-10 and 0-18 pg/mL for TNF-α [112]. Aforementioned concentrations were directly quantified from specific tissue

fluids by immunological assays, however, the focused µDialysate concentrations always only reflect a part of the concentrations in ISF of the individual tissue.

Investigation of the parallelism between dilution series from a study sample and spiked in-study validation samples was performed to detect possible matrix effects [17; 170; 204] and did not show deviations between dilution series of in-study and Cal samples (Tab. 3-4). In view of these results, matrix effects such as cross-reactivity of metabolism products with capture reagents or interference from endogenous compounds [205] appeared not to influence the bioanalytical method. Additionally, one incurred study sample was re-analysed throughout parallelism investigation. This second analysis resulted in the same concentration result as the first one (see section 3.1.2.5). Accordingly, requirements of incurred sample re-analysis were met [205; 206] with regards to accuracy. However, this analysis should be further addressed in future, especially in non-exploratory, studies [207], since the number of re-analysed samples from the clinical study (project III) was not in accordance with the EMA Guideline on BMV [17], which was caused by the pilot character of the conducted study.

To investigate internal intermediate precision, voltages of the detectors for identification as well as for quantification were changed on several of the individual validation days aiming for increased separation of the individual cytokine clusters during data acquisition. These adjustments did not influence the goodness of fit of the non-linear regression of Cal solutions, and did not affect concentration measurements of QC.
Due to simplification of sample processing and handling of a large number of sample replicates (i.e. up to 96 samples per run), Cal and QC replicates are regularly located sequentially on the first cavities of the microtitre plate. This fact potentially influences the goodness of in-study validation procedures and was therefore investigated. Section 3.1.2.6 outlines corresponding accuracy and precision ranges for sequentially and randomly distributed QC aliquots, which showed no differences.
Demonstrating external intermediate precision, a second “untrained” analyst was able to adequately perform sample processing and analysis, guided by SOP describing the bioanalytical method (see section 8.1) and supported by the manufacturer’s manuals.
The objective of the reinjection tests was to investigate the possibility of sample reinjection directly after the first plate read-out: if the analysis of samples failed due to unexpected device-dependent or other reasons, an immediate reinjection of samples could be required. Furthermore the requirement of the reinjection of Cal additionally to these ‘lost’ samples was to be investigated. Concluding from the results of section 3.1.2.6, a second analysis of samples by reinjection of the processed replicates on the 96-well-plate is associated with a loss of quality. Imprecision marginally increased in the reinjected samples, while inaccuracy

was higher for the predominant number of corresponding samples. Overall, reinjection resulted in lower MFI, thus, calculation of concentrations of reinjected samples using the calibration function of the first injection led to an underestimation of those concentrations. Therefore, additional reinjection of Cal samples is required. Immediate reinjection provides further information about samples, for which an uncertainty emerged during the first injection. Nevertheless, results would be affected by decreased correctness and reliability, but would predominantly meet the acceptance criteria, if Cal had been simultaneously reinjected (Tab. 3-9). Consequently, reinjection of samples having failed during first injection should be restricted to analysis runs, for which reanalysis of a second replicate of the concerned samples might not be feasible.

Several reasons for the observed concentration deviations might be the following hypothetic ones: (i) the emission of the fluorescence light might have decreased over time as a result of conformational changes or degradation of the dye molecules and of an increasing quenching by oxygen, respectively, potentially leading to a reduced emission intensity; (ii) the stability of the bead-antibody-cytokine-detection-antibody complex might have been limited due to short stability of the protein molecules and a possible change of affinity of this antibody-antigen complex in the medium; (iii) stability of the cytokines themselves might have been time-dependent (see section 3.1.2.1), hence cytokines bound in this complex might have been destructed and not measurable any longer.

As prerequisite for the investigation of effect of pH value on RR (see section 2.6.5 and 0) and analysing the external intermediate precision of the bioanalytical method, pH effect on the quantification of cytokines was determined. pH values of 5 and 8 visually changed the colour of sample solution throughout the predilution step in sample processing (see section 8.1.2). Samples were diluted in a ratio of 1:1 with AD, which contained a buffer (PBS supposed) and a coloured pH indicator. Accordingly, the buffering system of AD could not neutralise the pH-adjusted samples, which did not contain buffering substances.

Validity of the bioanalytical assay was partly affected by pH value of the analysed µD samples (3.1.2.6): In contrast to the robust concentration recovery of IL-6 and IL-8, substantial pH influence on the concentration recovery of IL-10 and TNF-α was observed. In view of these results, knowledge of pH values of the surrounding ISF has to be considered in *in vivo* µDialysate measurements for these two cytokines. Potential reasons for the observed pH influence leading to decreased concentration recoveries might be (i) probable changes in protein conformation due to the varying protonation of the amino acids at the different pH values (see Tab. 1-1 for isoelectric points), which may result in modifications of the epitope structure as the target structure of the analytical capture and detection antibodies or alteration of the paratopes of these antibodies added to the pH-modified samples; (ii) pH

dependence of the activity of ubiquitous proteolytic enzymes degrading the analytes; and (iii) the increased ionic strength of the pH-modified solutions.

To facilitate the comparison to already published results of the scientitifc community, in-house Cal, used for in-study analysis, had to be compared to international standards to ensure comparability of cytokine analysis results from different laboratories. International cytokine mass concentration standards for immunological assays did and currently do not exist. Therefore activity standards for biological assays, which were delivered by the National Institute for Biological Standards and Control (NIBSC) and represent the WHO recommended standards, had to be used for this approach. This utilisation was limited by the mass declaration of those standards with “approximately 1 µg” per lyophilisate [208–211]. Consequently, the calculated conversion factors for in-house analysed concentrations related to the international standards were approximations as well.

The differences between the CBA Flex Set Standards and the in-house Cal concerning their preparation consisted of the alternative method of dilution (serial vs. non-serial) and the diverse procedure of ‘top standard’ and stock solution preparation, respectively. While the top standard from BD was a solution of a single lyophilisate per cytokine from a certain batch, the in-house stock solution constituted a solution of four lyophilisates per cytokine from at least two batches of CBA standards. Those varying preparation methods could result in slight deviations between the Cal, nonetheless, the observed extensive divergence between analysis results and BD statements was not explainable.

The reasons for the published varying conversion factors of the CBA standards for Flex Sets on the one hand and for the Kits on the other hand were not explained by the company. The comment given by BD was: “The source of a recombinant protein (i.e., insect cell, E. coli, etc.) and the affinity of antibodies used can affect the measurement and performance of a protein in an immunoassay. The conversion factors provided in the subsequent tables [see values in 3.1.2.7] make it possible to compare protein concentrations in samples measured by different immunoassays that have been standardised to the same NIBSC/WHO standards. The conversion factor may change based on the batch of either standard. Therefore, the conversion factor is intended to be a guideline indicating whether a BD CBA assay over- or underestimates analyte concentrations relative to the NIBSC/WHO standards. Researchers are advised to incorporate both sets of standards in their assays if they wish to derive data from the NIBSC/WHO standards” [185].

Calculation of the ratios would provide a potential tool for comparison of study samples between different laboratories. However, this requires reliability and constancy of mass concentrations of the underlying in-house as well as the international standards. Alternatively, in-house standards could completely be replaced by international ones,

nonetheless demanding batch-to-batch conformity in mass values. Results of this thesis were not in accordance with those published by the manufacturer (BD) of the standards applied for in-house Cal solutions. Whereas BD used one lyophilisate batch per cytokine for comparison, the investigation described in section 2.4.2.9 applied several aliquots of a minimum of two batches for production of in-house solutions. One single lyophilisate per cytokine was employed in preparation of solution from WHO standards. If batch-to-batch variability of either BD CBA or WHO standards generated the deviations between previous results and the one presented in this thesis, the standards would not be appropriate and reliable for consistent in-study validation and comparison of concentration results between laboratories. Additional validation work has to be conducted in a routine manner to guarantee at least the consistency of in-house validation solutions despite of batch-to-batch variations of the supplied lyophilisates [201]. Since consistency of the in-house Cal and QC solutions has been evaluated and confirmed during the bioanalytical work presented in this thesis, the results are at least comparable within and between the different projects. Furthermore, the data can be related to the batch of WHO standards which were compared to the in-house Cal.

Based on international guidelines [17; 197] and validation results, recommendations for acceptance limits during in-study validation are highlighted in section 3.1.3. Further recommended QC procedures for cytokine and soluble-marker testing include replicate testing of two or more reference samples provided by the kit manufacturer, replicate testing of in-house frozen reference QC samples that represent normal and abnormal analyte contents, retesting 15% to 20% of randomly selected samples (i.e. incurred sample re-analysis), and comparing normal reference ranges each year [95]. These recommendations should be followed applying the validated bioanalytical method.

Immunoassays are bioanalytical methods in which quantitation of the analyte depends on the reaction of an antigen (i.e. the analyte) and an antibody. The above described adapted method belongs to the ligand-binding assays (LBA), which are essentially the only current bioanalytical option with sufficient sensitivity for the measurement of biologic macromolecules in such complex matrices as serum or plasma [205]. These procedures currently find most consistent application in the pharmaceutical industry to the quantitation of protein molecules. Immunoassays are also frequently applied in such important areas as the quantitation of biomarker molecules which indicate disease progression or remission, and antibodies elicited in response to treatment with macromolecular therapeutic drug candidates [184]. Historically, ELISA became the gold standard, yet this approach of measuring a single protein in each sample limits the amount of information which can be obtained from limited

volumes of human sample. In recent years commercially available multiplex technologies (refer to section 2.2.1) which detect large numbers of proteins in a limited volume have provided investigators with opportunities to begin addressing the complexity of inflammatory responses [212].

However, LBA do have a variety of drawbacks: (i) samples are usually diluted for LBA analysis instead of being processed by extraction; consequently, the analyte is not separated from its anabolism or metabolism products, which are widely unknown and might cause interferences from cross-reactivity with the capture reagent. Furthermore, the relative biological activity of these products compared to that of the parent molecule is unknown. (ii) Endogenous antibodies or soluble receptors for the macromolecule of interest might result in interferences with the assay. These potential interferences and the resulting inaccuracy need to be clearly acknowledged during interpretation of study data and derivation of conclusions about calculated pharmacokinetic parameters [205].

Since the core of the assay is an antigen-antibody reaction, immunoassays may be less precise than chromatographic assays; thus, criteria for accuracy and precision, both in pre-study validation experiments and in the analysis of in-study quality control samples, are more lenient than for chromatographic assays [184; 213].

LC-MS/MS would probably provide an alternative method, increasing the knowledge about incurred sample composition due to combination of chromatographic separation and specific fragmentation pattern [205]. LC-MS/MS could likewise be applied throughout pre-study and first in-study validation to affirm analyte concentration determinations from study samples and specificity issues complementary to LBA (cross-validation) [184; 202]. However, µDialysate is not effortlessly applicable to LC-MS/MS analysis due to high ionic strength of the RS based matrix and the additional human albumin molecules [214].

Another issue to address is the handling of a cytokine-containing matrix. Since µDialysate advantageously is not as complex in composition as blood or plasma, degradation and stability problems did not appear in a quantity and frequence as expected for those other matrices [194; 215]. For example, cytokine-secreting cells are separated from the analytes during µD, consequently, confounding factors on cytokine measurement cannot arise from post-sampling cytokine secretion or cell destruction.

4.2 Project II: *In vitro* microdialysis of cytokines

4.2.1 *In vitro* microdialysis investigations

Standardisation of *in vitro* µD investigations is highly desirable for comparability and reproducibility of various data from different experiments and furthermore from different laboratories. So far, no completely standardised *in vitro* µD system has been commercially available. The presented *in vitro* system had effectively been applied for the first time in µD investigations of antiinfective drugs [172], was subsequently utilised for µD of cytokines in the current investigation and can universally be used as a basic tool for *in vitro* µD investigations.
Handling of µD of cytokines required an enhanced amount of caution in the performance of the experiments compared to µD investigations of small drugs. Reasons for this fact predominantly resulted from the characteristics of µPerfusate and the catheter-surrounding matrix, which both were extended by addition of HA to RS, which is the common µPerfusate for the determination of small molecules. Protein solutions do permanently need special attention, beginning at the simplest pipetting step, due to increased viscosity and adsorption phenomena. HA was added to the µPerfusate for aforemententioned purposes (see section 4.1) and was a component of the catheter-surrounding medium as well to mimic the physiological composition of ISF. Hydrostatic, hydrodynamic as well as osmotic conditions *in vivo* were considered to be adequately represented *in vitro* by this matrix.
The following means to prevent failures in µD performance caused by the viscous µPerfusate were applied: Time periods of flushing the µD system by the µD pump were extended to remove air bubbles from the tubing and the membrane hollow part and to ensure homogenisation and equilibration of all system fluids; air remaining from the process of the connection of the syringe to the inlet tubing was avoided and the stirring velocity of the outer medium was intensified to assure constant homogenisation.
Stability of the four model cytokines in RS/HA at 37 °C was confirmed for a minimum of 4 h (see section 3.2.1). This time period adequately confirmed analyte stability in sampling vials over individual µD intervals throughout *in vitro* and *in vivo* investigations. However, stability was not sufficient to provide the opportunity of over-night sampling of cytokines, which would have been performed over a minimal interval of 12 h.
Loss of µDialysate volume was predominantly less than 30% (see 3.2.1) and was therefore compensated by planned increased sampling intervals to obtain sample volume surplus. No consistent trends concerning the dependence on FR were observed. While volumes sharply increased from 0.3 µL/min to 0.5 µL/min at 25 °C and subsequently slightly decreased, volume recoveries were vice versa at 37 °C. At the higher temperature adjusted by IVMS, the difference between µPerfusate temperature within the µD syringe and the catheter-surrounding medium was increased. Therefore, physico-chemical properties (e.g. fluid

densities) deviated to an extended amount in this setting. However, differences between the two temperature settings were not statistically significant. Whereas evaporation results consequentially increased with prolonged µD intervals (i.e. at lower FR), overall volume loss did not follow this trend and had to be additionally caused by a further influencing factor. This effect was attributed to the phenomenon of UF, which defines the fluid loss (or gain) of µPerfusate via the semi-permeable µD membrane [38; 39]. Theoretically, an increased loss of fluid volume would have been expected with low FR applying only RS as µPerfusate due to the hyperosmotic pressure of the surrounding medium. Using RS+HA did not show this trend in the current results, probably caused by the balance between the osmotic pressure at both sites of the µD membrane.

Since volume recoveries revealed high intra- and inter-catheter variability especially at 37 °C, additional factors, e.g. membrane properties with dependence on temperature, fluid-membrane interactions, and (time- and/or temperature-dependent) membrane clogging, were supposed to influence fluid loss.

UF has been a repeatedly published, major issue when performing µDialysate sampling of macromolecules [38; 39; 216; 217]. The applied µPerfusate RS/HA provided a simple but reliable matrix to diminish the effect of UF by creating an osmotic gradient comparable to the application of bovine serum albumin [218].

4.2.2 Adsorption of cytokines to the catheter components

The investigated intervals were the same like the procedures performed at the beginning of every single experiment with an unused ‘cytokine-naive’ µD catheter. The µD catheter was flushed at FR of 2.0 µL/min for the minimum of 60 min at all times prior to the µD experiments.

The results of the adsorption experiments confirmed the absence of cytokine adherence to the surfaces of the *in vitro* µD setting: experiments separately investigated different components of the µD catheter. The inner surface of the polyurethane tubing as well as the outer surface of the µD catheter membranes together with the outlet tubing did not show any adsorption effects exceeding bioanalytical method variability. However, the studied surrounding medium volume of 12 mL was considerably higher than the volume of catheter-surrounding ISF of e.g. human subcutaneous tissue. Subsequently, adsorption effects might not have been observed due to the larger volume. *In vivo*, a high amount of pro-inflammatory cytokines is expected during the first hours after catheter insertion due to the insertion trauma of the tissue [45]. Consequently, a saturation of adsorption of the inserted µD surfaces and the inner outlet tubing surface might be assumed. HA as an additive to the µPerfusate had previously been supposed to enhance RR of cytokines [30]. An explanation for the enhancement of RR due to adding albumin could be that it may occupy non-specific

binding sites on the membrane surface inhibiting binding of cytokines and probably forms an albumin-cytokine complex, with a higher molar mass, preventing the return into the external solution and thus decreases the flux of cytokines out of the catheter. Such an albumin-cytokine complex should not interfere with the LBA in a different way compared to the unbound cytokine. “Interestingly, for many of these cytokines, 0.1% HAS perfusate achieved the same increase in RR as the 3.5% HAS perfusate” [41]. Additionally, both components (RS/HA) are approved for clinical application, thus, the proposed µPerfusate can be applied *in vivo* as well.

4.2.3 Dependence of relative recovery and relative delivery on flow rate

At the *in vitro* µD investigations, RR could be determined across the entire investigated FR range for each individual cytokine (see section 3.2.3, first subsection). However, the results revealed substantial differences between the different cytokines: RR of IL-8 > IL-6 > TNF-α > IL-10. As expected, IL-8 as the smallest cytokine (8 kDa) showed the highest RR.

RR values of the cytokines over the FR range at 37 °C (median results for 0.3 µL/min and 0.5 µL/min: 26.1% and 29.6% for IL-6, 103% and 83.9% for IL-8, 13.0% and 14.0% for IL-10, 17.6% and 10.3% for TNF-α) can be compared to data previously published by other groups. Albeit, the application of catheter membranes (100 kDa) of different lengths as well as of different µPerfusate types have to be considered for this comparison: RR was less than 5.3% for TNF-α as well as for IL-10 and between 11.8% and 18.2% for IL-6 and IL-8 at 0.3 µL/min with an 10 mm CMA71® catheter and applying Ringer Dextran 60 solution as the µPerfusate [219]. RR of TNF-α and IL-6 were 4% up to 10% at FR of 0.5-2 µL/min with 10 mm CMA20® probes using wash buffer as µPerfusate [220]. Another investigation with the CMA20® probe and Krebs Ringer solution with 0.1% BSA (bovine serum albumin) at 0.5 µL/min revealed RR of 16.2% for IL-6 [221]. RR using 3.5% HA µPerfusate and CMA71® 10 mm catheters at 0.3 µL/min were: 73.4% for IL-8, 25.5% for IL-6, 8.7% for IL-10 and 31.2% for TNF-α [41] and were predominantly comparable to the here presented results (see above and section 3.2.3).

RR dependence on FR was shown to follow an exponential function (Eq. (10)) and the mass transfer coefficient *r* could be determined. The value of the mass transfer coefficient (Fig. 3-7) was inversely associated with the molar mass of the cytokines (see Tab. 1-1, section 1.3) and revealed decreased values compared to small and intermediate molar mass molecules such as antiinfective drugs (e.g. lipophilic VRC (349 $g \cdot mol^{-1}$) and daptomycin (1.6 kDa) with CMA66®, 20 kDa cut-off: 0.11 mm/min and 0.07 mm/min [172; 173]), as expected. To schematically show this relationship, reported mass transfer coefficients and results of the current *in vitro* investigation were plotted against the molar masses of the particular analytes (see Fig. 4-1). An exponential decrease of the mass transfer coefficient with increasing molar mass of the analyte is observed from this preliminary data evaluation.

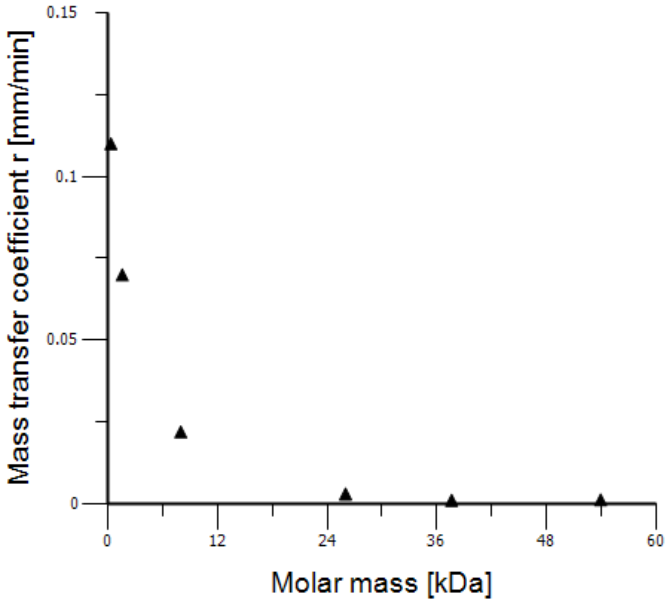

Fig. 4-1: Mass transfer coefficients versus molar mass of different analytes (cytokines from the *in vitro* recovery investigation (project II, 37 °C) and reported values of the antiinfective drugs voriconazole and daptomycin)

In contrast to RR, rD could only be reliably determined for IL-8 over the investigated FR range (see section 3.2.3, second subsection). The relation of rD to FR was demonstrated to follow an exponential function as well (Eq. (13)) and the mass transfer coefficient *r* could be determined. The phenomenon of negative values for IL-6, IL-10 and TNF-α was caused by observed µDialysate concentrations exceeding spiked µPerfusate concentrations. In consideration of the decreased RR at higher FR in recovery experiments, the cumulation of negative rD values at higher FR itself was not implausible. However, considering that diffusion of analyte molecules is hindered at high FR independently from the direction (into or outward the µD catheter), the rD should have converged to zero with increasing FR. Potential reasons for the observation of negative rD values might have been (i) fluid loss by ultrafiltration through the catheter membrane and subsequent analyte accumulation within the decreased µDialysate volume, (ii) fluid evaporation of the µDialysate sample during µD interval (see section 3.2.1 and 4.2.1 for these two first reasons), (iii) inhomogeneous protein suspension during µD experimens resulting in differences of quantified concentrations; (iv) analytical variability could have potentially resulted in negative values. But assuming a ‘true’ rD of zero (i.e., µDialysate concentration was equal to µPerfusate concentration), the influence of the analytical variability should be less or equal to the total error limit of the bioanalytical method [206] which was predominantly less or equal 30% (see section 3.1.2.3). However, rD values less than -30% were observed (see Fig. 3-8), therefore, analytical variability could not have been the only reason for the negative values. Although sample evaporation appeared during RR investigations as well, the potential influence on the

calculated results went in the opposite direction: if µDialysate volume was reduced and, thus, cytokine concentration accumulated, RR data would be overestimated (see section 2.6.5, Eq. (9)) whereas rD data would be underestimated (see Eq. (12)). In contrast, UF could potentially reduce RR in recovery experiments, because the outward water flow from inside the membrane would oppose the inward cytokine flow from the outer medium. In delivery experiments water and cytokine flow follow the same direction. On the other hand, rapid diffusion of the small water molecules could also hinder the already slow diffusion of the large cytokine molecules, subsequently, the volume of the µDialysate would be decreased while the amount of cytokine molecules would remain constant resulting in a higher µDialysate concentration compared to µPerfusate. Protein adherence on the catheter membrane, tubing or syringe surface would rather lead to overestimated rD results in view of consequentially decreased µDialysate concentrations compared to µPerfusate. Adherence processes, however, were not observed (see sections 3.2.2 and 4.2.2). Furthermore, the process of substance gain through the membrane always results in positive RR determination due to the direct determination of gained µDialysate concentration (each time equal to or greater than 0) as a fraction of the surrounding medium concentration. rD values of substance loss through the membrane are indirect measurements. Since the lost part was rarely measureable in the extensive volume of catheter-surrounding medium, determination of µDialysate concentrations as the remained part of µPerfusate concentrations was performed. If ‘true’ rD converges to zero (i.e., real µDialysate and µPerfusate concentrations equal), analytical and investigational errors and conditions can affect rD calculations to a higher extent. Thus, reliability of rD of cytokines increases with enhanced absolute values such as those for IL-8.

As optimal FR, 0.5 µL/min was selected for further RR and rD investigations as outlined below and can be recommended for future *in vivo* µD of cytokines. The selection was based on the high RR values at this FR and analytical plus experimental considerations: 25 µL sample volume was required for the bioanalytical assay and the time of µD intervals was 40% shorter at 0.5 µL/min compared with 0.3 µL/min. Furthermore, the higher FR was less susceptible to occasional interruptions of the µD flow. However, volume recovery was decreased at this FR regarding a temperature of 37 °C (see Fig. 3-4); this fact resulted in a high excess volume planned for µD samples of the clinical study, i.e., the µD interval was extended for a few minutes still shorter than the interval at 0.3 µL/min.

Regarding temperature (see section 3.2.3, first two subsections), the extent of the mass transfer coefficients *r* calculated from RR significantly varied between the two examined temperatures for all four cytokines, whereas rD results were significantly different only for for IL-8 and IL-10 (see Fig. 3-7). Shape and steepness of the curves (Fig. 3-6, Fig. 3-8) were

slightly different: rD and RR were increased at FR of 1.0, 2.0 and 5.0 µL/min for 37 °C compared to 25 °C, but the upper limit of rD and RR, caused by the 100 kDa cut-off of the membrane, was approximately reached at 0.3 and 0.5 µL/min. Subsequently, the steepness of the upper part of the curve was decreased at 37 °C compared to 25 °C. Increases of IL-8 rD and RR at 37 °C compared to 25 °C were of comparable extent (see Fig. 3-6, Fig. 3-8, upper right panels and Fig. 3-9). RR enhanced by increasing temperature has been previously observed for several analytes [222; 223] assigning this trend to the increased diffusion coefficient of solute molecules at higher temperatures. Further reasons for the temperature effect might be the influence on the properties of the membrane material such as a conceivable increase of the pore size at 37 °C. Kinetic molecule energy might also have been increased at the higher temperature leading to enhanced molecule dynamics and, thus, resulted in a higher probability of molecule contact with the µD membrane.
In contrast to the results of the other three cytokines, RR of TNF-α were increased at 25 °C compared to 37 °C, nonetheless, mass transfer coefficients were not significantly different at the two temperature settings (Fig. 3-7). One reason for this contradicting tendency of temperature effects might be a partly association of TNF-α monomers to homotrimers, essentially occurring at physiological temperature, which, as larger molecules, would result in decreased RR. Alternatively, TNF-α conformation could have changed at higher temperature and the modified conformation at 37 °C might have caused a higher molecule volume or an enhanced lipophilicity of the protein surface reducing the RR.
Equality of rD and RR over the investigated FR range from 0.3 µL/min to 5.0 µL/min was confirmed only for IL-8 at 25 °C as well as at 37 °C, therefore, the assumption of equal permeation in both directions across the catheter could be deduced for this model cytokine.

The two major findings in this thesis, which present limitations and have to be handled in *in vivo* µD investigations, are the negative rD values and the extensive intra- and inter-catheter variability. The diverse catheter performance could originate from the different rates of catheter clogging with advanced usage time or by catheter differences resulting from the production process, which influence the membrane passage of macromolecules but are not observed during µD of drugs or metabolite molecules. Since the delivery method failed *in vitro* (frequently negative results), retrodialysis is not applicable for catheter calibration *in vivo* as well. Thus, the demand of alternative clinical calibration methods for µD of cytokines has emerged from the results of this thesis.

4.2.4 Prediction of catheter-surrounding medium concentration by non-linear regression of microdialysate concentrations

The prediction of the concentration of the catheter-surrounding medium *in vitro* (see section 3.2.4) was a prerequisite for the application of the flow-rate-variation method as a µD calibration approach in the clinical study setting (section 2.7.1.3). However, usage of concentration data for non-linear regression was not planned throughout the performance of the experiments. Consequently, as rD and RR calculations did not require constant cytokine amounts, concentrations of the catheter-surrounding medium (recovery) and of the µPerfusate (delivery) were not consistently retained constant (but in a similar range) for different FR within one experiment. Hence, the optimal basis of the application of Eq. (14) and Eq. (15) for non-linear regression, which assumes a constant C_{medium} or $C_{\mu Perfusate}$, repectively, was not given. Applying the entire range of investigated FR, predictions from non-linear regression adequately described the catheter-surrounding medium concentrations of IL-8 for recovery as well as delivery experiments at the different temperatures as shown by Tab. 3-14 (column five). High correlation of predicted and observed data was certainly caused by the increased RR and rD of IL-8 compared to the other cytokines (see section 3.2.3 and 4.2.3), i.e. µDialysate concentrations approached to medium or µPerfusate concentrations with decreased FR.

Reducing the number of FR included in the non-linear regression considerably increased the residuals between predicted and observed concentrations (see Tab. 3-14). Most probably, the decreased amount of data, especially at the part of the concentration-FR curve with an increased slope, caused the higher inaccuracy of the predicted values. This reduction of included data points was performed in consideration of the practical realisation of *in vitro* and *in vivo* µD investigations, in which high FR (1-5 µL/min) were examined uninterruptedly within a few hours. Thus, the assumption of constant surrounding medium or µPerfusate concentrations was better met for the considered FR levels. Nevertheless, predicted concentrations appropriately described IL-8 concentrations exclusively for recovery testing at 37 °C and for delivery testing at 25 °C. Since recovery experiment at 37 °C most adequately simulated *in vivo* investigation settings, lower predictability of non-linear regression results for the alternative experimental settings was considered not relevant or subsequent analysis approaches of this thesis.

4.2.5 Concentration dependence of relative recovery

An essential basis for *in vivo* µD investigations of cytokines presented the demonstrated independence of RR from the catheter-surrounding ISF concentration of the analytes. A concentration-independent, constant reflection of interstitial cytokine concentrations by

means of observed µDialysate concentrations was demonstrated for all four cytokines in this thesis (see section 3.2.5).

4.2.6 pH value effect on relative recovery

Similar to the analysed cytokine concentration recovery in pH-adjusted pure cytokine solutions (see section 3.1.2.6), RR of IL-8 in µD investigations was not affected by the pH value of the catheter-surrounding medium (see section 0). Although measured concentrations of IL-6 were unchanged in pure solutions at different pH values, RR was decreased by 18%-19% at pH 8 suggesting a modification of molecule-membrane interaction with reduced µD membrane passage of IL-6. Thus, molecule structure regarding polarity or volume was presumably modified at different pH values but without altering the epitope targeted in the bioanalytical assay.

With the assumption that pH values of the catheter-surrounding medium may subsequently influence pH of the µDialysate, and considering the results of 3.1.2.6 for IL-10 and TNF-α at pH 5 (concentrations at pH 5 and 8 lower than at pH 7), RR values greater than (if pH of medium was 5 and µDialysate pH≈7) or equal to (if pH of medium and µDialysate was 5) the RR at pH 7 were expected. However, RR of IL-10 and TNF-α were decreased at pH 5 and increased with neutral and basic pH values. Hence, RR of IL-10 and TNF-α were substantially affected by acidic pH value as well as basic pH value. Helmy et al. assumed RR to increase not only with the molar mass, but also with shape and diffusion characteristics of the determined cytokines, as well as with the isoelectric points (see Tab. 1-1) while having higher RR if highly charged [41]. This assumption was not confirmed in the current investigation seeing that RR did not change at the pH values which were nearby the isoelectric points of the cytokines (see Fig. 3-13). Since the interaction between the cytokine molecules and the moieties of the polymer of the µD membrane have not been investigated and clarified yet, a hypothesis about in- or decreasing RR with the change in ion charge cannot be generated.

As clinical µD investigations would be predominantly performed in irritated tissues, the pH of ISF might differ from the physiological pH of around 7 [224–228], depending on the cause of irritation (e.g. trauma, infection or autoimmune response) and might in an extreme case be decreased to nearly 5 or increased to 8. Hence, extensive pH shifts during µD investigations would result in non-reproducible RR results (see section 0). Consequently, the relation between RR and pH value will have to be determined in detail prior to *in vivo* µD of cytokines in tissues with modified pH values in ISF.

4.3 Project III: Long-term pilot study on microdialysis of cytokines in healthy volunteers

4.3.1 Feasibility of long-term application of clinical microdialysis

The entire number of planned study samples could be obtained during the study course of approximately 56 h. The practical execution of the study plan did not result in any problems. Moreover, no drop-outs appeared. Observed AE were of mild intensity only. The majority of AE resulted from the transparent adhesive tape and from fixation of the outlet tubing guide channel to the skin. The latter can be diminished by placing mull between the guide channel and the skin. In summary, the study protocol was proofed to be overall clinically feasible.

Overnight samples of µDialysate could provide a beneficial source of large volumes of cytokine-containing µDialysate. However, due to instability of sampled cytokines under the conditions of overnight sampling (see section 3.2.1), measurement of these samples was not performed. Furthermore, overnight sampling would obtain *one* concentration for an interval of approximately 12 h and would, therefore, create a sparse data situation. The allocation of the concentration information to one point in time would be highly approximated. Therefore, overnight sampling is not recommended for µD of cytokines. Additionally, while the individuals slept (in a horizontal position), µDialysate ran back into the outlet tubing guide channel resulting in fluid loss (see section 3.3.3). For future µD trials with individuals in a resting position, this last limitation can be circumvented by using optimised outlet tubing guide channels (developed by Clinical Pharmacology of Medical University Vienna) preventing µDialysate from running back into the channel tube.

Additionally, some concentrations were near the LLOQ or BLQ, especially for IL-10 and TNF-α. Consequently, a more sensitive assay might probably provide more data for those samples. Nontheless, the measured µDialysate concentrations were all below 7421 pg/mL and, therefore, the validated calibration range could adequately cover the *in vivo* concentrations determined by µD.

Sample volume loss by ultrafiltration or evaporation

The initial reduction in sample volumes following insertion of the µD catheter was probably caused by modification of FR: subsequent to the activation of the µD pump, a ‘flush’ was automatically initiated, resulting in a rinsing of the catheter over 5 min at a FR of 15 µL/min. Afterwards, the pump adjusted FR to 0.5 µL/min. The automatical, fast down-regulation of FR could raise problems in the fluid flow. Once problems concerning µDialysate volume occurred in the equilibration period (see Tab. 3-17), FR of 1 µL/min or 2 µL/min was immediately applied to induct appropriate flow of µPerfusate. At a period of not less than 20 min prior to starting µDialysate sampling, FR was adjusted to 0.5 µL/min again. The

observed declines in volume could have resulted from a continued equilibration process within the µD inlet, outlet, and membrane tube, equalising the whole µD system with the adjusted FR.

During performance of the flow-rate-variation method, loss of fluid showed a course nearly parallel to *in vitro* results at 37 °C with a consistent shift of 10%-15% (Fig. 3-16). Lower volume recoveries were recorded during *in vitro* investigations probably caused by evaporation throughout the µD intervals from unlocked sampling vials. Evaporation could not reach the same extent in this study as in *in vitro* investigations, since the microvials were connected to the outlet tubing guide channels and hence, near-completely locked during the µD intervals. In contrast, the microvials were not locked or covered in the course of the IVMS investigations until the end of the µD intervals. Determined evaporation *in vitro* was not consistent over the FR range due to the different duration of µD intervals (see section 3.2.1). Evaporation can, therefore, not be the exclusive reason for the parallel shifted course of volume recovery over FR (Fig. 3-16). Sample volumes were decreased at 0.5 µL/min compared to the other FR both in the *in vitro* and the *in vivo* setting. The appearance of UF depends on osmotic and hydrostatic/hydrodynamic pressures. The osmotic pressure was equal in all *in vitro* settings, since catheter-surrounding medium and µPerfusate both consisted of RS/HA as the basic matrix, which is assumed to imitate physiological osmotic conditions. Hydrostatic pressure remains constant within IVMS. Hydrodynamic pressure at FR higher than or equal to 1 µL/min probably prevents perfusion fluid from “extravasation” into the catheter-surrounding medium by constantly pushing forward the water column inside the membrane. At 0.5 µL/min, the hydrodynamic pressure was conceivably not high enough to completely overcome the back pressure of the water column; the fluid was partly pressed through the membrane pores instead. Regarding the higher volumes at 0.3 µL/min the reason for this observation remains unknown. An increased interaction between µPerfusate and the surrounding medium/ISF can be assumed for this low FR. However, despite the fact that hydrodynamic pressure at the lowest FR could not be high enough to press fluid through the membrane pores to the same extent as with 0.5 µL/min, the flow of µDialysate was more in accordance with the pump velocity.

Trickler et al. observed a reduction of fluid loss by addition of BSA to PBS as the µPerfusate. Optimal retention of fluid volume was achieved with 7% of BSA [218], whereas in the current investigation only 0.5% HA had been added to RS as the µPerfusate. Ao et al. almost entirely reduced the effect of ultrafiltration by adding 0.1% BSA to PBS as µPerfusate using AD as the catheter-surrounding medium [52]. Furthermore, Fig. 3-16 indicates that IVMS settings (including application of RS/HA as catheter-surrounding medium, standardised heights and distances, controlled temperature of medium) do rather sufficiently than completely mimic *in vivo* conditions.

As a consequence of these measurements, the middle and high FR (1.0, 2.0 and 5.0 µL/min) proved to be optimal FR with regard to the prevention of UF appearance using CMA66® catheter. However, these FR did not show sufficient RR *in vitro* (see section 3.2.3) and were consequently not considered to be appropriate for the monitoring of cytokines *in vivo*. If the LLOQ of the bioanalytical method will be significantly improved in the future, the higher FR might be an option for *in vivo* µD of cytokines as well. FR of 0.3 µL/min was superior in volumes related to 0.5 µL/min; nonetheless, the length of µD intervals and more frequent problems with the consistency of fluid flow as well as remaining air bubbles rejected this FR for long-term *in vivo* investigations to monitor cytokine concentrations in ISF. Hence, 0.5 µL/min would probably be selected as FR for a future clinical application of µD of cytokines incorporating a small time period into the sampling schedule for an excess of sample volumes.

4.3.2 Bioanalysis of the study samples

All study samples were analysed without any problems. The bioanalytical assay was robust and valid over the time of in-study measurements (see section 3.3.4). The results of the individual sample for which prior dilution was required due to a small sample volume (ID 01, study day 1, 0.5 µL/min, last interval) were plausible compared to previous and subsequent sample concentrations.

A neutral and constant pH is a prerequisite for valid bioanalysis results and reliable calculations based on concentrations (see sections 3.1.2.6 and 4.1). The colour of the solution prepared from study samples during the predilution step (see section 8.1.2) is caused by a pH indicator. Since the colour of all investigated study samples was identical and deviated marginally from that of Cal and QC solutions only, it was concluded that no relevant pH variations were present. Therefore, pH values of the membrane surrounding ISF were assumed to have been physiological and constant throughout the entire study period.

4.3.3 Flow-rate-variation method for calibration of relative recovery of cytokines

The key prerequisite for *in vivo* application of the flow-rate-variation method is a constant analyte concentration in the catheter-surrounding ISF. This requirement was not fulfilled by the applied study situation. µDialysate concentrations of IL-6 and IL-8, which were selected for further data analysis, did not follow the expected exponentially decreasing profile (Fig. 3-19). Since IL-10 and TNF-α showed concentrations BLQ, both cytokines were excluded from data analysis. *In vivo* concentrations of IL-6 and IL-8 at high FR approached a parallel decrease when compared to *in vitro* results as illustrated in Fig. 3-18. However, this trend did not continue for low FR. Since concentrations were predominantly lower at low FR compared

to higher FR or since they were lower than expected by an exponential profile or from *in vitro* results (see section 3.2.3 and Fig. 3-11), ISF concentrations had supposably been decreasing from study day 2 (high FR) to study day 3 (low FR). This theory would explain the visible 'gap', which vertically shifted the upper part of the exponential profiles (at low FR) to lower concentrations (see Fig. 3-17, Fig. 3-18). This gap was especially observable in ID 04 for both, IL-6 and IL-8, concentrations. The study schedule was developed based on several references about the expected time for the decline of elevated cytokine concentrations caused by a trauma such as the µD catheter insertion [39; 43; 45; 229; 230]. The third sample of ID 02 at 2 µL/min deviated tremendously from the other two replicates at this FR. On the one hand, this 'outlier' could have been caused by a rapid change of the cytokine concentrations in ISF. However, since this would represent a simultaneous shift of at least three cytokines (third replicate sample was outlier for IL-6, IL-8, and IL-10; TNF-α was BLQ), the plausibility of this hypothesis would be questionable. Consequently, this systematic decrease of cytokine concentration was probably triggered by an unexplained error within sample handling, sample processing, bioanalysis, or a temporary disturbance of the performance of the catheter membrane.

Taking the above-mentioned issues into account, low FR were excluded from non-linear regression. Predicted values from the model fitted in the non-linear regression sufficiently described observed µDialysate concentrations at high FR (see Fig. 3-20). Predictions for IL-8 concentrations at FR of 0 µL/min, i.e. predictions of the concentrations of catheter-surrounding ISF, were subsequently used to calculate *in vivo* RR at high FR for the four µD catheters used in the study (see 2.6.6, 2.7.3.3 and 3.3.6). The resulting RR were significantly lower than the *in vitro* values (for *in vitro* RR, refer to Tab. 8-18). Nonetheless, *in vivo* and *in vitro* non-linear regression curves (Fig. 3-21) seemed to display parallel trends for the high FR. Median *in vivo* RR of IL-6 were 17.0%, 10.1% and 3.65% at 1.0, 2.0 and 5.0 µL/min, repectively, and median RR of IL-8 were 31.1%, 17.8% and 6.72% at the aforementioned FR. Few RR values calculated from *in vivo* concentrations were found in literature. Clausen et al. estimated RR of IL-6, IL-8 and TNF-α with a 950-kDa-membrane by flow-rate-variation method on three different days from the abdominal subcutaneous tissue of between two and ten healthy men (some µD catheter stopped working and individuals dropped out): mean RR of IL-6 at 1.0 µL/min were 70% (Day 1), 63% (Day 2), and 75% (Day 3); mean RR of IL-8 showed values of 51%, 43%, and 58%; and mean RR of TNF-α were 33%, 45%, and 49% [48]. These RR were increased compared to above-mentioned RR and, in contrast to the current results, IL-6 demonstrated higher RR than IL-8. However, the type and cut-off of the µD catheter were very different than this one used in this thesis and results were unfortunately less comparable. Dostalova et al. used the same method to

calculate *in vivo* RR for a CMA/71 catheter (100 kDa cut-off, 30 mm membrane length) in ten healthy lean women: mean RR of IL-6 were 53.6%, 32.3%, and 6.2% at 1.0, 2.0, and 5.0 µL/min, respectively; mean RR of IL-8 were calculated to be 50.7%, 28.2%, and 4.4% at 1.0, 2.0, and 5.0 µL/min, respectively; TNF-α could not be detected in this study [43]. Again IL-6 showed higher RR than IL-8. Both cytokines were gained by µD to a higher extent compared to the current study, although the insertion site was the same and the catheter properties were comparable except for the shape and diameter (CMA/71 is of concentric shape).

For future long-term µD studies, which aim to apply the flow-rate-variation method for calibration purposes, an alternative study schedule might be of the following design to better account for the initial variations in cytokine concentrations of the ISF: cytokine profiles would have to be observed at 0.5 µL/min over the first 3 days of the study. The detailed long-term observation of the cytokine release caused by insertion trauma could probably provide data sufficient for predictions of this cytokine release in subsequent settings. Consequently, differentiation of secretion of immunmodulators initiated by the trauma of µD catheter insertion from secretion caused by disease could potentially be enabled. Afterwards, the flow-rate-variation method would be performed on study day 4 within a time frame of approximately 15 h. This time frame would require the study ward to provide a recreation area with day beds to give the participants the opportunity to rest. The flow-rate-variation method should be performed consecutively investigating concentrations at the entire FR range. Whether the highest FR (5.0 µL/min) should be set first and *in vivo* catheter calibration continued with 2.0 µL/min, 1.0 µL/min, 0.5 µL/min, and 0.3 µL/min or the other way round, should potentially be investigated by optimal design approaches using the kinetic results of this thesis (see sections 3.3.7 and 4.3.4) as prior information. If the cytokine concentrations of ISF are supposed to stay constant, the order of FR does not matter but should be serial to change the µD settings in small steps. If a minor continous increase of cytokine concentrations is expected, mathematical simulations should evaluate the optimal study design with regards to the lowest variability of the investigated RR. Following the adjustment of the pump for the subsequent FR, an equilibration period of 20 min ought to be performed prior to continuation of µDialysate sampling over three intervals at each FR. Succeeding the last µD interval, study day 4 would end with withdrawing the µD catheter from subcutaneous tissue.

However, if baseline cytokine concentrations in ISF primarily ranged below 10^2 pg/mL, the concentrations in most of the µDialysate samples would scarcely be quantifiable in an adequate way, as the concentrations in µDialysate only reflect a part of the concentration in ISF.

4.3.4 Individual concentration-time profiles of cytokines in microdialysates

Overall, the cytokine profiles within the catheter-surrounding ISF of healthy volunteers were supposed to be mainly affected by the µD catheter insertion trauma of the microenvironment. The range of IL-6 and IL-8 concentrations (see section 3.3.7) was consistent with literature [43; 46; 48; 229; 231] and was anticipated considering concentrations in µDialysate as a fraction of concentrations in ISF. The fraction depends on the length, material and cut-off of the applied µD catheter, the composition of the µPerfusate, and the FR. While IL-6 started to decrease after reaching C_{max} within the first 6 h of study day 1 in two of the four individuals, all of the individuals showed C_{max} and subsequent declining concentrations of IL-8 within this time period (Fig. 3-22). At the beginning of study day 3, i.e. after approximately 48 h, the concentrations were much lower compared to study day 1 (two-log decrease of IL-6 and one-log decrease for IL-8) and predominantly continued to decline over the next hours. ID 03 and ID 01 revealed smaller gradients in IL-6 as well as IL-8 concentrations.

TNF-α and IL-10 concentrations were partially BLQ; however, TNF-α concentrations slightly exceeded LLOQ within the first 6 h and showed decreasing profiles for two participants and fluctuating values for ID 01 and ID 03. This response profile to the insertion trauma is coherent to the observation that maximal concentrations of TNF-α were detected 60-90 min after endotoxin infusion [64].

Since IL-6 and IL-8 may contribute to immune response reactions contrary to those of the other two cytokines, resulting in a partly inhibited/antagonised secretion of one another [212; 232], low concentrations of TNF-α and IL-10 could have resulted from this in ISF. Additionally, these cytokines revealed lowest RR during *in vitro* experiments. In view of usually further reduced *in vivo* RR, determination of the two cytokines could have been restricted by limited diffusion into µDialysate.

Cytokine secretion was published to be influenced by circadian variations, which are assumed to predominantly take place in central circulation affecting e.g. regulation of the body temperature [212; 233; 234]. The study schedule did not consider those rhythms. Additionally, the impact of fasting or fed state [212; 235] as well as of other potentially influencing factors, e.g. sex differences or physical activities, was not recorded.

To mathematically describe the endogenous cytokine concentration-time profiles of IL-6 and IL-8 in a first and preliminary approach, a 1-CMT PK model was applied. The fictional stimulus input was of 100 µg per cytokine and bioavailability was set to ‘1’. Implementation of an additional parameter for an absorption delay in time (t_{lag}) had to be performed to accurately describe the observed data (see section 2.7.3.3 and 3.3.7). This implementation accounted for the time gap from the insertion of the µD catheter (t=0) to the first concentration data point, which was placed to the middle of the first µD interval of 70 min

subsequent to an equilibration phase of 50-110 min. The baseline sample, obtained from the equilibration period, was not applicable to data analysis due to varying FR during this phase. Therefore, since concentrations at t=0 were not assessable, a change-from-baseline PK approach was not employable.

The resulting predicted concentration-time profiles adequately described data of IL-6 and IL-8 observed at study day 1 as displayed in Fig. 3-23. However, the model failed to accurately predict low IL-6 concentrations in ID 01, ID 02 and ID 04 and low IL-8 concentrations in ID 02 and ID 04 at study day 3. A 1-CMT model with two stimulus inputs (τ=24 h) was able to describe these late concentrations in an improved manner compared to the one stimulus input: the major deviations between observed/predicted IL-6 concentrations were 3.86/0.07 pg/mL in ID 01, 18.9/119 pg/mL in ID 02, 79.9/122 pg/mL in ID 03 and 3.72/0.01 pg/mL in ID 04 for one stimulus and 3.86/4.00 pg/mL in ID 01, 79.9/88.7 pg/mL in ID 03 and 3.72/5.62 pg/mL in ID 04 for two stimuli. However, the concentration-time profile of IL-6 could not be estimated for ID 02 with two input stimuli. Late IL-8 concentrations were more accurately predicted by the integration of two input stimuli: the major deviations between observed/predicted were 158/178 pg/mL in ID 01, 252/0.00 pg/mL in ID 02, 735/549 pg/mL in ID 03 and 103/0.00 pg/mL in ID 04 for one stimulus and 158/165 pg/mL in ID 01, 252/223 pg/mL in ID 02, 735/607 pg/mL in ID 03 and 103/123 pg/mL in ID 04 for two stimuli.

Consequently, the descending part of the cytokine concentration-time profile was assumed not to stick to the typical first-order elimination, instead, the decline was supposed to proceed with repeatedly differing elimination rates and/or to occasionally change into an increase due to further response reactions.

When observing all cytokine concentration-time profiles together in the individual study participants (see Fig. 3-24), a pattern of these profiles was visible at least for the IL-6 and IL-8, which are two cytokines rising early during immune reactions. Concentrations of these cytokines were in the same range and increased simultaneously until similar C_{max}, which also showed equal t_{max} except for ID 02 (with a delayed C_{max} of IL-6). Although not evaluable due to low concentrations, TNF-α declined parallel in ID 02 and ID 04 during the initial µD intervals. If those cytokine concentration patterns are investigated in a more detailed manner and in relation to a clinical outcome, diagnostic or predictive patterns might potentially be identified.

4.3.5 Conclusion and perspectives

The results of the presented pilot study indicate the principal feasibility, challenges as well as opportunities of the application of the µD technique for the determination of cytokines *in vivo*.

Limited predictability and ability of the quantification of *in vivo* RR reduce the quantity and the quality of information obtained via the µD method.
Individual cytokine-time profiles of IL-6 and IL-8 were sufficiently described for the four individuals by a common basic 1-CMT model. Hence, data resulting from a larger population could benefit from more elaborate PK approaches such as population PK enabling covariate analysis. If identifying useful covariates, the individual profiles may become further predictable and cytokine release caused by the trauma of µD insertion may potentially be separated from cytokine secretion during pathologic (disease generated) processes.

4.4 Project IV: Clinical long-term microdialysis study with voriconazole in healthy volunteers

This study was a pilot investigation of unbound target-site concentrations of the antifungal agent VRC by µD over a long period of time with regards to common µD investigations. Observing unbound plasma concentrations as well, the comparison of the drug accumulation and exposure in the central system with the exposure at the target site was enabled. In the following subsections, the performance and the results of the study will be discussed and conclusions of the potential meaning of these data for the drug therapy and its optimisation will be drawn.

4.4.1 Performance of study procedures and long-term microdialysis

The study aimed at determining unbound VRC concentrations in plasma and at the relevant target site of systemic fungal infections, i.e. the ISF of soft tissues. Additionally, PK parameters of VRC after single and multiple dosing were characterised and a first indication of factors influencing the parameters evaluated. Genotypes of the metabolising enzymes CYP2C9 and CYP2C19 that have been reported to potentially have an influence on the PK of VRC [189; 236; 237] were evaluated (only preliminary, hypothesis generating data was obtained). The unbound concentrations in UF and ISF during sequence therapy will be related to reported MIC values from the literature in one of the following subsections.
As this was the first human study of this drug employing the µD technique for determination of target site concentrations over several days (single and multiple dosing), the trial was divided in two consecutive parts: feasibility of the study performance, especially of the µD setting at the abdominal site and the long-term µD catheter insertion for PK data generation, was confirmed throughout the proof-of-principle investigation, i.e. the pilot study with the first three healthy volunteers, and published by Simmel et al. [173; 175]. To further evaluate VRC concentration-time profiles and PK parameters at the target site, the main study was

performed in additional six healthy volunteers applying the advantageous study schedule for rich sampling with the feasible long-term *in vivo* µD setting.

Two of the six µD catheters had to be removed during the main study due to lacking µD samples. One individual (ID 06) was considered to be a drop-out after catheter removal, presumably because lifestyle restrictions (see Tab. 8-5) were not adhered to. This study individual was replaced by an additional participant. The second removed catheter (in ID 09) was substituted by a new one only missing two µD intervals; however, results of the three following intervals were rejected from data analysis accomplishing compliance to the equilibration period of the inserted catheter. In spite of that, 93.3% of planned data was obtained from the related study individual. On the other hand, intra-individual variability of the calculated RR of ID 09 was increased compared to all other individuals. Apart from that the main part was performed as planned without any further incidents or complications. µD data were corrected for RR shown in Tab. 3-21 to obtain ISF concentrations. Overall RR results revealed low intra- and inter-individual variability (see Fig. 3-25, Tab. 3-21 and Tab. 3-22 in section 3.4.5).

The nine male study participants were comparable in body constitution and age (see section 3.4.1). Three healthy volunteers marginally exceeded ‘normal’ BMI [186]. Previous studies revealed significant influence of WT on the PK of VRC for WT lower than 40 kg only [137]. For this reason and owing to the examination of dose-/WT-normalised data, normalisation of concentrations regarding WT was not considered to be relevant for presentation of the results of the current study. Concentrations were however normalised by individual dose amounts listed in Tab. 3-19 to comprehensively assess inter-individual differences and to intra-individually compare concentration data concerning initial and maintenance IV as well as PO doses.

Genotype analysis showed a high number of alleles diverging from wild types. All study participants were analysed for selected polymorphism of CYP2C9 and CYP2C19. Pyrosequencing evaluated the occurence of the mutant alleles CYP2C9*2, CYP2C9*3 and CYP2C19*2. In view of the facts, that only the four last individuals were additionally analysed for CYP2C19*17 and that the prevalence of further CYP2C19 polymorphic alleles besides *2 and *17 is of marginal probability only (i.e. minor allele frequencies below or equal 0.0142 [150; 151; 238]), only these individuals were analysed for genotype influence on PK data. In addition, ID 02 was recognised for this data analysis, since his DNA was homozygous for CYP2C19*2 and further genetic variations concerning this isoenzyme were, therefore, excluded. Consequently, the genotype of ID 02 with regards to CYP2C19 was completely known although this ID was analysed for the incomplete set of mutant alleles only.

4.4.2 Drug distribution to the target site

Most PK data of VRC have only been obtained after single dose and only in plasma (commonly, from total concentrations, i.e. the sum of bound and unbound concentrations). In this thesis, the unbound concentration of VRC was determined in µD samples as this method did not allow the passage of proteins through the semipermeable membrane (see 1.2.1). In order to compare the concentrations determined from the target site with the systemic concentrations, plasma samples were ultrafiltered to measure the unbound concentrations in this matrix as well. Regarding the PD activity, which is caused by free molecules only, it is more appropriate to determine the unbound concentrations at the target site [239]. The µD technique allowed evaluating the concentration-time profile of VRC in ISF of the subcutaneous tissue, the compartment where most of the pathogens are considered to reside [240].

A total number of 1074 samples provided concentration data over approximately 84 h within the nine healthy volunteers. Hence, a rich data situation for evaluation of VRC concentration-time profiles in ISF and UF resulted from the study in spite of the small number of participants. For example, a number of only twelve healthy volunteers can be adequate to confirm bioequivalence in investigations for generic drug approvals [187]. Thus, nine individuals investigated in the current study should be sufficient to describe and, as the first time, preliminary evaluate tissue distribution and further PK parameters of VRC. However, in view of a population PK approach, which could reveal more information than the applied NCA with the aim to identify particular factors with an influence on the PK, the number of nine individuals is only sufficient if the influence is large.

All concentration-time data (except selected UF profiles of two individuals) revealed plausible profiles assuring adequate quality of the performance of the study. For the last two individuals, the highly scattered UF data points throughout visit 5 and visit 7 were probably caused by consistent blood sampling problems. Intravenous catheters of these participants had to be repeatedly rinsed with isotonic NaCl solution due to failing blood flow to the sampling vials. Therefore, results were potentially affected by a hindered representation of systemic concentrations by blood samples from an irritated or constricted vein and/or by remaining volumes of NaCl solution, i.e. plasma concentrations might have been diluted (although the first millilitres of sampled blood were always discarded).

Unbound ISF and plasma concentrations were individually outlined in section 3.4.7 for all study participants as well as geometric means of these concentrations. Since total plasma concentrations were determined in the majority of the clinical studies investigating VRC [241], comparison of the results from the literature with the current ones have to be performed with an assumption of drug-protein binding of approximately 60% [141]. UF

concentrations were measured instead of total plasma concentrations, as to our opinion UF was more meaningful for the comparison with the unbound VRC concentrations in ISF.
An equal number of data points (n) of the terminal phase of the concentration-time curve was selected to calculate the slope of the mono-exponential terminal phase throughout NCA. This approach was employed accounting for the inadequate regression curves resulting from the 'best-fit' method and the susceptibility of a subjective bias during visual examination of the terminal portion of the concentration-time profiles obtained in visits 1, 5 and 7 from the nine individuals. For all estimations, at least three or four of the terminal concentration-time points should be and have been involved [242] as well as it was confirmed that the selected time points belonged to the elimination phase of the profile.

The analysis revealed higher concentrations after multiple doses and showed a substantially increase in the inter-individual variability compared to single dose (see Fig. 3-26). Individual concentration-time profiles in plasma followed the typical course with a pronounced C_{max} after a steep increase in initial concentrations, followed by more slowly decreasing concentrations. The concentration-time curves in ISF followed a smoother pattern and were shifted with a time delay compared to the systemic exposure. Hence, ISF represented a kinetically distinct compartment and has to be considered as a peripheral compartment. C_{max} was reported to range between 3.0-4.7 µg/mL after a dose regimen of 6 mg/kg IV q12h on day 1 followed by a maintenance dose of 3 mg/kg q12h [141], which is comparable to the geomean unbound plasma C_{max} determined in the current investigation at visit 7 (1.92 µg/mL).
The individual profiles (Fig. 3-26) diverged tremendously in concentration ranges and in the degree of accumulation within the observed time frame of approximately 84 h. ID 02 and ID 08 showed the highest and most accumulating profiles, whereas ID 01 and ID 06 showed only low or even no accumulation of the drug. Reasons for these observations will be discussed with regard to genotype results in a subsequent section (4.4.4).
C_{max} accumulated in both matrices from single to multiple dosing and UF concentrations consistently exceeded those in ISF (Tab. 3-27). C_{max} values were slightly increased for visit 5 compared to visit 7 resulting from higher doses of the previous visits. As expected, the differences between the matrices were reduced after drug accumulation (Fig. 3-36, upper panel). Throughout IV administration C_{max} was reached in UF at the end of the infusion duration as had been expected (Fig. 3-35, Tab. 3-26). The profiles were right-shifted for ISF and t_{max} delayed for 0.75 h. t_{max} values decreased after PO dosing revealing rapid absorption of VRC in the fasted state of the healthy volunteers as also stated in the literature [115; 140; 141]. They were shortest at visit 7 due to reduced distribution effects after multiple dosing. Determination of C_{max} was probably also more imprecise in ISF due to sampling intervals

instead of time points and flatter concentration-time profiles, therefore, t_{max} varied in ISF to a higher extent between the individuals than in UF.

Less fluctuating concentrations within one dosing interval were reached after 48 h, observable from concentration-time profiles and from similar geometric means of (dose-normalised) C_{min} of every subsequent dosing interval (see section 3.4.7, Fig. 3-30). This observation resulted in the assumption of conditions almost achieving steady state for further data analysis. In 1053 patients from 10 clinical studies, the medians of average and maximum plasma concentrations, i.e. C_{av} and C_{max}, in individual patients across the studies were 2.51 µg/mL (inter-quartile range: 1.16-4.45 µg/mL) and 3.77 µg/mL (inter-quartile range: 2.03-6.31 µg/mL), respectively [137]. In the here described investigation, individual unbound plasma concentrations ranged from 0.18 µg/mL (lowest C_{min}) to 3.66 µg/mL (highest C_{max}) at visit 7. Accordingly, calculated total concentrations fluctuated between ca. 0.45 µg/mL and 9.15 µg/mL and varied in a similar way compared to the clinical studies. The medians of C_{av} and C_{max} were 0.91 µg/mL and 2.12 µg/mL in UF at the last visit, i.e. total concentrations of around 2.28 µg/mL and 5.30 µg/mL, being within the inter-quartile range of the published data.

With regards to the high ISF concentrations of VRC, the proportion of fat tissue potentially influenced the distribution of the lipophilic drug. Distribution effects are influenced by the extent and rate of blood flow to and within the tissue, by the physicochemical properties of the molecule affecting the endothelial permeability for the particular molecule and the diffusion of the lipophilic molecule in the extra- and intracellular fluid as well as the transport into the cells [239; 240]. For example, good penetration to CSF and brain tissue (i.e. tissue with high proportion of fat) was observed for VRC due to its lipophilic properties [243]. In animals and humans, concentrations in the CSF were approximately 50% reduced compared to plasma concentrations; concentrations in brain tissue were higher than those in the CSF [135]. The highest BMI were observed within ID 01, ID 02, ID 03, and ID 04. Since ID 02 and ID 04 did not belong to the homozygous wild types concerning CYP2C19, polymorphism effects could have superposed the effect of body composition. Steady-state concentrations (visit 7) in ISF of ID 01 and ID 03 considerably exceeded corresponding concentrations in UF, *AUC* ratios were significantly higher than 1 in these two individuals. In contrast, steady-state concentrations in UF were mainly increased compared to ISF in ID 08 and ID 09, potentially resulting from a high systemic accumulation rate due to polymorphism of the primary metabolic enzyme. This observation was similar in ID 02, showing an extent of drug exposure comparable to ID 08 and ID 09, but *AUC* ratios between ISF and UF approached to 1, i.e. exposure in ISF and UF was almost equal after multiple dosing; while BMI of ID 08 and ID 09 were 21.4 kg/m^2 and 23.4 kg/m^2, ID 02 showed a higher BMI of 25.3 kg/m^2; however,

these relatively small differences in BMI were not supposed to result in noticeable differences of drug distribution, therefore, BMI would hardly be assessable as a covariate in a population PK approach from the data of the current study.

Inter-individual variability within UF data was moderate at C_{max} of visit 1 (CV_{geom} of dose-normalised C_{max}: 25.2%, see section 3.4.8, Tab. 3-27) and subsequently started to increase (CV_{geom} of dose-normalised C_{min} (visit 1): 99.7%, see section 3.4.7, Fig. 3-28). Consequently, variability following the WT-individualised IV dose expanded due to distribution and elimination processes. This fact was furthermore observed from the different shapes and degrees of steepness of the descending parts of the concentration-time profiles in UF of the different individuals at visit 1. Subsequently, inter-individual variability (of C_{min}) stayed approximately consistent until 72 h and slightly increased in visit 6 and particularly in visit 7 as shown by Fig. 3-28 (right panel). In summary, the inter-individual variability increased over time during the first dose interval and furthermore increased after the switch from IV to PO dosing.

ISF concentration-time curves showed considerable differences compared to UF data. As expected, early concentrations did not reach such a sharp, obvious maximum compared to UF concentrations, implementing that the abdominal subcutaneous tissue represents a kinetically different and thus peripheral compartment. Individual profiles in ISF significantly deviated in concentrations rather than in shape and steepness. Inter-individual variability was initially high (CV_{geom} of dose-normalised C_{max}: 41.4%, see section 3.4.8, Tab. 3-27) and further increased to 58.8% at the end of visit 1 (CV_{geom} of dose-normalised C_{min}, see section 3.4.7, Fig. 3-29). Variability stayed at comparable degrees throughout the course of the study and was finally enlarged in visit 7 (see Fig. 3-29 and Fig. 3-31). Dose-normalised profiles (Fig. 3-30) showed plateau-like conditions beginning at 48 h as well. Similarly to UF concentration-time profiles, the terminal declines of the profiles in ISF were less pronounced after multiple doses compared to single dose. It cannot be ruled out that distribution processes were also occuring in ISF of the target site, since VRC might penetrate into cells and, then, might not be measureable in ISF. Consequently, ongoing distribution processes might have overlayed elimination processes in the declining part of the curves and the terminal phase might not have yet been reached.

AUC behaved comparably to C_{max}, i.e. values increased after multiple doses. Differences between both matrices reached a lower extent related to drug concentrations, resulting in the same *AUC* at visit 5 and only slight differences at visit 7 (Tab. 3-28). Whereas initial *AUC* was higher for UF than for ISF, similar values occurred after multiple doses, showing increased accumulation in the peripheral compartment compared to accumulation in plasma

(Fig. 3-36, lower panel). As observed in the other parameters, inter-individual variability of *AUC* in ISF was lower than in UF, except for visit 1, when variabilities were equal.
Relations between ISF and UF drug exposure and distribution were additionally confirmed by AUC_{ISF}/AUC_{UF} ratios shown in Tab. 3-29. Geometric means of ratios increased from visit 1 (0.74) to visit 5 (1.00) and visit 7 (1.10), demonstrating improved adipose tissue fluid distribution over time or with accumulating systemic concentrations, respectively. However, geometric means were mainly influenced by the inflated ratios of ID 01. Median values, less influenced by outliers, were 0.74 for visit 1, 0.94 for visit 5 and 1.03 for visit 7. Individual ratios also increased from visit 1 to visit 5 for all study participants except for ID 09. While ratios continued to increase for the first three individuals from visit 5 to visit 7, they stayed more or less equal for the other healthy volunteers. Overall, distribution of VRC was increased until and remained constant throughout steady-state conditions. A trend in the influence of BMI values was not observed.
These results indirectly showed enhanced drug accumulation in the tissue fluid compared to plasma, which was furthermore illustrated by the calculation of drug accumulation factors. Dose-normalised accumulation of the lipophilic drug in the subcutaneous adipose tissue fluid (six-fold) considerably exceeded that in plasma (four-fold) (Tab. 3-30). Nevertheless, drug distribution to the peripheral tissue slowly started at the first dosing interval, whilest drug was immediately exposed to the systemic circulation. Distribution of VRC was then enhanced after multiple dosing. In view of similar ratios and factors for visit 5 and visit 7 related to visit 1, increasing distribution was finished after the first PO dose and an equilibrium was predominantly established between ISF and UF concentrations.

Protein binding of VRC is published to range between 58% and 60% [130; 141], this allows 40% of the current drug molecules in plasma to penetrate into the target cells, blood cells or to permeate through vascular endothelium into the tissue. Similarly, the data on volume of distribution of 2-4.6 L/kg (3.9 L/kg in UF in the current study) indicated extensive distribution into extracellular and intracellular compartments, thus tissue concentrations may exceed serum concentrations [130]. Concentration profiles in ISF were not simply shifted in parallel to systemic concentrations and the distance as well as the position of the profiles related to curves in UF varied intra- and inter-individually (see Fig. 3-26). Consequently, drug distribution from blood to the adipose tissue fluid had to consist of further processes than pure diffusion, which would result in profiles with parallel slopes, if the blood flow to/in the tissue was sufficiently high and constant. Whereas terminal descending parts of the concentration-time profiles in UF and ISF overlapped at visit 1, declines were flatter for ISF at the last visits. Since the terminal slopes were similar after single dose, distribution and elimination effects appeared to result in a comparable extent of drug concentration decrease

after single dose. The redistribution process from peripheral tissue (ISF) to systemic circulation (UF) apparently was a limiting factor for the elimination process of VRC from the peripheral compartment after multiple dosing (Fig. 3-32). Geometric mean profiles in Fig. 3-32 showed accumulation of concentrations in ISF approaching concentrations in UF at visit 4. Subsequently, C_{max} in UF slightly exceeded values in ISF and concentrations decreased faster leading to lower C_{min} in UF than in ISF. These observations implied peripheral distribution by diffusion and delayed or limited redistribution by hindered diffusion or by other additional processes. Further, mechanistic, studies would have to be designed to investigate this preliminary observation and the causing processes.

The slopes in both matrices were flatter after multiple dosing and, consequently, concentration fluctuations were reduced at the nearly reached steady state for plasma (also visible from C_{max} and C_{min} in Fig. 3-27, right panel) as well as for ISF (Fig. 3-29). These observations were confirmed by direct comparison of geometric mean profiles in dependence of time after last dose (Fig. 3-33). A biphasic shape of the concentration-time profile in UF occurred after single dose. Since the visits correlated with the dosing intervals, a prolonged observation of the descending part of the concentration-time profiles exceeding 12 h was not feasible. Therefore, the final terminal slope of UF and ISF data might not have been observable throughout visit 1 due to interference of distribution processes overlaying the elimination rate. In view of the fact that the determined median $t_{1/2}$ in unbound plasma (4.42 h) at visit 1 was shorter than the reported $t_{1/2}$ (i.e. 6-9 h, as stated by Purkins et al. [140]), a triphasic shape with an unknown terminal slope could also be expected for a concentration-time profile exceeding 12 h after single dose.
Under the assumption of almost having reached steady state at visit 7, CL ranged from 0.08 L/h/kg to 0.54 L/h/kg in UF, which was comparable to published data for VRC with 0.2-0.5 L/h/kg [141] and revealed high inter-individual variability as well. It was slightly decreased in ISF, showing values between 0.07 L/h/kg and 0.39 L/h/kg. This lower CL for ISF provided another hint for a less efficient backtransport of VRC from the peripheral ISF to the systemic circulation. If distribution to the tissue and backtransport were rapid, equilibrated processes and elimination was of first order and restricted to the liver metabolism, then CL from UF and ISF would be equal. Current results seemed to indicate the backtransport from the ISF to be a rate-limiting step of the VRC elimination. However, geometric means were 0.27 L/h/kg and 0.23 L/h/kg for UF and ISF, respectively, and significance of this difference could not be confirmed due to the small population of nine participants and the high inter-individual variability.

4.4.3 Implication of non-linearity of pharmacokinetics of voriconazole

Under the assumption of almost having reached steady-state conditions as well as of an oral bioavailability of approximately 100% and constant PK parameters, i.e. linearity (over time/dose), comparison of systemic dose-normalised AUC_{τ} at visit 7 with dose-normalised $AUC_{0-\infty}$ after single dose should be equal. However, the extent of the extrapolated part of $AUC_{0-\infty}$ ranged from 6.5% to 72% for UF from the study individuals and between 18% and 77% for ISF, exceeding recommended quantities of up to 20% [181; 187]. Therefore, only individuals with an extrapolated part of $AUC_{0-\infty}$ of not more than 20% were selected for this analysis. The ratios of dose-normalised $AUC_{\tau,ss}$ (visit 7) and $AUC_{0-\infty}$ (visit 1) ranged between 1.9 and 3.9 in UF for these individuals and the ratio was 3.3 in ISF of ID 06 in the current study. I.e., the partial *AUC* after multiple doses was at least 2-fold higher than the *AUC* extrapolated to infinity after single dose. Therefore, since the ratios of individuals with a small extrapolated part of $AUC_{0-\infty}$ were significantly higher than '1', equality between single-dose (until infinity) exposure and the exposure close to steady state had to be denied for these individuals. This fact implicated that accumulation did apparently not follow linear PK conditions. Due to the fact, that the VRC accumulation visually seemed to be more than proportional for the other individuals, i.e. ID 02, 03, 08, and 09 (Fig. 3-26), as well, non-linear PK of VRC was also assumed for these data without a mathematical confirmation. Ratios between $AUC_{\tau,ss}$ and $AUC_{0-\infty}$ (after single dosing) highly exceeding '1' (=equality) revealed a non-linearity of PK parameters of VRC which could be time- and/or concentration-dependent. A time-dependent non-linearity would reflect a more than proportional increase of *AUC* over time in the current case.

However, an evaluation of time- or concentration-dependence was not possible due to the sequence dose regimen of the current study (see sections 1.4.1 and 2.8.1). Time-dependence has to be investigated by administering equal doses over several dosing intervals, while concentration-dependence might be considered by a single-/multiple-dose, cross-over design with different doses and an appropriate wash-out time.

The declines of geometric mean concentration-time profiles were flatter after multiple dosing compared to single dose for UF as well as ISF data (Fig. 8-14 and Fig. 8-13). Since the geometric mean descent throughout visit 1 was caused by distribution in addition to elimination processes (see previous section 4.4.2), comparison of the terminal phases might be biased. Terminal slopes of UF and ISF data (Tab. 8-24 and Tab. 8-25) revealed highest values for visit 1 and lower values for visit 5 and visit 7. However, the geomean of the slopes of ISF at visit 5 might have been biased by the slope of ID 09. Seven instead of ten time points could only be used for the estimation of λ_z, since sampling was interrupted for the µD catheter replacement (see sections 3.4 and 3.4.8). Probably the low geomean slope of ISF at

visit 5 resulted from that outlier value. Nontheless, the geomean slope of ISF data at visit 5 was similar to the unbiased one at visit 7, which was also remarkably lower than the geometric mean slope at visit 1.

Time-dependent reduction of elimination by mechanism-based autoinhibition [244] has been suggested as one cause of the decreasing slopes after multiple dosing. Resultant $t_{1/2}$ showed significantly higher values after multiple dosing (see Tab. 3-25) compared to reference values (circa 6 h) from the literature [115]. As a result of the saturable metabolism of VRC, some references supposed $t_{1/2}$ to be dose-dependent [193; 236]. The apparent $t_{1/2}$ of VRC was published to be approximately 6 h and increased when VRC concentration increased [49; 140; 218]. Since the approved sequence dosing, i.e. initial and maintenance doses with IV administration and subsequent oral doses, was investigated in the study, dose- or time-dependence of reduction in metabolism could not be evidently demonstrated. Dose-dependent non-linearity in PK of VRC was not determinable from the study setting (see above) in view of administration of only three equal doses close to steady-state conditions (subsequent to approximately 48 h). Different dose amounts of the sequence therapy could not be compared with regards to non-linearity, since they were administered at different points during the drug accumulation phase (see dosing schedule Tab. 2-4 in section 2.8.1). An optimal study design with regards to non-linearity of PK as well as sequence dosing would, amongst other, incorporate additional IV maintenance doses of 4 mg/kg reaching steady state (at around 20 h given $t_{1/2}$ of 6 h from the literature [115] or at approximately 25 h in plasma and 40 h in ISF with the data of this thesis (see Tab. 3-25)) previous to the switch to PO dosing of 200 mg. However, geometric means of terminal slopes showed approximately parallel courses for visit 5 compared to visit 7 in UF as well as in ISF. Consequently, linearity in PK with regards to time would be assumed. Nontheless, some of the individual terminal slopes showed different results for visit 5 and 7 not following any trend with regards to an increase or decrease.

4.4.4 Genotype effect on pharmacokinetic parameters

Variability of VRC plasma concentrations (see also section 4.4.2) has been mainly attributed to the metabolism via the polymorphic CYP2C19 P450 enzyme [130; 152]. The activity of the CYP2C19 pathway is highly dependent on genetic characteristics [135].

The investigation of the influence of genotypes on VRC PK parameters was restricted to the exploratory nature of the study. Furthermore, there was a limited number of those individuals, which were entirely characterised for polymorphism of the main VRC metabolising enzyme CYP2C19. In the last four participants, analysis of CYP2C19*3/*4/*17 was performed in addition to CYP2C19*2 and, hence, enlarged the probability of exact genotype knowledge. While these polymorphisms can occur in any individual, they are more common in certain

ethnic groups: the prevalence of the gain-of-function allele CYP2C19*17 (UM) is approximately 20% in Caucasians [151; 188] and represents, therefore, the most common mutant type of this population. The homozygous PM trait is uncommon in white and black populations worldwide (3%–5% Caucasians and Blacks, on the contrary 15%–20% Asians) [130; 135]. More detailed, roughly 2% to 5% of Caucasians are homozygous PM of CYP2C19, while 26% to 28% are heterozygous EM and 70% to 73% are homozygous EM [145]. Since prevalence of the loss-of-function allele CYP2C19*2 (i.e. PM, see above) is that low for Caucasians, and in view of tremendously reduced prevalences of other polymorphisms (<<1% [150; 151]), the overall conclusion of the absence of mutant alleles drawn from the determined absence of *2/*3/*4/*17-alleles was substantially indicated. ID 02 presented a homozygous CYP2C19*2 polymorphism and genotype was, thus, totally clarified. Remaining study participants (ID 01, ID 03-05) were excluded from the investigation of the genotype effect on the phenotype owing to the lack of detailed knowledge about their genotypes.

Mikulska et al. stated that homozygous PM have a three- to fourfold increase in systemic exposure compared to EM, while heterozygous PM have about a twofold increased exposure [130]. Consistent with this, for homozygous PM, the C_{max} and *AUC* of VRC were published to be two to five times higher than found for EM [193]. Individuals who are heterozygous PM have on average twofold higher VRC exposure than their homozygous EM counterparts [137]. In the current investigation, ID 02 (homozygous PM) and ID 08 (heterozygous PM) both showed about threefold increased partial *AUC* compared to ID 07, who exposed a homozygous wild type (EM). There are no dosage adjustments recommended in the Summary of Product Characteristics of Vfend® [138; 139] or in therapy guidelines [137; 245; 246] with regard to this observation at this point in time [135]. With regards to the extent of accumulation, ID 06 (heterozygous UM) showed the highest drug accumulation factor at visit 5. This observation might have resulted from the fast drug elimination in the circulation and a less efficient backtransport of VRC from the target-site to the blood (as the central elimination compartment).

CL, as the primary PK parameter of the elimination capacity, was applied for evaluation of the influence of the genotype. As illustrated in Fig. 3-37, the lowest values of CL were found in PM (0.28- and 0.24-fold compared to EM for UF and ISF, respectively) and IM (0.33- and 0.35-fold); they increased for the heterozygous carrier of the gain- as well as the loss-of-function alleles (i.e. PM/UM: 0.43- and 0.49-fold), and highly escalated for EM and UM (1.5- and 1.2-fold). Due to the number of five considered individuals, statistical significance testing was not performed. However, in view of the five different genotypes within this group of five, plausibility of results was undeniably pointed out: drug CL of plasma and ISF stepwise increased in relation to associated activity of the most important metabolising enzyme.

Consequently, the genotype status of the cytochrom P 450 isoenzyme 2C19 excessively influenced VRC elimination from the central blood system as well as from the peripheral adipose tissue as the target site of the drug. Based on previous publications on the effect of the CYP2C19 polymorphism on systemic concentrations (see above) and extended by the current results, which included the investigation at the target site, dose-individualisation accounting for genotype or phenotype characterisation is highly recommended in narrow therapeutic index drugs (see section 4.4.6). In order to reach a comparable drug exposure in the different genotype individuals, the amount of the maintenance dose should be increased to the fifth- or sixthfold from the PM to the UM.

4.4.5 Sequence therapy

Apart from multiple IV administration of VRC, sequence therapy has been introduced into drug therapy, i.e. a switch from direct administration into the systemic circulation to an absorption-based administration process, introducing further variability on the PK. A further important reason for assessing VRC concentrations during sequence therapy is that the IV dose is normalised to WT but the oral dose is given independently of this demographic dimension. As stated by Traunmüller et al., the time of VRC administrations per IV route seldom exceeded 14 days in clinical studies [132]. Therefore, the chosen sequence therapy approach represented a dose regimen common in clinical routine.

The amounts of the individual doses clearly showed the difference in VRC administration between IV and PO dosing; however, Tab. 3-19 does not account for differences between the infusion duration and the absorption period subsequent to PO doses, which do influence the rate and extent (t_{max}, C_{max}) of systemic drug occurence. Since the absolute bioavailability of VRC was published to almost reach 100% [115], *AUC* was rather dependent on dose and disposition processes than on the absorption process.

Some reports have suggested measuring C_{min} of VRC after oral intake of the 200 mg tablet due to less VRC exposure compared to the WT-individualised IV dose [193; 247]. If a patient started with, or was switched to, oral administration, this would almost certainly lead to reduced exposure to VRC than would be attained after IV administration for patients with more than 50 kg WT. This decrease was observed in the current investigation as well. Reasons for that are the higher amounts of recommended IV doses and bioavailibility (96%) reduction in non-fasted state (meals were served at least 2 h before or after dose administration; in case of having the meal before administratin of VRC, a fasting period of 2 h was not considered to be a ‘full’ fasted state in terms of PK). Hence, measuring plasma concentrations soon after the switch from IV to oral VRC administration would seem advisable to ensure adequate exposure [193].

The switch from WT-based IV to fixed-dosed PO administration slightly increased inter-individual variability: Variability of *AUC* (Tab. 3-28) and C_{max} (Tab. 3-27) in plasma stepwise increased from visit 1 to visit 5 and visit 7. $CV_{geom.}$ of C_{min} (see section 3.4.7) was high at visit 1 (99.7%), subsequently decreased by about 20% (visit 5) and finally increased to 126% (visit 7). Since first PO dose was administered at the beginning of visit 5, drug accumulation following WT-individualised IV administrations still influenced concentration-time profiles of this visit. Following three oral doses of 200 mg, concentrations and *AUC* marginally declined but variability expanded. However, the investigated population was in a small range with respect to body constitution (healthy young men, WT: 65.1-83.7 kg, BMI: 20.5-25.9 kg/m^2). PK variability after PO dosing was also high in patient populations as published by Miyakis et al. [248] and others [129; 247; 249]. In order to avoid highly variable drug concentrations, WT-based oral dosing, which is obligatory for VRC in children, might be useful also in adults. This dose recommendation would be feasible due to the availability of 50 mg tablets and the oral solution of VRC introduced in the year 2004 [130; 139]. If PO dosing is feasible in terms of the situation of the patient (e.g. ability to intentionally swallow the drug), it principally provides a more comfortable and cost-effective alternative to IV administration. In view of the high bioavailability of VRC in the fasted state, the oral solution, which can be individually dosed, presents an alternative drug formulation to tablets. On the other hand, the oral solution has to be repeatedly prepared from a powder due to reduced stability of the suspension; this preparation step carries the risk of mistakes in dosing and presents a higher practical effort.

Since inter-individual variability seemed to be influenced mainly by distribution and elimination processes, different dosing strategies should be combined: Distribution effects could be predicted by body-size descriptors and doses might be normalised to this factor, whereas elimination appeared to be predictable by determination of CYP2C19 genotype or alternative phenotype testing. This depends on which percentile of the inter-individual variability can be explained by the covariate. Overall, doses should potentially be adjusted to both, body-size descriptors and CYP2C19 isoenzyme activity. However, the current investigation could not confirm the influence of WT/BMI in view of the homogenous population. Moreover, data from literature did not reveal any need for dose adjustments due to body size descriptors; a WT of 40 kg was set as a single threshold for dose adjustment in terms of body composition [137]. Nonetheless, covariate analysis by means of the population PK approach could provide information to determine the potential influence of these factors in a healthy study population. This has already been attempted based on systeminc VRC concentrations [137], but not using the more specific and relevant concentrations in ISF. Furthermore, this analysis in healthy volunteers could serve as prior information for evaluation of covariates in different patient populations.

In the current study, steady state was almost reached at 48 h. Steady-state concentrations were achieved only after 5–6 days in previous studies of PO dosing, but, if an IV loading dose was given, steady-state concentrations were achieved within 1 day [198; 199]. Thus, intravenous route seems to be preferable for initial administration of VRC in critically ill patients suffering from life-threatening fungal infections in order to achieve therapeutic VRC concentrations as early as possible [130]. The recommended regimen is a loading dose of 6 mg/kg every 12 h for 2 doses, followed by a maintenance dose of 4 mg/kg every 12 h [135] as applied in this thesis. In the current study unbound plasma C_{min} were of comparable amounts after 24 h and 84 h (0.65 µg/mL and 0.61 µg/mL), but were higher (up to 0.93 µg/mL) between these time points rising with the maintenance IV doses. This observation is in accordance with the previous results, which showed that, with IV loading doses, concentrations in plasma equal to steady-state concentrations after PO doses can be obtained within 24 h. The outstanding issue is, which are the target steady-state concentrations, i.e., whether the effective concentrations are those of the steady state after PO doses of 200 mg or the concentrations after WT-individualised IV doses.

4.4.6 Pharmacokinetic/pharmacodynamic and -toxic relationships

Successful management of IFI reasonably relies on the accurate selection of an antifungal agent against the infection. Drug characteristics can help with the selection of drug therapy. These characteristics include the drug's spectrum of activity, PK (including the distribution to the infection site), and PD characteristics (especially the toxicity profile) [250]. VRC has been tested *in vitro* against yeast, filamentous fungi, and dimorphic fungi and appeared to exhibit antifungal activity against a wide variety of clinically important yeasts and moulds [115]. Descriptive or predictive relations between observed PK parameters and MIC values [213; 251] were considered applying published PK/PD indices. Although VRC reached the bedside more than 10 years ago and became the standard care in the treatment of invasive aspergillosis, reliable clinical PK/PD indices and breakpoints are still in high demand [241]. Moreover, the importance of this aspect has increased due to the recent emergence of azole resistance. Recently, clinical isolates of *A. fumigatus* exhibiting reduced susceptibility to VRC were associated with treatment failures, thereby complicating the clinical management of invasive aspergillosis [131].

PK/PD parameters

The MIC for the population of a fungal isolate is an *in vitro* value for the measure of the susceptibility to an antifungal agent and may provide enhanced utility in clinical guidance of antifungal therapy. A further parameter, the clinical breakpoint, is established by considering the MIC distribution for a antifungal agent (VRC) and a fungal species, pharmacokinetic (PK)

and pharmacodynamic (PD) parameters and clinical data in relation to different MIC values [130]. Because antifungal activity may vary largely according to the culture medium used, incubation time, assay method, and defined growth-inhibition end point, only those studies in which testing was performed according to EUCAST (European Committee for Antimicrobial Susceptibility Testing) guidelines for susceptibility testing for yeast and filamentous fungi [252; 253] were selected. “The EUCAST breakpoints are based on a compilation of microbiological, pharmacokinetic/pharmacodynamic data, and clinical experience. Epidemiological cut-off values were determined from MIC values obtained from multiple European laboratories” [254].

VRC activity against moulds, such as *Aspergillus spp*., is fungicidal and both time- and concentration-dependent [130; 133]. Unfortunately, however, there are no specific MIC data for *Aspergillus* species (determined using EUCAST methodology) that enable a relationship between MIC and clinical outcome to be established. Consequently, the Subcommittee on Antifungal Susceptibility Testing (AFST) has defined breakpoints from Monte Carlo simulations as follows: susceptibility ≤1 µg/mL, resistance >2 µg/mL [254]. A dynamic *in vitro* model of the human alveolus suggested that *AUC*/MIC and C_{min}/MIC ratios of 32.1 and 1, respectively, are associated with effects close to the maximal antifungal activity against *Aspergillus* [255]. The EC_{50} and EC_{80} for four *A. fumigatus* isolates were associated with $AUC_{0–12}$/MIC (95% CI) of 12.6 (9–17.8) and 24.0 (17–38.6), respectively. A C_{min}/MIC ratio of 1 was associated with the EC_{50} in another reference, and the susceptible, intermediate and resistant breakpoints were set to ≤0.5, 1–2 and ≥4µg/mL, respectively [131]. On the contrary, a C_{min}/MIC ratio of 2 to 5 was suggested to be used as a target for TDM of patients infected with a variety of fungal pathogens by Troke et al. [256]. Denning et al reported that plasma concentrations below 0.25 µg/mL correlated with a higher rate of clinical failure of invasive aspergillosis [129; 193]. Others reported a favourable response when VRC serum concentrations, measured at random timepoints, exceeded 2.05 µg/mL [257]. The FDA briefing document for VRC reported a PK/PD analysis of 280 patients with proven or probable invasive aspergillosis, suggesting a trend of higher success rates with mean total VRC plasma concentrations above 0.5 µg/mL: 56% success with values of 0.5-1.0 µg/mL, compared to 46% success with values below 0.5 µg/mL; i.e. an odds ratio of 1.5 [95% CI from 0.6 to 3.4] [137]. The majority of these PK estimates was based upon single trough concentrations. It would be interesting to determine if the use of additional monitoring time points to more accurately reflect the *AUC* will further enhance the strength of these concentration-effect relationships [145]. In a recent prospective investigation of VRC serum concentration monitoring in patients with IFI, treatment outcome was also statistically linked to drug concentration [247]. More than 180 concentrations of VRC were measured for 52 patients over more than 2,000 treatment days. Patients with VRC drug concentrations of less

than 1 µg/mL exhibited a response rate of just over 50%. Conversely, patients with concentrations above 1 µg/mL experienced a response rate of 90% [145]. Since almost none of the references clearly states, whether calculations were based on unbound or total VRC concentrations, a comparison of referenced values is difficult and probably inaccurate. Most likely, total concentrations were measured, since this is the most common bioanalytical approach in clinical studies and routine.

VRC showed a concentration-independent, fungistatic *in vitro* activity with a post-antifungal effect against *Candida* and *Cryptococcus* [130]. This activity against species of *Candida* is not uniform. The species most frequently involved in causing human infections were *Candida albicans*, *Candida parapsilosis*, *Candida tropicalis*, *Candida glabrata* and *C. krusei* and mostly exhibited MIC of VRC of less than 1 µg/mL. Wild-type isolates of *C. albicans*, *C. tropicalis* and *C. parapsilosis* exhibited MIC of ≤0.125 µg/mL, whereas MIC for *C. glabrata* and *C. krusei* were higher (commonly ≤1 µg/mL). Consequently, *Candida* infections should be identified to the species level. Since no European country has determined national breakpoints, the AFST committee of the EUCAST has established breakpoints for VRC for a few *Candida* species with sufficient data available, i.e., for *C. albicans*, *C. parapsilosis*, and *C. tropicalis* an susceptibility ≤0.125 µg/mL, and resistance >0.125 µg/mL [258].

In order to compare concentrations measured in the current work with reported MIC values, it is important to consider the matrices from which data have been generated. Since MIC values are determined *in vitro* applying drugs to a medium, composed of several ingredients such as serum proteins, concentrations do not refer to the unbound drug fraction. Consequently, published MIC values are overestimated when compared to measured unbound concentrations. Since protein binding is supposed not to have an impact on VRC activity *in vitro* [259], they commonly are compared to unbound drug concentrations from *in vivo* investigations.

Individual C_{min} (see Tab. 8-29) after multiple doses were at least 0.18 µg/mL for plasma and 0.54 µg/mL for ISF and exceeded a concentration of 1 µg/mL, which is the breakpoint for susceptibility of *Aspergillus* species, with values up to 2.37 µg/mL and 2.49 µg/mL, respectively, in ID 02, ID 08 and ID 09. Therefore, in view of the fact that breakpoints for *Aspergillus* were drawn from total concentrations and fraction unbound is about 40%-50% [247], ISF trough concentrations were adequate for *Aspergillus* species susceptible ≤1 µg/mL (*A. fumigatus* and *A. nidulans*). However, concentrations in plasma individually were below this breakpoint, resulting in critical non-effective values for fungi in the central system.

Considering MIC of the most clinically relevant *Candida* species, which are susceptible ≤0.125 µg/mL [258], initial VRC concentrations at visit 1 within the circulation as well as in the tissue were adequate to achieve a drug effect. For *C. glabrata* and *C. krusei* only three out of nine study participants reached appropriate C_{min} values.

Studies of the PD of triazoles in neutropenic and non-neutropenic murine models of systemic candidiasis have demonstrated that *AUC*/MIC is the most predictive PD index best related to outcome [130]. Monte Carlo simulations showed that a target *AUC*/MIC of 24 would inhibit 99% of isolates with an MIC ≤0.5 µg/mL if treatment were given intravenously, and 99% of isolates with MIC ≤0.25 µg/mL if treatment were given orally [258]. For the comparison of the data of the current work to MIC distributions, minimal $AUC_{12\,h}$ was duplicated and related to mean $AUC_{24\,h}$/MIC breakpoints. Comparing calculated $AUC_{24\,h}$ to MIC distributions evaluated *in vitro* and to pre-clinical models, geometric means of free, i.e. unbound, *AUC* at the target site (see section 3.4.7 and Tab. 3-28) revealed appropriate values for an antifungal effect. Individual *AUC* (Tab. 8-28) showed minimum amounts (in ID 01) competitive against fungi strains with MIC ≤0.28 µg/mL (*Aspergillus* spp.) and ≤0.38 µg/mL (*Candida* spp.).

Concerning clinical efficacy, species-related breakpoints had been previously determined, which were 0.125 µg/mL for *C. albicans*, *C. tropicalis* and *C. parapsilosis*. A clinical response of 76% has been achieved for infections due to these species when MIC were lower than, or equal to, the epidemiological cut-offs of 0.125 µg/mL for *C. albicans*, *C. tropicalis* and *C. parapsilosis* [258]. Although the data were limited, it has been shown that there was a decrease in the clinical response of patients when VRC trough total plasma concentrations were below 1 µg/mL. Regarding unbound concentrations, measured in the investigation of this thesis, about 40% of the individual plasma C_{min} after single and multiple doses (see Tab. 8-29) were below this cut-off of 0.40 µg/mL, i.e. 40% of 1 µg/mL. Only 7 out of 18 C_{min} in plasma exceeded the breakpoint for favourable response at visit 7, where steady state has almost been reached. Whereas C_{min} in ISF were predominantly decreased after single dose, i.e., 6 out of 9 concentrations were below 0.40 µg/mL, they completely exceeded the clinical-response breakpoint after multiple dosing except one single borderline C_{min} of 0.39 µg/mL.

All studies concerning clinical or toxic outcomes were performed investigating VRC concentrations from the systemic circulation, thus, research to determine the relationship of ISF concentrations to clinical breakpoints is highly warranted.

PK parameters related to toxicity

Considering the upper limit of the therapeutic concentration range of VRC, total (i.e. the bound plus the unbound fraction) C_{min} above 5.5 µg/mL in plasma have been associated with increased toxicity [247]. Very high concentrations of VRC have also been associated with reversible neurologic toxicity, i.e. 31% (5/16) of patients with C_{min} higher than 5.5 µg/mL experiencing encephalopathy as a SAE in one study, and none of 30 patients with C_{min} <5.5

µg/mL [145; 247; 250]. Concerning this toxicity cut-off, 2 out of 9 individuals of the study in this thesis surpassed this breakpoint at least at the last visit (i.e. near steady state).
Both Denning et al. as well as Potoski and Braun reported that there may be an association between abnormal liver function and plasma VRC concentrations higher than 6 µg/mL [129; 193; 260]. The median VRC blood concentration for patients reporting photopsia in clinical trials was 3.52 µg/mL; the median concentration for those without this visual symptom was 2.72 µg/mL. In the current study, photopsia seemed to occur independently from high or low drug exposure (see sections 3.4.3 and 3.4.7).

Adverse events

As stated by Traunmüller et al., the overall length of therapy was not related to the emergence and severity of AE during previous clinical studies. Moreover, discontinuation due to drug intolerability occurred only rarely and mainly in the first days of therapy [132].
No serious AE were observed throughout the course of the clinical study (see Tab. 3-20). A statistical analysis of the AE was not feasible, since the study population was too small and all observed AE were to be evaluated as 'very common', i.e. in 10% or more of the individuals, as they occurred in at least one of nine individuals. Frequent AE were visual disturbances, headache, rash and dizziness. The AE were of mild (26 AE) or moderate (3 AE) intensity and predominantly recovered or were resolved within the respective study visit, i.e., they were reversible. Most of the recorded events were typical for VRC and thus, causal relation was definable and plausible. Eight of nine healthy volunteers revealed transient visual abnormalities, this number considerably exceeded the incidence of about 30%, published by Jeu et al. [115]. Rash was documented only in ID 04, whereas during a previous clinical study it was reported among other skin reactions in 17.3% of the patients [115]. Six as well as three participants suffered from headache and nausea, respectively, also exceeding reported average incidences of 11.1% and 12.9% [115]. Results could have been biased by the study performance, which included at least three healthy volunteers at the same time. Consequently, participants' awareness for visual disturbances, headache and nausea could have been raised by the occurrence of AE within another individual, i.e. volunteers were unintentionally conditioned for AE. On the other hand, incidence of AE attributed to VRC treatment varied extensively between different clinical studies with different study populations (e.g. patient characteristics) or in combination with other infectious and immunosuppressive agents [115]. For example, Keady and Thacker stated rash, headache, nausea, and diarrhoea to be very common (≥10%) side effects; dizziness and hallucinations to be common (≥1% and <10%) side effects [116], which was a low incidence compared to frequencies published by Jeu et al. (see above) [115]. µD method-related events were of minimal frequency and of subordinated severity or concern.

4.4.7 Optimising drug therapy with therapeutic drug monitoring of VRC and genotyping

The occurrence of adverse side effects of VRC has been shown to directly correlate with increasing plasma concentrations [132; 147; 247]. On the other hand, distinct studies indicated a direct correlation between low plasma C_{min} and therapeutic failures [129; 257] (see also section 4.4.6). TDM, if feasible, seems especially advisable for multimorbid patients [132]. Several factors must be considered in determining the role of TDM in patient management [145; 261]: (i) a valid, rapid, and cost-effective drug assay must be readily available to perform a TDM. Such a bioanalytical method was previously developed [178] and applied in the current study (see sections 2.8.2.1, 3.4.4). Two further, pharmacological features then determine the relevance of TDM. (ii) The foremost characteristic is an unpredictable or highly inter-individual variable drug dose-concentration relationship, as discussed in sections 4.4.2 and 4.4.4. Next, (iii) there must be a clear relationship between concentrations of drug in plasma or at the target site and either toxicity or treatment efficacy (see section 4.4.6). Commonly, based on models obtained from data of prior investigations, TDM of plasma concentrations provides a tool able to show the drug exposure [130]. TDM has already been proposed as a potential tool for optimizing therapy with itraconazole, VRC, and posaconazole. Each of these drugs meets widely accepted criteria for TDM: a large degree of unexplained PK variability at standard doses, both inter- and intrapatient, a relatively narrow therapeutic window, and a fairly well defined clinical therapeutic range [248; 250].

Furthermore, TDM may potentially be used to overcome antifungal resistance by increasing drug concentrations for isolates with reduced susceptibility [131]. Additionally, when the IFI involves a pharmacologically protected site, such as the central nervous system (CNS) or eye, 5-fluorocytosine, fluconazole, or VRC are generally preferred antiinfectives [250]. TDM could be combined with simulations of the tissue concentrations by mathematical models, which have been built from data raised in investigations like the current one. Thus, a combination of *a-priori* and *a-posteriori* information could help in these clinically complicated cases as well.

In drugs that display non-linear PK, even small changes in the metabolic rate can have a disproportionate effect on plasma concentrations. Consequently, therapeutic monitoring of VRC concentrations may be necessary, particularly in patients who are not responding appropriately [115]. Additionally, there is a high potential for drug-drug interactions, which requires that careful attention is given to dosage regimens and monitoring of plasma concentrations and effects of interacting drugs [130; 135]. Several authors, therefore, suggest therapeutic monitoring of drugs metabolised by CYP2C19, as well as VRC itself, as long as VRC therapy is continued [132; 247].

Routine monitoring of plasma concentrations during the first 7 days of therapy may contribute to the early recognition of drug accumulation and the prevention of neurologic AE [145]. The relationship with CNS or visual side effects and high plasma concentrations of VRC has been well documented, thus immediate reduction or temporary discontinuation of the drug might be advisable, while awaiting the results of TDM [130]. However, in case of the visual phenomena, this potential PK/pharmacotoxic relationship should not warrant TDM for VRC because of the self-limited and fully reversible nature of this AE [145; 147]. Moreover, no cut-off value has been determined and proof was not forthcoming because of the heterogeneity of the clinical manifestations and the small number of cases [193]. C_{min} might provide a favourable tool for determination of exposure, since *AUC* calculation demands on more than one single concentration measurement and/or bases on reliable PK models, which will have to be more sophisticated due to non-linearity of PK parameters and high intra- and inter-individual variability. Given, however, the wide variability in VRC concentrations [147; 247], it can also be argued that an adequately sustained concentration of VRC, rather than a target concentration, ensures treatment success [248]. The occurrence of only short or negligible post-antifungal subinhibitory effects on *A. fumigatus* or *C. albicans in vitro* [141] supports this hypothesis. On the other hand, $AUC_{24\,h}$/MIC was determined to be the PK/PD index most predictive of efficacy (R^2: 82%), but $T_{>MIC}$ was of predictable value (R^2: 75%) as well [141].
However, a definitive C_{min} goal has not yet been identified for VRC [262]. TDM recommended C_{min} for VRC and posaconazole efficacy are each approximately >1 µg/mL. A minimum C_{max} of below 5 µg/mL has been recommended to limit the likelihood of VRC toxicity [247; 250]. Other authors stated a definitive goal for C_{min} of VRC likely to be in the range of 1 and 5 µg/mL [247; 257; 263]. Summarising the literature, C_{min} is likely to be in the range of 0.5 to 2.0 µg/mL for efficacy and less than 6.0 µg/mL for toxicity [145] (see also subsections of 4.4.6). Additionally, as the therapeutic window is narrow, with high risk of side effects at plasma concentrations 3–5 times higher than the minimal threshold for efficacy, TDM can help to maximise the efficacy and minimise the risk of toxicity [130].
Guidelines concerning dose modifications appear to be problematic as well due to the non-linear PK of VRC. Such guidelines about dose modifications for patients with very low or too high plasma concentrations need to be developed and validated to further support clinical management of patients with IFI using VRC. Until there is a consensus on how to manage dose adjustments, an approach with repeated plasma concentration monitoring is warranted after a dose adjustment to ensure adequate concentrations are reached [193].
On the other hand, concentration ranges and, thus, safety consideration may at least partly be predictable by identification of the CYP2C19 genotype status instead of or in combination with performing TDM. Genotype analysis of isoenzymes predominantly involved in metabolism of a broad range of drugs could be performed initially during early phases of

hospitalisation of patients with high likelihood or proven of immunosuppression. An alternative method would be provided by phenotyping applying agents specific for the different isoenzymes (i.e. CYP2C19, CYP2C9, and CYP3A4) or being metabolised by the same set of enzymes as the target drug. Subsequently, drug treatment could be adapted to genotype/phenotype status in an early stage of therapy enhancing the probability of favourable clinical outcomes and reducing toxicity rates. If the genotype cannot readily be determined routinely or does explain only a part of the interindividual variability, TDM offers a good alternative or a complementary approach to verify phenotypic outcome and to guide therapy [193; 248]. Although additional data are needed, it appears that there is high potential for initial VRC dose selection to be guided by CYP2C19 genotyping as clinical pharmacogenetic testing becomes widely available. Additionally, TDM of VRC will continue to provide patient-specific dosing recommendations, leading to more effective antifungal regimens [189]. In conclusion, initial genotype-based dose selection and verification of dose regimen by TDM will be a combined approach, which can benefit from a developed PK model for the prediction of individual systemic as well as target-site drug concentrations.

4.5 Conclusions for drug monitoring and biomarker profiling at the target site contributing to antifungal therapy optimisation

The four projects of this thesis were conducted as a stepwise approach for the optimisation of drug therapies. Especially, project III and project IV evaluated the applicability of the µD technique for potential biomarker profiling/monitoring and for drug monitoring at the target site, respectively, in clinical proof-of-principle settings. The combined approach of target-site drug and cytokine monitoring might be particularly beneficial in the therapy of antiinfective agents, since infections are often located in specific tissues. Infective diseases, e.g. invasive fungal infections, are inevitably associated with immune responses, which are mediated and characterised by cytokine secretion processes.

Fungal infections result from failure of the host immune system to eliminate pathogens [264]. For example neutropenic patients are at a high risk of infections, because TNF-α and MIP-1α are reduced [265]. In both, aspergillosis and candidiasis, cytokines belong to the first mechanism of defence [266]. Cytokines involved in the immune response against fungal pathogens include IL-1, IL-6, IL-8, IL-10, IL-15, TNF-α and TGF-β [267].

The development of T_H1 or T_H2 responses is an important determinant of the host's ability to control infection [268]. T_H1 responses are correlated with protection. Development of T_H1 responses is influenced by the combined action of several cytokines such as INF-γ, IL-6, TNF-α, and IL-12 in the relative absence of T_H2 cytokines, such as IL-4 and IL-10 which inhibit the induction of T_H1 responses [269]. Progression of fungal infection is associated with

predominance of T_H2 responses [268]. T_H1-mediated responses to fungal infections, characterised by TNF-α, IL-12 and IFN-γ production, are protective, whereas T_H2-linked responses, characterised by IL-4, IL-6 and IL-13 production, are maladaptive or deleterious [270; 271].

Stimulation by *Aspergillus* conidia leads to the release of pro-inflammatory cytokines including TNF-α, IL-1α and IL-1β. Stimulation by hyphae on the other hand leads to the release of the anti-inflammatory cytokine IL-10. TNF-α release is associated with the production of other pro-inflammatory proteins, e.g. IL-1, IL-6 and IL-8 and other chemokines like MIP-1α and MIP-2. *Aspergillus* conidia and hyphae induce nuclear factor (NF)-κB translocation, and release of TNF-α and MIP-2 [268]. *A. fumigatus* conidia can influence cytokine-mediated host responses, for example by inhibiting TNF-α-mediated apoptosis of primary human tracheal epithelial and respiratory cells [271; 272].

Many studies have shown that TNF-α plays an important role in inhibtion of fungal infections [266; 273]. TNF-α is necessary for the development of effective innate and adaptive immunity to fungal infections [267]. It stimulates antifungal effector functions of neutrophils and/or macrophages against *C. albicans*, *A. fumigatus* and *C. neoformans* [88; 274–276]. It also induces a number of other cytokines, including IFN-γ, IL-1, IL-6 and IL-12 [276].

It has been demonstrated that pro-inflammatory cytokines such as IL-1, IFN-γ, and TNF-α have important roles in the host defense against disseminated candidiasis [264]. Cytokines such as TNF-α, IL-6, G-CSF and GM-CSF have been determined to be important for neutrophil recruitment during candidiasis [59; 277].

Overall, cytokine secretion is influenced by the kind of infective agent (i.e. fungal species, conidiae or hyphae) and the pattern of cytokines, which are simultaneously active and co-working, is affected by the nature of host response and mediates the type of immune reaction.

Recent evidence suggests that host responses to fungal pathogens may additionally be influenced by the type of immunosuppressive regimen: the pattern of cytokine (TNF-α, IL-10) production and inflammatory response associated with *A. fumigatus* infection was different in mice pretreated with corticosteroids as compared with those pretreated with myelosuppressive chemotherapy [267; 278]. Patients who receive anti-TNF therapy showed increased susceptibility to invasive candidiasis and aspergillosis [271; 279].

Even after the advent of novel therapeutic agents, such as the second-generation triazoles (e.g. VRC) and the echinocandins, the treatment of IFI is often unrewarding [267]. For example, the overall mortality of invasive aspergillosis remains unacceptably high at 30–50% [125; 280; 281]. The candidaemia-associated mortality rate among cancer and other patients (10%-49%) remains still significant [267; 282; 283]. Therefore, instead of a monotherapy with

antifungals, therapies with antiinfectives should potentially supported by immunomodulatory agents. On the other hand, immunologic effects of antifungal agents have also been reported.

In addition to the aforementioned antifungal activity, VRC also possesses immunomodulatory effects. Antifungal agents also enter immune cells. There, VRC increased gene expression and release of cytokines, especially G-CSF, GM-CSF, IL-1, M-CSF and TNF-α by human monocytes exposed to *Aspergillus fumigatus* [284]. Various experiments showed a higher increase of the antifungal activity of mononuclear cells and polymorphnuclear neutrophils after incubation with fungal hyphae and VRC than with hyphae alone [273; 284–286]. *In vitro* models have shown that ergosterol depletion enhances the susceptibility of fungal cells to both oxidative and non-oxidative phagocytic damage. VRC also specifically induces the expression of Toll-like receptor 2, nuclear factor kappa B, and TNF-α in monocytes [130; 287].

Consequently, cytokine profiling evolvement might have the potential not only to monitor the fungal burden of the infected tissue, but also to directly observe the immunomodulatory effect of VRC.

From another point of view, therapy with cytokines, as an adjunct to antifungal therapy (as already mentioned above), is possibly of value [118]. Increasing the numbers of circulating granulocytes and monocytes in patients who have been neutropenic may be critical, but the temporal impact is small. G-CSF, GM-CSF, and IFN-γ also act by increasing phagocytosis of and damage to *Aspergillus* hyphae *in vitro* [288; 289]. Whether the magnitude of these effects is clinically important, in combination with the effect of antifungals, has yet to be clinically demonstrated; it was not the case in phase 1/2 studies of macrophage colony-stimulating factor [290]. In contrast, IL-10 seemed to have suppressive as well as stimulating effects on antifungal activity of immune cells [291] and high concentrations were associated with poor outcome in non-neutropenic patients with invasive aspergillosis [292].

In order to optimise the here presented µD method for cytokines, further cytokines than these used as model cytokines, which are related to the pathology of fungal infections or protection against fungi as well, could be included into determination by µD. Simultaneous determination of more cytokines over time increases the obtained quantity of data and could lead to a faster and enhanced identification of cytokine patterns and profiles for specific disease states or progresses.

For example, several clinical observations suggest an inverse relationship between IFN-γ and IL‑10 production in patients with fungal infections [270]. High concentrations of IL‑10, which negatively affect IFN-γ production, are detected in chronic candidal diseases, in the

severe forms of endemic mycoses and in neutropenic patients with aspergillosis, and thus have been linked to susceptibility to fungal infections [293; 294]. A recent study has shown that IL-22 is required for the control of *C. albicans* growth at mucosal sites in the absence of T_H1 and T_H17 cells [294; 295].

In clinical settings, cytokine secretion patterns of human tissue in immune response to invasive fungal infections were rarely investigated and elucidated. Most above-mentioned knowledge resulted from preclinical or *in vitro* data. Hence, the application of µD of cytokines in IFI and, furthermore, the simultaneous observation of VRC and cytokine ISF concentrations in clinical studies would enormously complement current knowledge. If correlations of cytokine patterns to clinical outcomes were detected, cytokine concentration determinations at the target site would be of diagnostic and prognostic use. The need for a finely regulated balance between T_H1 and T_H2 cytokines for the development of optimal immune response to fungal infections has been understood and emphasised by means of *in vitro* and preclinical studies [267] and provides the basis for determination of cytokine networks within the affected tissues in clinical settings.

Considering the way of scientific data management and analysis and the information obtained by the current work, the data generated from these clinical approaches could be furthermore analysed by more mechanistic PK models to obtain additional information. For example, a compartmental model of VRC combining IV and PO dosing and incorporating the information of all visits, e.g. after single and multiple doses, and of all matrices/compartments, i.e. plasma and ISF, could potentially describe the concentration-time profiles of UF and ISF in a beneficial way and additionally account for non-linearity. In future investigations, predictability of tissue concentrations by modelling and simulation approaches quantifying the influence of polymorphism and diseases should be evaluated. Furthermore, those models should be applied for simulations of PK of VRC in subpopulations at different therapy regimens aiming at the optimisation of the current therapy schedules.
Models adequately describing the PK of VRC could moreover be combined with cytokine concentration-time profiles from the target site resulting from VRC therapy. These PK/PD models, describing target-site effects by the input of systemic drug concentrations, potentially provide the basis for the reliable application of TDM with sparse blood sampling. If the inter-individual variability of VRC can be assigned to covariates by a population PK approach, an individual dosing and an accurate prediction of therapy effects might be possible applying the aforementioned mathematical approaches by patient characterisation only.

5 ABSTRACT

Cytokines as immunomodulatory proteins are secreted by immune and tissue cells mediating immune responses, e.g. inflammation. The use of microdialysis as a minimally invasive technique for sampling interstitial fluid might provide the basis for biomarker profiling for diseases and therapy monitoring. The objectives of this thesis were to develop reproducible bioanalytical methods and apply them to define feasibility and applicability limits for the quantification of cytokines in microdialysate.

A commercially available, flow-cytometry based cytokine assay for the four selected model cytokines Interleukin-6 (pro-), Interleukin-8 (pro-), Interleukin-10 (anti-) and Tumour Necrosis Factor-alpha (proinflammatory), which was previously adapted to microdialysate as the respective matrix, was successfully validated for the physiologically relevant concentration range of 5-10000 pg/mL.

In vitro microdialysis recovery and delivery investigations were performed utilising a standardised system. System suitability was investigated exploring analyte adsorption, pH effects, the influence of cytokine concentration and of temperature of the catheter-surrounding medium on the relative recovery. A mixture of Ringer's solution and human albumin solution (0.5%) was used as microperfusate and catheter-surrounding medium. Microdialysate was sampled using linear catheters at flow rates of 0.3, 0.5, 1.0, 2.0, and 5.0 µL/min. All samples were measured using the validated flow-cytometry method adapted to µDialysate. *In vitro* investigations confirmed the similarity of gain and loss of only Interleukin-8 via the microdialysis membrane. Delivery investigation of the remaining cytokines partly revealed implausible results, which led to the conclusion that the method of retrodialysis for *in vivo* catheter calibration of cytokines has to be excluded for clinical studies with microdialysis.

Consequently, the flow-rate-variation method was applied for the calibration of the microdialysis catheters in the subsequent *in vivo* investigation. Moreover, individual cytokine concentrations in microdialysate were observed over a period of three days. The *in vivo* long-term microdialysis setting was evaluated to be feasible for clinical studies. The study sampling schedule was critically checked and assessed as requiring optimisation. An alternative schedule was worked out and proposed for future clinical trials investigating microdialysis of the four model cytokines. Furthermore, this approach and investigation have in future to be extended to the population of patients with diseases predominantly effecting special tissues. For example, the potential of cytokine concentration measurement as a biomarker monitoring in infected tissues should be evaluated.

Another approach to increase understanding of drug distribution processes by the application of microdialysis to optimise drug therapy was acquired. In addition to the systemic exposure, concentrations of the antifungal agent voriconazole were monitored in the abdominal subcutaneous adipose tissue. In this clinical study, voriconazole showed an extensive distribution to the investigated target site. However, high variability was observed in drug distribution as well as in the systemic and target-site drug accumulation for the nine healthy volunteers. Genotyping of the polymorphic metabolic isoenzymes CYP2C9 and CYP2C9 revealed data for the preliminary assessment of an effect on VRC exposure. Especially for the polymorphism of CYP2C19, an essential influence on the systemic as well as the peripheral drug clearance was indicated by the current results.

The further evaluation of microdialysis of cytokines as biomarkers and the combination of both investigated approaches will potentially contribute to the optimisation of currently applied (antiinfective) drug therapies.

6 ZUSAMMENFASSUNG

Zytokine werden im Zuge der Immunantwort, z.B. im Rahmen einer Entzündung, als mediatorische Proteine von Immun- sowie Gewebszellen sezerniert. Die Mikrodialyse als minimal-invasive Technologie zur Gewinnung interstitieller Flüssigkeit kann eine Grundlage für die Erstellung von Biomarkerprofilen für Erkrankungen und deren Therapieüberwachung bilden. Die Zielstellung der vorliegenden Arbeit bestand in der Entwicklung einer reproduzierbaren bioanalytischen Methode und ihrer Anwendung zur Evaluierung der Umsetzbarkeit einer Quantifizierung von Zytokinen aus dem Mikrodialysat.

Ein kommerziell erhältlicher, durchflusszytometrischer Assay für die ausgewählten proinflammatorischen Modelzytokine Interleukin-6, Interleukin-8 und den antiinflammatorischen Mediatoren Interleukin-10 und Tumornekrosefaktor-alpha konnte erfolgreich für den physiologischen Konzentrationsbereich von 5 bis 10000 pg/mL validiert werden, nachdem er zuvor systematisch auf die Anforderungen des Mikrodialysats als relevante Matrix angepasst worden war.

In-vitro-Mikrodialyseuntersuchungen zur Zytokingewinnung und –freisetzung über die Mikrodialysemembran wurden an einem standardisiertem Mikrodialysesystem durchgeführt. Die Eignung der Systemparameter wurde anhand von Analytadsorptionserscheinungen an Mikrodialyskatheteroberflächen, von pH-Effekten, und des Einflusses von variierenden Zytokinkonzentrationen und der Temperatur des katheterumgebenden Mediums auf die sogenannte ‘Recovery’ untersucht. Eine mit Humanalbuminlösung versetzte Ringerlösung, welche einen Albumingehalt von 0.5 % aufwies, wurde als Mikroperfusat und äußeres Untersuchungsmedium für die Mikrodialyse eingesetzt. Die Untersuchungen wurden mit linearen Mikrodialysekathetern und bei Fließgeschwindigkeiten von 0.3, 0.5, 1.0, 2.0 und 5.0 µL/min durchgeführt. Die In-vitro-Experimente konnten die Annahme des gleichen Analytaustauschs in beide Richtungen über die Mikrodialysemembran (Rate der Gewinnung gleich der der Freisetzung) ausschließlich für Interleukin-8 bestätigen. Die Versuche zur Analytfreisetzung der restlichen Zytokine zeigten mitunter implausible Ergebnisse, was zur der Schlussfolgerung führte, dass die übliche In-vivo-Kalibiermethode für Mikrodialysekatheter, die Retrodialyse, nicht für die klinischen Anwendung der Mikrodialyse von Zytokinen geeignet ist.

Daraufhin wurde die sogenannte ‘Flow-rate-variation method’, eine schrittweise Variierung der Fließgeschwindigkeit, für die In-vivo-Studie angewendet. Daneben wurden die individuellen Zytokinkonzentrationen der über drei aufeinanderfolgende Tage gewonnenen Mikrodialysatproben analysiert. Das zur Langzeitanwendung entwickelte Mikrodialysesystem erwies sich als geeignet für klinische Studien. Das Probenentnahmeschema wurde kritisch

evaluiert und Vorschläge zur Optimierung in künftigen Studien zur Gewinnung der vier Modelzytokine wurden aufgezeigt. Darüber hinaus sollte die Überwachung von Zytokinkonzentrationen auf Patientenpopulationen mit beispielsweise mikrobiell infiziertem Gewebe ausgeweitet und auf ihre mögliche Anwendbarkeit als prädiktive Biomarkererhebung überprüft werden.

Als weitere Option der Optimisierung von Arzneimitteltherapien wurde die Mikrodialyse zur Untersuchung der Arzneistoffdistribution ins periphere Gewebe angewendet. Konzentrationen des Antimykotikums Voriconazol wurden sowohl systemisch als auch im subkutanen Fettgewebe des Unterbauchs bestimmt und miteinander verglichen. Voriconazol zeigte in dieser klinischen Studie eine ausgeprägte Verteilung in das untersuchte Gewebe, in welchem die Zielerreger für die Arzneimitteltherapie häufig lokalisiert sind. Jedoch wurde eine hohe Variabilität dieser Arzneistoffverteilung sowie der Akkumulation im System und im Zielgewebe zwischen den Probanden festgestellt. Die zusätzliche Genotypisierung der Probanden hinsichtlich des Polymorphismus des metabolisierenden Isoenzyms CYP2C19 lieferte eingeschränkt evaluierbare Daten zum Einfluss auf die individuelle Voriconazolexposition. Die präsentierten Ergebnisse konnten einen merklichen Einfluss auf die zentrale und periphere Arzneistoffclearance zeigen.

Eine weitere Evaluierung der Mikrodialyse zur Gewinnung von Zytokinen im Rahmen einer Biomarkerüberwachung und die Kombination dieser Kontrolle von Krankheits- bzw. Therapieeffekten und der Überprüfung von Arzneistoffkonzentrationen im Zielgewebe können einen wichtigen Beitrag zur Optimierung von vorhandenen antiinfektiven Arzneimitteltherapien leisten.

7 BIBLIOGRAPHY

1. C. Kloft, U. Jaehde. Dosisindividualisierung. In *Klinische Pharmazie,* p. 231–231. Ulrich Jaehde, Ed. (Wissenschaftliche Verlagsgesellschaft, Stuttgart, ed. 3, 2010).

2. H. Derendorf, T. Gramatté, H.G. Schäfer, A. Staab. Pharmakokinetik kompakt (Wiss. Verl.-Ges, Stuttgart, ed. 3, 2011).

3. N. Mukaida, A. Harada, K. Yasumoto, K. Matsushima. Properties of pro-inflammatory cell type-specific leukocyte chemotactic cytokines, interleukin 8 (IL-8) and monocyte chemotactic and activating factor (MCAF). *Microbiology and immunology* 36: 773 (1992).

4. P. Liu, H. Derendorf. Antimicrobial tissue concentrations. *Clinical Implications of Antimicrobial Pharmacokinetics* 17: 599 (2003).

5. T. Du Clos, C. Mold. C-reactive protein. *Immunologic Research* 30: 261-277 (2004).

6. S. Black, I. Kushner, D. Samols. C-reactive Protein. *Journal of Biological Chemistry* 279: 48487 (2004).

7. M. Brunner, O. Langer. Microdialysis versus other techniques for the clinical assessment of in vivo tissue drug distribution. *The AAPS journal* 8: E263-71 (2006).

8. J.W. Mouton, U. Theuretzbacher, W.A. Craig, P.M. Tulkens, H. Derendorf, O. Cars. Tissue concentrations: do we ever learn?. *The Journal of antimicrobial chemotherapy* 61: 235 (2008).

9. M. Stahl, R. Bouw, A. Jackson, V. Pay. Human microdialysis. *Current pharmaceutical biotechnology* 3: 165 (2002).

10. C. Joukhadar, H. Derendorf, M. Müller. Microdialysis. A novel tool for clinical studies of anti-infective agents. *European journal of clinical pharmacology* 57: 211 (2001).

11. Biomarkers Definitions Working Group. Biomarkers and surrogate endpoints: preferred definitions and conceptual framework. *Clinical pharmacology and therapeutics* 69: 89 (2001).

12. S. Gutman, L.G. Kessler. The US Food and Drug Administration perspective on cancer biomarker development. *Nat Rev Cancer* 6: 565 (2006).

13. K. Strimbu, J.A. Tavel. What are Biomarkers?. *Current opinion in HIV and AIDS* 5: 463 (2010).

14. ICH. GUIDELINE FOR GOOD CLINICAL PRACTICE. http://www.ich.org/fileadmin/Public_Web_Site/ICH_Products/Guidelines/Efficacy/E6_R1/Step4/E6_R1__Guideline.pdf. (26 February 2014).

15. ICH. General Considerations for Clinical Trials. http://www.ich.org/fileadmin/Public_Web_Site/ICH_Products/Guidelines/Efficacy/E8/Step4/E8_Guideline.pdf. (16 July 2015).

16. M. Arain, M.J. Campbell, C.L. Cooper, G.A. Lancaster. What is a pilot or feasibility study? A review of current practice and editorial policy. *BMC Medical Research Methodology* 10: 67 (2010).

17. European Medicines Agency. Guideline Bioanalytical method validation. (08 December 2011) ((30.10.2012)).

18. De la Peña, Amparo, P. Liu, H. Derendorf. Microdialysis in peripheral tissues. *Advanced Drug Delivery Reviews* 45: 189 (2000).

19. C.S. Chaurasia. In vivo microdialysis sampling: theory and applications. *Biomedical chromatography : BMC* 13: 317 (1999).

20. M.K. Lee, L. Di. Crosstalk the Microdialysis in Scientific Research: from Principle to its Applications. *Pharm Anal Acta* 5: 2 (2014).

21. U. Ungerstedt, C. Pycock. Functional correlates of dopamine neurotransmission. *Bulletin der Schweizerischen Akademie der Medizinischen Wissenschaften* 30: 44 (1974).

22. U. Ungerstedt, A. Hallstrom. In vivo microdialysis--a new approach to the analysis of neurotransmitters in the brain. *Life sciences* 41: 861 (1987).

23. N. Plock, C. Kloft. Microdialysis - theoretical background and recent implementation in applied life-sciences. *European journal of pharmaceutical sciences : official journal of the European Federation for Pharmaceutical Sciences* 25: 1 (2005).

24. M. Müller. Science, medicine, and the future: Microdialysis. *BMJ (Clinical research ed.)* 324: 588 (2002).

25. R. Sauermann, M. Zeitlinger. Microdialysis in Internal Organs and Tumors. In *Microdialysis in Drug Development,* pp. 303–333. Markus Müller, Ed. (Springer New York, 2013), vol. 4 *AAPS Advances in the Pharmaceutical Sciences Series*.

26. Committee for Proprietary Medicinal Products (CPMP). The European Agency for the Evaluation of Medicinal Products (EMA) (CPMP/EMA). Points To Consider On Pharmacokinetics and Pharmacodynamics in the development of antibacterial medicinal products. (2000) (http://www.ema.europa.eu/docs/en_GB/document_library/Scientific_guideline/2009/09/WC500003420.pdf (20/11/2014)).

27. Committee for Proprietary Medicinal Products (CPMP). The European Agency for the Evaluation of Medicinal Products (EMA) (CPMP/EMA). Note for guidance on evaluation of medicinal products indicated for treatment of bacterial infections. (2004) (http://www.lakemedelsverket.se/upload/halso-och-sjukvard/EMEAutveckling%20antibiotika.pdf (20/11/2014)).

28. Center for Drug Evaluation and Research (CDER). Food and Drug Administration (FDA). Guidance for Industry - Developing Antimicrobial Drugs — General Considerations for Clinical Trials. (1998) (http://www.fda.gov/downloads/Drugs/GuidanceComplianceRegulatoryInformation/Guidances/UCM070983.pdf (20/11/2014)).

29. C.S. Chaurasia, M. Muller, E.D. Bashaw, E. Benfeldt, J. Bolinder, R. Bullock, P.M. Bungay, E.C. DeLange, H. Derendorf, W.F. Elmquist, M. Hammarlund-Udenaes, C. Joukhadar, D.L. Kellogg, JR, C.E. Lunte, C.H. Nordstrom, H. Rollema, R.J. Sawchuk, B.W. Cheung, V.P. Shah, L. Stahle, U. Ungerstedt, D.F. Welty, H. Yeo. AAPS-FDA workshop white paper: microdialysis principles, application and regulatory perspectives. *Pharmaceutical research* 24: 1014 (2007).

30. G.F. Clough. Microdialysis of large molecules. *The AAPS journal* 7: E686-92 (2005).

31. CMA Microdialysis. Microdialysis in basic research (2009). 2009.

32. L. Stahle, P. Arner, U. Ungerstedt. Drug distribution studies with microdialysis. III: Extracellular concentration of caffeine in adipose tissue in man. *Life sciences* 49: 1853 (1991).

33. C.I. Larsson. The use of an "internal standard" for control of the recovery in microdialysis. *Life sciences* 49: PL73-8 (1991).

34. I. Jacobson, M. Sandberg, A. Hamberger. Mass transfer in brain dialysis devices--a new method for the estimation of extracellular amino acids concentration. *Journal of neuroscience methods* 15: 263 (1985).

35. P. Lönnroth, P.A. Jansson, U. Smith. A microdialysis method allowing characterization of intercellular water space in humans. *The American journal of physiology* 253: E228-31 (1987).

36. Y. Wang, S.L. Wong, R.J. Sawchuk. Microdialysis calibration using retrodialysis and zero-net flux: application to a study of the distribution of zidovudine to rabbit cerebrospinal fluid and thalamus. *Pharmaceutical research* 10: 1411 (1993).

37. Y. Deguchi, T. Terasaki, S. Kawasaki, A. Tsuji. Muscle microdialysis as a model study to relate the drug concentration in tissue interstitial fluid and dialysate. *Journal of pharmacobio-dynamics* 14: 483 (1991).

38. X. Ao, J.A. Stenken. Microdialysis sampling of cytokines. *Methods (San Diego, Calif.)* 38: 331 (2006).

39. A.J. Rosenbloom, R.L. Ferris, D.M. Sipe, S.A. Riddler, N.C. Connolly, K. Abe, T.L. Whiteside. In vitro and in vivo protein sampling by combined microdialysis and ultrafiltration. *Journal of immunological methods* 309: 55 (2006).

40. G.D. Keeler, J.M. Durdik, J.A. Stenken. Comparison of microdialysis sampling perfusion fluid components on the foreign body reaction in rat subcutaneous tissue. *European Journal of Pharmaceutical Sciences*.

41. A. Helmy, K.L. Carpenter, J.N. Skepper, P.J. Kirkpatrick, J.D. Pickard, P.J. Hutchinson. Microdialysis of cytokines: methodological considerations, scanning electron microscopy, and determination of relative recovery. *Journal of neurotrauma* 26: 549 (2009).

42. R.J. Schutte, S.A. Oshodi, W.M. Reichert. In vitro characterization of microdialysis sampling of macromolecules. *Analytical chemistry* 76: 6058 (2004).

43. I. Dostalova, P. Kavalkova, D. Haluzikova, J. Housova, M. Matoulek, M. Haluzik. The use of microdialysis to characterize the endocrine production of human subcutaneous adipose tissue in vivo. *Regulatory peptides* 155: 156 (2009).

44. G.F. Clough, J.A. Stenken, M.K. Church. High Molecular Weight Targets and Treatments Using Microdialysis - Microdialysis in Drug Development. In *Microdialysis in Drug Development,* pp. 243–268. Markus Müller, Ed. (Springer New York, 2013), vol. 4 *AAPS Advances in the Pharmaceutical Sciences Series*.

45. J.A. Stenken, M.K. Church, C.A. Gill, G.F. Clough. How minimally invasive is microdialysis sampling? A cautionary note for cytokine collection in human skin and other clinical studies. *The AAPS journal* 12: 73 (2010).

46. C. Pachler, D. Ikeoka, J. Plank, H. Weinhandl, M. Suppan, J.K. Mader, M. Bodenlenz, W. Regittnig, H. Mangge, T.R. Pieber, M. Ellmerer. Subcutaneous adipose tissue exerts proinflammatory cytokines after minimal trauma in humans. *American journal of physiology* 293: E690-6 (2007).

47. J.A. Stenken, C.R. Sides, G. Keeler, G. Bajpai, T. Vasicek, M. Jackson, J.M. Durdik. Microdialysis Sampling of Cytokines: Are we just measuring damage and can we do anything about it?. In *14th International Conference.* International Society for Monitoring Molecules in Neuroscience, Ed. (2012).

48. T. Clausen, P. Kaastrup, B. Stallknecht. Proinflammatory tissue response and recovery of adipokines during 4 days of subcutaneous large-pore microdialysis. *Journal of Pharmacological and Toxicological Methods* 60: 281 (2009).

49. K.A. Fitzgerald. The cytokine factsbook (Academic Press, San Diego, ed. 2, op. 2001).

50. D. Baron. Immunologie - Antikörper, Cytokine, Impfungen (Govi-Verl., Frankfurt am Main, ed. 1, 1996).

51. H. Ibelgaufts. Dictionary of cytokines (VCH, Weinheim u.a, 1995).

52. X. Ao, X. Wang, M.R. Lennartz, D.J. Loegering, J.A. Stenken. Multiplexed cytokine detection in microliter microdialysis samples obtained from activated cultured macrophages. *Journal of pharmaceutical and biomedical analysis* 40: 915 (2006).

53. J. van Snick, R.P. Nordan. Interleukin 6. In *Growth factors, differentiation factors, and cytokines.* Andreas Habenicht, Ed. (Springer, Berlin u.a, 1990).

54. E.C. Borden, P. Chin. Interleukin-6: a cytokine with potential diagnostic and therapeutic roles. *The Journal of laboratory and clinical medicine* 123: 824 (1994).

55. F.A. Houssiau, K. Bukasa, C.J. Sindic, J. van Damme, J. van Snick. Elevated levels of the 26K human hybridoma growth factor (interleukin 6) in cerebrospinal fluid of patients with acute infection of the central nervous system. *Clinical and experimental immunology* 71: 320 (1988).

56. K. Frei, T.P. Leist, A. Meager, P. Gallo, D. Leppert, R.M. Zinkernagel, A. Fontana. Production of B cell stimulatory factor-2 and interferon gamma in the central nervous system during viral meningitis and encephalitis. Evaluation in a murine model infection and in patients. *The Journal of experimental medicine* 168: 449 (1988).

57. M.W. Nijsten, de Groot, E R, ten Duis, H J, H.J. Klasen, C.E. Hack, L.A. Aarden. Serum levels of interleukin-6 and acute phase responses. *Lancet* 2: 921 (1987).

58. F.A. Houssiau, J.P. Devogelaer, J. van Damme, de Deuxchaisnes, C N, J. van Snick. Interleukin-6 in synovial fluid and serum of patients with rheumatoid arthritis and other inflammatory arthritides. *Arthritis and rheumatism* 31: 784 (1988).

59. J.L. Blanco, M.E. Garcia. Immune response to fungal infections. *Veterinary immunology and immunopathology* 125: 47 (2008).

60. E. Cenci, A. Mencacci, A. Casagrande, P. Mosci, F. Bistoni, L. Romani. Impaired Antifungal Effector Activity but Not Inflammatory Cell Recruitment in Interleukin-6–Deficient Mice with Invasive Pulmonary Aspergillosis. *The Journal of infectious diseases* 184: 610 (2001).

61. K. Matsushima, J.J. Oppenheim. Interleukin 8 and MCAF: novel inflammatory cytokines inducible by IL 1 and TNF. *Cytokine* 1: 2 (1989).

62. D.T. Graves, Y. Jiang. Chemokines, a family of chemotactic cytokines. *Critical reviews in oral biology and medicine : an official publication of the American Association of Oral Biologists* 6: 109 (1995).

63. J.J. Oppenheim, C.O. Zachariae, N. Mukaida, K. Matsushima. Properties of the novel proinflammatory supergene "intercrine" cytokine family. *Annual review of immunology* 9: 617 (1991).

64. T.S. Blackwell, J.W. Christman. Sepsis and cytokines: current status. *British journal of anaesthesia* 77: 110 (1996).

65. M. Tamura, M. Tokuda, S. Nagaoka, H. Takada. Lipopolysaccharides of Bacteroides intermedius (Prevotella intermedia) and Bacteroides (Porphyromonas) gingivalis induce interleukin-8 gene expression in human gingival fibroblast cultures. *Infection and immunity* 60: 4932 (1992).

66. S. Becker, J. Quay, J. Soukup. Cytokine (tumor necrosis factor, IL-6, and IL-8) production by respiratory syncytial virus-infected human alveolar macrophages. *Journal of immunology (Baltimore, Md. : 1950)* 147: 4307 (1991).

67. M. Seitz, B. Dewald, M. Ceska, N. Gerber, M. Baggiolini. Interleukin-8 in inflammatory rheumatic diseases: synovial fluid levels, relation to rheumatoid factors, production by mononuclear cells, and effects of gold sodium thiomalate and methotrexate. *Rheumatology international* 12: 159 (1992).

68. K. Kasahara, R.M. Strieter, S.W. Chensue, T.J. Standiford, S.L. Kunkel. Mononuclear cell adherence induces neutrophil chemotactic factor/interleukin-8 gene expression. *Journal of leukocyte biology* 50: 287 (1991).

69. H. Takematsu, H. Tagami. Quantification of chemotactic peptides (C5a anaphylatoxin and IL-8) in psoriatic lesional skin. *Archives of dermatology* 129: 74 (1993).

70. F.M. Brennan, C.O. Zachariae, D. Chantry, C.G. Larsen, M. Turner, R.N. Maini, K. Matsushima, M. Feldmann. Detection of interleukin 8 biological activity in synovial fluids from patients with rheumatoid arthritis and production of interleukin 8 mRNA by isolated synovial cells. *European journal of immunology* 20: 2141 (1990).

71. S. Chollet-Martin, P. Montravers, C. Gibert, C. Elbim, J.M. Desmonts, J.Y. Fagon, M.A. Gougerot-Pocidalo. High levels of interleukin-8 in the blood and alveolar spaces of patients with pneumonia and adult respiratory distress syndrome. *Infection and immunity* 61: 4553 (1993).

72. E.J. Miller, A.B. Cohen, S. Nagao, D. Griffith, R.J. Maunder, T.R. Martin, J.P. Weiner-Kronish, M. Sticherling, E. Christophers, M.A. Matthay. Elevated levels of NAP-1/interleukin-8 are present in the airspaces of patients with the adult respiratory distress syndrome and are associated with increased mortality. *The American review of respiratory disease* 146: 427 (1992).

73. G.D. Martich, R.L. Danner, M. Ceska, A.F. Suffredini. Detection of interleukin 8 and tumor necrosis factor in normal humans after intravenous endotoxin: the effect of antiinflammatory agents. *The Journal of experimental medicine* 173: 1021 (1991).

74. J.Y. Djeu, K. Matsushima, J.J. Oppenheim, K. Shiotsuki, D.K. Blanchard. Functional activation of human neutrophils by recombinant monocyte-derived neutrophil chemotactic factor/IL-8. *Journal of immunology (Baltimore, Md. : 1950)* 144: 2205 (1990).

75. K.W. Moore, A. O'Garra, de Waal Malefyt, R, P. Vieira, T.R. Mosmann. Interleukin-10. *Annual review of immunology* 11: 165 (1993).

76. G. Grutz. New insights into the molecular mechanism of interleukin-10-mediated immunosuppression. *Journal of leukocyte biology* 77: 3 (2005).

77. A. Marchant, C. Bruyns, P. Vandenabeele, D. Abramowicz, C. Gerard, A. Delvaux, P. Ghezzi, T. Velu, M. Goldman. The protective role of interleukin-10 in endotoxin shock. *Progress in clinical and biological research* 388: 417 (1994).

78. F. Capsoni, F. Minonzio, A.M. Ongari, V. Carbonelli, A. Galli, C. Zanussi. IL-10 up-regulates human monocyte phagocytosis in the presence of IL-4 and IFN-gamma. *Journal of leukocyte biology* 58: 351 (1995).

79. K. Asadullah, W. Sterry, H.D. Volk. Interleukin-10 therapy--review of a new approach. *Pharmacological reviews* 55: 241 (2003).

80. M.G. Netea, R. Sutmuller, C. Hermann, Van der Graaf, Chantal A. A., Van der Meer, Jos W. M., van Krieken, Johan H., T. Hartung, G. Adema, B.J. Kullberg. Toll-Like Receptor 2 Suppresses Immunity against Candida albicans through Induction of IL-10 and Regulatory T Cells. *The Journal of Immunology* 172: 3712 (2004).

81. T.J. Walsh, E. Roilides, K. Cortez, S. Kottilil, J. Bailey, C.A. Lyman. Control, immunoregulation, and expression of innate pulmonary host defenses against Aspergillus fumigatus. *Medical mycology* 43 Suppl 1: S165-72 (2005).

82. R.M. Strieter, S.L. Kunkel, R.C. Bone. Role of tumor necrosis factor-alpha in disease states and inflammation. *Critical care medicine* 21: S447-63 (1993).

83. P.E. Wakefield, W.D. James, C.P. Samlaska, M.S. Meltzer. Tumor necrosis factor. *Journal of the American Academy of Dermatology* 24: 675 (1991).

84. C.D. Raeburn, F. Sheppard, K.A. Barsness, J. Arya, A.H. Harken. Cytokines for surgeons. *American journal of surgery* 183: 268 (2002).

85. K.J. Tracey, A. Cerami. The biology of cachectin/tumor necrosis factor. In *Growth factors, differentiation factors, and cytokines.* Andreas Habenicht, Ed. (Springer, Berlin u.a, 1990).

86. E.3. Frei, D. Spriggs. Tumor necrosis factor: still a promising agent. *Journal of clinical oncology : official journal of the American Society of Clinical Oncology* 7: 291 (1989).

87. J.Y. Djeu, D.K. Blanchard, A.L. Richards, H. Friedman. Tumor necrosis factor induction by Candida albicans from human natural killer cells and monocytes. *Journal of immunology (Baltimore, Md. : 1950)* 141: 4047 (1988).

88. E. Roilides, A. Dimitriadou-Georgiadou, T. Sein, I. Kadiltsoglou, T.J. Walsh. Tumor necrosis factor alpha enhances antifungal activities of polymorphonuclear and mononuclear phagocytes against Aspergillus fumigatus. *Infection and immunity* 66: 5999 (1998).

89. A.P. Phadke, B. Mehrad. Cytokines in host defense against Aspergillus: recent advances. *Medical mycology* 43 Suppl 1: S173-6 (2005).

90. R. Medzhitov. Inflammation 2010: New Adventures of an Old Flame. *Cell* 140: 771 (2010).

91. L. Gullestad, T. Ueland, L.E. Vinge, A. Finsen, A. Yndestad, P. Aukrust. Inflammatory Cytokines in Heart Failure: Mediators and Markers. *Cardiology* 122: 23 (2012).

92. S. Alesci, P.E. Martinez, S. Kelkar, I. Ilias, D.S. Ronsaville, S.J. Listwak, A.R. Ayala, J. Licinio, H.K. Gold, M.A. Kling, G.P. Chrousos, P.W. Gold. Major depression is associated with significant diurnal elevations in plasma interleukin-6 levels, a shift of its circadian rhythm, and loss of physiological. *J Clin Endocrinol Metab* 90: 2522 (2005).

93. A. Deswal, N.J. Petersen, A.M. Feldman, J.B. Young, B.G. White, D.L. Mann. Cytokines and cytokine receptors in advanced heart failure: an analysis of the cytokine database from the Vesnarinone trial (VEST). *Circulation* 103: 2055 (2001).

94. J. Orus, E. Roig, F. Perez-Villa, C. Pare, M. Azqueta, X. Filella, M. Heras, G. Sanz. Prognostic value of serum cytokines in patients with congestive heart failure. *The Journal of heart and lung transplantation : the official publication of the International Society for Heart Transplantation* 19: 419 (2000).

95. N. Aziz, P. Nishanian, J.L. Fahey. Levels of Cytokines and Immune Activation Markers in Plasma in Human Immunodeficiency Virus Infection: Quality Control Procedures. *Clinical and Diagnostic Laboratory Immunology* 5: 755 (1998).

96. M. Perl. Contribution of anti-inflammatory/immune suppressive processes to the pathology of sepsis. *Frontiers in Bioscience* 11: 272 (2006).

97. S. Kumar, M. Rizvi. Prognostic serum tumor necrosis factor-alpha in paediatric patients with sepsis. *Journal of infection in developing countries* 3: 437 (2009).

98. C.E. Hack, M. Hart, van Schijndel, R J, A.J. Eerenberg, J.H. Nuijens, L.G. Thijs, L.A. Aarden. Interleukin-8 in sepsis: relation to shock and inflammatory mediators. *Infection and immunity* 60: 2835 (1992).

99. C. Marty, B. Misset, F. Tamion, C. Fitting, J. Carlet, J.M. Cavaillon. Circulating interleukin-8 concentrations in patients with multiple organ failure of septic and nonseptic origin. *Critical care medicine* 22: 673 (1994).

100. M. van Deuren, van der Ven-Jongekrijg, J, A.K. Bartelink, R. van Dalen, R.W. Sauerwein, van der Meer, J W. Correlation between proinflammatory cytokines and antiinflammatory mediators and the severity of disease in meningococcal infections. *The Journal of infectious diseases* 172: 433 (1995).

101. A. Marchant, J. Deviere, B. Byl, D. de Groote, J.L. Vincent, M. Goldman. Interleukin-10 production during septicaemia. *Lancet* 343: 707 (1994).

102. E.L. Tsalik, L.B. Jaggers, S.W. Glickman, R.J. Langley, V.J. van, L.P. Park, V.G. Fowler, C.B. Cairns, S.F. Kingsmore, C.W. Woods. Discriminative Value of Inflammatory Biomarkers for Suspected Sepsis. *The Journal of emergency medicine (*2011).

103. M. von Lilienfeld-Toal, M.P. Dietrich, A. Glasmacher, L. Lehmann, P. Breig, C. Hahn, I.G. Schmidt-Wolf, G. Marklein, S. Schroeder, F. Stuber. Markers of bacteremia in febrile neutropenic patients with hematological malignancies: procalcitonin and IL-6 are more reliable than C-reactive protein. *European journal of clinical microbiology & infectious diseases : official publication of the European Society of Clinical Microbiology* 23: 539 (2004).

104. M.B. Andersen, J. Pingel, M. Kjaer, H. Langberg. Interleukin-6: a growth factor stimulating collagen synthesis in human tendon. *Journal of applied physiology (Bethesda, Md. : 1985)* 110: 1549 (2011).

105. M.L. Cameron, F.H. Fu, H.H. Paessler, M. Schneider, C.H. Evans. Synovial fluid cytokine concentrations as possible prognostic indicators in the ACL-deficient knee. *Knee Surgery, Sports Traumatology, Arthroscopy* 2: 38 (1994).

106. A. Mire-Sluis. Cytokines and disease. *Trends in biotechnology* 11: 74 (1993).

107. R.M. Grossman, J. Krueger, D. Yourish, A. Granelli-Piperno, D.P. Murphy, L.T. May, T.S. Kupper, P.B. Sehgal, A.B. Gottlieb. Interleukin 6 is expressed in high levels in psoriatic skin and stimulates proliferation of cultured human keratinocytes. *Proceedings of the National Academy of Sciences of the United States of America* 86: 6367 (1989).

108. A. Kapp. The role of cytokines in the psoriatic inflammation. *Journal of dermatological science* 5: 133 (1993).

109. B.J. Nickoloff, H. Xin, F.O. Nestle, J.Z. Qin. The cytokine and chemokine network in psoriasis. *Clinics in dermatology* 25: 568 (2007).

110. B.J. Nickoloff, G.D. Karabin, J.N. Barker, C.E. Griffiths, V. Sarma, R.S. Mitra, J.T. Elder, S.L. Kunkel, V.M. Dixit. Cellular localization of interleukin-8 and its inducer, tumor necrosis factor-alpha in psoriasis. *The American journal of pathology* 138: 129 (1991).

111. H. Takematsu, H. Ohta, H. Tagami. Absence of tumor necrosis factor-alpha in suction blister fluids and stratum corneum from patients with psoriasis. *Archives of dermatological research* 281: 398 (1989).

112. A. Conway Morris, K. Kefala, T.S. Wilkinson, O.L. Moncayo-Nieto, K. Dhaliwal, L. Farrell, T.S. Walsh, S.J. Mackenzie, D.G. Swann, P.J. Andrews, N. Anderson, J.R. Govan, I.F. Laurenson, H. Reid, D.J. Davidson, C. Haslett, J.M. Sallenave, A.J. Simpson. Diagnostic importance of pulmonary interleukin-1beta and interleukin-8 in ventilator-associated pneumonia. *Thorax* 65: 201 (2010).

113. J.M. Swanson, E.W. Mueller, M.A. Croce, G.C. Wood, B.A. Boucher, L.J. Magnotti, T.C. Fabian. Changes in pulmonary cytokines during antibiotic therapy for ventilator-associated pneumonia. *Surgical infections* 11: 161 (2010).

114. K. Jansson, B. Redler, L. Truedsson, A. Magnuson, P. Matthiessen, M. Andersson, L. Norgren. Intraperitoneal cytokine response after major surgery: higher postoperative intraperitoneal versus systemic cytokine levels suggest the gastrointestinal tract as the major source of the postoperative inflammatory reaction. *American journal of surgery* 187: 372 (2004).

115. L.A. Jeu, F.J. Piacenti, A.G. Lyakhovetskiy, H.B. Fung. Voriconazole. *Clinical Therapeutics* 25: 1321 (2003).

116. S. Keady, M. Thacker. Voriconazole in the treatment of invasive fungal infections. *Intensive and Critical Care Nursing* 21: 370 (2005).

117. N. Yapar. Epidemiology and risk factors for invasive candidiasis. *Therapeutics and clinical risk management* 10: 95 (2014).

118. D.W. Denning. Invasive aspergillosis. *Clinical infectious diseases : an official publication of the Infectious Diseases Society of America* 26: 781-803; quiz 804-5 (1998).

119. J.-L. Vincent, J. Rello, J. Marshall, E. Silva, A. Anzueto, C.D. Martin, R. Moreno, J. Lipman, C. Gomersall, Y. Sakr, K. Reinhart. International study of the prevalence and outcomes of infection in intensive care units. *JAMA : the journal of the American Medical Association* 302: 2323 (2009).

120. E. Paramythiotou, F. Frantzeskaki, A. Flevari, A. Armaganidis, G. Dimopoulos. Invasive fungal infections in the ICU: how to approach, how to treat. *Molecules (Basel, Switzerland)* 19: 1085 (2014).

121. M.A. Pfaller, D.J. Diekema. Epidemiology of invasive candidiasis: a persistent public health problem. *Clinical microbiology reviews* 20: 133 (2007).

122. Centers for Disease Control and Prevention. Invasive Candidiasis Statistics - Candidiasis. http://www.cdc.gov/fungal/diseases/candidiasis/invasive/statistics.html. (09 April 2014).

123. M. Mikulska, V. Del Bono, S. Ratto, C. Viscoli. Occurrence, presentation and treatment of candidemia. *Expert review of clinical immunology* 8: 755 (2012).

124. D.P. Kontoyiannis. A clinical perspective for the management of invasive fungal infections: focus on IDSA guidelines. Infectious Diseases Society of America. *Pharmacotherapy* 21: 175S-187S (2001).

125. R. Herbrecht, D.W. Denning, T.F. Patterson, J.E. Bennett, R.E. Greene, J.-W. Oestmann, W.V. Kern, K.A. Marr, P. Ribaud, O. Lortholary, R. Sylvester, R.H. Rubin, J.R. Wingard, P. Stark, C. Durand, D. Caillot, E. Thiel, P.H. Chandrasekar, M.R. Hodges, H.T. Schlamm, P.F. Troke, B. de Pauw. Voriconazole versus amphotericin B for primary therapy of invasive aspergillosis. *The New England journal of medicine* 347: 408 (2002).

126. P.G. Pappas. Invasive candidiasis. *Infectious disease clinics of North America* 20: 485 (2006).

127. L. Drgona, A. Khachatryan, J. Stephens, C. Charbonneau, M. Kantecki, S. Haider, R. Barnes. Clinical and economic burden of invasive fungal diseases in Europe: focus on pre-emptive and empirical treatment of Aspergillus and Candida species. *European journal of clinical microbiology & infectious diseases : official publication of the European Society of Clinical Microbiology* 33: 7 (2014).

128. R. Herbrecht. Voriconazole: therapeutic review of a new azole antifungal. *Expert Review of Anti-infective Therapy* 2: 485 (2004).

129. D.W. Denning, P. Ribaud, N. Milpied, D. Caillot, R. Herbrecht, E. Thiel, A. Haas, M. Ruhnke, H. Lode. Efficacy and safety of voriconazole in the treatment of acute invasive aspergillosis. *Clinical infectious diseases : an official publication of the Infectious Diseases Society of America* 34: 563 (2002).

130. M. Mikulska, A. Novelli, F. Aversa, S. Cesaro, F.G. de Rosa, C. Girmenia, A. Micozzi, M. Sanguinetti, C. Viscoli. Voriconazole in clinical practice. *Journal of chemotherapy (Florence, Italy)* 24: 311 (2012).

131. M. Siopi, E. Mavridou, J.W. Mouton, P.E. Verweij, L. Zerva, J. Meletiadis. Susceptibility breakpoints and target values for therapeutic drug monitoring of voriconazole and Aspergillus fumigatus in an in vitro pharmacokinetic/pharmacodynamic model. *The Journal of antimicrobial chemotherapy (*2014).

132. F. Traunmuller, M. Popovic, K.H. Konz, F.M. Smolle-Juttner, C. Joukhadar. Efficacy and safety of current drug therapies for invasive aspergillosis. *Pharmacology* 88: 213 (2011).

133. E.K. Manavathu, J.L. Cutright, P.H. Chandrasekar. Organism-dependent fungicidal activities of azoles. *Antimicrobial agents and chemotherapy* 42: 3018 (1998).

134. European Medicines Agency - Committee for Medicinal Products for Human Use (CHMP). European Public Assessment Report (EPAR) - Vfend, INN-Voriconazole - Scientific discussion. (2006) (http://www.ema.europa.eu/docs/en_GB/document_library/EPAR_-_Scientific_Discussion/human/000387/WC500049753.pdf (20/11/2014)).

135. L.B. Johnson, C.A. Kauffman. Voriconazole: A New Triazole Antifungal Agent. *Clinical Infectious Diseases* 36: 630 (2003).

136. T.J. Walsh, E.J. Anaissie, D.W. Denning, R. Herbrecht, D.P. Kontoyiannis, K.A. Marr, V.A. Morrison, B.H. Segal, W.J. Steinbach, D.A. Stevens, J.A. van Burik, J.R. Wingard, T.F. Patterson. Treatment of Aspergillosis: Clinical Practice Guidelines of the Infectious Diseases Society of America. *Clinical Infectious Diseases* 46: 327 (2008).

137. FDA Antiviral Drugs Advisory Committee. Briefing document for voriconazole (oral and intravenous formulations). (.

138. Roerig, Division of Pfizer Inc. Summary of Product Characteristics Vfend®. (http://web.archive.org/web/20100705072024/http://media.pfizer.com/files/products/uspi_vfend.pdf (26/02/2014)).

139. European Medicines Agency - Committee for Medicinal Products for Human Use (CHMP). European Public Assessment Report (EPAR) - Vfend, INN-Voriconazole - Annex I - Summary of product characteristics. (2009. Last updated 29 September 2014).

140. L. Purkins, N. Wood, P. Ghahramani, K. Greenhalgh, M.J. Allen, D. Kleinermans. Pharmacokinetics and safety of voriconazole following intravenous- to oral-dose escalation regimens. *Antimicrobial agents and chemotherapy* 46: 2546 (2002).

141. U. Theuretzbacher, F. Ihle, H. Derendorf. Pharmacokinetic/pharmacodynamic profile of voriconazole. *Clinical pharmacokinetics* 45: 649 (2006).

142. D.J. Merrikin, J. Briant, G.N. Rolinson. Effect of protein binding on antibiotic activity in vivo. *The Journal of antimicrobial chemotherapy* 11: 233 (1983).

143. C.M. Kunin, W.A. Craig, M. Kornguth, R. Monson. INFLUENCE OF BINDING ON THE PHARMACOLOGIC ACTIVITY OF ANTIBIOTICS. *Annals of the New York Academy of Sciences* 226: 214 (1973).

144. C. Buerger, N. Plock, P. Dehghanyar, C. Joukhadar, C. Kloft. Pharmacokinetics of unbound linezolid in plasma and tissue interstitium of critically ill patients after multiple dosing using microdialysis. *Antimicrobial agents and chemotherapy* 50: 2455 (2006).

145. D. Andes, A. Pascual, O. Marchetti. Antifungal therapeutic drug monitoring: established and emerging indications. *Antimicrobial agents and chemotherapy* 53: 24 (2009).

146. H.M. Lazarus, J.L. Blumer, S. Yanovich, H. Schlamm, A. Romero. Safety and pharmacokinetics of oral voriconazole in patients at risk of fungal infection: a dose escalation study. *Journal of clinical pharmacology* 42: 395 (2002).

147. A.E. Boyd, S. Modi, S.J. Howard, C.B. Moore, B.G. Keevil, D.W. Denning. Adverse reactions to voriconazole. *Clinical infectious diseases : an official publication of the Infectious Diseases Society of America* 39: 1241 (2004).

148. K.L. McCarthy, E.G. Playford, Looke, David F M, M. Whitby. Severe photosensitivity causing multifocal squamous cell carcinomas secondary to prolonged voriconazole therapy. *Clinical infectious diseases : an official publication of the Infectious Diseases Society of America* 44: e55-6 (2007).

149. D.D. Miller, E.W. Cowen, J.C. Nguyen, T.H. McCalmont, L.P. Fox. Melanoma associated with long-term voriconazole therapy: a new manifestation of chronic photosensitivity. *Archives of dermatology* 146: 300 (2010).

150. NCBI. Database SNP (dbSNP). http://www.ncbi.nlm.nih.gov/snp. (13 October 2014).

151. J.C. Sanford, Y. Guo, W. Sadee, D. Wang. Regulatory polymorphisms in CYP2C19 affecting hepatic expression. *Drug metabolism and drug interactions* 28: 23 (2013).

152. J. Weiss, ten Hoevel, M. M., J. Burhenne, I. Walter-Sack, M.M. Hoffmann, J. RENGELSHAUSEN, W.E. Haefeli, G. Mikus. CYP2C19 genotype is a major factor contributing to the highly variable pharmacokinetics of voriconazole. *Journal of clinical pharmacology* 49: 196 (2009).

153. Central Research Division Pfizer Inc. Compound data sheet. Voriconazole. (2006). 2006.

154. G.C. Keustermans, S.B. Hoeks, J.M. Meerding, B.J. Prakken, W. de Jager. Cytokine assays: An assessment of the preparation and treatment of blood and tissue samples. *Methods* 61: 10 (2013).

155. BD Cytometric Bead Array: Multiplexed Bead-Based Immunoassays. http://www.bdbiosciences.com/documents/CBA_Brochure_Intl.pdf. (26 February 2014).

156. BD Biosciences Reagents - Bead-Based Immunoassays - Formats - Assay Principle. http://www.bdbiosciences.com/eu/research/cytometricbeadarray/formats/index.jsp. (26 February 2014).

157. BD CBA Soluble Protein Flex Set System. http://www.bdbiosciences.com/documents/CBA_SolubleProtein_FlexSet_System.pdf. (26 February 2014).

158. BD FACSArray™ Bioanalyzer. http://www.bdbiosciences.com/external_files/is/doc/mkt_lit/brochures/live/web_enabled/05-810076-2A1.pdf. (26 February 2014).

159. ERIC Huang. Flow Cytometry Core. http://www.ibms.sinica.edu.tw/html/flow/webpage_eng/index1.html. (26 February 2014).

160. BD FACSArray™ Bioanalyzer. http://www.bdbiosciences.com/documents/CBA_FACSArrayBioanalyzer_Setup.pdf. (07 December 2010).

161. J.W. Findlay, R.F. Dillard. Appropriate calibration curve fitting in ligand binding assays. *The AAPS journal* 9: E260-7 (2007).

162. J. Werner. Biomathematik und medizinische Statistik (Urban & Schwarzenberg, München u.a, ed. 2, 1992).

163. R Core Team. R: A Language and Environment for Statistical Computing (R Foundation for Statistical Computing, Vienna, Austria, 2012).

164. TIBCO Spotfire®. Curve Fit Models. https://docs.tibco.com/pub/spotfire/5.5.0-march-2013/UsersGuide/curve/curve_curve_fit_models.htm. (02 July 2015).

165. R.J. Carroll, D. Ruppert. Transformation and Weighting in Regression (Springer US, Boston, MA, s.l, 1988).

166. Human Soluble Protein Flex Set Compatibility. www.bdbiosciences.com/documents/CBA_Hu_Soluble_Protein_Flex_Set_Compatibility.xls. (26 February 2014).

167. D. Rodbard. Statistical estimation of the minimal detectable concentration (''sensitivity'') for radioligand assays. *Analytical biochemistry* 90: 1 (1978).

168. M. Swartz, I.S. Krull. Handbook of analytical validation (CRC Press, Boca Raton, FL, 2012).

169. The United States pharmacopeia (United States Pharmacopeial Convention, Rockville, Md, 2013).

170. B. DeSilva, W. Smith, R. Weiner, M. Kelley, J. Smolec, B. Lee, M. Khan, R. Tacey, H. Hill, A. Celniker. Recommendations for the bioanalytical method validation of ligand-binding assays to support pharmacokinetic assessments of macromolecules. *Pharmaceutical research* 20: 1885 (2003).

171. ICH. ICH HARMONISED TRIPARTITE GUIDELINE - Validation of analytical procedures: Text and Methodology. *IFPMA: Geneva (*2005).

172. F. Simmel, C. Kloft. Microdialysis feasibility investigations with the non-hydrophilic antifungal voriconazole for potential applications in nonclinical and clinical settings. *International journal of clinical pharmacology and therapeutics* 48: 695 (2010).

173. F. Simmel. Development, optimisation and application of in vitro and in vivo microdialysis methods contributing to characterise drug disposition processes. PhD thesis, MLU Halle-Wittenberg (2010).

174. WMA. Declaration of Helsinki - Ethical Principles for Medical Research Involving Human Subjects. http://www.wma.net/en/30publications/10policies/b3/. (26 February 2014).

175. F. Simmel, C. Kirbs, Z. Erdogan, E. Lackner, M. Zeitlinger, C. Kloft. Pilot investigation on long-term subcutaneous microdialysis: proof of principle in humans. *The AAPS journal* 15: 95 (2013).

176. CDER ICH. Guideline for Industry. http://www.fda.gov/downloads/Drugs/GuidanceComplianceRegulatoryInformation/Guidances/UCM073087.pdf. (27 February 2014).

177. CDER ICH. Guideline for Industry. http://www.fda.gov/downloads/Drugs/GuidanceComplianceRegulatoryInformation/Guidances/UCM073113.pdf. (27 February 2014).

178. F. Simmel, J. Soukup, A. Zoerner, J. Radke, C. Kloft. Development and validation of an efficient HPLC method for quantification of voriconazole in plasma and microdialysate reflecting an important target site. *Analytical and bioanalytical chemistry* 392: 479 (2008).

179. M. Niemi, I. Cascorbi, R. Timm, H.K. Kroemer, P.J. Neuvonen, K.T. Kivistö. Glyburide and glimepiride pharmacokinetics in subjects with different CYP2C9 genotypes. *Clinical pharmacology and therapeutics* 72: 326 (2002).

180. R. Timm, R. Kaiser, J. Lotsch, U. Heider, O. Sezer, K. Weisz, M. Montemurro, I. Roots, I. Cascorbi. Association of cyclophosphamide pharmacokinetics to polymorphic cytochrome P450 2C19. *The pharmacogenomics journal* 5: 365 (2005).

181. J. Gabrielsson, D. Weiner. Pharmacokinetic, pharmacodynamic data analysis (Apotekarsocieteten, Stockholm, ed. 3, 2000).

182. J. Gabrielsson, D. Weiner. Non-compartmental analysis. *Methods in molecular biology (Clifton, N.J.)* 929: 377 (2012).

183. Roerig, Division of Pfizer Inc. Label Vfend® - HIGHLIGHTS OF PRESCRIBING INFORMATION. (2011).

184. J.W. Findlay, W.C. Smith, J.W. Lee, G.D. Nordblom, I. Das, B.S. DeSilva, M.N. Khan, R.R. Bowsher. Validation of immunoassays for bioanalysis: a pharmaceutical industry. *J Pharm Biomed Anal* 21: 1249 (2000).

185. BD Biosciences. BD™ Cytometric Bead Array (CBA). http://www.bdbiosciences.com/documents/cba_product_list.pdf. (11 August 2014).

186. World Health Organisation (WHO). Global Database on Body Mass Index. http://apps.who.int/bmi/index.jsp?introPage=intro_3.html. (21 July 2014).

187. European Medicines Agency. Guideline o the Investigation of Bioequivalence. (European Medicines Agency; http://www.ema.europa.eu/docs/en_GB/document_library/Scientific_guideline/2010/01/WC500070039.pdf (12/10/2014)).

188. A. Li-Wan-Po, T. Girard, P. Farndon, C. Cooley, J. Lithgow. Pharmacogenetics of CYP2C19: functional and clinical implications of a new variant CYP2C19*17. *British Journal of Clinical Pharmacology* 69: 222 (2010).

189. A. Owusu Obeng, E.F. Egelund, A. Alsultan, C.A. Peloquin, J.A. Johnson. CYP2C19 Polymorphisms and Therapeutic Drug Monitoring of Voriconazole: Are We Ready for Clinical Implementation of Pharmacogenomics?. *Pharmacotherapy (*2014).

190. G. Wang, H.-P. Lei, Z. Li, Z.-R. Tan, D. Guo, L. Fan, Y. Chen, D.-L. Hu, D. Wang, H.-H. Zhou. The CYP2C19 ultra-rapid metabolizer genotype influences the pharmacokinetics of voriconazole in healthy male volunteers. *European journal of clinical pharmacology* 65: 281 (2009).

191. S. Kumar, M. Rizvi. Prognostic serum tumor necrosis factor-alpha in paediatric patients with sepsis. *Journal of infection in developing countries* 3: 437 (2009).

192. A. Signore, E. Procaccini, A. Annovazzi, M. Chianelli, d.L. van, A. Mire-Sluis. The developing role of cytokines for imaging inflammation and infection. *Cytokine* 12: 1445 (2000).

193. Brüggemann, Roger J M, J.P. Donnelly, R.E. Aarnoutse, A. Warris, Blijlevens, Nicole M A, J.W. Mouton, P.E. Verweij, D.M. Burger. Therapeutic drug monitoring of voriconazole. *Therapeutic drug monitoring* 30: 403 (2008).

194. P.W. Thavasu, S. Longhurst, S.P. Joel, M.L. Slevin, F.R. Balkwill. Measuring cytokine levels in blood. Importance of anticoagulants, processing, and storage conditions. *Journal of immunological methods* 153: 115 (1992).

195. L. Flower, R.H. Ahuja, S.E. Humphries, V. Mohamed-Ali. EFFECTS OF SAMPLE HANDLING ON THE STABILITY OF INTERLEUKIN 6, TUMOUR NECROSIS FACTOR-α AND LEPTIN. *Cytokine* 12: 1712 (2000).

196. A. Friebe, H.-D. Volk. Stability of Tumor Necrosis Factor α, Interleukin 6, and Interleukin 8 in Blood Samples of Patients With Systemic Immune Activation. *Archives of Pathology & Laboratory Medicine* 132: 1802 (2008).

197. Food and Drug Administration (FDA). Guidance for industry: bioanalytical method validation. *Rockville, MD: CDER (*2001).

198. K.L. Kellar, M.A. Iannone. Multiplexed microsphere-based flow cytometric assays. *Experimental hematology* 30: 1227 (2002).

199. A. Tarnok, J. Hambsch, R. Chen, R. Varro. Cytometric bead array to measure six cytokines in twenty-five microliters of serum. *Clinical chemistry* 49: 1000 (2003).

200. S.X. Leng, J.E. McElhaney, J.D. Walston, D. Xie, N.S. Fedarko, G.A. Kuchel. ELISA and multiplex technologies for cytokine measurement in inflammation and aging research. *The journals of gerontology* 63: 879 (2008).

201. J.W. Lee, V. Devanarayan, Y.C. Barrett, R. Weiner, J. Allinson, S. Fountain, S. Keller, I. Weinryb, M. Green, L. Duan. Fit-for-purpose method development and validation for successful biomarker measurement. *Pharmaceutical Research* 23: 312 (2006).

202. J.W. Lee, M. Hall. Method validation of protein biomarkers in support of drug development or clinical diagnosis/prognosis. *Journal of chromatography* 877: 1259 (2009).

203. M.L. Cameron, F.H. Fu, H.H. Paessler, M. Schneider, C.H. Evans. Synovial fluid cytokine concentrations as possible prognostic indicators in the ACL-deficient knee. *Knee Surgery, Sports Traumatology, Arthroscopy* 2: 38 (1994).

204. M.-A. Valentin, S. Ma, an Zhao, F. Legay, A. Avrameas. Validation of immunoassay for protein biomarkers: bioanalytical study plan implementation to support pre-clinical and clinical studies. *Journal of pharmaceutical and biomedical analysis* 55: 869 (2011).

205. J.W. Findlay. Specificity and Accuracy Data for Ligand-binding Assays for Macromolecules Should be Interpreted with Caution. *The AAPS journal* 10: 433 (2008).

206. J.W. Findlay. Some important considerations for validation of ligand-binding assays. *Journal of chromatography* 877: 2191 (2009).

207. D.M. Fast, M. Kelley, C.T. Viswanathan, J. O'Shaughnessy, S.P. King, A. Chaudhary, R. Weiner, A.J. DeStefano, D. Tang. Workshop Report and Follow-Up--AAPS Workshop on Current Topics in GLP Bioanalysis: Assay Reproducibility for Incurred Samples--Implications of Crystal City Recommendations. *The AAPS journal* 11: 238 (2009).

208. NIBSC. WHO International Standard - INTERLEUKIN-6 (IL-6, Human rDNA derived) 1st International Standard (19/03/2008).

209. NIBSC. WHO International Standard - 1st Standard for Interleukin-8 (Human, rDNA derived) (23/04/2013).

210. NIBSC. WHO International Standard - Interleukin-10 (Human, rDNA derived) (09/04/2013).

211. NIBSC. WHO International Standard - 3rd International Standard forTumour Necrosis Factor-alpha (Human, rDNA derived) (26/11/2013).

212. X. Zhou, M.S. Fragala, J.E. McElhaney, G.A. Kuchel. Conceptual and methodological issues relevant to cytokine and inflammatory marker measurements in clinical research. *Current opinion in clinical nutrition and metabolic care* 13: 541 (2010).

213. European Medicines Agency. Guideline on the evaluation of medicinal products indicated for treatment of bacterial infections. (European Medicines Agency; .

214. J.R. Yates, C.I. Ruse, A. Nakorchevsky. Proteomics by mass spectrometry: approaches, advances, and applications. *Annual review of biomedical engineering* 11: 49 (2009).

215. S.S. Tworoger. Collection, Processing, and Storage of Biological Samples in Epidemiologic Studies: Sex Hormones, Carotenoids, Inflammatory Markers, and Proteomics as Examples. *Cancer Epidemiology Biomarkers & Prevention* 15: 1578 (2006).

216. M. Averbeck, S. Beilharz, M. Bauer, C. Gebhardt, A. Hartmann, K. Hochleitner, F. Kauer, U. Voith, J.C. Simon, C. Termeer. In situ profiling and quantification of cytokines released during ultraviolet B-induced inflammation by combining dermal microdialysis and protein microarrays. *Experimental dermatology* 15: 447 (2006).

217. Y. Wang, J.A. Stenken. Affinity-based microdialysis sampling using heparin for in vitro collection of human cytokines. *Analytica chimica acta* 651: 105 (2009).

218. W.J. Trickler, D.W. Miller. Use of osmotic agents in microdialysis studies to improve the recovery of macromolecules. *Journal of pharmaceutical sciences* 92: 1419 (2003).

219. F. Sjögren, C.D. Anderson. Are cutaneous microdialysis cytokine findings supported by end point biopsy immunohistochemistry findings?. *The AAPS journal* 12: 741 (2010).

220. X. Ao, R.F. Rotundo, D.J. Loegering, J.A. Stenken. In vivo microdialysis sampling of cytokines produced in mice given bacterial lipopolysaccharide. *Journal of microbiological methods* 62: 327 (2005).

221. P. Desai, P. Shah, R. Patlolla, M. Singh. Dermal Microdialysis Technique to Evaluate the Trafficking of Surface-Modified Lipid Nanoparticles upon Topical Application. *Pharmaceutical Research* 29: 2587 (2012).

222. V.I. Chefer, A.C. Thompson, A. Zapata, T.S. Shippenberg. Overview of Brain Microdialysis. *Current protocols in neuroscience / editorial board, Jacqueline N. Crawley … [et al.]* CHAPTER: Unit7.1 (2009).

223. H.-Y. Zhang, H.-Y. Shi, E.-Y. Wang. Effect of environment temperature on the recovery of microdialysis probe for monoamine neurotransmitter. *Zhejiang da xue xue bao. Yi xue ban = Journal of Zhejiang University. Medical sciences* 38: 271 (2009).

224. J.K. Chai. The pH value of granulating wound and skin graft in burn patients. *Zhonghua zheng xing shao shang wai ke za zhi* 8: 177-8, 246 (1992).

225. Z. Gerevich, Z.S. Zadori, L. Koles, L. Kopp, D. Milius, K. Wirkner, K. Gyires, P. Illes. Dual effect of acid pH on purinergic P2X3 receptors depends on the histidine 206 residue. *The Journal of biological chemistry* 282: 33949 (2007).

226. I. Goldie, A. Nachemson. Synovial pH in rheumatoid knee joints. II. The effect of local corticosteroid treatment. *Acta orthopaedica Scandinavica* 41: 354 (1970).

227. W.E. Jacobus, G.J. Taylor, D.P. Hollis, R.L. Nunnally. Phosphorus nuclear magnetic resonance of perfused working rat hearts. *Nature* 265: 756 (1977).

228. Y.C. Woo, S.S. Park, A.R. Subieta, T.J. Brennan. Changes in tissue pH and temperature after incision indicate acidosis may contribute to postoperative pain. *Anesthesiology* 101: 468 (2004).

229. F. Sjögren, C. Anderson. Sterile trauma to normal human dermis invariably induces IL1beta, IL6 and IL8 in an innate response to "danger". *Acta dermato-venereologica* 89: 459 (2009).

230. J. Riese, S. Boecker, W. Hohenberger, P. Klein, W. Haupt. Microdialysis: a new technique to monitor perioperative human peritoneal mediator production. *Surgical infections* 4: 11 (2003).

231. F. Sjögren, K. Davidsson, M. Sjostrom, C.D. Anderson. Cutaneous Microdialysis: Cytokine Evidence for Altered Innate Reactivity in the Skin of Psoriasis Patients?. *The AAPS journal (*2012).

232. D.A. Vignali, L.W. Collison, C.J. Workman. How regulatory T cells work. *Nature reviews. Immunology* 8: 523 (2008).

233. P.M. Liebmann, G. Reibnegger, M. Lehofer, M. Moser, P. Purstner, H. Mangge, K. Schauenstein. Circadian rhythm of the soluble p75 tumor necrosis factor (sTNF-R75) receptor in humans--a possible explanation for the circadian kinetics of TNR-alpha effects. *International immunology* 10: 1393 (1998).

234. A.N. Vgontzas, E.O. Bixler, H.-M. Lin, P. Prolo, G. Trakada, G.P. Chrousos. IL-6 and its circadian secretion in humans. *Neuroimmunomodulation* 12: 131 (2005).

235. C. Payette, P. Blackburn, B. Lamarche, A. Tremblay, J. Bergeron, I. Lemieux, J.-P. Despres, C. Couillard. Sex differences in postprandial plasma tumor necrosis factor-alpha, interleukin-6, and C-reactive protein concentrations. *Metabolism: clinical and experimental* 58: 1593 (2009).

236. R. Hyland. Identification of the Cytochrome P450 Enzymes Involved in the N-Oxidation of Voriconazole. *Drug Metabolism and Disposition* 31: 540 (2003).

237. I. Scholz, H. Oberwittler, K.-D. Riedel, J. Burhenne, J. Weiss, W.E. Haefeli, G. Mikus. Pharmacokinetics, metabolism and bioavailability of the triazole antifungal agent voriconazole in relation to CYP2C19 genotype. *British Journal of Clinical Pharmacology* 68: 906 (2009).

238. M.G. Scordo, A.P. Caputi, C. D'Arrigo, G. Fava, E. Spina. Allele and genotype frequencies of CYP2C9, CYP2C19 and CYP2D6 in an Italian population. *Pharmacological research : the official journal of the Italian Pharmacological Society* 50: 195 (2004).

239. T. Felton, P.F. Troke, W.W. Hope. Tissue penetration of antifungal agents. *Clinical microbiology reviews* 27: 68 (2014).

240. M. Müller, A. dela Peña, H. Derendorf. Issues in Pharmacokinetics and Pharmacodynamics of Anti-Infective Agents: Distribution in Tissue. *Antimicrobial Agents and Chemotherapy* 48: 1441 (2004).

241. A. Florent, P. Gandia, P. Seraissol, E. Chatelut, G. Houin. Determination of plasma unbound fraction of voriconazole in patients treated with a prophylactic or a curative treatment. *Therapeutic drug monitoring* 36: 752 (2014).

242. Y. Kwon. Handbook of Essential Pharmacokinetics, Pharmacodynamics and Drug Metabolism for Industrial Scientists (Kluwer Academic Publishers, Boston, MA, 2002).

243. M.K. Grudzien, K. Palka, F.A. Plucinski, A.P. Mazurek. Molecular properties impact on bioavailability of second generation triazoles antifungal agents. *Acta poloniae pharmaceutica* 70: 869 (2013).

244. M. Rowland, T.N. Tozer. Clinical pharmacokinetics (Williams and Wilkins, Baltimore, Md, ed. 4, 2005).

245. M.D. Richardson, B.L. Jones, R. Rautemaa. Therapeutic guidelines in systemic fungal infections (Remedica, London, ed. 4, 2007).

246. David N. Gilbert, R. C. Moellering, G. M. Eliopoulos, H. F. Chambers, M. S. Saag, Eds. The Sanford guide to antimicrobial therapy 2010 (Antimicrobial Therapy, Sperryville, VA, ed. 40, 2010).

247. A. Pascual, T. Calandra, S. Bolay, T. Buclin, J. Bille, O. Marchetti. Voriconazole Therapeutic Drug Monitoring in Patients with Invasive Mycoses Improves Efficacy and Safety Outcomes. *Clinical Infectious Diseases* 46: 201 (2008).

248. S. Miyakis, van Hal, S J, J. Ray, D. Marriott. Voriconazole concentrations and outcome of invasive fungal infections. *Clinical microbiology and infection : the official publication of the European Society of Clinical Microbiology and Infectious Diseases* 16: 927 (2010).

249. T. Hussaini, Rüping, Maria J. G. T, F. Farowski, J.J. Vehreschild, O.A. Cornely. Therapeutic Drug Monitoring of Voriconazole and Posaconazole. *Pharmacotherapy* 31: 214 (2011).

250. D. Andes. Optimizing antifungal choice and administration. *Current medical research and opinion* 29 Suppl 4: 13 (2013).

251. J.W. Mouton, M.N. Dudley, O. Cars, H. Derendorf, G.L. Drusano. Standardization of pharmacokinetic/pharmacodynamic (PK/PD) terminology for anti-infective drugs: an update. *The Journal of antimicrobial chemotherapy* 55: 601 (2005).

252. M. C. Arendrup, M. Cuenca-Estrella, C. Lass-Flörl, W. Hope, Subcommittee on Antifungal Susceptibility Testing (AFST) of the ESCMID European Committee for Antimicrobial Susceptibility Testing (EUCAST). Method for the determination of broth dilution minimum Inhibitory concentrations of antifungal agents for yeasts. http://www.eucast.org/fileadmin/src/media/PDFs/EUCAST_files/AFST/EUCAST_EDef_7_2_revision.pdf. (16 October 2014).

253. Subcommittee on Antifungal Susceptibility Testing (AFST) of the ESCMID European Committee for Antimicrobial Susceptibility Testing (EUCAST). EUCAST Technical Note on the method for the determination of broth dilution minimum inhibitory concentrations of antifungal agents for conidia-forming moulds. *Clinical microbiology and infection : the official publication of the European Society of Clinical Microbiology and Infectious Diseases* 14: 982 (2008).

254. Subcommittee on Antifungal Susceptibility Testing (AFST) of the ESCMID European Committee for Antimicrobial Susceptibility Testing (EUCAST). EUCAST Technical Note on Voriconazole and Aspergillus spp. *Clinical Microbiology and Infection* 19: E278 (2013).

255. A.R. Jeans, S.J. Howard, Z. Al-Nakeeb, J. Goodwin, L. Gregson, J.B. Majithiya, C. Lass-Florl, M. Cuenca-Estrella, M.C. Arendrup, P.A. Warn, W.W. Hope. Pharmacodynamics of Voriconazole in a Dynamic In Vitro Model of Invasive Pulmonary Aspergillosis: Implications for In Vitro Susceptibility Breakpoints. *The Journal of infectious diseases (*2012).

256. P.F. Troke, H.P. Hockey, W.W. Hope. Observational study of the clinical efficacy of voriconazole and its relationship to plasma concentrations in patients. *Antimicrobial agents and chemotherapy* 55: 4782 (2011).

257. J. Smith, N. Safdar, V. Knasinski, W. Simmons, S.M. Bhavnani, P.G. Ambrose, D. Andes. Voriconazole therapeutic drug monitoring. *Antimicrobial agents and chemotherapy* 50: 1570 (2006).

258. Subcommittee on Antifungal Susceptibility Testing (AFST) of the ESCMID European Committee for Antimicrobial Susceptibility Testing (EUCAST). EUCAST Technical Note on voriconazole. *Clinical microbiology and infection : the official publication of the European Society of Clinical Microbiology and Infectious Diseases* 14: 985 (2008).

259. F. Cafini, D. Sevillano, L. Alou, F. Gomez-Aguado, M.T. Corcuera, N. Gonzalez, J. Guinea, J. Prieto. Effect of protein binding on the activity of voriconazole alone or combined with anidulafungin against Aspergillus spp. using a time-kill methodology. *Revista espanola de quimioterapia : publicacion oficial de la Sociedad Espanola de Quimioterapia* 25: 47 (2012).

260. B.A. Potoski, J. Brown. The safety of voriconazole. *Clinical infectious diseases : an official publication of the Infectious Diseases Society of America* 35: 1273 (2002).

261. G.L. Drusano. How does a patient maximally benefit from anti-infective chemotherapy?. *Clinical infectious diseases : an official publication of the Infectious Diseases Society of America* 39: 1245 (2004).

262. A. Howard, J. Hoffman, A. Sheth. Clinical application of voriconazole concentrations in the treatment of invasive aspergillosis. *The Annals of pharmacotherapy* 42: 1859 (2008).

263. M.J. Dolton, J.E. Ray, S.C.-A. Chen, K. Ng, L.G. Pont, A.J. McLachlan. Voriconazole Pharmacokinetics and Therapeutic Drug Monitoring: A Multi-Center Study. *Antimicrobial agents and chemotherapy (*2012).

264. D.A. Stevens, B.J. Kullberg, E. Brummer, A. Casadevall, M.G. Netea, A.M. Sugar. Combined treatment: antifungal drugs with antibodies, cytokines or drugs. *Med Mycol* 38 Suppl 1: 305 (2000).

265. F. Reichenberger, J.M. Habicht, A. Gratwohl, M. Tamm. Diagnosis and treatment of invasive pulmonary aspergillosis in neutropenic patients. *European Respiratory Journal* 19: 743 (2001).

266. B.J. Kullberg, '.W. van. Cytokines in the treatment of fungal infections. *Biotherapy* 7: 195 (1994).

267. C. Antachopoulos, E. Roilides. Cytokines and fungal infections. *British journal of haematology* 129: 583 (2005).

268. S. Shoham, S.M. Levitz. The immune response to fungal infections. *British journal of haematology* 129: 569 (2005).

269. L. Romani. Immunology of invasive candidiasis. In *Candida and candidiasis.* Richard A. Calderone, Ed. (ASM Press, Washington, DC, c 2002).

270. L. Romani. Immunity to fungal infections. *Nat Rev Immunol* 4: 11 (2004).

271. T.M. Hohl, A. Rivera, E.G. Pamer. Immunity to fungi. *Current Opinion in Immunology* 18: 465 (2006).

272. N. Berkova, S. Lair-Fulleringer, F. Femenia, D. Huet, M.-C. Wagner, K. Gorna, F. Tournier, O. Ibrahim-Granet, J. Guillot, R. Chermette, P. Boireau, J.-P. Latge. Aspergillus fumigatus conidia inhibit tumour necrosis factor- or staurosporine-induced apoptosis in epithelial cells. *International immunology* 18: 139 (2006).

273. M. Simitsopoulou, E. Roilides, F. Paliogianni, C. Likartsis, J. Ioannidis, K. Kanellou, T.J. Walsh. Immunomodulatory Effects of Voriconazole on Monocytes Challenged with

Aspergillus fumigatus: Differential Role of Toll-Like Receptors. *Antimicrobial Agents and Chemotherapy* 52: 3301 (2008).

274. K. Kawakami, M.H. Qureshi, Y. Koguchi, T. Zhang, H. Okamura, M. Kurimoto, A. Saito. Role of TNF-alpha in the induction of fungicidal activity of mouse peritoneal exudate cells against Cryptococcus neoformans by IL-12 and IL-18. *Cellular immunology* 193: 9 (1999).

275. A. Mencacci, E. Cenci, A. Bacci, C. Montagnoli, F. Bistoni, L. Romani. Cytokines in candidiasis and aspergillosis. *Current pharmaceutical biotechnology* 1: 235 (2000).

276. M.G. Netea, B.J. Kullberg, d.M. Van. Proinflammatory cytokines in the treatment of bacterial and fungal infections. *BioDrugs* 18: 9 (2004).

277. B.J. Kullberg, M.G. Netea, A.G. Vonk, van der Meer, J W. Modulation of neutrophil function in host defense against disseminated Candida albicans infection in mice. *FEMS immunology and medical microbiology* 26: 299 (1999).

278. V. Balloy, M. Huerre, J.-P. Latge, M. Chignard. Differences in patterns of infection and inflammation for corticosteroid treatment and chemotherapy in experimental invasive pulmonary aspergillosis. *Infection and immunity* 73: 494 (2005).

279. S.G. Filler, M.R. Yeaman, D.C. Sheppard. Tumor necrosis factor inhibition and invasive fungal infections. *Clinical infectious diseases : an official publication of the Infectious Diseases Society of America* 41 Suppl 3: S208-12 (2005).

280. D.W. Denning. Therapeutic outcome in invasive aspergillosis. *Clinical infectious diseases : an official publication of the Infectious Diseases Society of America* 23: 608 (1996).

281. W.W. Hope, D.W. Denning. Invasive aspergillosis: current and future challenges in diagnosis and therapy. *Clinical microbiology and infection : the official publication of the European Society of Clinical Microbiology and Infectious Diseases* 10: 2 (2004).

282. B. Moriyama, L.A. Gordon, M. McCarthy, S.A. Henning, T.J. Walsh, S.R. Penzak. Emerging drugs and vaccines for candidemia. *Mycoses* 57: 718 (2014).

283. C. Viscoli, C. Girmenia, A. Marinus, L. Collette, P. Martino, B. Vandercam, C. Doyen, B. Lebeau, D. Spence, V. Krcmery, B. de Pauw, F. Meunier. Candidemia in cancer patients: a prospective, multicenter surveillance study by the Invasive Fungal Infection Group (IFIG) of the European Organization for Research and Treatment of Cancer (EORTC). *Clinical infectious diseases : an official publication of the Infectious Diseases Society of America* 28: 1071 (1999).

284. M. Simitsopoulou, E. Roilides, C. Likartsis, J. Ioannidis, A. Orfanou, F. Paliogianni, T.J. Walsh. Expression of Immunomodulatory Genes in Human Monocytes Induced by Voriconazole in the Presence of Aspergillus fumigatus. *Antimicrobial Agents and Chemotherapy* 51: 1048 (2007).

285. A.L. Baltch, L.H. Bopp, R.P. Smith, W.J. Ritz, P.B. Michelsen. Anticandidal effects of voriconazole and caspofungin, singly and in combination, against Candida glabrata, extracellularly and intracellularly in granulocyte-macrophage colony stimulating factor (GM-CSF)-activated human monocytes. *Journal of Antimicrobial Chemotherapy* 62: 1285 (2008).

286. S. Vora, S. Chauhan, E. Brummer, D.A. Stevens. Activity of Voriconazole Combined with Neutrophils or Monocytes against Aspergillus fumigatus: Effects of Granulocyte Colony-Stimulating Factor and Granulocyte-Macrophage Colony-Stimulating Factor. *Antimicrobial Agents and Chemotherapy* 42: 2299 (1998).

287. R. Ben-Ami, R.E. Lewis, D.P. Kontoyiannis. Immunocompromised Hosts: Immunopharmacology of Modern Antifungals. *Clinical Infectious Diseases* 47: 226 (2008).

288. E. Roilides, A. Holmes, C. Blake, D. Venzon, P.A. Pizzo, T.J. Walsh. Antifungal activity of elutriated human monocytes against Aspergillus fumigatus hyphae: enhancement by granulocyte-macrophage colony-stimulating factor and interferon-gamma. *The Journal of infectious diseases* 170: 894 (1994).

289. E. Roilides, K. Uhlig, D. Venzon, P.A. Pizzo, T.J. Walsh. Prevention of corticosteroid-induced suppression of human polymorphonuclear leukocyte-induced damage of Aspergillus fumigatus hyphae by granulocyte colony-stimulating factor and gamma interferon. *Infection and immunity* 61: 4870 (1993).

290. J. Nemunaitis, K. Shannon-Dorcy, F.R. Appelbaum, J. Meyers, A. Owens, R. Day, D. Ando, C. O'Neill, D. Buckner, J. Singer. Long-term follow-up of patients with invasive fungal disease who received adjunctive therapy with recombinant human macrophage colony-stimulating factor. *Blood* 82: 1422 (1993).

291. E. Roilides, A. Dimitriadou, I. Kadiltsoglou, T. Sein, J. Karpouzas, P.A. Pizzo, T.J. Walsh. IL-10 exerts suppressive and enhancing effects on antifungal activity of mononuclear phagocytes against Aspergillus fumigatus. *The Journal of Immunology* 158: 322 (1997).

292. E. Roilides, T. Sein, M. Roden, R.L. Schaufele, T.J. Walsh. Elevated Serum Concentrations of Interleukin-10 in Nonneutropenic Patients with Invasive Aspergillosis. *The Journal of infectious diseases* 183: 518 (2001).

293. L. Romani, P. Puccetti. Protective tolerance to fungi: the role of IL-10 and tryptophan catabolism. *Trends in microbiology* 14: 183 (2006).

294. L. Romani. Immunity to fungal infections. *Nat Rev Immunol* 11: 275 (2011).

295. A. De Luca, T. Zelante, C. D'Angelo, S. Zagarella, F. Fallarino, A. Spreca, R.G. Iannitti, P. Bonifazi, J.-C. Renauld, F. Bistoni, P. Puccetti, L. Romani. IL-22 defines a novel immune pathway of antifungal resistance. *Mucosal immunology* 3: 361 (2010).

296. BD Cytometric Bead Array (CBA) Kit for the BD FACSArray Bioanalyzer - Instruction Manual. https://www.bdbiosciences.com/documents/CBA_BDFACSArray_Bioanalyzer_Kit_Manual.pdf. (30 June 2015).

297. FCAP Array Software User's Guide. http://www.bdbiosciences.com/external_files/pm/doc/manuals/live/web_enabled/FCAPArraySoftwareUG_641489.pdf. (26 February 2014).

298. FCAP Array Software with BD FACSArray Bioanalyzer. http://www.bdbiosciences.com/documents/CBA_FCAP_Tutorial.pdf. (26 February 2014).

299. BD Cytometric Bead Array (CBA) Human Soluble Protein Master Buffer Kit - Instruction Manual. http://www.bdbiosciences.com/ds//pm/others/23-13480.pdf. (30 June 2015).

300. MILLIPORE. MultiScreen® Separations System. http://www.millipore.com/userguides.nsf/a73664f9f981af8c852569b9005b4eee/e0f9962bc5e5c2f885256b260052584d/$FILE/P17479.pdf. (28 February 2014).

301. M. Burian, S. Grosch, I. Tegeder, G. Geisslinger. Validation of a new fluorogenic real-time PCR assay for detection of CYP2C9 allelic variants and CYP2C9 allelic distribution in a German population. *British journal of clinical pharmacology* 54: 518 (2002).

302. C. Markert, R. Hellwig, J. Burhenne, M.M. Hoffmann, J. Weiss, G. Mikus, W.E. Haefeli. Interaction of ambrisentan with clarithromycin and its modulation by polymorphic SLCO1B1. *European journal of clinical pharmacology* 69: 1785 (2013).

303. B.E. Caplin, R.P. Rasmussen, P.S. Bernard, C.T. Wittwer. LightCycler hybridization probes - The most direct way to monitor PCR amplification for quantification and mutation detection. *Biochemica* 1: 5 (1999).

PUBLICATIONS

Journal Articles

C. Kirbs, C. Kloft.
In vitro microdialysis recovery and delivery investigation of cytokines as prerequisite for potential biomarker profiling. European Journal of Pharmaceutical Sciences, in press (2013). http://dx.doi.org/10.1016/j.ejps.2013.11.006

F. Simmel, C. Kirbs, Z. Erdogan, E. Lackner, M. Zeitlinger, C. Kloft
Pilot Investigation on Long-Term Subcutaneous Microdialysis: Proof of Principle in Humans. The AAPS Journal, Volume 15, Issue 1: 95 (2013).
doi: 10.1208/s12248-012-9412-z.

Abstracts

Oral presentation

C. Kirbs, C. Kloft.
In vitro microdialysis of cytokines. 7th International Symposium on Microdialysis, Poitiers, France, 23.-24.05.2013.
Abstract 1.4 http://microdialysis.conference.univ-poitiers.fr/spip.php?article93&lang=en

Poster presentations

C. Kirbs, C. Kloft.
In vitro microdialysis of cytokines. 7th International Symposium on Microdialysis, Poitiers, France, 23.-24.05.2013.
Abstract 1.4 http://microdialysis.conference.univ-poitiers.fr/spip.php?article93&lang=en

C. Kirbs, A. Simm, C. Kloft.
In vitro microdialysis of cytokines applying a validated cba/facs quantification method. 9th Joint Meeting of the International Cytokine Society (ICS) and the International Society for Interferon and Cytokine Research (ISICR), Florence, Italy, 09.-12.10.2011. Cytokine, Volume 56, Issue: 34 (2011). http://dx.doi.org/10.1016/j.cyto.2011.07.099

C. Kirbs, F. Simmel, M. Zeitlinger, E. Lackner, C. Rimmbach, C. Kloft.
Clinical long-term microdialysis study with voriconazole in healthy volunteers. European Congress of Clinical Microbiology and Infectious Diseases, Mailand, Italien, 07.-10.05.2011. Final Programme, 106 (2011).
and in Clinical Microbiology and Infection, Volume 17, Issue Supplement s4: 196 (2011). doi: 10.1111/j.1469-0691.2011.03558.x

C. Kirbs, A. Simm, J. Wohlrab, C. Kloft.
A valid method for quantification of cytokines from microdialysate contributing to biomarker profiling. Jahrestagung der Deutschen Pharmazeutischen Gesellschaft (DPhG), Braunschweig, Deutschland, 04.-07.10.2010. Tagungsband, 138 (2010).

Diploma thesis

C. Kirbs
Entwicklung einer durchflusszytometrischen Methode zur Quantifizierung der Zytokine Interleukin-6, -8, -10 und Tumor-Nekrose-Faktor-alpha aus 100-kDa-Mikrodialysat. Institute of Pharmacy, Martin-Luther-Universitaet Halle-Wittenberg, Halle, Germany (2011).

CURRICULUM VITAE

The biography is not included in the online version for reasons of data protection

Der Lebenslauf ist in der Online-Version aus Gründen des Datenschutzes nicht enthalten.

8 APPENDIX

8.1 SOP: Quantification method of the cytokines IL-6, IL-8, IL-10 and TNF-α from microdialysate by BD™CBA/BD FACSArray™

8.1.1 Preparation of 'Mixed Beads' and 'Mixed Detection Reagents'

Refer to the manuals of the BD FACSArray™ Bioanalyzer (*BD Cytometric Bead Array (CBA) Kit for the BD FACSArray Bioanalyzer - Instruction Manual* [296]), the FCAP Software (*FCAP Array Software User's Guide* [297]; *FCAP Array Software with BD FACSArray Bioanalyzer* [298]), and of the commercial assay (*BD FACSArray™ Bioanalyzer - BD™ CBA Flex Sets: Instrument Setup, Data Acquisition, and Analysis - Instruction Manual* [160]; *BD Cytometric Bead Array (CBA) Human Soluble Protein Master Buffer Kit - Instruction Manual* [299]) for the performance and instructions of the method. The following instructions amend these manuals with regards to the adapted method.

Preparation of Mixed Beads ('Capture Beads' of the individual cytokines + 'Capture Bead Diluent') and Mixed Detection Reagents ('Detection Reagents' of the individual cytokines + 'Detection Reagent Diluent') follows a scheme of calculations:

- Preparation of bead suspension ('Mixed Beads') and detection antibody solution ('Mixed Detection Reagents') for intended number of tests by dilution of the individual concentrates (concentrated fifty-fold)
  - Sample calculation for quantification of four model cytokines in 96 microtitre-plate cavities (example: 32 samples, 3 replicates):
    - Determination of number of 'Flex Sets' (reagent kit for one cytokine) for multiplex-assay: 4 (four cytokines)
    - Determination of number of tests (surplus for correct pipetting): 96 tests + 4 tests surplus = 100 tests
    - Calculation of total volume of Mixed Beads for the experiment (25 µl per test): 100 tests x 25 µl = 2500 µl bead suspension
    - Determination of volume of each Capture Bead (0.5 µl bead concentrate per cytokine and test): 100 tests x 0.5 µl = 50 µl per Capture bead
    - Sum of Capture Bead volumes: 50 µl x 4 cytokines = 200 µl (total volume)
    - Calculation of volume of Capture Bead Diluent by subtraction total Capture bead volume from volume of bead suspension: 2500 µl – 200 µl = 2300 µl
  - Spin down unopened Capture Bead concentrates
  - Vortex each Capture Bead vial for at least 15 seconds to resuspend the beads thoroughly

- Add calculated xx µl (example: 50 µL) of each Capture Bead concentrates to calculated xxxx µl (example: 2300 µL) of Capture Bead Diluent (= bead suspension)

- Preparation of detection antibody solution (‘Mixed Detection Reagents’) following the same scheme: mixing Detection Reagents concentrates (concentrated fifty-fold) of each cytokine (without vortexing) with Detection Reagent Diluent
  - Store at 4 °C, protected from light, until ready to use

8.1.2 Sample processing

The method was validated for frozen samples only, therefore, fresh samples are not under the scope of this SOP.

- Prearrangements:
  - Thaw sample vials at RT for a minimum of 15 min (volumes ≤150 µL)
  - Spin down sample vials
- Predilution samples in the microtitre plate:
  - Calculation of required volume of Assay Diluent: Number of tests x 25 µL + ca. 500 µL surplus
  - Fill Assay Diluent into reagent reservoir for use with electronical multichannel pipette
  - Pipette 25 µL of Assay Diluent into the required number of cavities of the microtitre plate (round-bottom, PVC) and put the cover lid onto the plate
  - Vortex samples/Cal/QC cautiously at low rpm (≤speed level 4-5)
  - Add 25 µL sample/Cal/QC to the intended cavities:
    - Use one channel of the electronical multichannel pipette
    - Pre-wet pipette tip with sample/Cal/QC
    - Pipette required number of replicates (25 µL) of the individual sample/Cal/QC into cavities using the same tip
  - Shake covered plate for 5 min at 500 rpm
- Processing of prediluted samples:

  Cover individual unused cavities with adhesive tape prior to vacuum filtration! Remove cover lid from microtitre plate for vaccum filtration! Pipette reagents with electronical multichannel pipette from labelled reagent reservoirs. Avoid contact of the bottom of the microtitre filter plate (i.e. membranes!) with absorbent materials (e.g. cellulose) while cavites are filled with fluids.
  - Fill 100 µL Wash Buffer into required cavities of microtitre filter plate
  - Apply to the vacuum manifold (refer to the manual *MILLIPORE MultiScreen® Separations System – User’s Guide* [300]):
    - Assemble vacuum manifold as described in the manual [154]
    - Adjust vacuum pressure to 2-4“ Hg by pressure regulation valves applying a common PVC-microtitre plate (without filter bottom)
    - Start filtration of the filter plate and stop after 1-2 s, repeat filtration

- Gently tap the bottom of the plate onto absorbent material to remove any residual fluid

- Vortex Mixed Beads for ca. 5 s at high rpm (speed level 9)
- Pipette 25 µL of Mixed Beads into each required cavity
- Add 25 µL prediluted sample/Cal/QC (out of the microtitre plate) to the filter plate
- Shake covered plate for 5 min at 500 rpm
- Incubate for 1 h protected from light
- Pipette 25 µL of Mixed Detection Reagents into each cavity
- Shake covered plate for 5 min at 500 rpm and incubate for 2 h protected from light
- Vacuum filtrate filter plate
- Fill 100 µL Wash Buffer into cavities of microtitre filter plate, shake plate (see above)
- Vacuum filtrate filter plate
- Fill 150 µL Wash Buffer into cavities
- Cover filter plate and store protected from light until analysis

➢ Shake filter plate prior to analysis (see above)

8.1.3 Data acquisition and analysis with BD FACSArray™

In case the device had not been in use for a while (> 1 week), the bidestilled water in the sheath fluid container has to be exchanged with sheath fluid ('FACS Flow') and the device initially rinsed. See *BD FACSArray™ Bioanalyzer - BD™ CBA Flex Sets: Instrument Setup, Data Acquisition, and Analysis - Instruction Manual* for using instructions of the device and the FCAP Array™ Software.

➢ (Perform Instrument Setup including) pre-testing of Mixed Beads

➢ (save 'Instrument Setup Experiment' as template and export to the FCAP Array™ Software)

➢ Create experiment in the FCAP Array™ Software

➢ Export experiment (including integration of the Instrument Setup template) and import into BD FACSArray System Software

➢ Check instrument and experiment parameters

➢ Experiment parameters:

- Sample flow rate: 1 µL/s
- Sample volume: **30 µL**
- Mix volume: 60 µL
- Mixing speed: 200 µL/s
- Number of mixes: 1
- Wash volume: 200 µL

➢ Analysis of the samples on microtitre plate(s):

- Measure the first filled cavity (Cal 1/1)
- Export data to the FCAP Array™ Software
- Check number and signals of detected cluster
- In case of failure (e.g. no cluster detection): analyse and fix problem
- In case of correct functioning (detection of all clusters): Continue with the analysis of the remaining cavities

- Export acquired data to data analysis software (FCAP Array™)
- Pre-analyse experiment (create digital data from signals) and export
- Export experiment into PDF and ECXEL documents
- Save data on storage medium
- Perform wash (required washing duration depending on frequence of use: 'weekly' or 'monthly' clean as recommened in the manual)
- Exchange sheath fluid with bidistilled water, if required (if in use less than once per week)
- Exit programes, switch off device and computer

Data will subsequently be analysed with Microsoft Office Excel and Phoenix™ WinNonlin®. MFI of the all clusters, i.e. cytokines, are determined for every calibration sample with known concentration and calibration functions generated by non-linear regression (see section 2.4.1.1) [160; 297; 298]. Concentrations of QC and unknown samples are calculated using calibration function. Validity of QC will be checked before calculated sample concentrations can be used.

8.2 Laboratory investigations for the clinical long-term microdialysis study with voriconazole in healthy volunteers (project IV)

At the screening visit and in a reduced manner at the final examination (see Tab. 8-3) a laboratory screening was conducted to ascertain participants to be healthy:

- Haematology: erythrocytes concentration, white blood cell count, haemoglobin, mean corpuscular volume, mean corpuscular haemoglobin, mean corpuscular haemoglobin concentration, haematocrit, thrombocytes concentration.
- Clinical chemistry: total bilirubin, AP, ASAT, ALAT, γ-GTP, LDH, creatinine.
- Virology: HIV, HepB antigen and HepC antibody (only at screening).
- Urinalysis: Stix® Test and drug screening for amphetamines, barbiturates, opiates, cocaine and methadone (only at screening).
- Coagulation test: activated partial thromboplastin time, normotest.

- Genotype: genotype of the CYP isoenzymes 2C9, 2C19 by pyrosequencing and hybridization probes format (see section 2.8.2.2).
- Measurement of visual acuity: distance best-corrected visual acuity (BCVA) by standard Early Treatment Diabetic Retinopathy Study charts. Near BCVA with Jaeger reading charts at distances of 20 cm or 40 cm (All tests for visual activity were performed by qualified ophthalmologists).

8.3 Analysis of genotype of Cytochrome P450 isoenzymes 2C9 and 2C19 of the healthy volunteers (project IV)

Genotype analysis of the first five individuals [173]

Preparation of genomic DNA from blood samples was supported by the NucleoSpin® Blood isolation kit. In order to control the purification process, the concentration of the eluted DNA was determined by spectrometric analysis (λ=220 nm to 750 nm). Real time polymerase chain reaction (RT-PCR) was applied for the amplification of the selected alleles *2 and *3 of CYP2C9 and *2 of CYP2C19 from the purified DNA. To control the PCR process and to detect the PCR product, respectively, electrophoresis was carried out. Previous to the pyrosequencing® procedure, single-stranded DNA had to be prepared from the PCR product using the Vacuum Prep Tool®. The single-stranded templates were then analysed with the Pyrosequencing® system.

Genotype analysis of the subsequent four individuals

For genotyping genomic DNA was isolated from leucocytes using the QIAamp DNA Blood Mini Kit (Qiagen, Hilden, Germany) according to the manufacturer's instructions. The presence of the CYP2C9*2/3 alleles [301] and CYP2C19*2/*3/*4/*17 alleles [237; 302] in the DNA of the participants was determined by using the hybridisation probes format on a LightCycler480® (Roche Applied Sciences, Mannheim, Germany). Application of the LightCycler® system allowed to combine RT-PCR with highly sensitive and sequence-specific fluorophore-labelled probes (primers and probes designed and synthesised by TIB Molbiol, Berlin, Germany) with melting curves for discrimination between wild type, mutant and heterocygote products for genotyping [303].

8.4 Tables

Tab. 8-1: Study schedule of long-term pilot study on microdialysis of cytokines (project III)

Study procedure	Screening visit	Study day 1	Study day 2	Study day 3	Final examination
Informed written consent	X				
Inclusion and exclusion criteria	X	X			
Demographics	X				
Physical examination, anamnesis	X				
Weight, BMI	X				
Insertion of microdialysis catheter		X			
Perfusion of microdialysis catheter, microdialysis sampling		X	X	X	
Visual inspection of puncture sites		X	X	X	X
Monitoring of (Adverse) events/problems		X	X	X	X

Tab. 8-2: Data items in the data set of long-term pilot study on microdialysis of cytokines (project III)

Data item	Unit	Item description
ID	---	Identification No. for study individuals (data belonging to a individual No.); 2 digits, starting with 01 and consecutive
CYT	---	IL-6, IL-8, IL-10, TNF-α
FR	[µL/min]	Perfusion flow rate achieved by microdialysis pump
TASM	[h]	'Time after start of microdialysis'. Rel. time elapsed from microdialysis catheter insertion (set to 0.00); all events before insertion set to 0.00; time refers to start of current microdialysis interval [Ex: 8.50 => 8 hours and 30 min after insertion]
TAMI	[h]	'Time after microdialysis catheter insertion'. Rel. time elapsed from microdialysis catheter insertion (set to 0.00); all events before insertion set to 0.00; time refers to middle of current microdialysis interval [Ex: 8.50 => 8 hours and 30 min after insertion]
TINT	[min]	'Time of microdialysis interval'. Rel. time elapsed from start of current microdialysis interval (set to 0.00); time refers to the *end* of microdialysis interval
TMID	[min]	'Mid time of mcirodialysis interval'. Rel. time elapsed from start of current microdialysis interval (set to 0.00); time refers to *middle* of microdialysis interval
TIPL	[h]	"Time planned". Planned rel. time elapsed from microdialysis catheter insertion (set to 0.00); time refers to middle of current microdialysis interval; introduced for comparison of DV of individuals [Ex: 8.50 => 8 hours and 30 min after insertion]
DV	[pg/mL]	Value of dependent variable (i.e. measured cytokine concentration value): 0.00: if EVID is 1 Measured values: if EVID is 0
EVID	---	Identification No. of event 0: observation event (only DV observation) 1: insertion of microdialysis catheter
FLDV	---	Additional information about value of dependent variable (i.e. measured value): 0: measured cytokine concentration values between LLOQ and ULOQ 1: < LLOQ ("BQL"), but measurable 2: < LLOQ ("BQL"), not measurable (=baseline noise) 3: "NV" i.e. no value; if no measured sample result was available 4: > ULOQ, extrapolated from non-linear regression

Data item	Unit	Item description
FLSA	---	Additional information about type of sample: 0: µD sample planned/scheduled 1: equilibration, baseline, or over-night sample 2: no sample
REµD	(%)	Inaccuracy in nominal sample volume. ($Volume_{observed}$-$volume_{calculated}$) / $volume_{calculated}$ ·100
Recµ	(%)	Recovered sample volume. 100+(($volume_{observed}$-$volume_{calculated}$) /$volume_{calculated}$ ·100)
FLRE	---	0: observation of volume recovery; 1: no observation of volume recovery
DAY	---	Data belonging to study day from 0:00-23:59 1: study day 1 (microdialysis catheter insertion) 2: study day 2 3: study day 3
AGE	year	Age of individual at the day of inclusion into the study ; 25-36 years
WT	kg	Body weight; 50-72 kg
HT	cm	Body height; 165-178 cm [Ex: 175 => 1 m and 75 cm]
BMI	[kg/m^2]	Body weight divided by squared height = (WT/HT/HT); 18.5-25.8 kg/m^2
SEX	---	1: female; 2: male
COM1-3	---	Three freetext items for comments on bioanalysis or on investigation performance, other comments

Tab. 8-3: Study schedule of clinical long-term microdialysis study with voriconazole in healthy volunteers (project IV main part, for pilot part refer to [173])

Study procedures	**Screening visit**	**Study day 1**		**Study day 2**		**Study day 3**		**Study day 4**	**Final examination**
		Visit 1	**Visit 2**	**Visit 3**	**Visit 4**	**Visit 5**	**Visit 6**	**Visit 7**	
Written informed consent	**X**								
Demographics[1]	**X**								
Medical history, concomitant diseases	**X**								
Physical examination	**X**								**X**
ECG, eye examination	**X**								**X**
Genotype sample	**X**								
Weight, BMI	**X**	**X**[12]							**X**[12]
Vital signs[2]	**X**	**X**		**X**		**X**		**X**	**X**
Drug history[3]	**X**	**X**							
Virology[4]	**X**								
Drug screening in urine	**X**								
Urinanalysis	**X**								**X**
Coagulation test	**X**								**X**
Clinical chemistry/haematology	**X**								**X**
Inclusion/Exclusion criteria	**X**								
Procedures before administration of voriconazole									
Documentation of concomitant medication		**X**	**X**	**X**	**X**	**X**	**X**	**X**	
Recording food intake within 2 h prior to PO administration						**X**	**X**	**X**	
Insertion of microdialysis catheter		**X**							
In vivo calibration of microdialysis catheter				**X**[5]				**X**[5][6]	

Study procedures	Screening visit	Study day 1		Study day 2		Study day 3		Study day 4	Final examination
		Visit 1	Visit 2	Visit 3	Visit 4	Visit 5	Visit 6	Visit 7	
Administration of VFEND® IV		X [7]	X [7]	X [8]	X [8]				
Administration of VFEND® PO						X [9]	X [9]	X [9]	
Plasma for PK		X[10]	X[11]	X[11]	X[11]	X[10]		X[10]	
Microdialysate for PK		X[10]	X[11]	X[11]	X[11]	X[10]		X[10]	
Adverse event monitoring		X	X	X	X	X	X	X	X

[1] Initials, birth date, height

[2] Before drug administration: blood pressure (BP), heart rate, temperature

[3] Volunteer must not have taken any drugs during the last 14 days (except paracetamol, max. 1.5 g/d)

[4] Testing for HIV and Hepatitis B

[5] RD sampling

[6] 12 h after 7th administration

[7] VFEND® Loading dose (i.v.): 6 mg/kg over 120 min

[8] VFEND® Maintenance dose (i.v.): 4 mg/kg over 80 min

[9] VFEND Maintenance dose (p.o.): 200 mg

[10] Extensive sampling

[11] Sparse sampling

[12] Only weight

Tab. 8-4: Inclusion criteria, exclusion criteria, and reasons for withdrawal for study volunteers

Inclusion criteria
– Healthy males aged between 18 and 50 years
– Body mass index between 20 and 28 kg/m^2
– No regular concomitant (topical or systemic) medication within the last 4 weeks prior to the start of the trial
– Written informed consent given by volunteers after being provided with detailed information about the nature, risks, and scope of the clinical study as well as the expected desirable and adverse effects of the drug
– No legal incapacity and/or other circumstances rendering the individual unable to understand the nature, scope and possible consequences of the study
Exclusion criteria
– Known allergy or hypersensitivity against study drug or drug class
– Participation in another clinical study within the last 6 weeks prior to study
– Blood donation within the last 4 weeks prior to study
– Application of live or killed virus or bacteria vaccines within 14 days prior to study
– Alcohol or drug abuse
– Abuse of nicotine
– History of severe allergic or anaphylactic reactions to any medication
– History of or ongoing optic dysfunction (all volunteers will undergo mandatory testing at screening)
– Ongoing bacterial, viral, fungal, or atypical mycobacterial infection
– Presence of malignancy within the past 5 years, including lymphoproliferative disorders
– History of or ongoing hepatic cirrhosis regardless of cause or severity
– History of or ongoing hospital admission for cardiac disease, stroke, or pulmonary disease within the last 5 years
– History of or ongoing symptoms for blood coagulation disorders
– Seropositivity for human immunodeficiency virus (HIV), all volunteers will undergo mandatory

testing at screening – Seropositivity for hepatitis B or C virus (HepB antigen, HepC antibody), all volunteers will undergo testing at screening – Clinically significant thrombocytopenia, bleeding disorders or a platelet count < 50,000 / µL – White blood cell count <3000/L or >14,000/L, all volunteers will undergo mandatory testing at screening – Hepatic enzymes (aspartate aminotransferase (ASAT), alanine aminotransferase (ALAT), alkaline phosphatase (AP), gamma-glutamyltranspeptidase (γGTP), lactate dehydrogenase (LDH)) and bilirubin 3 times the upper limit of normal, all volunteers will undergo mandatory testing at screening – Serum creatinine 2 times the upper limit of normal, all volunteers will undergo mandatory testing at screening – Abnormalities in ECG that are considered clinically relevant, all volunteers will undergo mandatory testing at screening – Unreliability and/or lack of cooperation – Other objections to participate in the study in the opinion of the investigator
Reasons for Withdrawal:
– Unreliability and/or lack of cooperation – Signs of clinically relevant illness that might hamper the performance of the study according to the protocol or the evaluation of safety – Alcohol or drug abuse – Other objections to participate in the study in the opinion of the investigator

Tab. 8-5: Lifetsyle restrictions and recommendations for appropriate handling of microdialysis setting

Lifestyle restrictions
– Consumption of any food or drinks (except water) for about 2 h before oral drug administration – Intake of concomitant medication except in case of emergency or treatment of AE – Smoking – Intake of alcohol or grapefruit juice from 24 h before until end of the study – Excessive intake of coffee, tea and any other food containing xanthines (i.e. coke, chocolate, etc.)
Behavioural recommendations
– Microdialysis catheters will be kept in place according to the sampling schedule. Throughout the period during which catheters are inserted, individuals will not be allowed to take baths and it will be obligatory to cover the catheter with a plastic wrap and the pump with a plastic bag in order to avoid wetting them when taking a shower. – In addition, the investigator will instruct the individuals to refrain from intensive sports or activities to avoid premature dislocation of the microdialysis catheters.

Tab. 8-6: Data items in the data set of clinical long-term microdialysis study with voriconazole in healthy volunteers

Data item	Unit	Item description
ID	---	Identification No. for study individuals (data belonging to a individual No.);3 digits, starting with 101 and consecutive

Data item	Unit	Item description
TIME	h	'Time'. Rel. time elapsed from start of 1st drug administration (set to 0.00); all events before 1st admin. set to 0.00 [Ex: 8.50 => 8 hours and 30 min after 1st dose]
TILD	h	'Time after last dose'. Rel. time elapsed from start of most recent drug administration (set to 0.00); all events before most recent admin. setF to 0.00 [Ex: 8.50 => 8 hours and 30 min after 1st dose]
TIPL	h	'Time planned'. Planned rel. time after start of 1st drug administration; events before 1st admin. set to 0.00
TALD	h	'Time planned after last dose'. Planned rel. time elapsed from start of most recent drug administration (set to 0.00), all events before most recent admin. set to 0.00 [Ex: 8.50 => 8 hours and 30 min after most recent dosing]
AMT	mg	Actual administered amount of drug; (0 if observation) 200-498 mg [if FLDV=0 then AMT >0 and if EVID=1 then AMT>0]
RATE	mg/h	Infused voriconazole amount administered in 1 h, i.e. RATE = AMT [mg]/infusion duration [h] 0: if no dosing event or no infusion -1: if PO zero order absorption; estimation of absorption rate
DV	µg/mL	Value of dependent variable (i.e. measured value): 0: if EVID is 1, 2 (i.e. dosing, other or reset event) Measured values between LLOQ and ULOQ: if EVID is 0 -99: see also FLCR, no dependent variable "NV" i.e. no value: if no measered sample result is available (see FLCR)
CMT	---	Assignment of compartment number in model: a) first-order and zero/first-order absorption 1: depot (for dosing) 2: central (for observation) 3: peripheral 1 (for e.g. observation) b) zero-order absorption 2: central (for dosing and observation) 3: peripheral 1 (for e.g. observation)
EVID	---	Identification No. of event: 0: observation event (only DV observation) 1: dosing event 2: no event
ADMA	---	Administered formulation of voriconazole 0: no administration 1: solution IV (120/80 min infusion (6/4 mg VRC/kgWT) 2: tablet PO (200 mg VRC)
FLDV	---	Identifier for different records (detailed): 0: dosing record 1: PK observations 2: no observation/dosing
FLCA	---	Identifier for different matrices 60: dialysate from concentric catheter 0: ultrafiltrate (unbound plasma concentration)
FLAM	---	Analytical method used for measuring PK/PD 0: no analytical method, e.g. for dosing events 1: HPLC (LLOQ = 0.15 µg/mL plasma)
FLCR	---	Additional information about values of dependent variable (i.e. measured value, conc. µD uncorrected): 0: measured values between LLOQ and ULOQ: if EVID is 0 1: < LLOQ ("BQL"), but measurable 2: < LLOQ ("BQL"), not measurable 3: "NV" i.e. no value; if no measured sample result is available 4: if EVID ≠ 0 5: if measured results are not listed due to reasons given in comments
VISI	---	Data belonging to observations of one visit according to study protocol (incl. dosing record), all events before 1st admin. set to 0 1: of 1st visit 2: of 2nd visit ..., x: of x visit

Data item	Unit	Item description
DAY	day	Data belonging to study day from 0:00-23:59: 1: day 1 (administration) 2: day 2 3: day 3 etc.
OCC	---	Data belonging to observations (incl. dosing record) following one drug administration, all events before 1st admin. set to 0: 1: of 1st dose 2: of 2nd dose ..., x: of x dose
DOS1	mg	Actual dose administered in all records within one ID (covariate); 0 if event before 1st admin.
DOS2	mg	Actual dose administered in one record within one ID (covariate); 0 if event before 1st admin.
AGE	year	Age of individual at the day of inclusion into the study; 21-46 years
HT	m	Body height; 1.71-1.84 m [Ex: *1.75* => 1 m and 75 cm]
WT	kg	Body weight; 65.1-82.8 kg
BMI	kg/m²	body weight divided by squared height = (WT/HT/HT); 20.63-25.72 kg/m^2
COME	---	0: no co-medication given 1: co-medication given
COM1-5	---	Five freetext items for comments on plasma or microdialysate appearance or processing; other comments (0, 1, 2 or text)

Tab. 8-7: Stability (Arithmetic mean of calculated concentration recoveries; n=3, CV, %) of IL-6, IL-8, IL-10 and TNF-α in stock solution/microdialysate at different storing conditions. QC_{Stab} 1: low, QC_{Stab} 2: intermediate, and QC_{Stab} 3: high cytokine concentration

Stability	C [pg/mL]	Storage	Mean Stability, %				CV, %			
			IL-6	IL-8	IL-10	TNF-α	IL-6	IL-8	IL-10	TNF-α
Stock solution	**150000**	Ultrafreezer (-80 °C)	112	102	104	105	1.92	4.25	6.87	7.27
		Refridgerator (5 °C)	102	101	99.2	92.2	10.7	9.82	7.20	6.95
		Bench-top (RT)	101	101	98.4	100	2.12	3.74	0.00	7.17
Freeze-thaw	**Low**	Cycle 1	103	89.8	102	102	9.83	10.4	15.0	9.14
		Cycle 2	104	82.5	97.0	91.0	6.77	8.38	12.3	8.19
		Cycle 3	101	82.0	100	86.6	11.1	11.9	11.7	9.70
		Cylce 4	98.3	81.2	96.0	82.8	7.29	6.78	11.1	4.05
		Cycle 5	101	79.9	95.0	77.5	7.55	6.00	1.96	2.72
		Cycle 6	92.7	68.8	82.8	69.7	6.27	4.96	7.04	3.07
	Inter-mediate	Cycle 1	95.6	98.5	95.6	93.6	9.48	7.05	8.83	10.0
		Cycle 2	98.2	96.9	93.4	92.0	4.46	4.26	4.78	4.44
		Cycle 3	92.0	89.5	87.1	77.6	4.72	4.13	3.56	2.07
		Cylce 4	87.3	84.4	82.7	73.8	8.55	9.00	13.7	10.5
		Cycle 5	103	96.0	93.8	78.2	4.00	1.16	2.27	1.81
		Cycle 6	90.8	86.1	86.5	74.6	11.1	10.1	6.04	10.5
	High	Cycle 1	107	91.7	97.5	104	7.57	7.82	7.88	4.79
		Cycle 2	92.4	81.2	86.3	83.5	4.66	6.68	2.46	3.55

Stability	C [pg/mL]	Storage	Mean Stability, %				CV, %			
			IL-6	IL-8	IL-10	TNF-α	IL-6	IL-8	IL-10	TNF-α
		Cycle 3	109	102	109	97.4	11.3	15.0	12.2	16.5
		Cylce 4	98.6	90.6	88.8	80.6	8.53	8.19	12.7	8.47
		Cycle 5	101	92.2	94.9	78.5	8.81	7.33	9.16	4.97
		Cycle 6	112	98.6	102	85.8	5.29	2.44	5.98	1.67
Short-term at RT	**Low**	1 h	95.2	92.7	99.7	88.1	8.02	11.1	6.69	8.46
		2 h	91.5	89.9	92.1	89.4	8.71	5.65	4.24	11.8
		4 h	89.5	87.2	93.9	86.9	4.68	4.25	3.30	4.10
		6 h	98.3	98.7	94.1	81.7	7.17	9.48	9.58	11.6
		9 h	102	95.9	91.9	78.2	5.66	2.36	4.32	0.61
		12 h	107	98.8	94.2	78.2	2.10	2.84	2.41	7.65
		15 h	101	97.3	93.4	72.6	3.15	4.63	0.00	0.88
		24 h	95.3	94.4	90.9	59.1	0.77	6.65	2.49	6.46
	Inter-mediate	1 h	83.9	83.1	81.5	78.2	2.15	1.06	2.68	4.60
		2 h	101	90.5	96.7	98.2	9.31	5.37	10.0	14.1
		4 h	95.3	96.0	93.3	83.0	5.43	3.41	3.85	10.9
		6 h	80.7	87.8	84.6	74.0	3.32	2.53	2.53	7.55
		9 h	90.4	87.0	93.7	79.0	1.44	4.33	2.09	1.49
		12 h	90.7	97.9	90.4	78.0	1.34	4.68	7.07	4.25
		15 h	88.3	91.5	84.1	72.0	10.4	4.44	7.56	10.1
		24 h	95.0	93.7	92.9	64.6	5.56	4.71	3.18	6.49
	High	1 h	118	103	104	105	11.5	4.81	11.3	8.55
		2 h	112	106	120	117	29.2	23.8	25.6	29.7
		4 h	84.6	80.1	82.9	78.6	5.77	1.94	3.04	7.33
		6 h	108	92.5	104	95.3	6.55	4.29	6.54	4.41
		9 h	87.4	77.6	80.6	74.6	14.8	11.0	11.1	2.87
		12 h	87.8	81.8	83.4	77.1	8.13	9.27	7.20	7.07
		15 h	117	101	109	91.0	2.82	3.12	9.57	1.47
		24 h	127	98.7	114	86.1	4.62	8.09	3.03	8.39
Long-term at -80 °C	**Low**	2 month	113	71.6	116	112	3.64	17.8	12.6	8.01
		8 month	86.1	85.6	89.1	90.7	4.54	6.18	2.50	3.27
	Inter-mediate	2 month	102	105	106	108	5.07	3.25	8.33	5.48
		8 month	90.3	87.2	85.7	89.5	8.62	6.18	9.48	8.99
	High	2 month	94.2	85.0	94.7	88.3	3.18	5.65	5.06	6.25
		8 month	84.4	83.7	88.6	89.0	7.24	4.02	7.75	3.57
Post-preparative	**Low**	2nd microtitre plate	86.8	79.2	77.8	93.0	11.6	15.5	20.7	8.14
	Inter-mediate	2nd microtitre plate	84.5	83.9	81.9	89.9	11.4	10.6	13.3	7.52

Stability	C [pg/mL]	Storage	Mean Stability, %				CV, %			
			IL-6	IL-8	IL-10	TNF-α	IL-6	IL-8	IL-10	TNF-α
	High	2nd microtitre plate	83.8	73.9	82.6	82.3	17.0	15.6	14.3	12.1

Tab. 8-8: Within-day and inter-assay imprecision (expressed as coefficient of variation, CV) and inaccuracy (as mean percentage deviation, RE) of determined IL-6 concentrations in microdialysate calibrators (highest values at concentrations ≤10 pg/mL in violet, highest values at concentrations >10 pg/mL in blue)

C_{nom} [pg/mL]	C_{calc} [pg/mL] Range of means	Range of Imprecision CV, %	Range of Inaccuracy RE, %
Within-day variability (n=2, 3 or 5) [1]			
4	3.95 - 4.68	2.92 – 12.1	-1.35 - +16.9
6	5.62 – 6.37	1.77 – 10.8	-6.34 - +6.09
10	9.08 – 9.98	3.88 – 14.4	-9.22 - -0.17
20	18.2 – 21.0	5.85 – 11.4	-8.88 - +5.18
50	46.9 – 55.4	1.84 – 18.2	-6.11 - +10.7
100	98.1 – 107	1.06 – 6.89	-1.87 - +7.11
500	483 – 521	1.36 – 13.3	-3.47 - +4.19
1000	957 – 1029	0.68 – 17.5	-4.30 - +2.89
4000	3820 – 4091	0.72 – 10.2	-4.50 - +2.28
6000	5668 – 6161	2.21 – 10.4	-5.53 - +0.46
9000	8676 – 9206	1.14 – 8.40	-3.60 - +2.29
10000	9744 – 10883	0.00 – 10.6	-2.56 - +8.83
C_{nom} [pg/mL]	C_{calc} [pg/mL] mean ± S.D.	Imprecision CV, %	Inaccuracy RE, %
Inter-assay variability (n=17) [1]			
4	4.24 ± 0.37	8.84	+ 6.03
6	5.93 ± 0.45	7.54	- 1.19
10	9.70 ± 0.92	9.48	- 2.97
20	19.7 ± 1.71	8.67	- 1.62
50	50.5 ± 5.89	11.7	+ 0.97
100	102 ± 4.44	4.34	+ 2.20
500	508 ± 26.6	5.24	+ 1.55
1000	988 ± 93.0	9.44	- 1.23
4000	3943 ± 197	5.00	- 1.41
6000	5929 ± 367	6.19	- 1.18
9000	9007 ± 503	5.58	+ 0.08

10000	10294± 553	5.37	+ 2.94

[1] Validation runs 1+3: n=3, run 2: n=5, runs 4-6: n=2

Tab. 8-9: Intra-assay and inter-assay imprecision (expressed as coefficient of variation, CV) and inaccuracy (as mean percentage deviation, RE) of determined IL-8 concentrations in microdialysate calibrators (highest values at concentrations ≤10 pg/mL in violet, highest values at concentrations >10 pg/mL in blue)

C_{nom} [pg/mL]	C_{calc} [pg/mL] Range of means	Range of Imprecision CV, %	Range of Inaccuracy RE, %
Intra-assay variability (n=2, 3 or 5) [1]			
4	3.42 – 4.31	0.00 – 24.5	-14.6 - +7.83
6	5.62 – 6.65	4.53 – 21.2	-6.35 - +10.9
10	9.35 – 10.8	2.88 – 9.43	-6.47 - +8.06
20	18.2 – 21.9	0.45 – 6.44	-8.92 - +9.31
50	45.0 – 54.5	2.33 – 12.6	-9.97 - +8.98
100	96.5 – 106	0.63 – 7.47	-3.50 - +5.83
500	472 – 513	1.41 – 9.64	-5.59 - +2.64
1000	964 – 1017	1.38 – 13.7	-3.56 - +1.67
4000	3893 – 4295	0.73 – 7.95	-2.68 - +7.37
6000	5844 – 6118	2.77 – 8.95	-2.61 - +1.97
9000	8871 – 9222	0.41 – 8.87	-1.44 - +2.47
10000	9349 – 10468	3.64 – 5.71	-6.51 - +4.68
C_{nom} [pg/mL]	C_{calc} [pg/mL] mean ± S.D.	Imprecision CV, %	Inaccuracy RE, %
Inter-assay variability (n=17) [1]			
4	3.94 ± 0.56	14.2	- 1.58
6	6.13 ± 0.64	10.5	+ 2.22
10	9.96 ± 0.77	7.74	- 0.35
20	20.1 ± 1.54	7.68	+ 0.41
50	50.0 ± 5.24	10.5	- 0.07
100	100 ± 4.84	4.82	+ 0.48
500	503 ± 22.8	4.54	+ 0.53
1000	990 ± 76.1	7.69	- 1.03
4000	4058 ± 212	5.23	+ 1.44
6000	6007 ± 313	5.22	+ 0.12
9000	9063 ± 458	5.05	+ 0.70
10000	9916 ± 507	5.11	- 0.84

[1] Validation runs 1+3: n=3, run 2: n=5, runs 4-6: n=2

Tab. 8-10: Intra-assay and inter-assay imprecision (expressed as coefficient of variation, CV) and inaccuracy (as mean percentage deviation, RE) of determined IL-10 concentrations in microdialysate calibrators (highest values at concentrations ≤10 pg/mL in violet, highest values at concentrations >10 pg/mL in blue)

C_{nom} [pg/mL]	C_{calc} [pg/mL] Range of means	Range of Imprecision CV, %	Range of Inaccuracy RE, %
Intra-assay variability (n=2, 3 or 5) [1]			
4	3.94 – 4.62	2.89 – 17.8	-1.52 - +15.5
6	5.38 – 6.24	1.18 – 19.7	-10.3 - +3.92
10	8.82 – 9.79	3.34 – 11.2	-11.8 - -2.09
20	18.1 – 21.6	0.84 – 8.37	-9.64 - +7.76
50	45.9 – 55.4	3.22 – 13.9	-8.10 - +10.7
100	97.5 – 106	0.31 – 7.23	-2.51 - +6.35
500	471 – 511	0.34 – 5.50	-5.86 - +2.29
1000	964 – 1008	2.60 – 17.3	-3.60 - +0.82
4000	3970 – 4247	0.68 – 7.56	-0.75 - +6.17
6000	5680 – 5947	2.05 – 9.87	-5.33 – -0.88
9000	8740 – 9396	1.08 – 7.48	-2.88 – +4.40
10000	9576– 10509	1.09 – 7.47	-4.24 - +5.09
C_{nom} [pg/mL]	C_{calc} [pg/mL] mean ± S.D.	Imprecision CV, %	Inaccuracy RE, %
Inter-assay variability (n=17) [1]			
4	4.25 ± 0.37	8.72	+ 6.26
6	5.92 ± 0.59	10.0	- 1.34
10	9.59 ± 0.68	7.08	- 4.08
20	20.2 ± 1.78	8.83	+ 0.85
50	50.0 ± 5.79	11.6	+ 0.09
100	102 ± 4.64	4.55	+ 2.07
500	501 ± 21.1	4.21	+ 0.29
1000	990 ± 93	9.35	- 1.00
4000	4034 ± 181	4.48	+ 0.86
6000	5879 ± 350	5.95	- 2.02
9000	9072 ± 447	4.93	+ 0.80
10000	10132 ± 494	4.88	+ 1.32

[1] Validation runs 1+3: n=3, run 2: n=5, runs 4-6: n=2

Tab. 8-11: Intra-assay and inter-assay imprecision (expressed as coefficient of variation, CV) and inaccuracy (as mean percentage deviation, RE) of determined TNF-α concentrations in microdialysate calibrators (highest values at concentrations ≤10 pg/mL in violet, highest values at concentrations >10 pg/mL in blue)

C_{nom} [pg/mL]	C_{calc} [pg/mL] Range of means	Range of Imprecision CV, %	Range of Inaccuracy RE, %
Intra-assay variability (n=2, 3 or 5) [1]			
4	3.98 – 4.78	3.01 – 25.2	-0.54 - +19.5
6	5.18 – 6.12	1.50 – 18.7	-13.7 - +2.06
10	9.18 – 10.6	2.68 – 13.0	-8.16 - +5.61
20	18.9 – 21.0	4.36 – 11.6	-5.28 - +4.85
50	46.7 – 55.9	0.80 – 23.1	-6.51 - +11.8
100	96.1 – 109	1.46 – 9.23	-3.93 - +9.49
500	464 – 509	0.97 – 11.1	-7.29 - +1.73
1000	955 – 1021	0.32 – 14.2	-4.51 - + 2.06
4000	3976 – 4276	2.08 – 10.4	-0.59 - +6.89
6000	5905 -6387	1.29 – 10.0	-1.58 - +6.45
9000	8672 – 9080	0.97 – 6.86	-3.65 - +0.89
10000	9516 – 10553	0.87 – 5.87	-4.84 - +5.53
C_{nom} [pg/mL]	C_{calc} [pg/mL] mean ± S.D.	Imprecision CV, %	Inaccuracy RE, %
Inter-assay variability (n=17) [1]			
4	4.20 ± 0.57	13.6	+4.99
6	5.77 ± 0.66	11.4	-3.79
10	9.82 ± 0.79	8.08	-1.82
20	20.3 ± 1.61	7.97	+1.31
50	50.9 ± 5.55	10.9	+1.87
100	101 ± 6.14	6.07	+1.13
500	494 ± 26.5	5.35	-1.13
1000	987 ± 78.2	7.93	-1.33
4000	4063 ± 200	4.93	+1.57
6000	6114 ± 388	6.35	+1.91
9000	8902 ± 386	4.34	-1.09
10000	9972 ± 468	4.70	-0.28

[1] Validation runs 1+3: n=3, run 2: n=5, runs 4-6: n=2

Tab. 8-12: Intra-assay and inter-assay imprecision (expressed as coefficient of variation, CV) and inaccuracy (as mean percentage deviation, RE) of determined IL-6 concentrations in microdialysate quality control samples (highest values at concentrations ≤10 pg/mL in violet, highest values at concentrations >10 pg/mL in blue)

C_{nom} [pg/mL]	C_{calc} [pg/mL] Range of means	Range of Imprecision CV, %	Range of Inaccuracy RE, %
Intra-assay variability (n=3 or 5) [1]			
5	4.80 – 5.75	5.93 – 16.8	-3.93 - +14.9
15	12.8 – 15.1	1.08 – 9.85	-15.0 - +0.60
200	195 – 213	1.97 – 10.3	-2.27 - +6.35
1000	914 – 1019	2.03 – 12.0	-8.61 - +1.92
7000	6104 – 7321	1.10 – 5.00	-12.8 - +4.58
9500	8383 – 10222	1.45 – 9.14	-11.8 - +7.60
C_{nom} [pg/mL]	C_{calc} [pg/mL] mean ± S.D.	Imprecision CV, %	Inaccuracy RE, %
Inter-assay variability (n=20) [1]			
5	5.11 ± 0.59	11.6	+2.30
15	14.3 ± 1.09	7.61	-4.49
200	203 ± 13.8	6.81	+1.60
1000	984 ± 77.6	7.89	-1.59
7000	6793 ± 473	6.96	-2.95
9500	9151 ± 718	7.85	-3.68

[1] Validation runs 1, 3-6: n=3, run 2: n=5

Tab. 8-13: Intra-assay and inter-assay imprecision (expressed as coefficient of variation, CV) and inaccuracy (as mean percentage deviation, RE) of determined IL-8 concentrations in microdialysate quality control samples (highest values at concentrations ≤10 pg/mL in violet, highest values at concentrations >10 pg/mL in blue)

C_{nom} [pg/mL]	C_{calc} [pg/mL] Range of means	Range of Imprecision CV, %	Range of Inaccuracy RE, %
Intra-assay variability (n=3 or 5) [1]			
5	3.18 – 4.90	4.78 – 30.4	-36.5 - -1.91
15	12.4 – 15.4	4.30 – 10.4	-17.0 - +2.93
200	177 – 205	0.56 – 6.93	-11.7 - +2.39
1000	896 – 997	0.96 – 12.3	-10.4 - -0.27

C_{nom} [pg/mL]	C_{calc} [pg/mL] Range of means	Range of Imprecision CV, %	Range of Inaccuracy RE, %
7000	5905 – 7095	1.68 – 4.82	-15.6 - +1.36
9500	8503 – 9140	1.24 – 4.63	-10.5 - -3.78
C_{nom} [pg/mL]	C_{calc} [pg/mL] mean ± S.D.	Imprecision CV, %	Inaccuracy RE, %
Inter-assay variability (n=20) [1]			
5	3.87 ± 0.74	19.2	-22.6
15	13.7 ± 1.34	9.81	-8.95
200	192 ± 12.4	6.45	-3.98
1000	922 ± 66.3	7.20	-7.83
7000	6406 ± 400	6.24	-8.48
9500	8765 ± 379	4.32	-7.74

[1] Validation runs 1, 3-6: n=3, run 2: n=5

Tab. 8-14: Intra-assay and inter-assay imprecision (expressed as coefficient of variation, CV) and inaccuracy (as mean percentage deviation, RE) of determined IL-10 concentrations in microdialysate quality control samples (highest values at concentrations ≤10 pg/mL in violet, highest values at concentrations >10 pg/mL in blue)

C_{nom} [pg/mL]	C_{calc} [pg/mL] Range of means	Range of Imprecision CV, %	Range of Inaccuracy RE, %
Intra-assay variability (n=3 or 5) [1]			
5	4.32 – 6.48	11.3 – 26.9	-13.6 - +29.5
15	13.6 – 16.4	2.25 – 9.59	-9.09 - +9.13
200	199 – 216	1.33 – 8.84	-0.59 - +7.84
1000	952 – 1032	0.92 – 11.6	-4.76 - +3.22
7000	6252 – 7188	0.59 – 7.09	-10.7 - +2.68
9500	8575 – 10369	1.34 – 5.74	-9.73 - +9.15
C_{nom} [pg/mL]	C_{calc} [pg/mL] mean ± S.D.	Imprecision CV, %	Inaccuracy RE, %
Inter-assay variability (n=20) [1]			
5	5.23 ± 0.93	17.8	+4.52
15	14.8 ± 1.07	7.20	-1.02
200	209 ± 12.7	6.06	+4.47

1000	1003 ± 66.5	6.63	+0.32
7000	6845 ± 434	6.35	-2.21
9500	9293 ± 643	6.92	-2.18

[1] Validation runs 1, 3-6: n=3, run 2: n=5

Tab. 8-15: Intra-assay and inter-assay imprecision (expressed as coefficient of variation, CV) and inaccuracy (as mean percentage deviation, RE) of determined TNF-α concentrations in microdialysate quality control samples (highest values at concentrations ≤10 pg/mL in violet, highest values at concentrations >10 pg/mL in blue)

C_{nom} [pg/mL]	C_{calc} [pg/mL] Range of means	Range of Imprecision CV, %	Range of Inaccuracy RE, %
Intra-assay variability (n=3 or 5) [1]			
5	4.64 – 5.51	6.13 – 27.8	-7.11 - +10.1
15	14.7 – 18.0	4.87 – 16.5	-1.96 - +20.1
200	218 – 247	3.22 – 5.13	+9.16 - +23.7
1000	1064 – 1150	1.05 – 11.8	+6.41 - +15.0
7000	6836 – 7702	2.35 – 6.68	-2.34 - +10.0
9500	9220 – 10657	0.53 – 5.65	-2.95 - +12.2
C_{nom} [pg/mL]	C_{calc} [pg/mL] mean ± S.D.	Imprecision CV, %	Inaccuracy RE, %
Inter-assay variability (n=20) [1]			
5	5.13 ± 0.87	17.0	+2.65
15	16.7 ± 1.68	10.1	+11.0
200	233 ± 13.1	5.61	+16.5
1000	1098 ± 75.4	6.87	+9.75
7000	7362 ± 427	5.80	+5.17
9500	9766 ± 580	5.94	+2.80

[1] Validation runs 1, 3-6: n=3, run 2: n=5

Tab. 8-16: Parameter values of non-linear regression (4-parameter logistic) at six validation runs

Cyto-kine	**Para-meter**	**Value**								
		Day 1	**Day 2**	**Day 3**	**Day 4**	**Day 5**	**Day 6**	**Mean**	**SD**	**CV, %**
IL-6	A	1.10	1.08	1.10	1.05	1.09	1.09	**1.09**	0.02	***1.75***
	B	2.32	2.03	2.36	2.17	2.06	1.97	**2.15**	0.16	***7.49***

Cyto-kine	Para-meter	Value								
		Day 1	Day 2	Day 3	Day 4	Day 5	Day 6	Mean	SD	CV, %
	C	3.92	4.41	3.88	4.37	4.64	5.16	**4.40**	0.48	***10.8***
	D	6.47	7.32	6.30	7.09	7.68	8.36	**7.20**	0.77	***10.7***
IL-8	A	1.25	1.22	1.24	1.09	1.04	1.03	**1.14**	0.10	***8.98***
	B	2.68	2.43	2.65	2.45	1.85	1.80	**2.31**	0.39	***16.8***
	C	3.74	4.04	3.77	3.79	5.39	5.61	**4.39**	0.87	***19.8***
	D	5.85	6.35	5.86	6.08	8.96	9.19	**7.05**	1.58	***22.4***
IL-10	A	1.15	1.12	1.15	1.06	0.71	0.75	**0.99**	0.20	***20.8***
	B	2.61	2.24	2.61	2.47	1.77	1.74	**2.24**	0.40	***17.8***
	C	3.90	4.41	3.91	4.26	5.59	6.36	**4.74**	1.01	***21.3***
	D	6.27	7.29	6.26	6.77	9.49	10.6	**7.78**	1.83	***23.5***
TNF-α	A	0.48	0.45	0.46	0.41	0.46	0.61	**0.48**	0.07	***14.4***
	B	2.04	1.61	1.79	1.75	1.63	1.81	**1.77**	0.16	***8.82***
	C	4.24	5.56	5.35	6.67	8.02	6.56	**6.07**	1.31	***21.5***
	D	7.23	9.45	9.00	11.2	13.6	10.9	**10.2**	2.17	***21.3***

Tab. 8-17: Imprecision (expressed as coefficient of variation, CV) and inaccuracy (as relative error, i.e. mean percentage deviation, RE) of determined cytokine concentrations (calculated with the calibration function from in-house Cal) of in-house and NIBSC calibration solution samples

C_{nom} [pg/mL]	Mean C_{calc} [pg/mL]				CV, %				RE, %			
	IL-6	IL-8	IL-10	TNF-α	IL-6	IL-8	IL-10	TNF-α	IL-6	IL-8	IL-10	TNF-α
In-house Cal (n=2)												
4	4.33	3.83	3.85	4.27	1.87	5.86	9.26	8.55	+8.21	-4.36	-3.81	+6.68
6	5.71	5.74	6.02	5.76	7.49	6.98	6.95	7.85	-4.84	-4.30	+0.37	-4.05
10	10.3	11.4	10.9	10.6	9.11	11.7	5.23	15.3	+3.48	+13.5	+8.56	+5.99
20	18.6	19.5	19.5	18.3	0.00	6.94	7.40	1.83	-6.97	-2.65	-2.37	-8.37
50	48.2	47.0	46.3	47.8	2.31	1.91	2.91	4.55	-3.67	-5.98	-7.30	-4.37
100	106	101	103	108	2.10	0.78	3.67	0.69	+5.79	+0.75	+2.79	+8.24

C_{nom} [pg/mL]	Mean C_{calc} [pg/mL]				CV, %				RE, %			
	IL-6	**IL-8**	**IL-10**	**TNF-α**	**IL-6**	**IL-8**	**IL-10**	**TNF-α**	**IL-6**	**IL-8**	**IL-10**	**TNF-α**
500	536	532	535	517	6.67	1.35	2.27	9.59	+7.20	+6.46	+6.94	+3.31
1000	969	983	996	1007	6.07	4.85	2.99	8.64	-3.08	-1.71	-0.37	+0.7
4000	3841	3802	3730	3706	0.72	0.00	0.37	5.32	-3.98	-4.95	-6.74	-7.34
6000	5420	5716	5609	5605	0.37	2.14	4.54	7.45	-9.67	-4.73	-6.51	-6.58
9000	8838	8963	9340	9255	0.77	0.93	0.80	1.04	-1.80	-0.41	+3.77	+2.83
10000	11432	10877	10643	10816	6.69	3.83	3.23	1.41	+14.3	+8.77	+6.43	+8.16
	IL-6	**IL-8**	**IL-10**	**TNF-α**	**IL-6**	**IL-8**	**IL-10**	**TNF-α**	**IL-6**	**IL-8**	**IL-10**	**TNF-α**
NIBSC Cal (n=2)												
4	4.66	5.89	2.57	3.91	1.74	10.3	8.03	3.47	+16.4	+47.2	-35.8	-2.17
6	5.83	8.04	2.96	4.37	4.46	5.10	20.9	5.05	-2.87	+34.0	-50.7	-27.2
10	10.4	13.3	5.47	6.11	6.22	3.50	8.05	2.10	+3.81	+32.6	-45.3	-38.9
20	20.4	26.5	12.1	15.1	7.78	10.7	15.1	10.2	+1.75	+32.6	-39.7	-24.7
50	56.0	69.5	34.1	38.5	6.77	0.00	8.80	7.85	+12.1	+39.0	-31.8	-23.0
100	104	120	61.0	74.4	1.76	4.50	1.05	6.42	+3.96	+20.4	-39.0	-25.6
500	535	609	316	363	7.00	6.77	2.26	2.26	+6.96	+21.9	-36.8	-27.5
1000	1069	1222	642	749	5.08	6.33	4.57	2.24	+6.87	+22.2	-35.8	-25.1
4000	4091	5117	2825	3058	7.99	4.21	0.00	4.62	+2.29	+27.9	-29.4	-23.5
6000	6487	8238	4271	4435	2.63	1.82	4.06	5.36	+8.12	+37.3	-28.8	-26.1
9000	9650	12301	6312	6630	3.88	1.96	1.53	5.47	+7.22	+36.7	-29.9	-26.3
10000	11676	14545	7882	8044	10.2	8.59	4.30	16.2	+16.8	+45.5	-21.2	-19.6

Tab. 8-18: Median and range (Min-Max) of relative recoveries on subsequent flow rates at 25 °C and 37 °C

Flow rate [µL/min]	Human IL-6		Human IL-8		Human IL-10		Human TNF	
	Median	**Min-Max**	**Median**	**Min-Max**	**Median**	**Min-Max**	**Median**	**Min-Max**
				Relative recovery at 25°C, %				
0.3	26.8	22.2-29.0	89.9	82.9-101	9.50	8.64-11.3	29.4	22.9-38.8
0.5	16.8	15.0-23.3	72.5	65.7-81.8	5.91	5.35-8.24	15.9	13.9-24.0
1.0	9.50	8.45-11.7	49.0	44.9-53.0	3.36	2.95-4.50	6.40	5.56-7.42
2.0	5.36	4.87-6.14	30.0	28.9-33.1	1.72	1.48-2.07	2.76	2.18-3.08

5.0	2.60	1.95-3.48	15.3	12.8-22.0	0.75	0.62-1.00	0.68	0.50-1.06
				Relative recovery at 37°C, %				
0.3	26.1	21.6-47.6	103	76.6-113	13.0	7.65-21.5	17.6	13.9-26.7
0.5	29.7	19.3-56.4	83.9	68.8-116	14.0	9.52-23.7	10.3	7.54-20.8
1.0	16.1	8.75-25.0	60.8	44.1-77.4	7.28	4.47-10.3	5.07	3.09-8.72
2.0	13.2	4.59-15.1	48.7	32.8-61.6	4.95	2.56-6.19	3.86	1.63-4.93
5.0	4.42	1.46-4.93	19.0	12.4-25.0	1.29	0.89-2.16	0.98	0.50-1.49

Tab. 8-19: Median and range (Min-Max) of relative deliveries on subsequent flow rates at 25 °C and 37 °C

Flow rate [µL/min]	**Human IL-6**		**Human IL-8**		**Human IL-10**		**Human TNF**	
	Median	**Min-Max**	**Median**	**Min-Max**	**Median**	**Min-Max**	**Median**	**Min-Max**
				Relative delivery at 25°C, %				
0.3	21.1	8.56-48.4	88.1	82.8-92.0	6.43	-19.8-14.8	21.6	-20.0-26.6
0.5	15.0	4.26-30.5	80.2	73.1-81.9	2.08	-2.82-9.71	12.4	-4.19-17.5
1.0	11.9	-11.2-19.1	56.3	42.0-62.1	0.33	-12.4-5.66	3.57	-9.60-8.50
2.0	3.70	-2.69-12.3	30.8	27.7-41.2	-3.13	-11.5-3.24	1.37	-11.4-5.51
5.0	-4.53	-16.0-2.32	13.5	2.69-17.6	-6.51	-19.3-(-0.75)	-7.29	-20.7-(-0.38)
				Relative delivery at 37°C, %				
0.3	34.8	21.8-43.0	89.0	87.7-89.7	-9.13	-22.6-0.96	12.9	-2.52-17.3
0.5	19.9	-37.1-40.2	84.9	83.9-89.6	4.49	-38.0-11.4	18.3	-19.6-28.8
1.0	14.7	-4.72-32.2	71.3	64.4-75.4	-12.0	-19.2-23.5	-7.24	-13.2-38.6
2.0	-17.0	-29.5-(-2.66)	41.2	36.4-53.8	-9.89	-39.3-(-0.97)	7.07	-3.73-15.6
5.0	-29.1	-47.9-(-20.2)	17.3	5.11-22.4	-10.3	-20.9-(-6.07)	-14.4	-36.7-(-1.97)

Tab. 8-20: Non-linear regression parameters calculating microdialysate concentrations via the flow-rate-variation method from the long-term pilot study on microdialysis of cytokines

Cytokine	**ID**	**Parameter**	**Estimate**	**Standard error**	**CV, %**
IL-6	01	r	0.002	0.009	587
IL-6	01	C_{ISF}	100.8	544.9	540

Cytokine	ID	Parameter	Estimate	Standard error	CV, %
IL-6	02	r	0.006	0.009	166
IL-6	02	C_{ISF}	100.9	124.9	124
IL-6	03	r	0.008	0.003	33.9
IL-6	03	C_{ISF}	106.0	24.59	23.2
IL-6	04	r	0.012	0.014	114
IL-6	04	C_{ISF}	103.2	69.56	67.4
IL-8	01	r	0.037	0.011	30.4
IL-8	01	C_{ISF}	291.7	34.53	11.8
IL-8	02	r	0.021	0.004	17.0
IL-8	02	C_{ISF}	226.5	17.85	7.88
IL-8	03	r	0.024	0.007	28.9
IL-8	03	C_{ISF}	482.9	63.91	13.2
IL-8	04	r	0.048	0.013	28.2
IL-8	04	C_{ISF}	120.4	12.00	9.97
IL-10	02	r	0.001	0.008	833
IL-10	02	C_{ISF}	100.1	788.1	788
IL-10	03	r	0.001	0.010	962
IL-10	03	C_{ISF}	100.1	912.5	912
IL-10	04	r	0.001	0.011	1059
IL-10	04	C_{ISF}	100.1	1004.4	1003
TNF-α	01	r	0.001	0.010	1045
TNF-α	01	C_{ISF}	100.1	990.6	990

Tab. 8-21: Weighted correlation coefficients of the non-linear regression of microdialysate concentrations via the flow-rate-variation method from the long-term pilot study on microdialysis of cytokines

Cytokine	ID	*R*
IL-6	1	0.3497
IL-6	2	0.4413
IL-6	3	0.9654

Cytokine	ID	*R*
IL-6	4	0.1355
IL-8	1	0.8642
IL-8	2	0.9674
IL-8	3	0.8979
IL-8	4	0.8363

Tab. 8-22: Parameter of the one-compartment model estimating microdialysate concentrations over time from the long-term pilot study on microdialysis of cytokines

ID	Cytokine	Parameter	Estimate	Standard error	CV, %
01	IL-6	V_F	0.0580	0.075	129
01	IL-6	K01	0.5503	1.573	286
01	IL-6	K10	0.3486	0.340	97.4
01	IL-6	Tlag	1.5459	2.062	133
01	IL-8	V_F	0.0905	0.004	4.92
01	IL-8	K01	0.8660	0.141	16.3
01	IL-8	K10	0.1077	0.004	3.79
01	IL-8	Tlag	2.2262	0.028	1.24
02	IL-8	V_F	0.0125	0.002	12.8
02	IL-8	K01	1.7947	1.932	108
02	IL-8	K10	0.1821	0.011	5.97
02	IL-8	Tlag	1.8248	0.192	10.5
03	IL-6	V_F	0.0171	0.591	3457
03	IL-6	K01	0.2958	10.13	3425
03	IL-6	K10	0.2994	10.42	3480
03	IL-6	Tlag	2.3543	0.111	4.72
03	IL-8	V_F	0.0096	1.324	13764
03	IL-8	K01	0.2131	29.29	13744
03	IL-8	K10	0.2141	29.51	13784
03	IL-8	Tlag	2.2245	0.154	6.94
04	IL-6	V_F	0.0084	0.378	4487
04	IL-6	K01	0.4880	22.09	4526
04	IL-6	K10	0.4865	21.79	4479

ID	Cytokine	Parameter	Estimate	Standard error	CV, %
04	IL-6	Tlag	1.3151	0.054	4.13
04	IL-8	V_F	0.0015	0.002	102
04	IL-8	K01	0.1996	0.010	4.88
04	IL-8	K10	2.0206	2.029	100
04	IL-8	Tlag	1.3196	0.103	7.81

V_F volume of distribution not corrected for bioavailability
K01 absorption rate
K10 elimination rate
Tlag lag time

Tab. 8-23: Mean relative recoveries and variability of retrodialysis samples 1 and 2 (CMA60) within one visit and one individual (n=2; n=1 for visit 3 ID 02)

Individual	Visit	Mean RR, %	SD, %	CV, %
01	1	91.4	0.93	1.0
01	3	87.4	5.09	5.8
01	5	82.2	0.20	0.2
01	7	81.8	2.16	2.6
02	1	91.0	0.41	0.4
02	3	88.5	-	-
02	5	84.4	2.04	2.4
02	7	83.8	3.67	4.4
03	1	81.5	0.64	0.8
03	3	82.9	0.72	0.9
03	5	89.5	2.34	2.6
03	7	76.5	2.71	3.5
04	3	91.0	3.76	4.1
04	7	83.1	0.35	0.4
05	3	86.9	0.65	0.7
05	7	83.4	2.50	3.0
06	3	84.6	0.78	0.9
06	7	96.9	1.26	1.3
07	3	83.5	1.42	1.7
07	7	88.8	1.58	1.8
08	3	80.7	1.37	1.7

Individual	Visit	Mean RR, %	SD, %	CV, %
08	7	80.2	4.64	5.8
09	3	73.8	3.09	4.2
09[1]	7	91.9	2.59	2.8

[1] insertion of a new catheter during visit 5

Tab. 8-24: Terminal slope λ_z [1/h] of VRC concentration-time profiles in ultrafiltered plasma (UF) and interstitial fluid (ISF). In brackets: number of data points involved in the analysis of λ_z

ID	Matrix	Visit 1	Visit 5	Visit 7
01	UF	0.1662 (8)	0.0929 (9)	0.1185 (8)
	ISF	0.1026 (10)	0.0666 (9)	0.0702 (10)
02	UF	0.0469 (8)	0.0095 (9)	0.0179 (8)
	ISF	0.0695 (10)	0.0120 (9)	0.0251 (10)
03	UF	0.1070 (8)	0.0283 (9)	0.0403 (8)
	ISF	0.0873 (10)	0.0376 (9)	0.0427 (10)
04	UF	0.1590 (8)	0.0904 (9)	0.1028 (8)
	ISF	0.1333 (10)	0.0679 (10)	0.0504 (10)
05	UF	0.2339 (8)	0.1031 (9)	0.0973 (8)
	ISF	0.1327 (10)	0.0815 (10)	0.0716 (10)
06	UF	0.1770 (8)	0.1122 (9)	0.1355 (8)
	ISF	0.1889 (10)	0.0623 (10)	0.0528 (10)
07	UF	0.1567 (8)	0.1074 (9)	0.1097 (8)
	ISF	0.1494 (10)	0.0841 (10)	0.0739 (10)
08	UF	0.0233 (8)	0.0619 (9)	0.0667 (5)
	ISF	0.0249 (10)	0.0242 (10)	0.0268 (10)
09	UF	0.0494 (8)	0.0465 (9)	0.0152 (8)
	ISF	0.0670 (10)	0.0081 (7)	0.0381 (10)

Tab. 8-25: Geometric mean of terminal slope λ_z [1/h]

Matrix	Visit 1	Visit 5	Visit 7
	$\bar{x}_{geom}$	$\bar{x}_{geom}$	$\bar{x}_{geom}$
UF	0.0999	0.0585	0.0616
ISF	0.0930	0.0381	0.0468

Tab. 8-26: Maximum concentration C_{max} [µg/mL] and related time t_{max} (time after dose) [h]

ID	Matrix	C_{max}			t_{max}		
		Visit 1	Visit 5	Visit 7	Visit 1	Visit 5	Visit 7
01	UF	1.21	1.08	0.71	2.25	2.25	2.50
	ISF	0.61	1.02	1.32	1.75	3.75	0.25
02	UF	1.88	3.22	3.26	1.75	1.00	2.00
	ISF	0.94	2.80	3.13	2.75	0.75	3.25
03	UF	1.76	1.65	1.70	1.75	1.75	1.00
	ISF	0.86	1.67	2.25	3.75	0.75	1.25
04	UF	1.00	1.87	1.32	1.00	0.50	1.00
	ISF	0.47	1.12	0.73	3.75	1.75	1.75
05	UF	1.36	2.45	1.32	2.00	0.50	1.00
	ISF	0.46	1.44	1.05	1.75	1.25	1.25
06	UF	1.52	1.40	2.12	2.25	0.50	0.50
	ISF	0.94	1.18	0.97	2.25	4.50	1.75
07	UF	1.53	2.82	2.31	2.00	1.50	1.78
	ISF	1.20	1.63	1.21	2.25	1.75	1.25
08	UF	2.15	4.19	3.66	2.00	2.50	1.75
	ISF	0.79	2.80	2.45	3.75	3.25	2.25
09	UF	1.83	2.72	2.88	2.25	2.50	1.00
	ISF	1.30	2.19	1.82	3.25	0.75	1.25

Tab. 8-27: Dose-normalised C_{max} [µg/mL/g]

ID	Matrix	Visit 1	Visit 5	Visit 7
01	UF	2.44	5.38	3.55
	ISF	1.22	5.12	6.62
02	UF	3.91	16.1	16.3
	ISF	1.96	14.0	15.7
03	UF	3.57	8.24	8.49
	ISF	1.75	8.36	11.3
04	UF	2.23	9.35	6.59
	ISF	1.05	5.61	3.65
05	UF	3.24	12.3	6.59
	ISF	1.09	7.20	5.24
06	UF	3.91	6.99	10.6

ID	Matrix	Visit 1	Visit 5	Visit 7
	ISF	2.41	5.90	4.87
07	UF	3.77	14.1	11.6
	ISF	2.96	8.14	6.04
08	UF	4.90	21.0	18.3
	ISF	1.81	14.0	12.3
09	UF	3.96	13.6	14.4
	ISF	2.83	11.0	9.12

Tab. 8-28: Determined partial *AUC* [µg·h/mL] and dose-normalised partial *AUC* [µg·h/mL/g]. Visit 1: $AUC_{0\text{-}12h}$, visit 5: $AUC_{48\text{-}60h}$, visit 7: $AUC_{72\text{-}84h}$.

ID	Matrix	Determined partial *AUC*			Dose-normalised partial *AUC*		
		Visit 1	Visit 5	Visit 7	Visit 1	Visit 5	Visit 7
01	UF	4.93	6.41	4.50	9.91	32.0	22.5
	ISF	4.39	9.92	10.5	8.82	49.6	52.4
02	UF	10.9	29.5	31.9	22.7	147	159
	ISF	7.54	27.4	34.3	15.7	137	171
03	UF	7.09	14.3	13.3	14.4	71.4	66.4
	ISF	6.35	14.6	18.8	12.9	72.8	94.2
04	UF	4.32	10.7	7.49	9.61	53.3	37.4
	ISF	3.20	10.1	6.82	7.10	50.3	34.1
05	UF	5.19	10.9	8.25	12.4	54.5	41.2
	ISF	2.92	10.7	8.52	6.94	53.4	42.6
06	UF	7.69	8.36	7.33	19.7	41.8	36.6
	ISF	4.84	10.2	8.30	12.4	51.1	41.5
07	UF	7.25	14.5	10.9	17.9	72.6	54.3
	ISF	5.70	12.6	9.93	14.0	62.8	49.7
08	UF	11.6	37.1	30.6	26.5	185	153
	ISF	7.20	30.9	26.0	16.4	154	130
09	UF	10.6	23.0	22.2	23.1	115	111
	ISF	9.81	19.3	18.0	21.3	96.5	89.9

Tab. 8-29: Observed C_{min} [µg/mL] at visit 1, visit 5 and visit 7.

ID	Matrix	Visit 1	Visit 5	Visit 7
01	UF	0.13	0.35	0.18
	ISF	0.19	0.64	0.54
02	UF	0.71	2.25	2.37
	ISF	0.47	2.03	2.49
03	UF	0.28	0.92	0.78
	ISF	0.34	1.02	1.49
04	UF	0.11	0.45	0.31
	ISF	0.18	0.60	0.39
05	UF	0.08	0.45	0.34
	ISF	0.14	0.63	0.45
06	UF	0.18	0.41	0.23
	ISF	0.20	0.61	0.54
07	UF	0.27	0.61	0.46
	ISF	0.26	0.65	0.55
08	UF	0.68	2.07	2.29
	ISF	0.57	2.17	1.90
09	UF	0.75	1.46	1.39
	ISF	0.67	1.50	1.23

8.5 Figures

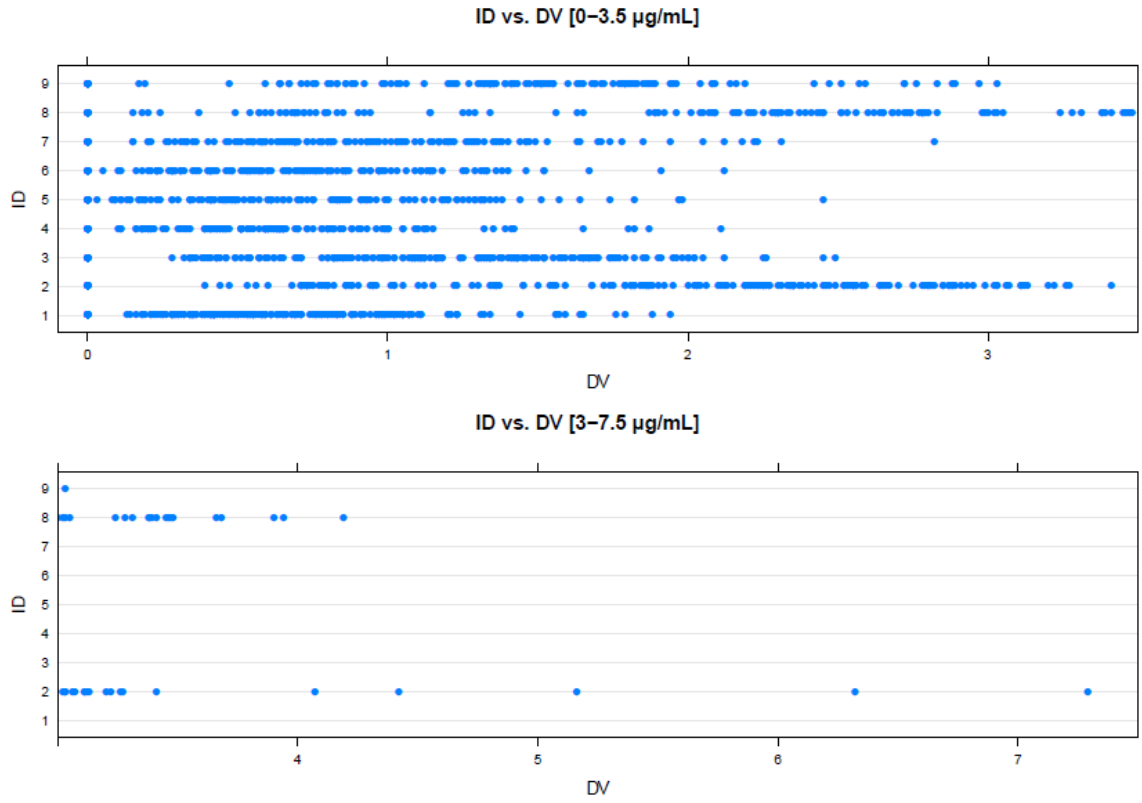

Fig. 8-1: Data set checkout plot (so-called index plots) of identification number vs. concentration of voriconazole.

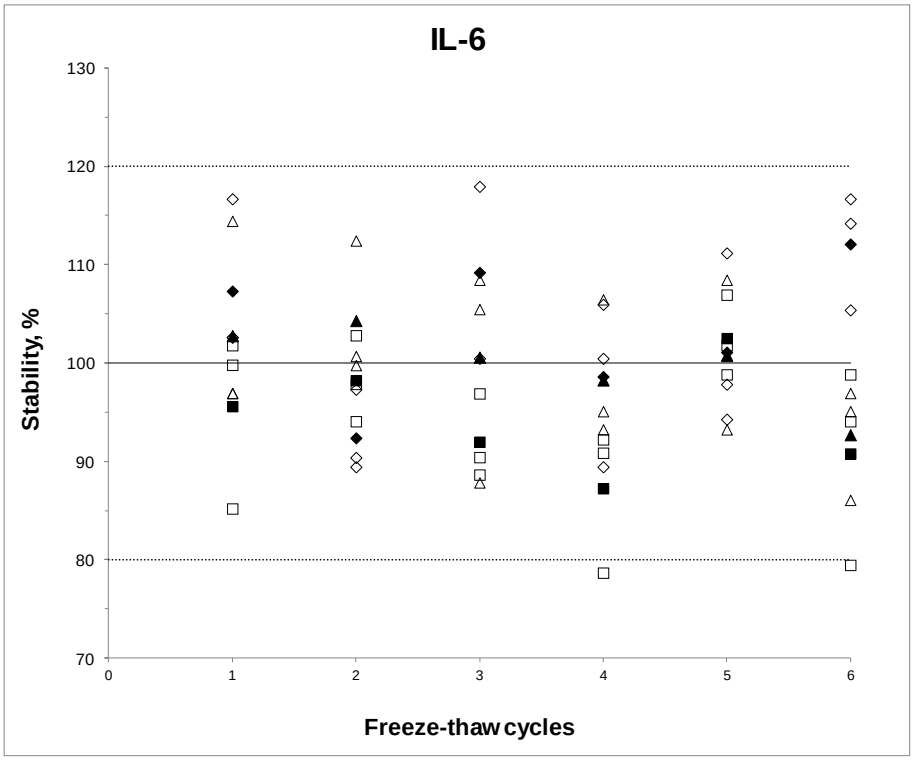
IL-6
Stability, %
130
120
110
100
90
80
70
0
1
2
3
4
5
6
Freeze-thaw cycles

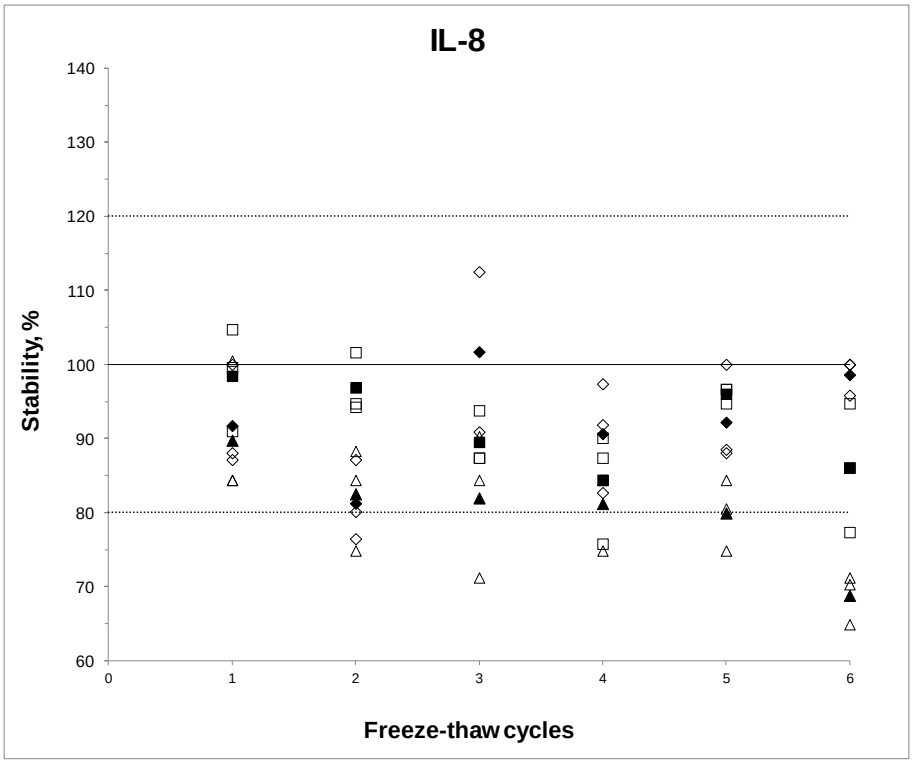
IL-8
Stability, %
140
130
120
110
100
90
80
70
60
0
1
2
3
4
5
6
Freeze-thaw cycles

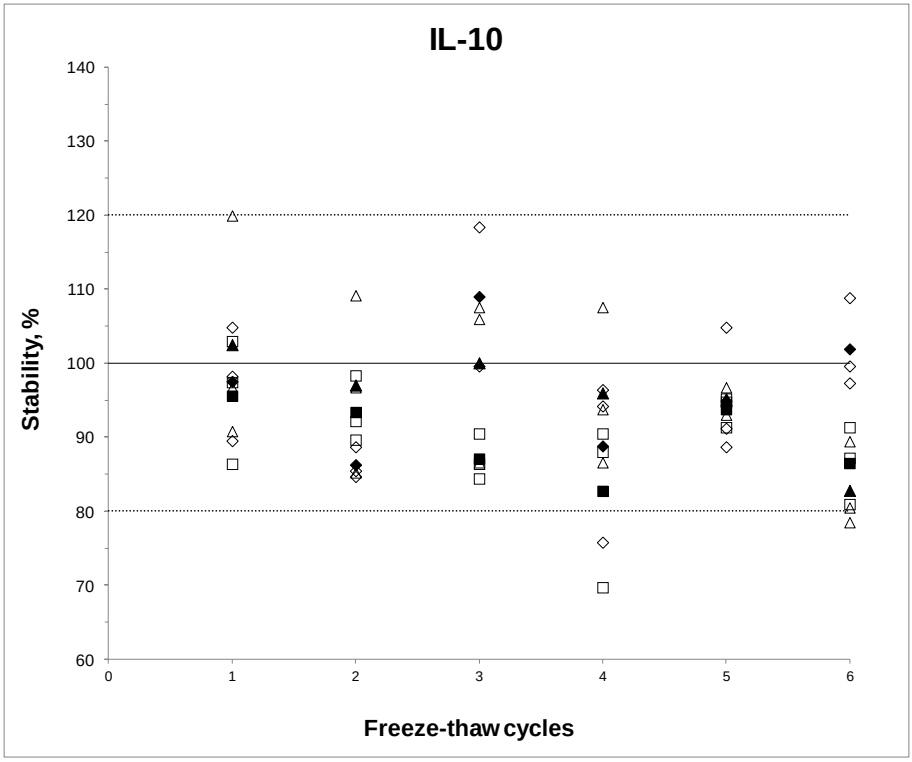

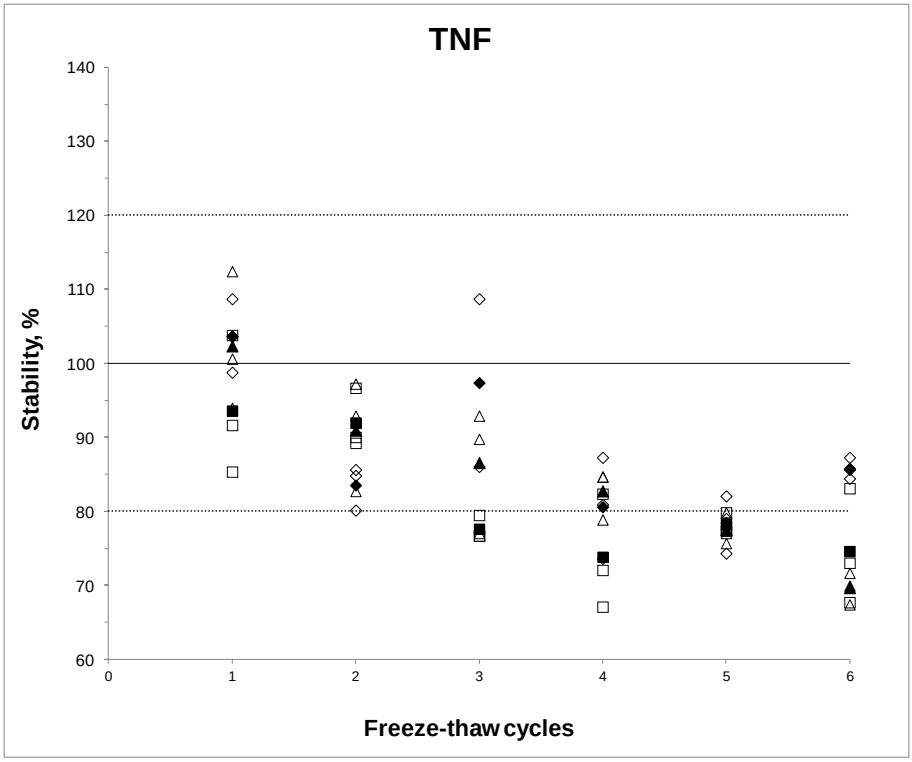

Fig. 8-2: Freeze-thaw stability of IL-6, IL-8, IL-10 and TNF-α in microdialysate. Low (triangles), intermediate (squares) and high (diamonds) concentrations. Arithmetic means (filled symbols); acceptance range (dotted lines) 80%-120%.

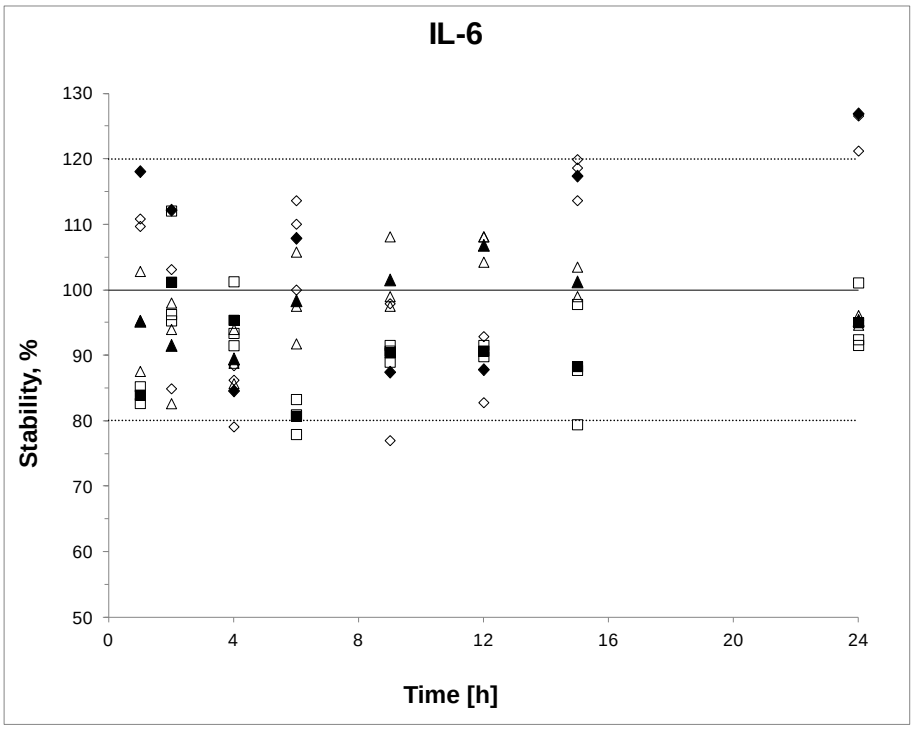
IL-6
Stability, %
130
120
110
100
90
80
70
60
50
0
4
8
12
16
20
24
Time [h]

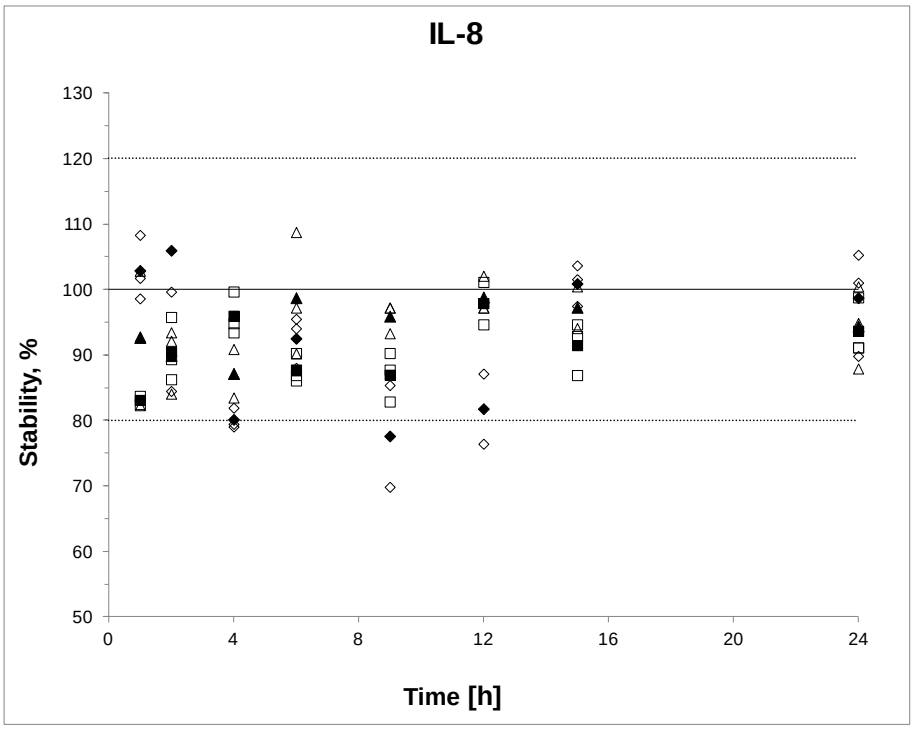
IL-8
Stability, %
130
120
110
100
90
80
70
60
50
0
4
8
12
16
20
24
Time [h]

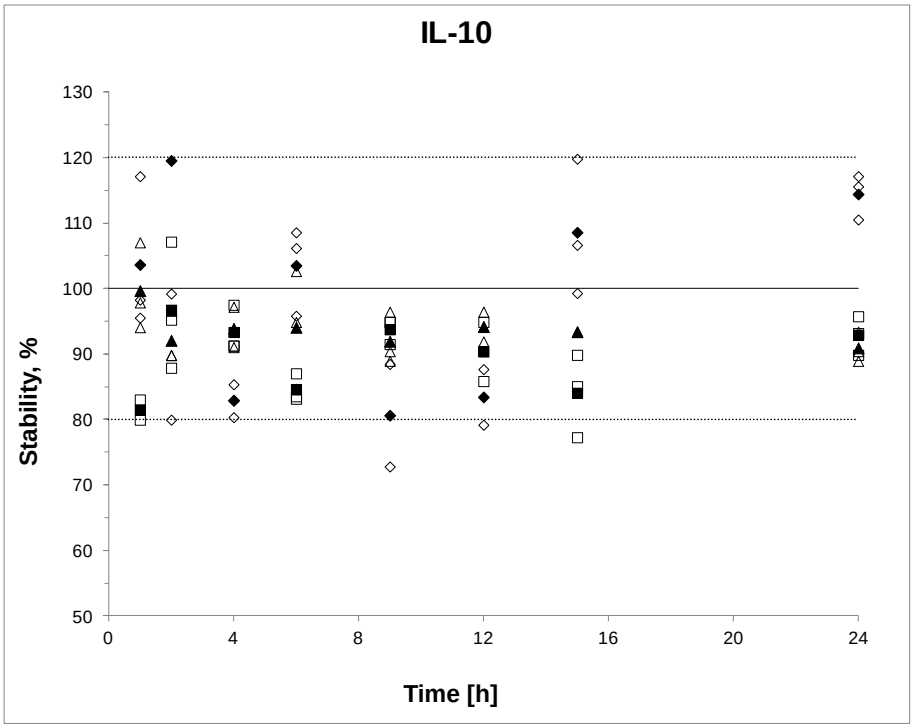

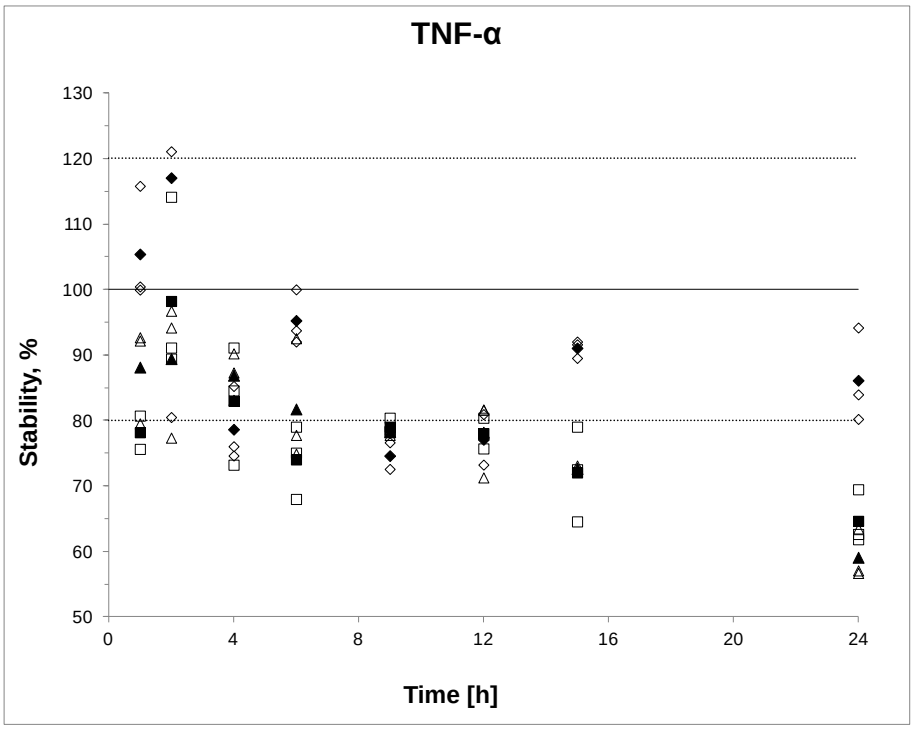

Fig. 8-3: Short-term stability of IL-6, IL-8, IL-10 and TNF-α in microdialysate at room temperature. Low (triangles), intermediate (squares) and high (diamonds) concentrations. Arithmetic means (filled symbols); acceptance range (dotted lines) 80%-120%.

IL-6

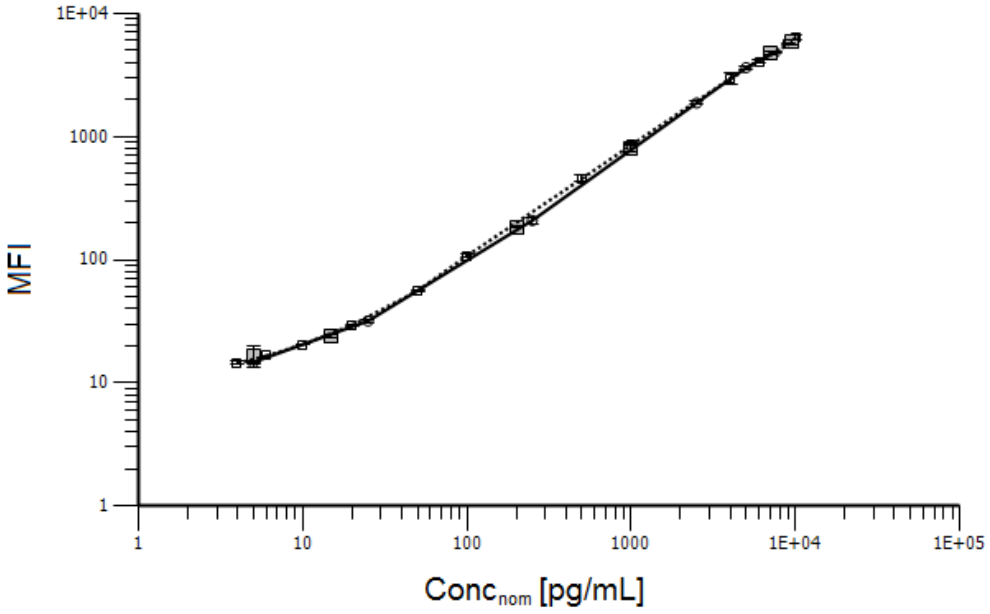
1E+04
1000
100
10
1
MFI
1
10
100
1000
1E+04
1E+05
Conc nom [pg/mL]

IL-8

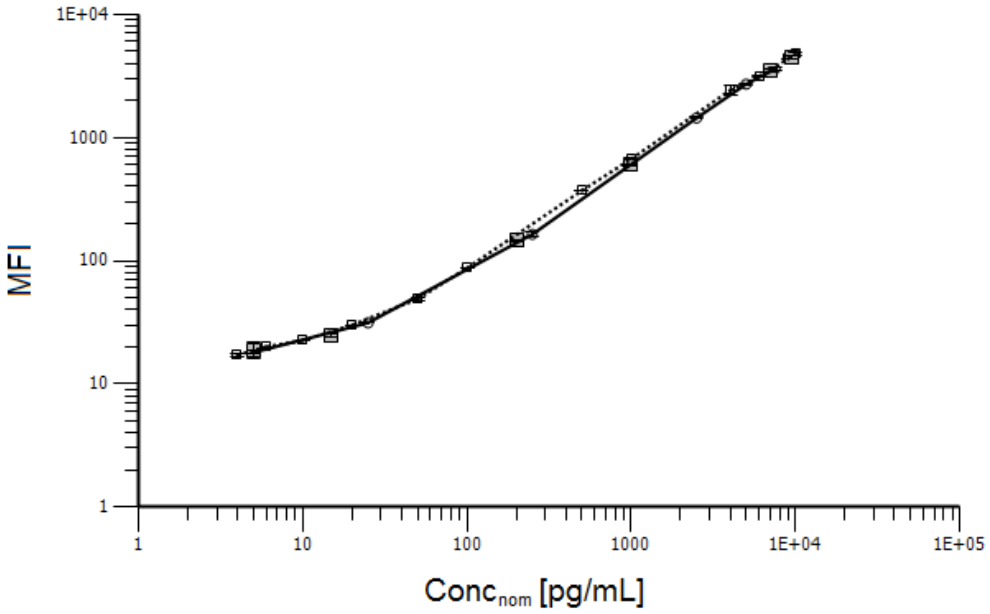
1E+04
1000
100
10
1
MFI
1
10
100
1000
1E+04
1E+05
Conc nom [pg/mL]

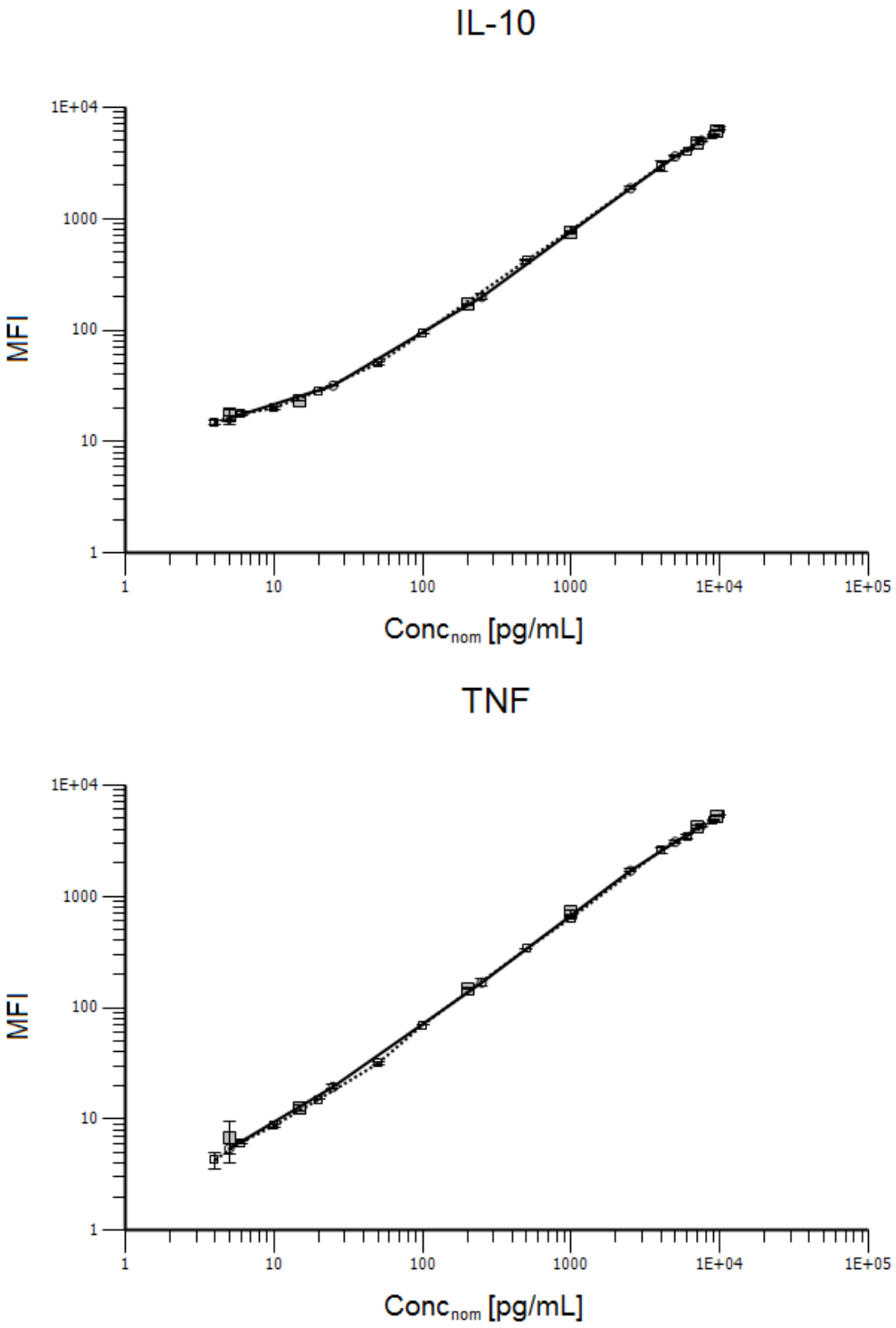

Fig. 8-4: MFI-concentration profiles of IL-6, IL-8, IL-10 and TNF-α from dilutional-linearity samples (line), calibration solutions (dotted line, squares) and quality control samples (grey filled squares). Arithmetic means (symbols) ± SD (error bars).

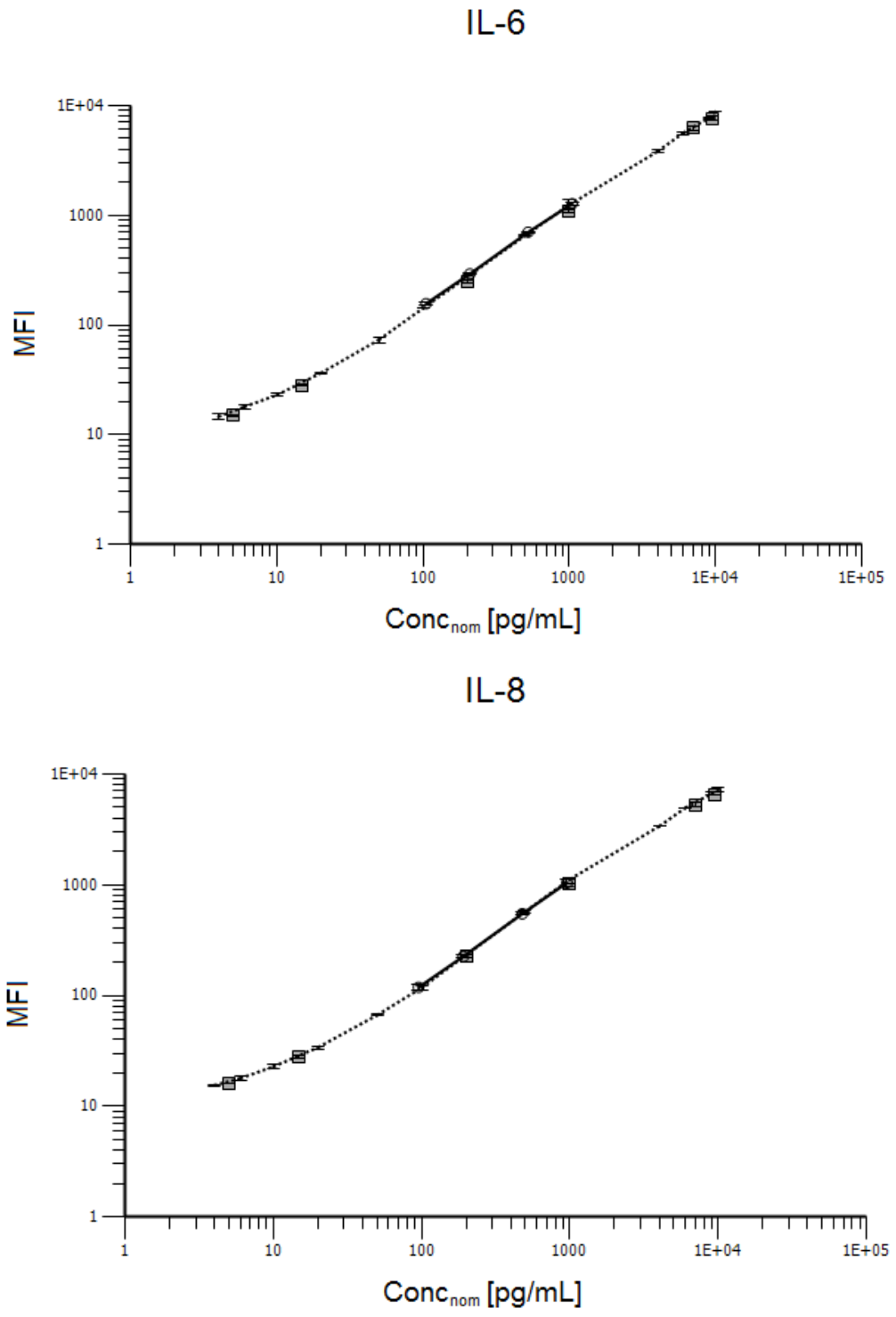

Fig. 8-5: MFI-concentration profiles of IL-6 and IL-8 from parallelism samples (line), calibration solutions (dotted line, squares) and quality control samples (grey filled squares). Arithmetic means (symbols) ± SD (error bars).

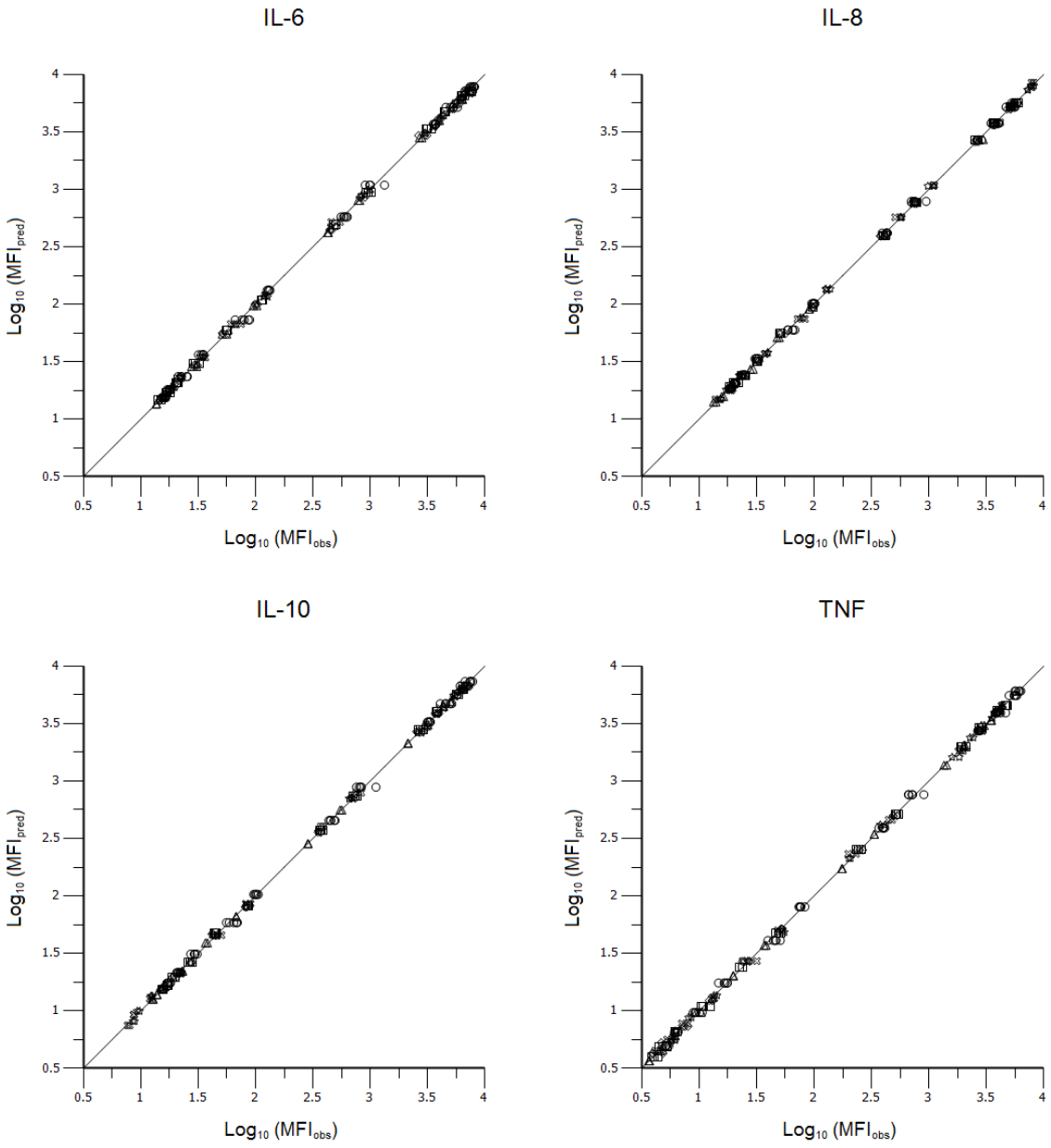

Fig. 8-6: Goodness-of-fit plots of non-linear regression of calibration solutions at six validation runs. Predicted versus observed MFI and line of identity. Symbols: Validation days 1 (□), 2 (○), 3 (◊), 4 (Δ), 5 (✪), 6 (*)

IL-6

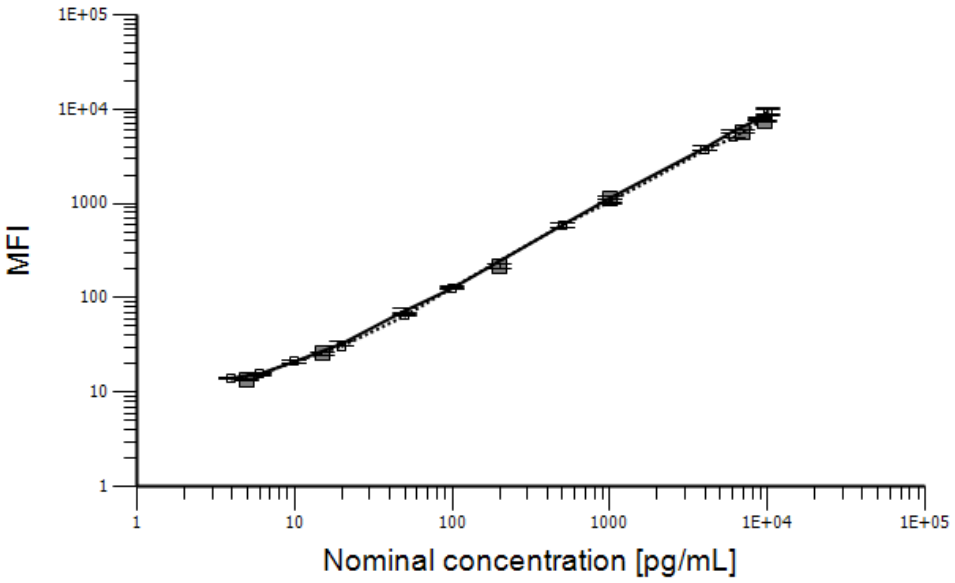
1E+05
1E+04
1000
100
10
1
MFI
1
10
100
1000
1E+04
1E+05
Nominal concentration [pg/mL]

IL-8

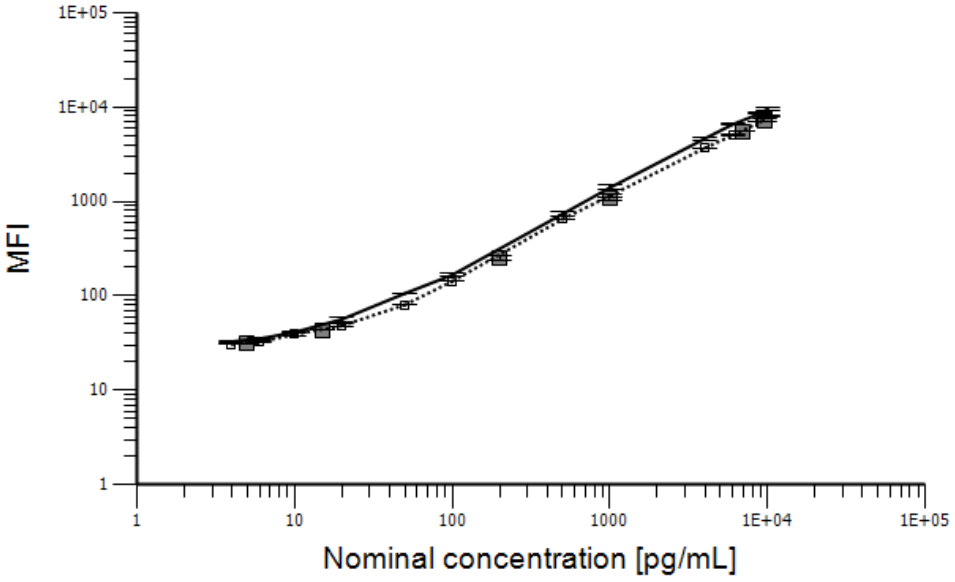
1E+05
1E+04
1000
100
10
1
MFI
1
10
100
1000
1E+04
1E+05
Nominal concentration [pg/mL]

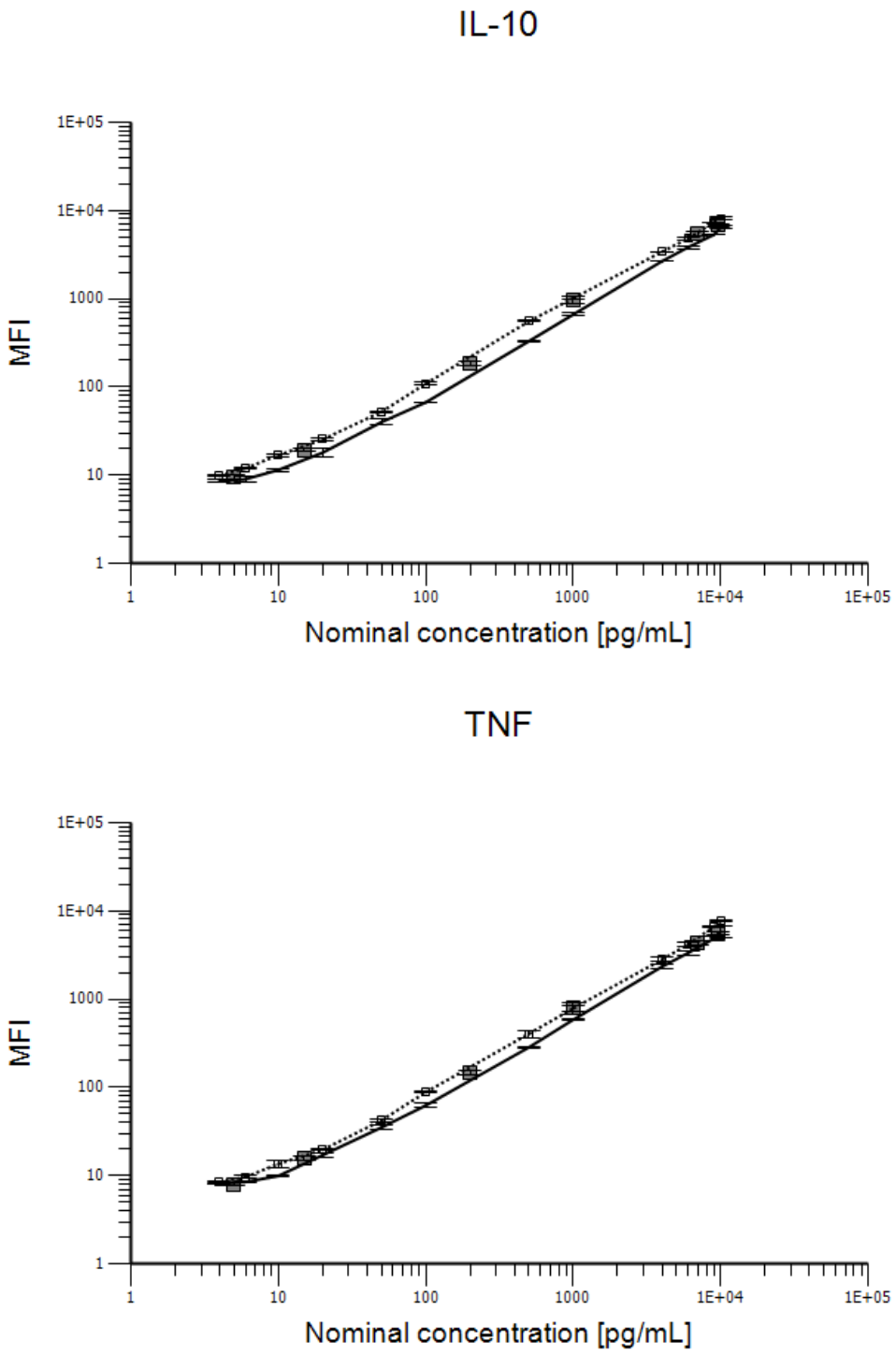

Fig. 8-7: MFI-concentration profiles of IL-6, IL-8, IL-10 and TNF-α from NIBSC calibration solutions (line), in-house calibration solutions (dotted line, squares) and quality control samples (grey filled squares). Arithmetic means (symbols) ± SD (error bars).

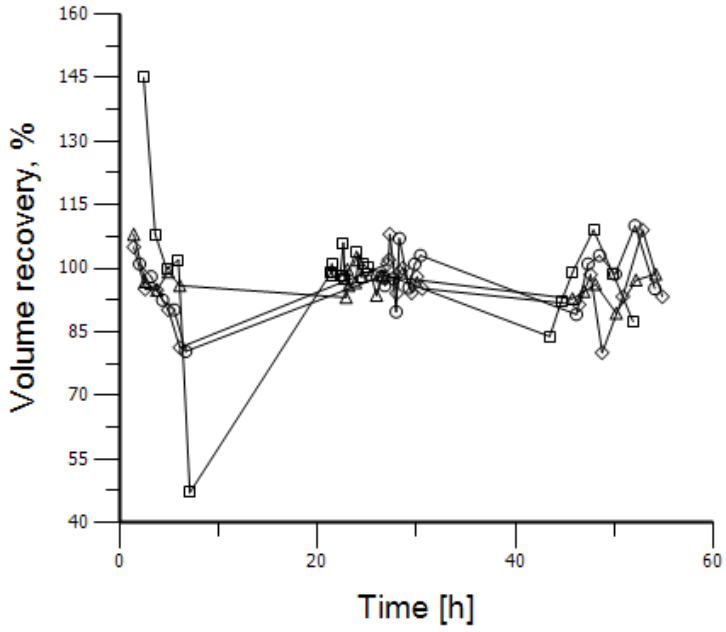

Fig. 8-8: Volume recovery of the individual microdialysate samples at study days 1-3. The x-axis refers to the planned time (i.e. at the middle of the microdialysis interval) after insertion of the microdialysis catheter. Symbols: ID 01 (□), ID 02 (○), ID 03 (◊) and ID 04 (Δ)

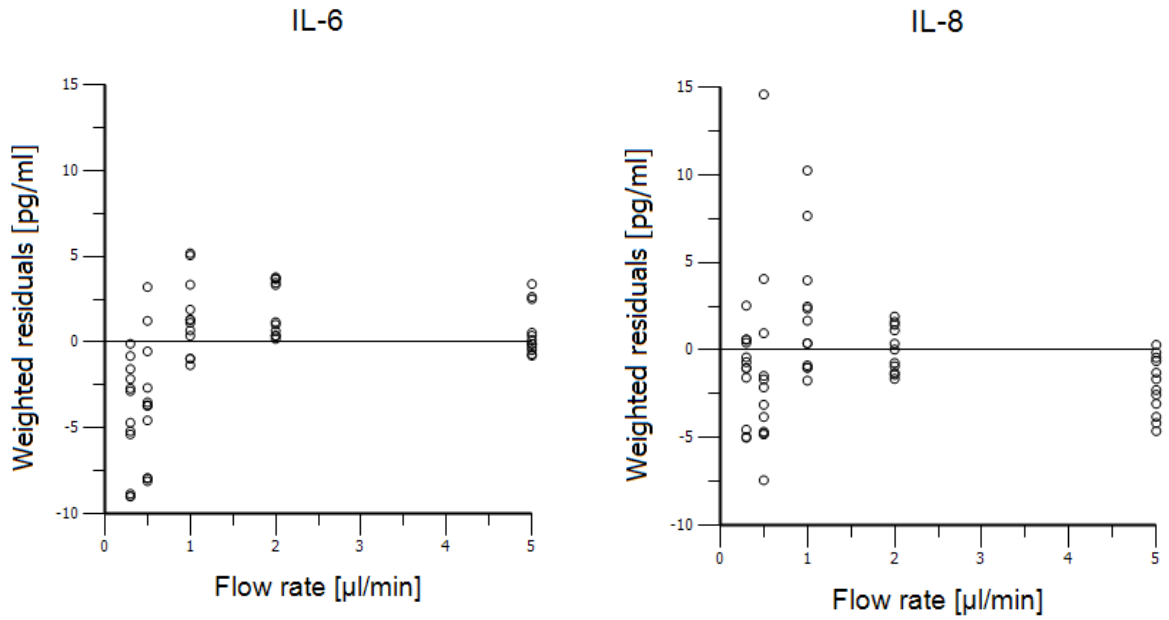

Fig. 8-9: Weighted residuals between observed and predicted (by non-linear regression) microdialysate concentrations of IL-6 and IL-8 vs. flow rate from the four study individuals.

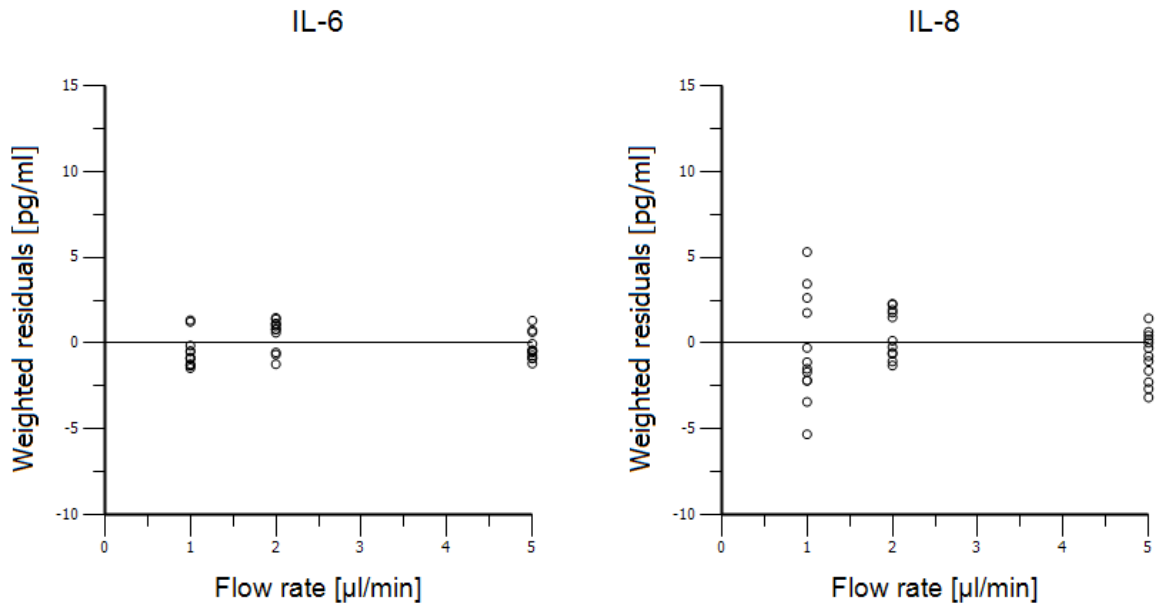

Fig. 8-10: Weighted residuals between observed and predicted (by non-linear regression without flow rates of 0.3 and 0.5 µL/min) microdialysate concentrations of IL-6 and IL-8 vs. flow rate from the four study individuals

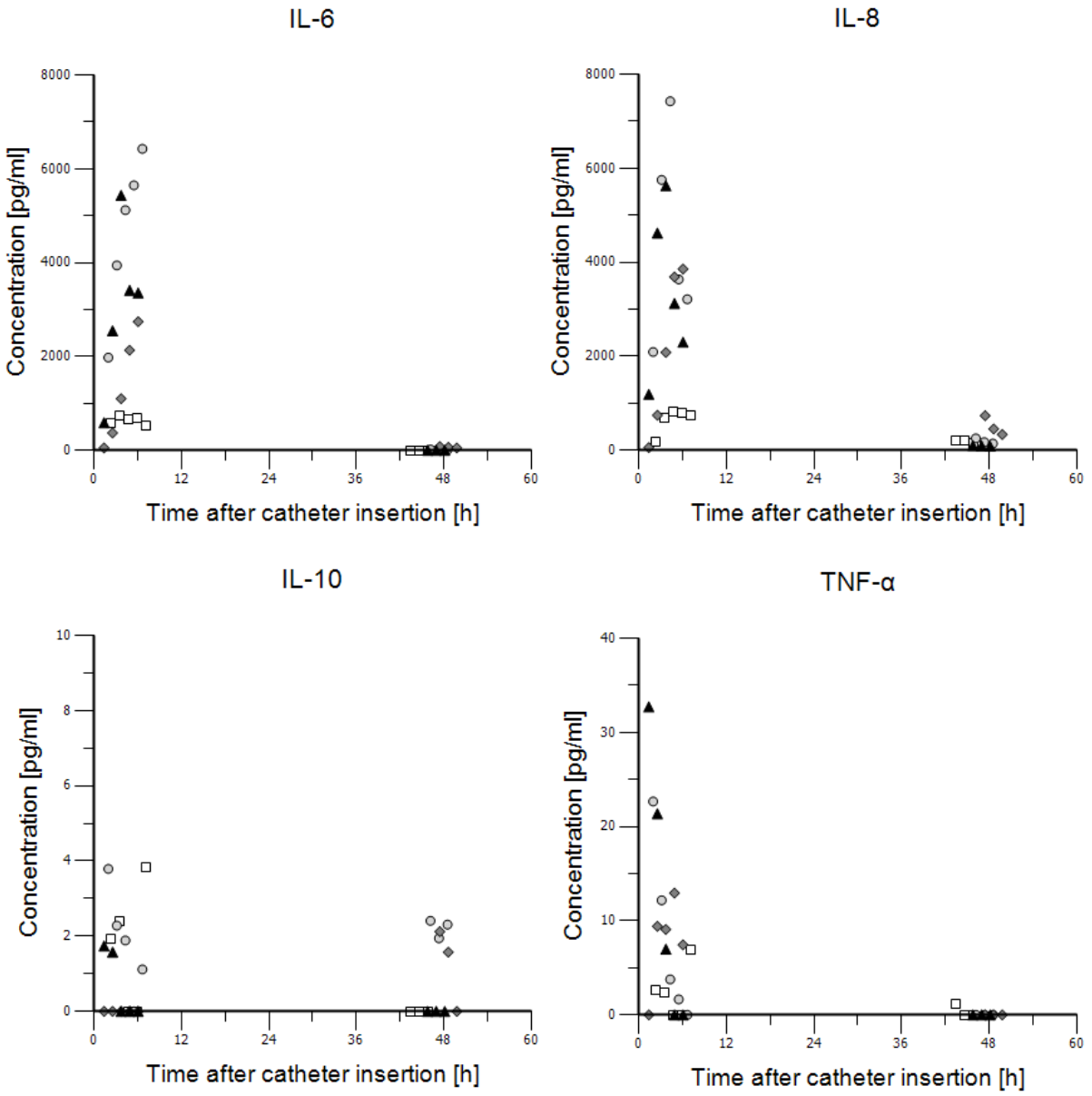

Fig. 8-11: Concentration-time profiles of IL-6, IL-8, IL-10 and TNF-α in ID 01 (□), ID 02 (○), ID 03 (◊) and ID 04 (Δ)

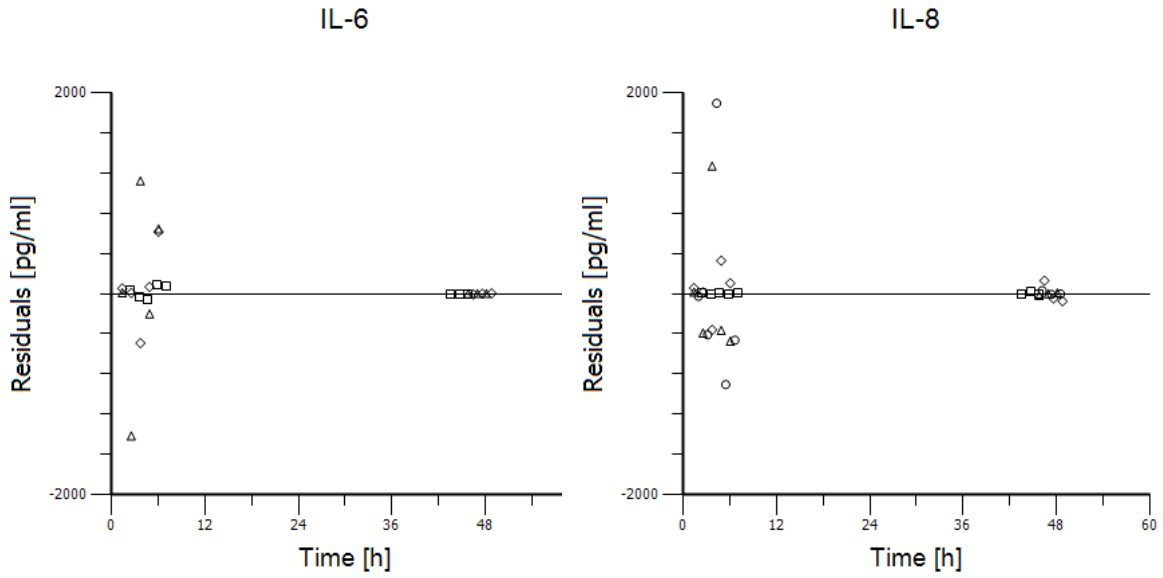

Fig. 8-12: Residuals between observed and predicted (by 1-copartment model) microdialysate concentrations of IL-6 and IL-8 vs. time after microdialysis insertion in ID 01 (□), ID 02 (○), ID 03 (◊) and ID 04 (Δ).

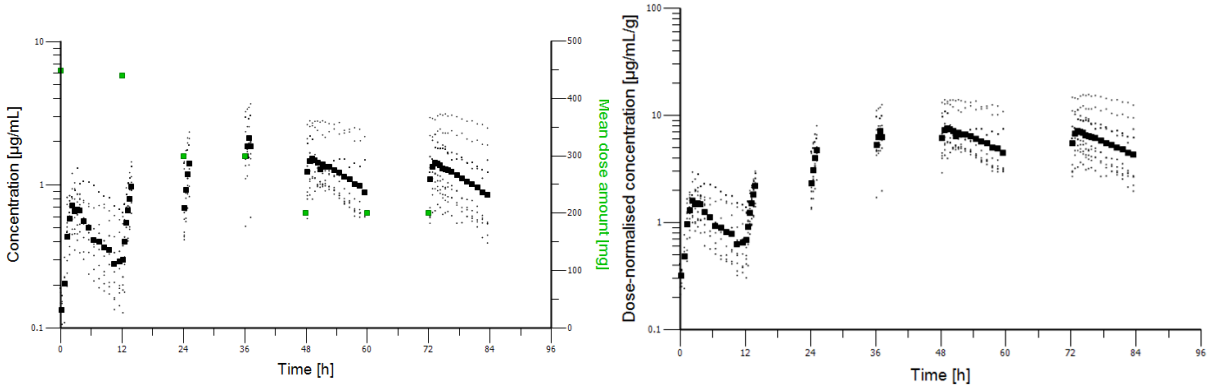

Fig. 8-13: Individual ISF concentration-time profiles (left panel) and dose-normalised profiles of voriconazole in ID 01 (squares), ID 02 (circles), ID 03 (diamonds), ID 04 (triangles), ID 05 (cross), ID 06 (four-point star), ID 07 (five-point star), ID 08 (six-point star) and ID 09 (ten-point star) and geometric mean (black filled squares) concentrations in semi-logarithmic plots.

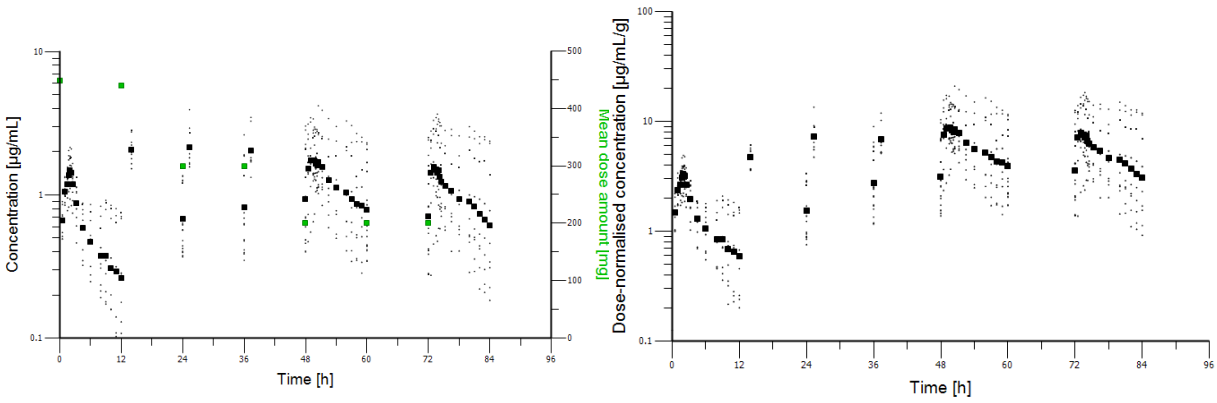

Fig. 8-14: Individual UF concentration-time profiles (left panel) and dose-normalised profiles of voriconazole in ID 01 (squares), ID 02 (circles), ID 03 (diamonds), ID 04 (triangles), ID 05 (cross), ID 06 (four-point star), ID 07 (five-point star), ID 08 (six-point star) and ID 09 (ten-point star) and geometric mean (black filled squares) concentrations in semi-logarithmic plots.

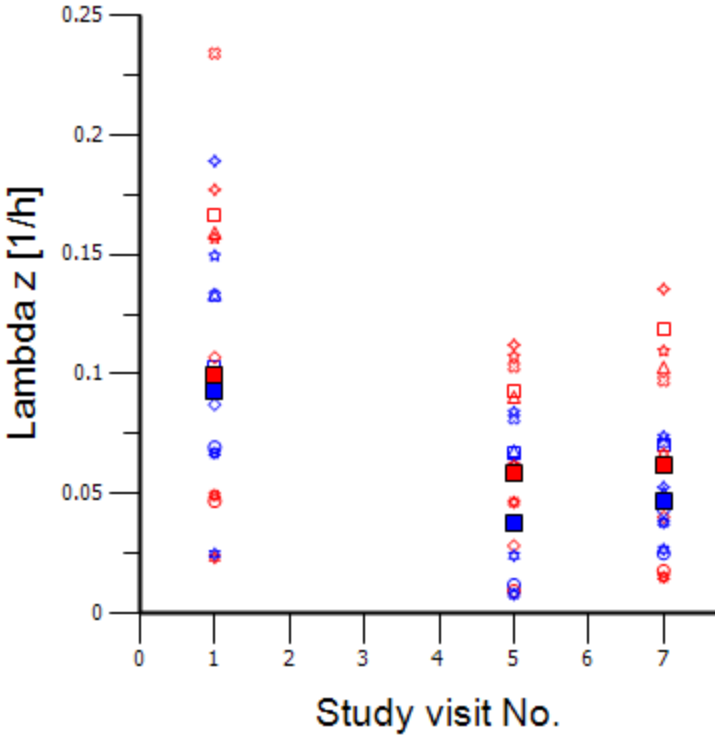

Fig. 8-15: λ_z after single (visit 1) and multiple dosing (visits 5, 7) in ID 101 (squares), ID 02 (circles), ID 03 (diamonds), ID 04 (triangles), ID 05 (cross), ID 06 (four-point star), ID 07 (five-point star), ID 08 (six-point star) and ID 09 (ten-point star). UF (red colour), ISF (blue colour). Geometric means (filled squares).

DANKSAGUNG

Ein besonderer Dank gilt meiner Betreuerin Frau Prof. Charlotte Kloft für die spannenden Projekte, welche ich bearbeiten und vorantreiben durfte, des Weiteren für ihre thematische, fachliche und mentale Unterstützung, Ausbildung, Beratung und Motivation und für das herzliche Miteinander.

Darüber hinaus möchte ich folgenden Menschen (und Arbeitskreisen) ganz besonders danken:

Herrn Prof. Markus Zeitlinger, Frau Edith Lackner und vielen Assitenzärzten und auch Medizinstudenten am AKH Wien (Klinische Pharmakologie und Innere Medizin, Medizinische Universität Wien) für die tolle Zusammenarbeit im Rahmen des Projektes IV und auch für die weitere Unterstützung sowie den fachlichen als auch menschlichen Austausch,

Dem Unternehmen Becton Dickinson, jedoch vor allem Herrn Prof. Andreas Simm und Herrn Dr. Alexander Navarrete Santos (Klinik für Herz- und Thoraxchirurgie, Universitätsklinikum Halle (Saale)) für das Zurverfügungstellen, den Transfer und das Training am BD FACSArray™ sowie der überaus netten, unkomplizierten und spannenden Kommunikation,

Herrn Dr. Christian Rimmbach (Institut für Pharmakologie, Ernst-Moritz-Arndt-Universität Greifswald) und Frau Prof. Johanna Weiß (Klinische Pharmakologie und Pharmakoepidemiologie, Universitätsklinikum Heidelberg) für die Genotypisierung der Isoenzyme der Probanden aus der klinischen Studie (Projekt IV),

Den Studienteilnehmern für ihre Bereitschaft, zur klinischen Forschung beizutragen, und sich den damit verbundenen Unannehmlichkeiten auszusetzen,

Herrn Dr. Martin Kees für die ärztliche Leitung der Mikrodialysestudie (Projekt III) und viele weitere kompetente, sachliche wie auch freundschaftliche Ratschläge,

Meiner Mentorin Frau Dr. Franziska Drescher für die tatkräftige Einführung in den Arbeitskreis, die Hilfestellungen und die optimale Vorbereitung der Übernahme des Projektes IV und die langjährige Unterstützung,

Der ‘guten Seele’ Frau Dorothea Frenzel für ihren praktischen, theoretischen und zwischenmenschlichen Beistand und für die tollen ‘Obstpausen’ und vieles mehr während des Überbrückungsjahres an der MLU, außerdem der ‘Mittagsrunde’, Frau Martina Mannd und Frau Antje Peters, für die vielen schönen Augenblicke zusammen,

Meinen lieben ‘Herren’, Herrn Dr. Holger Brosig, Herrn Dr. Ingo Siebenbrodt und Herrn Dr. Werner Herrmann, für die vielen lustigen Stunden miteinander im Labor oder bei den Kaffeepausen sowie für die tatkräftige Hilfe und die gute Verständigung,

Den beiden liebenswerten Damen, Frau Beatrice Rackwitz und Frau Cornelia Böhnstedt, für ein stets offenes Ohr und angenehme, rege Gespräche sowie die Bereitschaft zu Helfen,

Den befreundeten Arbeitsgruppen am Institut für Pharmazie der Martin-Luther-Universität Halle-Wittenberg, insbesondere den ‘Immings’, den ‘Sippels’ und den ‘Mäders’, für das außergewöhnliche Klima am Institut, die tollen Gespräche auf den Gängen, den interdisziplinären Austausch, die häufigen ‘Besprechungsrunden’, die tollen Feiern und vor allem für die Aufnahme und die Unterstützung während des Überbrückungsjahres,

Meinen Berliner Mitdoktorand(inn)en, Iris Minichmayr, Helena Edlund, Johanna Melin, Eva Göbgen, Daniela Burau, Christine Weiser, Andrea Henrich und Sebastian Wicha, als auch den Potsdammern, vor allem Alexander Solms, für den projektbezogenen, fachlichen, sowie auch den privaten Meinungsaustausch, für die Korrekturhilfen, für die äußerst schöne Zeit an der Freien Universität Berlin und dafür, dort auch Freunde gewonnen zu haben,

Und natürlich auch dem Hallenser Urgestein, Marcus Scholz, Valerie Nock, Ronald Niebecker, André Schäftlein, Monika Frank, Anne Keunecke und Julia Michael, für die vielen Korrekturstunden an dieser und anderen Arbeiten, für die unendlich vielen schönen, lustigen, fröhlichen Runden zusammen, die gemeinsam verbrachten Bürozeiten, die ausgelassenen Feiern und die geteilten Rückschläge sowie die gemeinsamen Schritte vorwärts als auch die daraus entstandenen, andauernden Freundschaften,

Weiterhin meinen langjährigen Freunden, allen voran Stefan Hoffmann, für ihre stete Unterstützung und das harmonische Miteinander,

Und natürlich meiner Familie für den Rückhalt, den sie mich unentwegt spüren lässt, und für die unbedingte Herzlichkeit und Hingebung.